Study of chars prepared from biomass wastes : material and energy recovery

Jenny Juliana Pena

▶ **To cite this version:**

Jenny Juliana Pena. Study of chars prepared from biomass wastes : material and energy recovery. Chemical and Process Engineering. Ecole nationale supérieure Mines-Télécom Atlantique, 2018. English. NNT : 2018IMTA0104 . tel-03032643

HAL Id: tel-03032643

https://theses.hal.science/tel-03032643v1

Submitted on 1 Dec 2020

HAL is a multi-disciplinary open access archive for the deposit and dissemination of scientific research documents, whether they are published or not. The documents may come from teaching and research institutions in France or abroad, or from public or private research centers.

L'archive ouverte pluridisciplinaire **HAL**, est destinée au dépôt et à la diffusion de documents scientifiques de niveau recherche, publiés ou non, émanant des établissements d'enseignement et de recherche français ou étrangers, des laboratoires publics ou privés.

UNIVERSITE BRETAGNE SCIENCES LOIRE POUR L'INGENIEUR

IMT Atlantique
Bretagne-Pays de la Loire
École Mines-Télécom

THESE DE DOCTORAT DE

L'ÉCOLE NATIONALE SUPERIEURE MINES-TELECOM ATLANTIQUE
BRETAGNE PAYS DE LA LOIRE - IMT ATLANTIQUE
COMUE UNIVERSITE BRETAGNE LOIRE

ECOLE DOCTORALE N° 602
Sciences pour l'Ingénieur
Spécialité : « *Génie des procédés et bioprocédés* »

Par

« Jenny PEÑA »

« Study of chars prepared from biomass wastes: material and energy recovery»

« Valorisation énergétique et matière de chars issus de biomasses résiduelles »

Thèse présentée et soutenue à « IMT Atlantique », le « 12 Novembre 2018 »
Unité de recherche : GEPEA (UMR CNRS 6144)
Thèse N° : 2018 IMTA0104

Rapporteurs avant soutenance :

Pierre LE-CLOIREC — Ecole Nationale Supérieure de Chimie de Rennes
Marco BARATIERI — Università de Bozen-Bolzano

Composition du Jury :

Président :	Laurence LE COQ	Professeur IMT Atlantique
Examinateurs :	Pierre LE CLOIREC	Professeur Ecole Nationale Supérieure de Chimie de Rennes
	Marco BARATIERI	Professeur Università di Bozen-Bolzano
	Manuel RODRIGUEZ	Professeur Universidad de Los Andes
Dir. de thèse :	Claire GERENTE	Maître Assistant HDR IMT Atlantique
Encadrant de thèse :	Audrey VILLOT	Maître Assistant IMT Atlantique

Invité(s)
Simon THOUIN Ingénieur ADEME

Acknowledgments

I wish to express my gratitude to Professor Claire GÉRENTE and Dr Audrey VILLOT for allowing me to prepare my doctorate in the best conditions. I want to thank them especially for their efforts and the support they have shown me throughout this study under their direction.

I am very honored by the presence as reviewers of Professor Pierre LE CLOIREC and Professor Marco BARATIERI for having accepted to participate in this jury. I would like to thank Professor Manuel RODRIGUEZ of Universidad de Los Andes and Professor Laurence LE COQ for having accepted to participate in this jury.

This work was done with the financial support of L'Agence de l'Environnement et de la Maîtrise de l'Energie (ADEME) and Region Pays de la Loire. I thank M. Simon THOUIN for taking part in the jury of this thesis in representation of ADEME. I am also very grateful to all the teams of the professors of the Department, secretaries (especially, Mme Dominique Briand), technicians (particularly, Mr Eric Chevrel), colleagues and friends. Finally, I would like to express my gratitude to my dear cousin Carolina Gutierrez and my family, whose support has been essential throughout my studies, especially during this work.

Scientific production

Scientific articles

Peña J., Villot A., Gérente C. Pyrolysis chars and physically activated carbons prepared from buckwheat husks for catalytic purification of syngas. Submitted to Biomass and Bioenergy Journal. September 2018 (Annexe 6).

Oral presentations

Peña J., Villot A., Gérente C. Valorization of millet and buckwheat husks chars and activated carbons in H_2S removal from biogas. 7th International conference on Engineering for Waste and Biomass Valorization – Prague, Czech Republic. 02 – 05 July 2018.

Peña J., Goh K., Villot A., Gérente C., Le Coq L. Biomass valorization by means of thermochemical conversion processes: pyrolysis and surface activation. 7th International Symposium on Carbon for Catalysis, Strasbourg, France, 12 – 16 June, 2016.

Posters

Peña J., Villot A., Gérente C. Buckwheat husk based materials as new catalyst in syngas upgrading. 7th International conference on Carbon for Energy Storage and Environmental Protection – Lyon, France. 23 – 26 October 2017.

Peña J., Villot A., Gérente C. Raw and activated char's selectivity in syngas upgrading application: Implementation in a fixed bed column. 16éme Congrès de la Société Français de Génie des Procédés (SFGP 2017) – Nancy, France. 11 – 13 July 2017.

M. Elsayed, Peña J., Villot A., Gérente C. Y. Andres. Energy potential from buckwheat husks through a thermochemical and biochemical approaches. 25th European Biomass Conference and Exhibition - Stockholm, Sweden. 12 – 15 June 2017.

Peña J., Villot A., Gérente C. Upgrading of pyrolysis chars in syngas purification: Characterization and implementation in a fixed bed column. 25th European Biomass Conference Exhibition - Stockholm, Sweden. 12 – 15 June 2017.

Acronyms

AC: Activated carbon

AD: Anaerobic digestion

AEE: Apparent energy efficiency

AEE_{elec}: Apparent energy efficiency which takes into account the electrical consumption

AAEM: Alkali and Alkaline Earth Metals

AS: Amine scrubbing

BH: Buckwheat Husk

BH-Char: Pyrolysis char from buckwheat husk

BH-CO_2: Activated char prepared from CO_2 activation of buckwheat husk

BH-H_2O: Activated char prepared from steam activation of buckwheat husk

CHP: Combined Heat and Power

D_p: Pore diameter

EB: Ethylbenzene

EBC: European Biochar Certificate

ESP: Electrostatic Precipitator

FAO: Food and agriculture Organization of United Nations

GC: Gas Chromatography

HHV: Higher Heating Value

HPWS: High Pressure Water Scrubbing

IEA: International Environment Agency

ISS: Inorganic Solvent Scrubbing

IUPAC: International Union of Pure and Applied Chemistry

LHV: Lower Heating Value

MH: Millet Husk

MH-Char: Pyrolysis char from millet husk

MH-CO_2: Activated char prepared from CO_2 activation of millet husk

MH-H_2O: Activated char prepared from steam activation of millet husk

MT: Mine tailings

NER: Net Energy Ratio

OPS: Organic Physical Scrubbing

PAH: Poly-aromatic Hydrocarbons

PSA: Pressure Swing Adsorption

RH: Relative Humidity

SEM: Scanning Electron Microscopy

SOFC: Solid Oxide Fuel Cells

TGA: Thermo-gravimetric Analysis

VOC: Volatile Organic Compounds

List of contents

List of tables

List of figures

General introduction

Context of the study

Currently, the world is consuming 99.3 million barrels per day of oil and the demand is expected to increase to 116 million barrels a day by 2030 according to the International Energy Agency [1]. It is agreed that it is necessary to reduce the oil-dependence and to mitigate climate change, thus other alternatives of energy production must be considered. It is well known that a single energy supply method is not sufficient thus combined solutions are required. In that sense, biomass is one of the suitable alternatives to replace fossil fuels since is a carbon-rich material available worldwide. Different thermo-chemical conversion processes are available to convert biomass into energy such as pyrolysis and gasification. Pyrolysis is the thermal decomposition of organic matter in the absence of oxygen that allows obtaining three phases: a combustible gas phase, a liquid phase (oil) and a solid phase (char). Gasification is the process of transforming the solid char and the liquid phase produced by pyrolysis into synthesis gas (syngas) in presence of an oxidizing agent (air, oxygen, steam, carbon dioxide) added in appropriate proportion. Lastly, pyro-gasification is a pyrolysis step followed by a gasification step and the so-called "gasification" processes are actually pyro-gasification processes in practice, except if they directly gasify coal. Usually in pyro-gasification processes a char phase remains as well.

Pyro-gasification is a key process to deal with several major issues worldwide [2]: i) contribute to the future energy supply at an affordable and stable price, ii) deal with the waste generation and pollution, and iii) reduce greenhouse gas emissions. The advantages of pyro-gasification are multiple. It is able to treat wastes that are not directly burned in existing facilities. Most pyro-gasification equipments are able to treat solid wastes with less than 20 % of humidity [3] and some gasifiers can also accept slurry feeds [4]. In addition, this technology is very flexible in terms of the feedstock used (biomass, waste, coal), energy recovery (electricity or biofuel) and capacity (from few kW to several tens MW). Therefore, this diversity is an advantage since it is possible to adapt to the specificities of different local contexts which can contribute to the decentralized energy production. This process is more compact compared to conventional incinerator or boilers, thus this flexibility allows to better fit at local scale. Consequently, this technology is going to grow in the near future as indicated by the Global Syngas Technologies Council [5] which announces that the cumulative worldwide capacity of gasification plants is

expected to raise from 150,000 MWth in 2014 to 280,000 MWth in 2018. In addition, the research community is dedicating a lot of effort to the further development and optimization of this technology.

The expected growth of pyro-gasification implies a larger production of char which represents a potential limitation for the development of this process under the principles of circular economy. Currently, resources are taken to manufacture a product which is used and disposed away; this is better known as linear economy. In contrast, the approach of circular economy is to reduce, reuse and recycle. Therefore, fewer amounts of resources are needed, products are manufactured from used materials and after their use they are recycled. In a circular economy, the value of products, materials and resources is preserved in the economy for as long as possible and wastes are minimized. The action plan adopted by the European Commission on 2015 states that the transition to a circular economy requires action in the whole process chain from production to the end life of products involving the creation of markets for waste-derived materials [6]. In addition, the European commission will encourage best practices in the industrial sector and parameters such as durability, upgradability, recyclability will be systematically examined. Consequently, in a circular economy the use of resources involving reuse or various recycling steps should be promoted. For instance, materials from biomass should be reused or recycled several times [7].

According to the report No. 6/2017 of the European Environment Agency, in the circular economy scenario, reuse, redistribution and refurbishment of products have received less attention thus there are no mature strategies in that direction. Most efforts are dedicated to improving the material and energy efficiency, however the inner circles or circular economy such as reuse and recycle have been given less importance. This is a key approach since it limits the waste generation and increases the economy independence of extraction and import of resources. In addition, it has environmental and economic advantages and is recognized as the instrument that allows achieving sustainable growth and development. Therefore closing the loop of products life-cycles by means of reusing and recycling is beneficial for the environment and the economy [8].

Nowadays, chars from pyro-gasification processes are considered residues and don't have further use, besides the most common application is their implementation as soil conditioners. In Europe, Switzerland is the first country that has officially authorized this use in order to close material cycles [9]. In this regard, the European Biochar Certificate

[10] states that char must present carbon content higher than 50 % dry, molar H/C ratio of 0.1 – 0.7 and O/C molar ratio of 0.4. Not all chars can meet these requirements, in particular those with elevated ash content. Besides, there is not a clear trend regarding the impacts of char in soil. For example, some authors have found that the composition of the feedstock and the temperature of pyrolysis determine the phytotoxicity of chars [11]. Moreover, char application rates and frequency remain poorly understood [12]. However, other studies have highlighted the benefits of applying chars in soil such as mitigation of global warming by carbon sequestration and improving soil quality in terms of fertility, pH, soil cation exchange [13].

In line with circular economy, the biorefinery concept should be adopted in order to integrate different technologies and be able to reuse or recycle materials as long as possible. Biorefinery is defined as the sustainable processing of biomass into a spectrum of marketable products and energy according to the IEA Bioenergy Task 42 [14]. In that sense, combined technologies make possible to use the residue from the first process as an input for the second. As happens in an oil refinery, in a biorefinery the raw material is continuously upgraded and refined leading to a cascade of several process [15]. Raw materials for a biorefinery are provided from agriculture, forestry, industries and aquaculture. The products from a biorefinery are material and energy products, the first ones provide energy while the second ones are used for their chemical or physical properties. The most important energy products are gaseous biofuels (biogas, syngas, hydrogen), solid and liquid biofuels. In conclusion, the approach of biorefinery increases the value of biomass as material an energy resource.

In this project, the principles of circular economy are coupled with the biorefinery concept in order to valorize chars prepared from biomass by thermo-chemical conversion process according to Figure 1-1. Two biomasses are selected and submitted to pyrolysis and physical activation which is assimilated as a pyro-gasification process. In the biorefinery scenario, the raw and activated chars are integrated with other processes such as the syngas and biogas treatment. Then the exhausted chars should be recycled as precursors for gasification or as additives for building materials.

To do so, two wastes from agriculture were selected: buckwheat and millet husks. These wastes have been barely studied in the literature and they can contribute to the development of a circular economy without compromising other well-known alternative valorizations. According to FAO (2016), the total world production of buckwheat is 2.800

million tons with a distribution between Europe (510,299 tons), Asia (2,130,344 tons), America (138,113 tons) and Africa (21,325 tons). On the other hand, millet world production is 30,353 million tons concentrated in Asia (16,141 million tons), Africa (13,552 million tons), Europe (332,199 tons), America (291,993 ton) and Australia (36,038 tons). The production of buckwheat and millet grains has experienced an increase of 27 % and 38 % respectively from 2010 to 2016. This increase is explained by the increasing interest in food science given that it contributes to vegan or gluten-free diets.

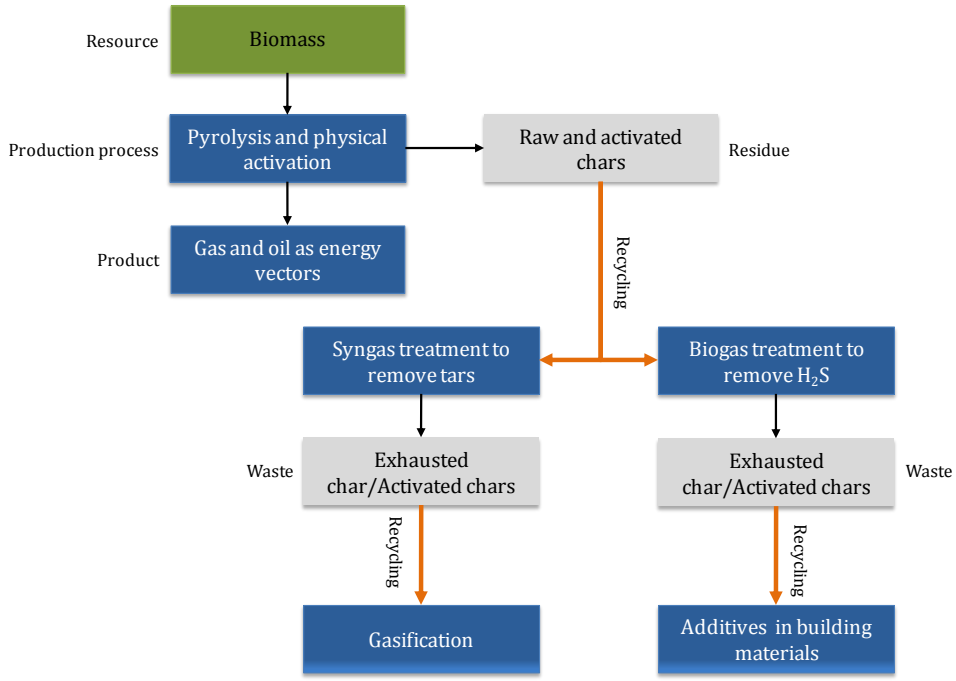

Figure 1-1. Schema of the study according to principles of circular economy.

Objective

The objective of this work is to study the possibility of integrating different technologies through the implementation of chars from pyro-gasification in syngas and biogas treatment. In that sense, it is necessary to relate their physical and chemical properties to their efficiency in both applications. This work aims to contribute to the transition to a circular economy by recovering the solid residue of pyro-gasification and using it in other applications. Due to the nature of the initial waste (buckwheat and millet husks) and the different activation methods, resulting materials have very different chemical compositions and physical structures. This variety makes it possible to study the influence of the physical and chemical properties of materials on their purification efficiency. The characterization of materials is carried out in order to obtain a detailed description of their properties (organic composition, mineral species and textural properties). The

experiments of syngas and biogas treatment are focused on two main pollutants: tars in syngas and H_2S in biogas. Lastly, the exhausted materials must be reuse or recycle in order to avoid waste generation as determined by the principles of circular economy.

This manuscript aims to describe the methodology to achieve the objectives presented above, and to present the main results obtained during these three years of research. This document is composed of five chapters:

Chapter 1 consists of a literature review of the main subjects addressed in this thesis. The purpose of this chapter is to provide a detailed description of chars, methods of production and activation as well as the different alternatives of valorization, with a particular attention paid to their implementation in the syngas and biogas.

Chapter 2 presents the materials and methods used for production and activation of the chars, the characterization of their chemical and textural properties as well as their implementation in syngas and biogas cleaning tests (tar cracking and H_2S adsorption).

Chapter 3 is dedicated to the preparation and characterization of raw and activated chars. First, the chemical compositions of the materials are exposed. This first step distinguishes two families of materials according to the biomass used. The impact of pyrolysis, CO_2 activation and steam activation on the chemical and textural properties is presented. In addition, the mass and energy balances for each process are calculated and different indicators of energy efficiency are proposed.

Chapter 4 presents the purification efficiency of materials in the tar cracking of ethylbenzene. The impact of gas composition is analyzed, and the performance of the materials is compared and related to their physical and chemical properties. The characterization of exhausted samples makes it possible to identify the deactivation mechanism and the nature of the active sites for the cracking reactions of tars. An exploratory study of the life end of exhausted samples is assessed.

Chapter 5 summarizes the main results obtained from hydrogen sulfide removal at room temperature by adsorption on materials. The adsorption capacity of samples is compared and interpreted according to their chemical and textural properties. The impact of the composition of the gas on the H_2S adsorption is studied and the involved reaction

mechanisms are then discussed. Finally, the ultimate use of samples containing sulfur compounds is proposed.

Chapter 1. Literature review

Introduction

With the aim of integrating different technologies through the recycling of chars from pyro-gasification, multiple topics must be addressed. This first chapter aims to provide the essential information for the understanding of this thesis. The literature review comprises the characteristics of a collection of biomass with different nature which involves organic composition and mineral species that can be found in agricultural wastes. In addition, the different types of pyrolysis are introduced as well as the activation methods that improve the properties of chars from pyrolysis. In the same way, the influence of the oxidizing agent in the activation stage is assessed. Different paths of char valorization are presented paying particular attention to the implementation of syngas and biogas treatment. Accordingly, the composition of syngas and its various pollutants are introduced, and the treatment technologies are presented. Finally, the biogas composition including its several contaminants is described. Likewise, the existing technologies for cleaning biogas are exposed.

1.1. Biomass wastes as char precursor

Biomass is organic matter coming from vegetation and animals and is considered a renewable source of energy. Therefore, biomass is a carbon-rich material found around the world that can potentially contribute to the replacement of fossil fuels. There are several types of biomass such as plant crops, wood, algae and municipal residues. According to the European Commission the biomass is defined as the biodegradable fraction of products, waste and residues from biological origin from agriculture (including vegetal and animal substances), forestry and related industries including fisheries and aquaculture, as well as the biodegradable fraction of industrial and municipal waste (DIRECTIVE 2009/28/EC OF THE EUROPEAN PARLIAMENT AND OF THE COUNCIL of 23 April 2009 on the promotion of the use of energy from renewable sources and amending and subsequently repealing Directives 2001/77/EC and 2003/30/EC).

This work is focused on biomass wastes from plant crops thus; well-known biomasses such as coal or sewage sludge from water treatment plants are excluded. In general, most wastes including biomass residues are disposed in landfills or incinerated. However, biomass wastes are sources of energy that can be recovered through several conversion processes. Conversion

technologies are flexible including thermo-chemical processes such as combustion, pyrolysis and gasification whereas biological technologies comprise anaerobic digestion. Availability of biomass wastes from plant crops in France are presented in Table 1-1.

Table 1-1. Crop production in France in 2014 (FAOSTAT).

Crop	Production (tons)	Crop	Production (tons)
Pulses, nes	6 000	Broad beans, horse beans, dry	278 645
Beans, dry	7 500	Sorghum	397 936
Poppy seed	8 000	Oats	443 528
Mustard seed	14 000	Peas, dry	512 094
Lupins	15 020	Pulses	842 259
Oilseeds nes	18 891	Sunflower seed	1 559 100
Lentils	23 000	Maize	1 854 180
Linseed	23 319	Triticale	2 022 500
Olives	23 700	Oilcrops Primary	2 820 272
Millet	40 000	Rapeseed	5 522 980
Hempseed	57 162	Potatoes	8 054 500
Rice, paddy	83 400	Roots and Tubers	8 054 500
Cereals, nes	111 250	Barley	11 770 680
Buckwheat	111 300	Coarse Grain	17 101 227
Rye	128 153	Sugar beet	37 630 688
Grain	221 700	Wheat	38 966 600
Soybeans	227 262	Cereals	56 151 227

Usually, husks and straws remain as wastes after plant crops are processed. Nevertheless, it is important to consider that some of these wastes have already alternative uses and therefore their availability is limited. For example, sunflower and soybean husk are used for animal feeding; oat hulls and oat mill feed are mostly valuable for ruminant and rabbit feeding due to their high fiber content; while rye and barley husks are used for composting.

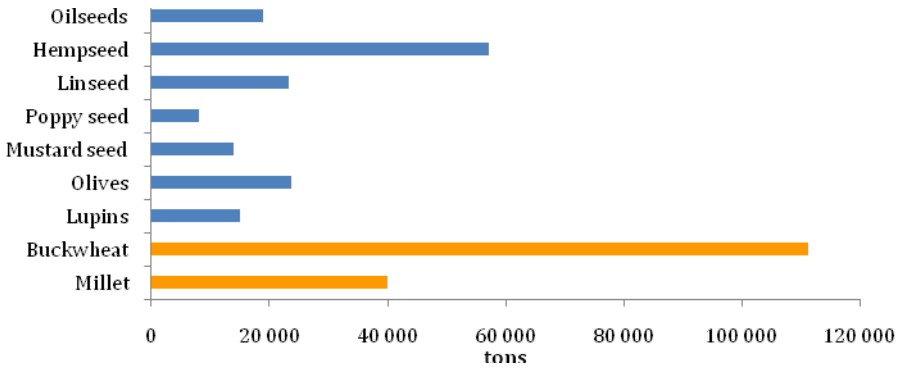

Figure 1-1. Crop production in France 2014 (potential waste candidates for char production). (FAOSTAT)

On the other hand, some of these wastes such as rice husk or hull and corn cobs have been deeply studied in pyrolysis and char production from biomass. Considering these criteria, suitable materials for char preparation available in France reduce to wastes remaining from crop production represented in Figure 1-1. The information provided by the figure shows that wastes from buckwheat and millet crops are available in France and their production is higher compared to other residues.

Biomass composition is defined in terms of cellulose, hemicellulose, lignin and extractives content. A more detailed composition can be given in terms of C, H and O which provide, for most part, its heating value. In general, carbon and oxygen contents of biomass vary in the 40 – 50 % range depending on the origin. However, there are some particular residues such as Cassava peel with higher C (59.3 %) and lower O (28.7 %), contrary to *Delorix regia* fruit pods with lower C (34.2 %) and higher O (58.9 %) [16]. Biomass also contains small quantities of N, S and Cl. The inorganic part of biomass is composed of Si, Al, Ti, Ca, Mg, Na, K, S, P and other minor elements that are important for its ash characterization. The content of biomass is usually lower than 8 %, nevertheless there are residues with elevated ash content like rice derivates (15 – 17%) [17].

Four references allowed synthesizing the biomass composition for a conglomerate of several agricultural wastes depicted in Table 1-2. The properties of these residues are presented in terms of proximate analysis (moisture, ash, volatiles, fixed carbon), elemental analysis (C, H, N, S, O), cellulose, hemicellulose and lignin contents, as well as higher heating value (HHV).

1.1.1. Moisture content

The moisture content of some agricultural wastes such as sugarcane bagasse, palm fiber and peat is higher than 20 % (Table 1-2), which requires that pyrolysis process is preceded by a drying stage (100–200 °C [18]) in order to eliminate most of the moisture [3]. This step allows less energy consumption during pyrolysis and also limits the water fraction in gas and liquid phases. Thus, it is important to consider this property in order to reduce the energy consumption of the process and maximize the potential value of by-products (gas and bio-oil). In addition, the water content of the bio-oil depends on the initial moisture content of the biomass and water formation during pyrolysis [19]. Therefore, biomass residues with moisture content lower than 20% are preferred in order to minimize the energy demand of the whole process.

1.1.2. Cellulose, hemicellulose and lignin content

Biomass chemical composition influences pyrolysis process due to different chemical pathways for cellulose, hemicelluloses and lignin fragmentation [20]. Usually, cellulose is the most abundant component in biomass, accounting for approximately 10 to 45 % as indicated in Table 1-2. In addition, a number of other polysaccharides called hemicelluloses are present in biomass, in the range of 15–35 %. Likewise, lignin is another macromolecular component in biomass, accounting for about 10–30 % weight of the material. Lignocellulosic biomass is also composed by extractives referring to the non-structural components that can be extracted by solvents (e.g., water, ethanol, acetone, benzene and toluene), such as fatty acids, simple sugars, waxes and sterols which account for 0–15 % of the feedstock [19]. According to other authors, cellulose and hemicelluloses determine the amount of carbon oxides produced (CO and CO_2) in the gas from pyrolysis, they also contribute to the bio-oil yield, while lignin increases the average molecular weight and viscosity of the bio-oils [19,21]. In addition, lignin favors the char yield thus biomass with high lignin content (> 15%) is preferred to produce chars or activated carbons considering that the higher percentage of fixed carbon is related to higher percentages of lignin [22].

1.1.3. Inorganic composition

Lignocellulosic biomass is known for having inorganic elements such as potassium, magnesium and calcium which are essential nutrients for growth. Major elements present in biomass ash are: Na, K, Ca, Mg, Fe, P, Al and Si [23,24]. Some authors report the inorganic composition as element percentage (Table 1-3) or oxide percentages (Table 1-4) in ashes. The highest contents in ashes, expressed as element or oxides are the Si, K and Ca and in a lesser extent Na and Mg. For example, some biomass ashes are extremely rich in Si: rice and its byproducts contain 90 % of Si, the millet husks have 85 % of Si (or 73 % expressed as SiO_2), the bagasse with 61 % of Si and the coconut shells, the palm husks with respectively 69 and 63 % of SiO_2. Others are particularly rich in potassium such as the corn cob (43 % as K), the coir pith (39 %), the coconut shell (34 %), the cotton husk (50 % as K_2O) and the coffee byproducts (between 37-44 %). Regarding the calcium, the ash from mustard husks exhibit 43 % of CaO and the peat is close to 32 %. The ashes from groundnut shell show respectively 25 % of Ca or CaO. The ashes from subabul wood are the highest concentrated in Ca with 68 %. The ashes from coconut shells are rich in Na (20-22 %) or Na_2O (4.8 %) as well as the soya husks with 5 % of Na_2O. The magnesium seems particularly present in the ashes from bagasse (22 % of Mg) and from buckwheat husks (17 %), the phosphorus from sunflower husks and pepper waste (9-10% of

P_2O), the iron from subabul wood (7 % of Fe) and groundnut shells (10 % of Fe_2O_3), the aluminium from sunflower husks (15 % of Al_2O_3) and finally the sulfur from mustard husks (14% of sufur as sulphate). According to the provided information, it can be noticed that millet and buckwheat husks have very different inorganic composition.

Some of these elements have demonstrated catalytic effect on the characteristics of pyrolysis products. As others have highlighted, Mg increases the solid content and the presence of high molecular weight compounds in bio-oil which results in higher viscosity [25]. In the same way, Ca decreases the gas yield, decreases the aromatic fraction and acidic compounds and increases polycyclic aromatic hydrocarbons (PAHs) [26]. Other authors have evidenced that release of alkali and alkaline earth metallic (AAEM) species depends on several aspects such as biomass properties, inorganic composition, heating rate and temperature of pyrolysis [27,28]. It seems that pyrolysis at a slow heating rate (10 °C/min) results in minimal (often < 20 %) transformation of AAEM species.

Table 1-2. Main characteristics of agricultural wastes.

Agricultural waste	Proximate analysis (wt. %)				Ultimate analysis (wt. %)					Cellulose (wt. %)	Hemicellulose (wt. %)	Lignin (wt. %)	HHV (MJ/Kg)	Ref
	Moisture	Ash	Volatiles	Fixed carbon	C	H	N	S	O					
Almond shell	10.0	0.6	80.3	9.1	50.5	6.6	0.2	0.0	42.7	32.5	25.5	24.8	-	[16]
Almond tree pruning	10.6	1.2	72.2	16.0	51.3	6.5	0.8	0.0	41.4	33.7	20.1	25.0	-	
Bagasse	-	6.2	83.3	-	41.6	5.6	0.0	-	52.9	-	-	-	-	
Bamboo	2.4	6.5	69.6	21.4	45.5	4.6	0.2	-	-	-	-	-	-	
Banana empty fruit bunch	5.2	15.7	78.8	0.2	41.8	5.1	1.2	0.2	51.7	8.3	21.2	19.1	-	
Birch	4.4	0.2	-	-	48.4	5.6	0.2	-	45.8	-	-	-	-	
Cassava peel	11.4	0.3	59.4	28.9	59.3	9.8	2.1	0.1	28.7	-	-	-	-	
Cocoa pod husk	-	-	-	-	-	-	-	-	-	42.9	35.3	1.0	-	
Coconut shell	8.2	0.1	73.1	18.6	48.6	6.5	0.1	0.1	44.6	19.8	68.7	30.1	-	
Corn cob	4.3	0.9	78.7	16.1	46.8	6.0	0.9	-	46.3	-	-	-	-	
Delorix regia fruit pods	0.2	2.8	92.0	5.0	34.2	4.5	1.9	0.4	58.9	13.9	24.1	23.4	-	
Durian shell	11.3	4.8	-	-	39.3	5.9	1.0	0.1	53.7	-	-	-	-	
Grape stalk	15.7	10.2	51.1	23.1	46.1	5.7	0.4	0.0	36.6	-	-	-	-	
Kola nut pod	-	-	-	-	-	-	-	-	-	38.7	40.4	21.3	-	
Olive stone	10.4	1.4	74.4	13.8	44.8	6.0	0.1	0.0	49.1	30.8	17.1	32.6	-	
Palm shell	8.0	1.1	72.5	18.5	50.0	6.9	1.9	0.0	41.0	29.0	47.7	53.4	-	
Palm stem	6.1	4.0	72.5	17.5	45.6	5.9	0.8	-	47.7	-	-	-	-	
Pomegranate seed	5.4	1.8	78.7	14.1	49.7	7.5	4.0	0.7	38.1	27.0	25.5	39.7	-	
Rice husk	-	16.7	65.7	-	36.5	4.8	0.9	-	41.1	-	-	-	-	
Rice stalk	14.2	14.9	66.3	4.6	40.8	7.7	1.2	0.5	49.9	-	-	-	-	
Salix	7.3	0.8	-	-	48.8	6.2	1.0	-	43.4	-	-	-	-	
Wallnut shell	11.0	1.3	71.8	15.9	45.1	6.0	0.3	0.0	48.6	40.1	20.7	18.2	-	
Wheat straw	3.3	3.2	-	-	46.5	6.3	0.9	-	46.3	-	-	-	-	
Woody birch	6.6	0.2	81.2	12.0	48.4	5.6	0.2	-	45.8	-	-	-	-	
Akhrot shell	8.8	1.2	80.0	18.8	49.8	5.6	0.4	-	42.9	-	-	-	20.0	[17]
Bamboo wood	11.5	2.0	86.8	11.2	48.8	6.3	0.2	-	42.8	-	-	-	20.5	

Agricultural waste	Proximate analysis (wt. %)				Ultimate analysis (wt. %)					Cellulose (wt. %)	Hemicellulose (wt. %)	Lignin (wt. %)	HHV (MJ/Kg)	Ref
	Moisture	Ash	Volatiles	Fixed carbon	C	H	N	S	O					
Block wood	12.2	2.1	83.3	14.6	46.9	6.1	1.0	-	44.0	-	-	-	18.3	
Casurina wood	12.7	1.8	78.6	19.6	48.5	6.2	0.3	-	43.1	-	-	-	18.8	
Coconut coir pith	19.8	5.2	66.0	28.8	43.4	5.0	1.6	-	44.9	-	-	-	18.1	
Coconut shell	8.3	0.7	77.2	22.1	50.2	5.7	0.0	-	43.4	-	-	-	20.5	
Cotton gin waste	5.0	1.6	83.4	15.0	42.7	6.1	0.2	-	49.5	-	-	-	17.5	
Eucalyptus wood	16.4	3.4	75.4	21.3	46.0	5.8	0.3	-	44.5	-	-	-	18.6	
Groudnut shell	8.1	5.7	72.7	21.6	48.6	5.6	0.6	-	39.5	-	-	-	19.8	
Jawar straw	7.5	8.9	76.0	15.2	42.1	5.6	0.0	-	43.4	-	-	-	18.0	
Jujuba wood	12.5	2.3	83.6	14.1	47.6	6.1	0.2	-	43.8	-	-	-	19.8	
Mango wood	14.1	3.0	85.6	11.4	46.2	6.1	0.3	-	44.4	-	-	-	19.2	
Millet grain waste	5.2	8.4	77.1	14.5	40.6	5.2	0.4	-	45.4	-	-	-	15.2	
Millet straw	5.1	5.3	78.3	16.5	43.7	5.9	0.0	-	45.2	-	-	-	18.0	
Neem wood	12.3	1.9	85.9	12.2	48.3	6.3	0.1	-	43.5	-	-	-	20.3	
Ply wood	13.8	2.1	82.1	15.8	48.1	5.9	1.5	-	42.5	-	-	-	19.0	
Rice husk	8.5	21.2	61.8	17.0	38.5	5.2	0.5	-	34.6	-	-	-	14.7	
Rice husk bran	8.5	18.6	61.8	19.5	38.9	5.1	0.6	-	36.8	-	-	-	15.3	
Rice straw	8.1	20.4	65.7	13.9	35.7	4.6	0.3	-	39.0	-	-	-	14.9	
Subabul wood - dry	7.6	1.2	81.0	18.5	48.2	5.9	0.0	-	44.8	-	-	-	19.8	
Sugarcane bagasse	51.0	3.2	83.7	13.2	45.5	6.0	0.2	-	45.2	-	-	-	18.7	
Wheat straw	8.9	6.9	82.1	11.0	43.0	5.4	0.0	-	44.8	-	-	-	18.0	
Bagasse	-	2.9	84.2	-	43.8	5.8	0.4	-	47.1	41.3	22.6	18.3	16.3	
Coconut coir	-	0.9	82.8	-	47.6	5.7	0.2	-	45.6	47.7	25.9	17.8	14.7	
Coconut shell	-	0.7	80.2	-	50.2	5.7	0.0	-	43.4	36.3	25.1	28.7	20.5	
Coir pit	-	7.1	73.3	-	44.0	4.7	0.7	-	43.4	28.6	15.3	31.2	18.1	[24]
Corn cob	-	2.8	85.4	-	47.6	5.0	0.0	-	44.6	40.3	28.7	16.6	15.7	
Corn stalks	-	6.8	80.1	-	41.9	5.3	0.0	-	46.0	42.7	23.6	17.5	16.5	
Cotton gin waste	-	5.4	88.0	-	42.7	6.0	0.1	-	49.5	77.8	16.0	0.0	17.5	

Agricultural waste	Proximate analysis (wt. %)				Ultimate analysis (wt. %)					Cellulose (wt. %)	Hemicellulose (wt. %)	Lignin (wt. %)	HHV (MJ/Kg)	Ref
	Moisture	Ash	Volatiles	Fixed carbon	C	H	N	S	O					
Groundnut shell	-	5.9	83.0	-	48.3	5.7	0.8	-	39.4	35.7	18.7	30.2	18.7	
Millet husk	-	18.1	80.7	-	42.7	6.0	0.1	-	33.0	33.3	26.9	14.0	17.5	
Rice husk	-	23.5	81.6	-	38.9	5.1	0.6	-	32.0	31.3	24.3	14.3	15.3	
Rice straw	-	19.8	80.2	-	36.9	5.0	0.4	-	37.9	37.0	22.7	13.6	16.8	
Subabul wood	-	0.9	85.6	-	48.2	5.9	0.0	-	45.1	39.8	24.0	24.7	19.8	
Wheat straw	-	11.2	83.9	-	47.5	5.4	0.1	-	35.8	30.5	28.9	16.4	18.0	
Sunflower husk	9.1	1.9	69.1	19.9	51.4	5.0	0.6	0.0	43.0	-	-	-	-	
Cotton husk	6.9	3.2	73.0	16.9	50.4	8.4	1.4	0.0	39.8	-	-	-	-	
Mustard husk	5.6	3.9	68.6	22.0	46.1	9.2	0.4	0.2	44.7	-	-	-	-	
Palm fiber	36.4	5.3	46.3	12.0	51.5	6.6	1.5	0.3	40.1	-	-	-	-	
Pepper waste	9.7	7.4	58.4	24.4	45.7	3.2	3.4	0.6	47.0	-	-	-	-	
Soya husk	6.3	5.1	69.6	19.0	45.4	6.7	0.9	0.1	46.9	-	-	-	-	[29]
Groundnut shell	7.9	3.1	68.1	20.9	50.9	7.5	1.2	0.0	40.4	-	-	-	-	
Coconut shell	4.4	3.1	70.5	22.0	51.2	5.6	0.0	0.1	43.1	-	-	-	-	
Coffee (mbuni) husk	11.4	4.1	64.6	20.0	43.9	4.8	1.6	0.1	49.6	-	-	-	-	
Coffee (parchment) husk	10.2	0.9	72.0	17.0	46.8	4.9	0.6	0.6	47.1	-	-	-	-	
Peat	37.0	4.3	41.0	17.7	57.1	5.9	2.3	0.8	43.1	-	-	-	-	

The information that is not available in the consulted references is represented by the "– "symbol.

Table 1-3. Ash composition of agricultural wastes: mineral elements.

Agricultural wastes	Ash composition of biomass: major elements (wt. %)								Ash composition of biomass: trace elements (wt. %)							Ref
	Al	Ca	Fe	Mg	Na	K	P	Si	Co	Cr	Cu	Mn	Ni	S	Zn	
Bagasse	-	5.34	0.44	22.03	0.33	9.44	1.00	61.01	-	-	0.06	0.03	0.06	0.21	0.06	[24]
Coconut coir	-	5.55	2.18	6.19	20.45	28.37	0.55	34.79	0.01	0.02	0.79	0.05	0.02	0.74	0.29	
Coconut shell	1.28	26.33	2.02	6.82	21.81	34.47	1.65	4.49	0.01	0.01	0.09	0.02	0.23	0.61	0.16	
Coir pith	2.48	4.69	1.26	12.16	15.87	39.47	1.76	19.60	0.00	0.00	1.86	0.04	0.03	0.71	0.06	
Corn cob	-	0.84	0.11	7.78	0.65	43.04	2.05	45.30	-	-	-	0.09	0.03	0.07	0.05	
Corn stalks	5.35	13.11	1.45	16.58	18.09	0.09	5.95	37.50	0.02	0.03	0.09	0.03	0.04	1.58	0.09	
Cotton gin waste	-	11.80	2.36	15.55	4.10	22.40	2.32	41.05	-	0.02	-	0.12	0.03	0.18	0.07	
Groundnut shell	7.13	25.40	2.14	6.95	0.91	34.64	0.54	21.46	0.00	-	0.02	0.09	0.02	0.59	0.10	
Millet husk	-	3.55	0.58	6.32	0.81	2.19	0.72	85.56	-	-	-	0.02	0.03	0.18	0.05	
Rice husk	-	0.76	0.23	0.68	0.06	3.84	0.14	93.62	-	-	0.01	0.05	0.01	0.07	0.53	
Rice straw	-	2.41	0.10	3.18	2.58	2.73	0.38	88.22	-	-	-	0.23	0.02	0.11	0.02	
Subabul wood	-	67.54	6.88	13.12	1.03	6.88	1.12	2.19	-	-	0.01	0.02	0.01	0.74	0.45	
Wheat straw	2.53	7.91	0.14	4.47	8.11	29.86	0.22	45.87	-	-	0.01	0.03	0.03	0.81	0.02	

The information that is not available in the consulted references is represented by the "– "symbol.

Table 1-4. Ash composition of agricultural wastes: Oxides.

Agricultural waste	Ash composition of biomass wastes: oxides (%wt)														Ref
	SiO_2	Fe_2O_3	TiO_2	P_2O_5	Al_2O_3	CaO	MgO	SO_3	Na_2O	K_2O	ZnO	CuO	MnO	Na_2O	
Sunflower husk	17.8	6.4	0.2	9.4	14.5	14.6	8.5	6.8	0.1	21.1	-	-	-	-	[29]
Cotton husk	10.8	1.9	0.0	4.0	1.3	20.7	7.5	1.7	1.3	49.6	-	-	-	-	
Coffee husk	3.8	0.2	0.2	4.1	7.5	9.2	ù	0.4	0.6	43.8	-	-	-	-	
Mustard husk	16.9	0.8	0.1	2.0	1.5	42.8	9.2	14.3	2.0	7.4	-	-	-	-	
Palm husk	63.2	3.9	0.2	2.8	4.5	-	3.8	2.8	0.8	9.0	-	-	-	-	
Pepper waste	13.2	2.9	0.1	9.6	7.2	8.6	3.9	9.1	0.9	30.3	-	-	-	-	
Soya husk	1.7	2.5	0.2	4.9	7.4	21.4	7.1	3.7	5.3	30.5	-	-	-	-	
Groundnut shell	27.7	10.3	0.1	3.7	8.3	24.8	5.4	10.4	0.8	8.5	-	-	-	-	
Coconut shell	69.3	6.4	0.0	1.6	8.8	2.5	1.6	0.0	4.8	8.8	-	-	-	-	
Coffee (mbuni) husk	13.5	2.2	-	3.7	3.9	10.7	4.0	-	0.4	38.1	-	-	-	-	
Coffee (parchment) husk	16.6	2.4	-	3.4	4.5	9.8	3.7	-	0.5	36.9	-	-	-	-	
Peat	24.6	8.2	-	5.4	8.1	31.7	1.2	-	0.4	0.6	-	-	-	-	
Millet Husk	73.1	4.2	-	1.6	0.0	10.5	0.0	1.4	-	7.5	-	-	0.4	-	[30]
Buckwheat Husk	4.0	0.4	-	-	0.3	1.0	16.7	-	-	22.0	0.1	trace	0.3	0.3	[31]

The information that is not available in the consulted references is represented by the "– "symbol.

1.2. Char production by thermo-chemical reactions

Char is a solid material formed by the thermo-chemical decomposition of biomass. Chars can be obtained by means of thermo-chemical reactions through several processes such as pyrolysis, gasification and hydrothermal carbonization which are presented below.

1.2.1. Pyrolysis

Pyrolysis is the thermal decomposition of organic matter under inert atmosphere that leads to a solid residue called char, moisture and volatiles of biomass are driven off leading to the formation of liquids (condensable vapors) and gases (non-condensable vapors). More precisely, this decomposition releases most of the non-carbon elements particularly hydrogen, oxygen and nitrogen in the form of gases and tars [16]. The operation also creates rudimentary porosity limited to macropores [32].

Depending on the process conditions, pyrolysis can be divided into six categories, which are shown in Table 1-5.

Table 1-5. Types of pyrolysis [19,33,34]**.**

Type of pyrolysis	Operating condition	Reactor types	Liquid (%wt)	Gas (%wt)	Solid (%wt)
Flash pyrolysis	Rapid heating (<0.5s), very small particle sizes (<0.5 mm), temperature (400 - 1000 °C).	Fixed bed reactor, Tubular reactor, Bubbling fluidized bed reactor, Circulating fluidized bed reactor, Ablative pyrolyzer, Rotating cones reactor, Auger reactor, Cyclone reactor.	60 - 70	10 -15	15 - 25
Fast pyrolysis	Atmospheric pressure, small particle size (< 3mm), short residence time (0.5 - 2s), moderate temperature (400 - 550 °C) in absence of oxygen.		65 - 75	13 - 25	12 -19
Slow pyrolysis	Low heating rate, moderate temperature (350 - 750 °C), atmospheric pressure, long residence time (5 – 30 min) in absence of oxygen.		30 - 50	15 - 30	30 - 60
Intermediate pyrolysis	Moderate temperature (< 500 °C), moderate vapor residence time (4 - 10s) and atmospheric pressure.		45 - 55	25 - 35	15 - 25
Vacuum pyrolysis	Moderate temperature (300 - 500 °C), pressure below atmospheric (< 50KPa).		45 - 60	17 - 27	19 - 27
Ablative pyrolysis	Moderate temperature (450 - 600 °C), atmospheric pressure, particle size < 3.5 mm.		60 - 80	6 - 10	12 -20

It can be noticed that each type of pyrolysis results in different phase yields. Usually, when the product of interest is the liquid phase fast pyrolysis is used under moderate temperature and very short vapor residence time conditions (0.5-2 s). On the contrary, char is the main product of

slow pyrolysis at a slow heating rate (5 – 20 °C/min) [35], longer vapor residence time (5-30 min), and moderate temperature (350-750 °C). At industrial scales, large retorts (batch or continuous), agitated drum kilns, rotary kilns and screw pyrolyzers are used to carry out this process [34].

Operating conditions such as temperature and heating rate influence pyrolysis products. Based on literature, rapid heating and cooling of primary vapor favor high liquid yield, in contrast slow heating leads to a higher char formation considering that secondary pyrolysis reactions are reduced [36,37]. In the same way, higher temperatures result into lower char but higher gas and bio-oil yield because of the stripping of more volatile matter from the char and the increase of secondary cracking reactions of the gas phase [34,38–41]. Temperature not only influences char yield but also the resulting properties of pyrolysis products.

According to Park et al., [39] the lighter fraction of bio-oil composed mostly of water increases with temperature. Likewise, the fraction of H_2 and CH_4 in the gas phase gradually increases above 400 °C, thus pyrolysis gas at higher temperatures (600 – 700 °C) present higher percentage of H_2 and CH_4 leading to a superior energetic value of the gas. In fact, in this study the HHV of the gas phase was increased from 4.1 MJ/Kg at 300 °C to 11.5 MJ/Kg at 700 °C. As the yield of pyrolysis products varied with temperature, the energy distribution also did. At 300 °C the energy was distributed as follows: 65 % in the char, 35 % in bio-oil and 3 % in the gas. When temperature was raised to 700 °C, 40 % of energy was contained in the char, 40 % in bio-oil and 28 % in the gas.

1.2.2. Gasification

Gasification is the partial oxidation that transforms organic materials to gaseous products using oxidizing agents (air, oxygen, steam, carbon dioxide). The pyro-gasification is a pyrolysis step followed by a gasification stage and the so-called "gasification" processes are actually pyro-gasification processes in practice, except if they directly gasify char. The desirable product from pyro-gasification process is the gas phase (H_2, CO, CO_2, N_2), however a liquid phase (tars and oil) and a solid phase (char) are also produced. Usually, the yield of char in gasification is lower than pyrolysis (5 – 10 %) [42]. There are different types of gasifiers such as fixed/moving bed, fluidized bed and entrained bed which properties are summarized in Table 1-6.

The fixed bed gasifier also known as moving bed can operate in counter current (updraft) or co-current flow (downdraft) [43,44] while in the entrained bed biomass and gasifying agent are in suspended flow mode. The fixed-bed gasifier presents the largest residence times (15 – 30 min)

and the temperature of the outlet gas is in the 400 – 500 °C range. This technology is inexpensive and achieves high carbon conversion however the updraft reactor leads to high tar production while the downdraft requires feed with low ash content limiting its scale up potential.

Table 1-6. Properties of different types of gasifiers [43,45].

Gasifier description	Advantages	Disadvantages
Fixed/Moving bed	**Fixed/Moving bed, updraft**	
Updraft: Gasifying agent is injected at the bottom and fuel is injected at the top Downdraft: gasifying and fuel are injected at the top Required particle size 2 - 50 mm Gas exit temperature 400 - 500 °C Pressure 0.15 - 2.45 Mpa Residence time 15 - 30 min	Simple, inexpensive process Operates satisfactorily under pressure High carbon conversion efficiency Low dust levels in gas High thermal efficiency	Large tar production Potential channeling Potential bridging, small feed size Potential clinkering
	Fixed/Moving bed, downdraft	
	Simple process Only traces of tar in product gas	Minimum feed size Limited ash content allowable in feed Limits to scale up capacity Potential for bridging and clinkering
Fluidised bed		
Fuel and gasifying agent are injected at the bottom or sides Required average particle size is 8 mm Operation temperature 900 - 1050 °C Residence time 10 – 100 s	Flexible feed rate and composition High ash fuels acceptable Able to pressurize High CH_4 in product gas High volumetric capacity Easy temperature control	Operating temperature limited by ash clinkering High product gas temperature High tar and fines content in gas Possibility of high C content in fly ash
	Circulating fluidised bed	
	Flexible process Up to 850 °C operating temperature	Corrosion and attrition problems Poor operational control using biomass
	Double fluidised bed	
	Oxygen not required High CH_4 due to low bed temperature Temperature limit in the oxidizer	More tar due to lower bed temperature Difficult to operate under pressure
Entrained bed		
Fuel concurrently react with gasifying agent in suspended (i.e. entrained) flow mode Require pulverized feedstock, particle size < 1 mm Operation temperature may exceed 1500 °C Residence time is in the order of 1 s Pressure 2.94 – 3.43 MPa	Very low in tar and CO_2 Flexible to feedstock (accepts both solid and liquid fuels)	Low in CH_4 Extreme feedstock size reduction required Complex operational control Carbon loss with ash Ash slagging Raw syngas requires significant cooling before being cleaned.

The fluidized bed gasifier operates in the 900 – 1050 °C temperature range with shorter residence times of 10 – 100 s. This technology is able to deal with feedstock with varied composition and high ash content. It can be operated at variable loads (high volume capacity) and the temperature is easily controlled. However, this reactor leads to high tar and particles content and remaining carbon from the feedstock. The entrained bed gasifier requires extreme small solid biomass, but it accept liquid fuels. It operates at very high temperatures and short residence times. This technology presents disadvantages such as the carbon loss with ash, ash slagging and the gas product requires significant cooling.

Therefore, the selection of the type of gasifier depends on the type of feedstock (solid, liquid, size and composition), the characteristics of the product gas and the operating limitations related to temperature, pressure and load capacity.

1.2.3. Hydrothermal conversion

Pyrolysis and gasification required limited moisture (<20 %) in the feedstock in order to increase the energy efficiency and fuel conversion. There are several biomass resources that have high moisture content that imposes a drying stage previous to the process to avoid comprising its performance. Hydrothermal conversion is able to overcome this limitation and deals with biomass mixed with water in a close reactor at high pressure. This technology allows the conversion of non-traditional biomass such as: wet animal manures, human waste, sewage sludge, municipal waste, aquaculture and algal residues [46]. Hydrothermal conversion is a cost effective pre-treatment and its advantages are: i) does not require any chemicals, ii) limited equipment corrosion problems, (iii) simple and economical operation [47].

The hydrothermal conversion can be described as follows: at temperature close to 100 °C, the water-soluble portion of the biomass becomes liquid, and above 150 °C hydrolysis takes place. In the meantime, cellulose and hemicellulose, decompose into their monomeric chains. At approximately 200 °C and 1 MPa, solid biomass turns slurry. Finally, at around 300 °C and 10 MPa, liquefaction occurs and the oily product is obtained [48]. Therefore, operating conditions such as temperature and pressure determine the type of hydrothermal conversion of biomass and the distribution of products. Hydrothermal carbonization is carried out in the 180 – 250 °C range of temperature; it operates at pressures up to 20 bar and the processing time varies from 1 to 12 hours.

Hydrothermal process can be classified in three types: carbonization, liquefaction and gasification. In hydrothermal carbonization the main phase is the solid (50 – 80 %) better known as hydrochar, a liquid phase in less proportion (5 – 20 %) and a gas phase (2 – 5 %) [46]. The hydrothermal liquefaction is carried out at temperatures varying between 250 - 400 °C and the desirable product of this process is the oil (40 – 60 %) [49]. Lastly, when hydrothermal conversion is carried out at temperatures above 400 °C it is call hydrothermal gasification whose main product is the gas phase composed of CO, CO_2, CH_4 and H_2[42].

1.3. Energy vectors from pyrolysis

In a context of energy transition and use of renewable energy, by-products of pyrolysis i.e char, bio-oil and gas can be considered as energetic vectors depending on their features. Therefore, information regarding their characteristics and energetic value is provided in this section.

1.3.1. Bio-oil

Bio-oil is a complex mixture of carbon, hydrogen, oxygen, organic acids, esters, alcohols, ketones, phenols, aldehydes, alkenes, furfurals, sugars and some inorganic species [40] coming from the condensed vapor fraction of pyrolysis. This liquid is a dark-brown free flowing fluid at room temperature. It consists of two phases: a lighter aqueous phase of low molecular weight and a non-aqueous phase of heavier molecules. The heavier fraction is mainly composed of aromatics and is a suitable substitute for fuel, thus it can be used in engines and turbines for power generation [19,33,35]. Because of its inconsistent nature, thermal instability and corrosive properties, it must undergo several upgrading steps to be refined to meet the requirements proposed in the ASTM D7544 -09 standard for bio-oils intended for industrial burners (Table 1-7).

Table 1-7. Chemical and physical requirements of bio-oil produced from pyrolysis of biomass [50]**.**

Bio-oil property	Unit	ASTM D7544-09
Higher Heating Value	MJ/kg	15 min
Bio-oil's solid content	wt. %	2.5 max
Water content	wt. %	30 max
Acidity	pH	Report
Kinematic viscosity	cSt (40 °C)	125 max
Density	kg/dm^3 (20 °C)	1.1 - 1.3
Sulfur content	wt. %	0.05 max
Ash content	wt. %	0.25 max

The methods to improve bio-oil quality can be classified in physical and chemical methods summarized in Table 1-8. The purpose of this treatment stage is to enhance stability, reduce viscosity and to remove particles contents of bio-oil. As far as the lighter part is concerned, it consists mostly of chemicals such as acetic acid and hydroxyacetone, which emits VOCs.

Table 1-8. Methods to upgrade bio-oil from pyrolysis of biomass [51]**.**

Physical methods	Chemical methods
Emulsion	**Catalytic hydrogenation**
Separates the polar compounds in order to be able to mix bio-oil with diesel	Oxygen in the form H_2O or CO_2 is removed from bio-oil in order to improve homogeneity, reduce polarity and improve heating value (HHV). Disadvantages: catalyst deactivation and cost of H_2
Filtration	**Fluidised catalytic cracking**
Removes alkali metals, solid particles and char which decrease storage stability and cause problems in applications	Bio-oil macromolecules are cracked into smaller molecules using catalyst
Solvent addition	**Catalytic esterification**
Organic solvents (usually alcohols) are used to reduce viscosity of bio-oil and improve its stability	Removes most of the acids reducing corrosiveness of bio-oil and increases its stability. Disadvantages: large amount of carbon residue leading to rapid deactivation of catalyst
Distillation	**Steam reforming**
Bio-oil is divided into quasi gasoline, diesel and aviation kerosene through distillation	It uses heat and steam to produce hydrogen under the action of catalyst

The composition of pyrolysis condensate varies with pyrolysis type, biomass and operating conditions. The presence of aldehydes and ketones in the oily phase make this product hydrophilic, therefore it is difficult to dehydrate. The elemental composition of bio-oil can vary as follows: C (55 – 64 %), H (5 – 8 %), N (0.05 – 1.0 %) and O (27 – 40 %) [52]. The higher heating value (HHV) of the bio-oils varies from 16 and 35 MJ/kg [53] while that of the fossil fuels HHV varies in the range 42 – 45 MJ/kg. Properties of this phase are presented elsewhere [21,53] which exhibits a comparative frame between this potential energy vector and other fuels. Some of these properties are discussed below:

a. Moisture content: water content in pyrolysis liquid varies in the range from 10 to 65 % weight [53,54]. Water in pyrolysis liquid is product of chemical reactions and directly from biomass humidity [19,40]. It is important to highlight that the heating value of the pyrolysis bio-oil increases with high lignin content of biomass. Water content increases with temperature, promoting decarboxylation and dehydration reactions. The use of bio-oil as fuel may be limited by the water content since it affects viscosity in a complex manner, modifies density, stability, pH and homogeneity. It also has been stated that in slow pyrolysis the water content of bio-oil is high [38,55].
b. Viscosity: pyrolysis liquid is highly viscous (25 – 1000 cSt) compare to fossil diesel fuel (3–8 cSt at 40 °C). Viscosity is reduced if pyrolysis liquid has less hydrophobic compounds. Its chemical composition can change in time (aging) leading to larger molecules as product of polymerization and condensation reactions [53].
c. pH: Bio-oil has low pH ranging from 2 to 4 due to the presence of carboxylic acids. Usually, char particles and ash can be also found in this phase, although ash content is usually very low [19,40,56].

1.3.2. Gas

Gas from pyrolysis can be used for the production of heat or electricity or can be returned to the pyrolysis unit as carrier gas [19,33,55]. Pyrolysis gases consist of condensable and non-condensable fractions. The non-condensable gases are CO_2, CO, H_2, CH_4 and N_2 (if N_2 is used as the carrier gas) in various proportions. Other light hydrocarbons such as ethane (C_2H_6), ethylene (C_2H_4), and small amounts of propane (C_3H_8), ammonia (NH_3), nitrogen oxides (NO_X), sulfur oxides (SO_X) and alcohols are also present [19,21]. Usually, condensable aromatic organics referred to tars are present in this phase too and can vary from 0.5 - 100 g/m^3 [57]. In addition the gas composition can vary with biomass type [53,55].

The HHV is an important fuel property which defines the energy content of a sample. The LHV is calculated from the HHV and is the amount of heat available from a fuel after the latent heat of vaporization. The HHV of pyrolysis gas can vary in a wide range depending on pyrolysis temperature according to literature. In the study of Gómez et al., [38] slow pyrolysis of different biomass wastes was carried out. They found that the lower heating value (LHV) of gas varied in the range of 1.8 – 15.3 MJ/m^3 in function of the biomass type and temperature (350 – 550 °C). The results of Park et al., [39] showed that the HHV is higher as operating temperature increases from 300 °C (4.1 MJ/kg) to 700 °C (11.4 MJ/kg). This is related to the increase in the production of H_2 from the cracking of hydrocarbons while CO and CO_2 fraction decrease at higher temperatures [21]. According to their study, the gas profile for pyrolysis at 600 °C was described as follows. Release of CO_2 and CO was dominant in the early stage of pyrolysis, resulting mainly from decomposition of cellulose and hemicellulose. Later, the CO_2 and CO concentration reduced rapidly above 400 °C, while H_2 and CH_4 gradually increased, mainly from the slow decomposition of lignin. A more detailed explanation [19] states that CO_2 and CO originate from the decomposition and reforming of carbonyl (C=O) and carboxyl (COO) groups. The CH_4 formation is attributed to the decomposition of weakly bonded methoxyl (-O-CH_3) and methylene (-CH_2-) groups in addition to the secondary decomposition of the oxygenated compounds. In the same way, the secondary decomposition and reforming of the aromatic C=C and C–H groups at high temperatures leads to formation of H_2.

1.3.3. Char

Char is the solid phase obtained from the thermo-chemical conversion of biomass in an oxidant-limited atmosphere. This charred material can represent between 15 to 30 wt. % of initial mass and have 25 % of its exploitable energy [58]. The LHV of chars is high varying from 25 to 32 MJ/kg (Table 1-9). This energy can be recovered as fuel through gasification process; therefore,

due to the high LHV of chars they can be used as feedstock of gasification in order to transform carbon to gaseous fuel. However, gasification of chars with high ash content can cause problems in the gasifier adding costs to the process and decreasing the life of the unit [45]. In the same way, the presence of some mineral elements like Si decreases the gas yield in char gasification and trap char particles above 870 °C [24,59].

1.4. Uses of chars

The valorization of pyrolysis chars depends on their features. Char properties such as elemental composition also called ultimate analysis (C, H, N, S, O), proximate analysis (fixed carbon, volatile matter and ash), the HHV, moisture content, the functional groups among others depend strongly on biomass characteristics and operation conditions. Chars can be valorized as materials, in fact, the combination of each biomass and pyrolysis parameters will lead to a char with certain properties that makes it suitable for a specific application. The elemental composition, proximate analysis, LHV and pH of chars from pyrolysis can vary as indicated in Table 1-9. The elemental composition fluctuates as follows: C (between 70 - 90 wt. %), H (0.7 - 5.2 wt. %), O (1.8 – 23 wt. %) and N (0.6 – 3.3 wt. %) and traces of sulfur can be found for different precursors and operating temperatures from 300 to 950 °C. Among remarkable values, the rice husks exhibit an extremely low concentration of carbon with 31 % and high content of oxygen (19 %). This is consistent with Table 1-2. The chars exhibiting oxygen contents higher than 15 % generally present a depletion of carbon (69 - 81 %) which is the case of almond shells (pyrolized at 350 °C), pine wood pellets (at 350 °C), olive-tree pruning (at 350 °C), rice straw (between 300 and 600°C) and switch grass (at 400 and 500 °C).

In the same way, the proximate composition of raw chars depends in a great extent of the feedstock: moisture (1 - 23 wt. %), fixed carbon (9 - 92 wt. %), volatile matter (6 - 87 wt. %) and ash content (3 - 55 wt. %). According to literature biomass with elevated lignin content is related to higher fixed carbon [41,60–62]. This is connected to the fact that lignin is resistant to thermal decomposition due to its complex structure [63] and thus the charred residue of pyrolysis is formed from the decomposition of lignin while cellulose and hemicellulose produce volatile products [34,36].

It can be observed in Table 1-9 that pH of chars varies depending on the composition of its precursor and the conditions of pyrolysis. Chars with high ash content such as rice derivates have basic pH due to the mineral species. It can also be observed that pH increases with temperature of pyrolysis and percentage of ash. HHV and LHV are generally ranged between 27

and 32 MJ/kg except for the rice byproducts. Lastly, it should be noticed that pyrolysis chars present poor porosity according to the BET surface area (5 – 85 m^2/g). This porosity corresponds to micropores (pore diameters under 2 nm) and mesopores (pore diameters ranged between 2 and 50 nm). The macroporosity (pore diameters above 50 nm) obtained from mercury porosimetry is rarely found. In the work of Brewer et al. [32], the chars from pyrolysis of dried grass and dried wood performed at temperature < 450 °C resulted in BET surface areas under 10 m^2/g and porosity increased in the 550 – 700 °C temperature range reaching higher porosity 100 – 400 m^2/g.

The potential uses of chars from pyrolysis are summarized in Table 1-10. Chars can be valorized in different applications such as: catalysts, soil quality improvement, fuel cells, sorbents, storage materials or precursors of activated carbons. In general, the advantages of implementing chars are the low cost of production, availability and sustainability; however, there are some disadvantages as well. For example, the efficiency of raw chars as catalyst can be low, besides the mineral content and PAHs can contaminate the soil and finally the variability of char properties. The valorization of chars depends on its properties thus the importance of their characterization. According to Qian et al., [13] chars with high electrical conductivity, porosity and stability at lower temperatures are chosen as electrodes in microbial fuel cells while chars with relatively high oxygen groups are preferred in direct carbon fuel cells.

The interest or limitations of using chars in different applications is explained as follows:

a. Catalyst for syngas cleaning: Chars can be used in syngas cleaning as a catalyst with no metals or as a catalyst support. The catalytic activity of char for tar cracking is associated to its porosity and mineral content [13]. However, potential problems include the degradation of surface properties and deactivation due to coking [64].
b. Soil amendment: char contains high concentrations of N, P, Ca, and K, which may provide soil with nutrients [13]. The char increases the pore fraction of soil. Nevertheless, a high degree of aromaticity is associated to strong resistance to chemical oxidation. For this reason, the degree of aromatic condensation of char should be considered in determining the persistence of char in the environment [64] and its potential impact in the long term. Switzerland is the first country in Europe which has officially authorized char use in agriculture introducing this application for closing material cycles [9]. Switzerland has based its regulation policies in the European Biochar Certificate (EBC) developed with the aim of ensuring sustainable biochar production and low hazard use in agriculture. This accreditation contains several criteria that should be met in order to use char in agriculture as well as a list of biomass feedstock approved for use in biochar preparation.

This inventory includes husks from agriculture as eligible precursor with a special requirement: that only waste not/no longer usable for human consumption or as animal feed should be used [65]. According to EBC, char must present carbon content > 50% dry, the molar H/C ratio of 0.1 – 0.7 and O/C molar ratio of 0.4.

c. Sorbent for contaminant reduction in soil and water: The poor porosity of chars may limit its implementation as a sorbent in removing contaminants since the adsorption capacity of a char will depend on surface area, pore structure, and the surface chemistry [13]. For example, the adsorption capacity of chars in liquid phase is influenced by the quantity of negative charges which are related to the mineral species from the raw biomass precursor. Furthermore, the adsorption performance depends on the operating conditions of the char preparation. The increase of temperature in pyrolysis results in an increase in carbon content and porosity but decreases the number of oxygen functional groups on the char surface [42].

d. Activated carbon: The two main steps that are required for the preparation of activated carbon from char which are pyrolysis followed by the chemical or physical activation of the char. Physical activation occurs at high temperature in the presence of oxidizing agents, such as carbon dioxide, steam or air. The advantage of physical activation is that it does not involve any chemicals whereas chemical activation uses chemicals as activating agent as will be explained in the next section. In the work of Benedetti et al., [66] the properties of six chars from different biomass gasification plants were studied. It was demonstrated that chars from gasification process have varied porosity up to 587m^2/g and composition (CHN and ash content) similar to that of activated carbons. The authors concluded that there is a great potential for char from biomass gasification to be used as activated carbon in adsorption applications.

Table 1-9. Main characteristics of chars from pyrolysis.

Precursor and T (°C) of pyrolysis	Moisture (wt. %)	Proximate analysis (wt. %) (dry basis)			Ultimate analysis (wt. %) (dry basis)					LHV (MJ/kg)	HHV (MJ/kg) (dry basis)	pH	A_{BET} (m^2/g)	Ref
		Fixed carbon	Volatile matter	Ash	C	H	O	N	S					
Casuria wood (950 °C)	23.2	71.5	15.2	13.2	77.5	0.9	5.6	2.7	-	-	27.1	-	-	[17]
Coconut shell (750 °C)	16.4	9.9	87.2	2.9	89.0	0.7	6.0	1.4	-	-	31.1	-	-	
Eucalyptus wood (950 °C)	21.0	19.2	70.3	10.5	76.1	1.3	11.1	1.0	-	-	27.6	-	-	
Red wood	-	72.0	23.9	4.1	78.8	3.5	13.2	0.2	-	-	30.5	-	-	
Rice husk (750 °C)	6.5	8.5	46.3	45.2	31.5	2.5	19.3	1.5	-	-	10.9	-	-	
Subabul wood (950 °C)	15.4	74.5	21.7	4.0	83.6	2.0	10.5	0.0	-	-	30.4	-	-	
Olive stone (350°C)	3.3	81.4	17.1	1.6	84.3	3.1	12.2	0.31	0.05	30.6	-	-	-	[38]
Olive stone (450°C)	2.9	86.6	11.7	1.6	87.9	2.6	9.1	0.4	0.05	31.9	-	-	-	
Olive stone (550°C)	3.3	91.7	6.4	1.9	90.8	1.6	7.1	0.4	0.05	32.1	-	-	-	
Almond shell (350°C)	3.7	66.0	31.9	2.2	76.4	3.9	19.3	0.3	0.05	27.7	-	-	-	
Almond shell (450°C)	4.0	83.4	14.4	2.2	86.6	2.8	10.1	0.4	0.05	30.0	-	-	-	
Almond shell (550°C)	3.9	88.0	8.9	3.1	90.4	2.1	7.1	0.4	0.05	31.7	-	-	-	
Pine wood pellets (350°C)	3.9	68.5	30.2	1.4	79.5	3.6	16.5	0.3	0.05	30.3	-	-	-	
Pine wood pellets (450°C)	3.6	79.2	19.1	1.7	85.2	2.8	11.6	0.4	0.05	30.6	-	-	-	
Pine wood pellets (550°C)	4.3	84.4	13.2	2.5	88.4	2.5	8.6	0.4	0.08	31.2	-	-	-	
Olive-tree pruning (350°C)	4.2	62.0	29.8	8.2	73.9	4.0	20.9	1.1	0.06	24.8	-	-	-	
Olive-tree pruning (450°C)	3.9	71.9	19.2	8.9	82.9	2.7	13.2	1.2	0.06	27.2	-	-	-	
Olive-tree pruning (550°C)	3.7	78.6	13.7	7.7	86.3	2.3	10.3	1.0	0.06	28.8	-	-	-	
Rice straw (300°C)	-	28.1	34.5	37.4	68.7	5.2	22.8	3.3	-	-	16.6	9	4.5	[39]
Rice straw (400°C)	-	35.4	18.8	45.9	75.5	4.6	16.9	3.0	-	-	15.3	10.1	21.2	
Rice straw (500°C)	-	38.7	10.6	50.7	81.4	2.3	15.1	1.1	-	-	13.5	10.5	45.8	
Rice straw (600°C)	-	39.9	6.9	53.2	87.5	2.1	7.5	2.9	-	-	13.9	10.6	84.8	
Rice straw (700°C)	-	39.5	5.9	54.6	91.2	1.3	7.0	0.6	-	-	13.6	10.6	22.5	
Switch grass (400 °C)	-	70.0	20.0	10.0	75.2	4.9	17.7	1.9	0.3		28.9	-	-	[40]
Switch grass (500 °C)	-	70.0	18.0	12.0	78.3	3.6	16.5	1.3	0.3		29	-	-	
Switch grass (600 °C)	-	80.0	8.0	14.0	82.0	2.4	14.1	1.2	0.3		29.4	-	-	
White ash (400 °C)	-	-	-	3.1	87.6	2.5	6.3	0.6	-	32.4	-	7.2	-	
White ash (500 °C)	-	-	-	3.8	90.2	1.5	4.1	0.5	-	33.5	-	7.9	-	
Switch grass (300 °C)	-	-	-	8.7	76.1	3.9	10.7	0.7	-	28.9	-	8.2	-	

Precursor and T (°C) of pyrolysis	Moisture (wt. %)	Proximate analysis (wt. %) (dry basis)			Ultimate analysis (wt. %) (dry basis)					LHV (MJ/kg)	HHV (MJ/kg) (dry basis)	pH	A_{BET} (m^2/g)	Ref
		Fixed carbon	Volatile matter	Ash	C	H	O	N	S					
Switch grass (400 °C)	-	-	-	10.3	80.8	3.0	5.3	0.6	-	30.2	-	8.4	-	
Switch grass (500 °C)	-	-	-	10.6	86.3	1.9	0.5	0.6	-	31.5	-	8.6	-	
Corn stover (300 °C)	-	-	-	11.7	69.9	4.0	13.4	0.9	-	28.0	-	7.3	-	
Corn stover (400 °C)	-	-	-	14.8	74.8	3.2	6.2	1.1	-	28.8	-	7.8	-	
Corn stover (500 °C)	-	-	-	15.1	78.1	2.1	3.8	0.9	-	30.5	-	8.1	-	
Red pepper stalk	2.52	66.14	22.4	9.3	86.6	2.4	8.3	2.6	0.0	-	-	12.2	32.5	[67]

Table 1-10. Applications of pyrolysis chars taken from [13]**.**

Application	Purpose	Advantage	Disadvantage
Catalyst	Syngas cleaning, biodiesel production, Fischer-Tropsh synthesis, Biogas treatment, Air pollution control	Easy to recycle supported metal, co-catalyst, low cost.	Relative low efficiency and low abrasive resistance compared with commercial catalyst
Soil amendment	Carbon sequestration, soil quality improvement	Low cost, sustainable resource, retain water and nutrient, reduce fertilizer consumption, reduce greenhouse gas emission and nutrient losses	Possible heavy metal and polyaromatic hydrocarbons (PAHs) contaminant
Fuel cell	Fuel for fuel cell, Electrode of Supercapacitors	Renewable fuel compared with coal	High ash content, relative low voltage and power output
Sorbent of contaminant	Adsorption of organic contaminants and heavy metals present in soil and water.	Low cost, abundant and sustainable resource, and oxygenated groups on char surface facilitate adsorption	Effectiveness of organic/inorganic contaminants remediation is still uncertain, and persistence of heavy metals
Storage material	CO_2 sequestration, H_2 storage	Low cost, abundant and sustainable resource, high recyclability	Require surface treatment
Activated carbon	Precursor for making activated carbon	Low cost, abundant and sustainable resource	Properties vary with different precursors, may not produce desired granular or spherical activated carbon

1.5. Improvement of char properties by activation

As result from pyrolysis process, porosity in the char is created to some extent (4.5 – 84 m^2/g) [32]. Char can be upgraded by means of activation of its surface. The purpose of activation is basically to develop porosity in the solid [16] and to create some ordering of the structure [68]. Therefore, the final product has well-developed and accessible internal structure. Activation stage can be carried out through physical or chemical agents that develop surface porosity in the char and create functional groups with different properties. In both methods the precursor reacts with the activating agent to create porosity; however they differ not only in the practical procedure, but also in the mechanism by which the activating agent promotes porosity [69]. In the next pages, both methods will be described, however deeper focus will be addressed to physical activation which corresponds to the purpose of this study.

1.5.1. Chemical activation

When direct chemical activation is carried out, the precursor is impregnated with a chemical agent such as KOH, H_3PO_4 and K_2CO_3 and then dried. After that, the sample is activated under inert atmosphere and temperature. Thus, usually carbonization and activation are carried out simultaneously. Finally, the sample is submitted to a washing stage with distilled water or HCl solution until reaching neutral pH of the washed liquor.

Simultaneous activation and carbonization of impregnated biomass was compared to carbonization (500 °C, 2h) followed by activation of impregnated char (500 – 900°C, 1.5 – 4h) [70]. The activated carbon obtained from direct impregnation of KOH onto pistachio-nut shells was in the powder form making it difficult to separate from the volatile matter. Therefore, it is preferred to carry out a two-step chemical activation (pyrolysis followed by activation of KOH-impregnated char) in order to obtain a granular activated carbon. It has been stated that chemical activation with KOH usually results in powdered carbons from different biomass precursors which include rubber wood, sawdust, coconut husk, bamboo, rice husk and apricot shell [71,72], however a powdered carbon can cause problems in gas applications which is the intended used in this study, therefore granular activated carbons are preferred.

1.5.1.1. Oxidizing agents in chemical activation

In chemical activation dehydrating agents and oxidants are employed in order to create porosity in the surface of the sample. Among used chemical agents the most common are KOH and H_3PO_4. The potassium hydroxide is reported to be more appropriate for coal based precursors whereas phosphoric acid is widely known to be a suitable impregnating agent for lignocellulosic materials [71].

1.5.1.2. Influence of chemical activation agents on porosity development

Moreno et al. [73] studied and compared KOH and H_3PO_4 activation methods using olive-mill waste water as precursor material. They found that phosphoric acid activation follows two paths: i) H_3PO_4 behaves as an acidic catalyst promoting bond cleavage reactions and formation of cross-links; ii) it also reacts with organic species to form phosphate linkages, such as phosphate and polyphosphate esters, that connect and cross-link biopolymer fragments. On the other hand, the oxygen in KOH eliminates and avoids cross-linking and as a result it stabilizes the carbon atoms in crystallites. In addition other authors have explained that the release of carbon atoms by activation reaction and removal of potassium salts during the washing step generates micropores in the sample [74].

The activation temperature is different for the chemical agents: phosphoric acid usually reacts at temperatures below 450 °C and KOH acts at temperatures above 700 °C. In terms of porosity [72], it has been stated that phosphoric acid and potassium hydroxide enhance pore development, initially centered in the micropore region. At higher loadings of KOH and H_3PO_4 the pore size distribution becomes more heterogeneous. KOH only produces widening of the microporosity to more heterogeneous micropores, whereas H_3PO_4 develops large mesopores and even macropores. Non-uniform porosity created by phosphoric acid is explained considering the mixture of molecules from H_3PO_4 to $H_{13}P_{11}O_{34}$ at the maximum temperature of treatment regardless mass ratio of the chemical agent.

In the work of Fierro et al., [75] activated carbons were prepared by chemical activation using phosphoric acid. Parameters like effect of impregnation ratio (acid/lignin = 0.7 – 1.75), carbonization temperature (400–650 °C) and impregnation times were studied. The optimum temperature for porosity development in lignin-derived ACs was found to be 600 °C. Authors suggested that low impregnation ratios promote creation of micropores whereas acid/lignin ratios equal to or higher than 1.0 slightly influence the pore size distribution. Increasing the impregnation times reduced the BET surface area and total pore volume due to the damage of

the polymeric structure. Finally, it was stated that further increase of activation temperature and impregnation ratio leads to widening of pore size distribution with a higher relative contribution of mesoporosity.

Hayashi et al., [61] investigated the influence of carbonization at different temperatures (500 – 900 °C) on the surface area and pore volume of ACs prepared with H_3PO_4 and KOH. They pointed out that maximum surface areas were obtained at carbonization temperature of 600 °C for H_3PO_4 activation (1000 m^2/g); whereas a higher temperature of 800 °C was necessary in the KOH activation to reach the maximum surface area (1500 m^2/g). The pore volumes of ACs increased with temperature over the range of 500 – 600 °C, and then decreased at higher values for materials activated with H_3PO_4. It was suggested that above 600 °C, the carbon structure shrinks resulting in the decrease of surface area and pore volume.

1.5.1.3. Influence of chemical activation agents on functional groups

The use of different chemical agents influences the surface chemistry of activated carbons. Activated carbons prepared by H_3PO_4 and KOH activation were characterized in terms of surface chemistry by Guo and Lua [76]. Phenols, carboxylic acids (or carboxylic anhydrides) and carbonyl groups which are typical acidic functional groups were present on the H_3PO_4 impregnated sample. In contrast, the main surface functional groups existing on the KOH-impregnated carbon were presumed to be alkaline groups of pyrones (cyclic ketone), other keto-derivatives of pyran and alkaline chromenes groups. Furthermore, other authors have obtained ACs with acidic surface from KOH and H_3PO_4 activation with surface pH of 2.5 and 6.5 respectively [73].

1.5.1.4. Influence of chemical activation agents on mineral content

A remarkable difference between KOH and H_3PO_4 is their influence in ash content of activated materials [73]. The activation with H_3PO_4 results in ACs with higher ash content than ACs from KOH activation. The high mineral fraction resulting from H_3PO_4 activation is explained considering that: i) organic constituent of the raw material can combine with phosphoric acid giving insoluble phosphates which are then trapped inside the carbon matrix, and ii) phosphate and polyphosphate species are incorporated to the carbon matrix, through C-O-P bonds, connecting and cross-linking different organic species. On the contrary, KOH activated carbon reduces the ash content as demonstrated elsewhere [77]. This was highlighted in the work of Moreno et al., [73] who showed that the activation of olive-mill waste water with either KOH (800 °C) or H_3PO_4 (500 °C) resulted in 0.4 and 12.6 % of ash content respectively.

In conclusion, the chemical activation method results in a well-developed porous structure with high BET surface area however; it seems that potassium hydroxide is more effective than phosphoric acid to develop porosity. The temperature influences development of porosity in the materials until reaching a maximum which depends on the chemical agent used. The optimum activation temperature varies in a wide range; in fact H_3PO_4 reacts at lower temperature (400 – 500 °C) than KOH (700 – 800 °C) does. KOH and H_3PO_4 are the most common chemicals employed in this activation method. Usually, porosity is concentrated in the micropore region without appreciable contribution of mesopores. Likewise, increasing impregnation ratios promote creation of pores whereas higher chemical/sample ratios slightly influence the pore size distribution. Potassium hydroxide activation is mainly directed towards the preparation of powdered activated carbons which is not suitable for the gas treatment applications by fixed beds whereas phosphoric acid results in granular ACs. In addition, mineral content is affected depending on the chemical employed; it can be pronouncedly reduced (using KOH) or increased (using H_3PO_4) due to different reaction mechanisms. In general, chemical method results in activated carbons with functional groups of acid character.

1.5.2. Physical activation

In physical activation, usually the raw material is first carbonized and then activated by steam, carbon dioxide, air or their mixture as oxidizing agents. Usually, the physical activation is preceded by the carbonization or pyrolysis of the precursor followed by the activation stage. During pyrolysis, the moisture and volatile matter are removed from the raw material. Then, in the activation phase the porosity of the carbonized material is created. Usually, temperature of physical activation ranges between 600 and 900 °C [68,78–81]. The influence of steam and CO_2 in the properties of activated carbons is explained below. The physical activation and pyro-gasification process are similar considering that both comprise a carbonization (pyrolysis) step followed by an oxidation stage carried out with steam, CO_2 or air as mentioned before. In fact, the characteristics of chars from pyro-gasification are very similar to those of activated carbons prepared by physical activation as demonstrated by Ahmad et al., [82]. Therefore, physical activation can be considered as a partial gasification since the difference between both process relays in the conversion degree of char. Hence, this segment considers relevant references from gasification in order to explain the influence of certain parameters.

1.5.2.1. Influence of oxidizing agents on porosity development

The mechanism of porosity development in steam activation increases the pore depth but also the pore diameter. Therefore, steam activation creates microporosity meso- and macroporosity

[83]. Other authors state that carbon dioxide creates mainly micropores while the steam activation results in a higher degree of mesoporosity [70].

Ruiz-Fernández et al. [83] have underlined different conclusions about the mechanism of porosity development. First, it is important to consider that CO_2 molecule is linear (O=C=O; C=O bond length, 116.3 pm), while the steam molecule is angular (O–H bond length, 95.84 pm; angle, 104.5° as shown in Figure 1-2).

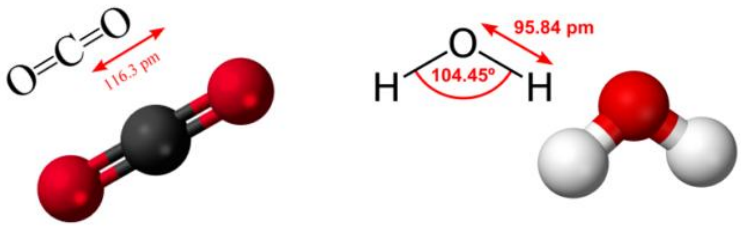

a) **b)**

Figure 1-2. a) Carbon dioxide molecule and b) Water molecule.

Moreover, the critical molecular dimension is smaller for steam than for CO_2 resulting in easier diffusion and reaction rate with steam than with CO_2. Therefore, the larger dimension of the CO_2 molecule results in restricted accessibility towards micropores. However, it is important to keep in mind that linear orientations parallel to the surface are more favorable as the wall separation in slit-shaped pores decreases and the CO_2 molecule can diffuse in narrower micropores than the steam molecule. Lastly, the molar mass of the oxidizing agents varies as follows: $CO_2 > H_2O$ and, according to Graham's law, their diffusion rate in pores is inversely proportional to their molar weight.

In the investigation carried out by Yang et al., [84] the influence of steam and carbon dioxide (CO_2) on the porosity of activated carbons was studied. Walnut shells were carbonized at 500 °C and then activated at 900 °C with either CO_2 (1000 mL/min) or steam (M_{H2O}:M_C = 1:2) for 2.0 hours. The results showed that the samples prepared by steam activation had higher surface area (771 m^2/g) and pore volume (V_{total} = 0.499 cm^3/g) than those by CO_2 activation (552 m^2/g and 0.293 cm^3/g respectively). In addition, the CO_2 activated sample was mainly microporous (78 %) while the steam activated carbon had more mesopores (68%). These results were in agreement with those from Guizani et al., [85]. They studied the gasification of chars with steam and CO_2 to different conversion degrees. Their findings suggested that for an equivalent conversion level i.e. 50 %, H_2O-chars presented higher surface area (1225 m^2/g) and pore

volume than CO_2-chars (842 m^2/g). Furthermore beyond 50 % of conversion, a widening of the porosity or mesopore development was noticed for H_2O gasification.

1.5.2.2. Influence of oxidizing agents on functional groups

It is well known that raw chars and activated carbons have surface functional groups which can influence the performance of these materials in certain applications. The presence and amount of these groups depend on the precursor, oxidizing agent and operating conditions of the carbonization and activation processes. In general, it seems that chemical agents create acidic functional groups (acidic or neutral pH) [71,73,77] while physical activation produce carbons with alkaline pH as will be further discussed in this section. Some of the oxygen functional groups are presented in Figure 1-3.

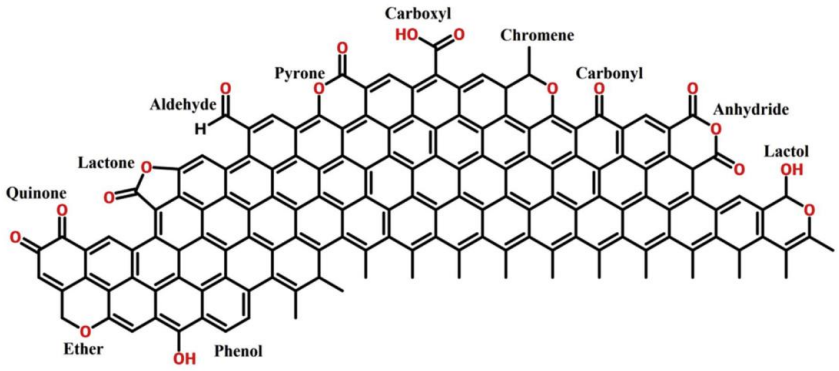

Figure 1-3. Schematic of oxygen functional groups on the surface of carbons, taken from [78].

Several authors have studied the surface functional groups of carbons activated with either steam or CO_2, however there is not a clear trend about the influence that these two oxidizing agents may have. According to literature, one explanation for this outcome is the operating temperature. As reported by some authors, surface functional groups are destroyed during the heat treatment. Usually, pyrolysis at low temperatures (≈500 °C) yields acidic chars, while higher pyrolysis temperatures (≈900 °C) generate basic chars [86,87]. This is in agreement with the results of You et al., [64] who highlighted that the high temperature in a gasifier decomposes functional groups such as hydroxyl, carboxyl, and carbonyl and the resulting material have less functional groups than the char produced from the previous pyrolysis. However, in many cases the alkaline pH of activated carbons is also explained by the high contents of alkali and alkaline earth metals in the form of carbonates [87,88].

The presence of the same functional groups on carbons resulting from H_2O or CO_2 gasification was found by Klinghoffer et al., [89]. In their study they characterized the functional groups via

temperature programmed desorption (TPD). This technique involves heating the char under inert atmosphere and each type of functional group desorbs at a specific temperature as either CO or CO_2. The TPD profiles of materials were somewhat different. The main distinction found was that the CO_2 activated sample showed a slightly higher release of CO_2 and CO at 750 °C and 1000 °C respectively. Their results led them to conclude that both activation methods (steam and CO_2) produce carbons with acidic and basic groups on the surface. In the same way, Guizani et al., [90] studied the differences in the surface chemistry of CO_2 and steam gasified chars. The TPD profiles of both samples were very similar. However, release of CO_2 in the range of 150 - 350 °C (carboxyles decomposition) and release of CO in the range of 700 – 900 °C (quinone decomposition) was higher for the char gasified under CO_2 at early stage of conversion (20 %).

Yang et al., [84] investigated the effect of steam and carbon dioxide activation methods on the physicochemical properties of AC. The functional groups were characterized via FTIR analysis. The FTIR spectra of samples were comparable with little differences. The CO_2 activated materials showed stronger intensity in the peak representing O-H groups while the steam activated samples presented higher intensity in the C-O groups. For the C=O functional groups, the same results were observed for the ACs prepared by the two activation methods. They concluded that a higher number of O–H (phenol, carboxyl and lactol) groups were produced during the CO_2 activation process, while steam activation favored the development of the C–O (ether, pyrone, chromene) groups on the surface of materials.

In conclusion several studies have tried to determine the influence of oxidizing agents in the surface functional groups; however, results are not conclusive since both activation methods are able to create both basic and acidic groups. According to these studies, there seems to be a trend and is that the CO_2 activation creates a slightly higher number of oxygen functional groups than the steam activation.

1.5.2.3. Influence of oxidizing agents on release of AAEMs

The transformation and release of AAEMs during activation depend on the precursor and upon how these elements are associated in the char, the ash composition, the temperature, atmosphere in the reactor and the heating rate of the process. The AAEMs can be organically and/or inorganically bonded on the carbonaceous material. The organically associated elements are mostly metal cations, which are bound to anionic groups of the organic matrix. The inorganically associated elements may exist as soluble salts and/or minerals. Some of the ash-forming elements are believed to be highly reactive during thermal conversion processes [91].

Release of K during activation

Different trends in the release of K during gasification with CO_2 or H_2O have been reported. For instance, Bai et al,. [92] found that the gasification of bituminous coal with either steam or CO_2 does not influence the release of K. However, Hai-Bo et al., [93] stated that the potassium release under CO_2 is similar to that under N_2 while Tchoffor et al., [91] concluded that the transformation of potassium under H_2O is higher than in N_2.

Different mechanisms explaining the release of K along activation have been proposed. First, K can be released as KCl since during gasification the char is less compact therefore there is less diffusional resistance to the evaporation of KCl [91]. In parallel, the char-bound K can be released or retained in the ash in function of the degree of char conversion and the concentration of Si in the char [91,93]. At the early stage of gasification (low conversion of char), the organic matrix prevents the formation of potassium silicates [94] and thus, the preservation of K in the ash is limited. Then at late stage of activation (high char conversion) when the organic matrix of the char is almost completely converted, the formation of K silicates is favored enhancing the retention of K. In this sense, more K is released from materials with low Si content during gasification.

Another mechanism for the transformation of K is the decomposition of K_2CO_3 at temperatures close to 900 °C explained by the following reactions [91], which means that in the steam gasification K is released as KOH through the decomposition of K_2CO_3.

$$K_2CO_3 \rightarrow CO_2 + K_2O \qquad \textbf{R 1-1}$$

$$K_2O \rightarrow 2K + \frac{1}{2}O_2 \qquad \textbf{R 1-2}$$

$$K_2O + H_2O \rightarrow 2KOH \qquad \textbf{R 1-3}$$

A general mechanism for the release of AAEMs which takes into account the element state is proposed elsewhere [95]. The existing state of an element (i.e. K and Ca) is not the same under different oxidizing agents. Free radicals can interact with the char matrix and participate in substitution reactions leading to the release of AAEMs according to the reaction: *R + Char-X → Char-R + X*, where *X* represents the AAEMs species and *R* denotes free radicals. More free radicals, such as H radical, would be formed in steam than in CO_2 activation. The free radicals break the Char-AAEM bonds resulting in the transformation of AAEMs. In addition to the

previous mechanism, the release of K is enhanced by a smaller particle size, fast heating rate and high temperature [94].

Release of Ca during activation

In general, authors have agreed that calcium follows different transformation mechanisms under H_2O or CO_2 [92,96,97]. Ca is found in the char as calcite ($CaCO_3$) when the char is submitted to gasification with CO_2. This indicates that CaO on the char adsorbed CO_2 to form $CaCO_3$ according to R 1-4. In addition, $CaCO_3$ presents a vast variability in the particle size with an irregular shape, indicating agglomeration and a poor dispersion on the surface of the material [92,96]. On the other hand, in steam activation the CaO of the char reacts with H_2O to form $Ca(OH)_2$ (R 1-4) though it may be an instantaneous reaction. Then, $Ca(OH)_2$ is decomposed into H_2O and CaO and this reaction takes place repeatedly in both directions decreasing the size of CaO allowing higher dispersion [96]. Therefore, steam seems to be a good oxidizing agent since it prevents the sintering behavior of Ca via the hydration reaction R 1-4. However, according to Bai et al., [92] the faster sintering of $CaCO_3$ can be also explained considering that the melting points of CaO and $CaCO_3$ are 1307 °C and 670 °C, respectively.

$$CaO + CO_2 \leftrightarrow CaCO_3 \qquad \textbf{R 1-4}$$

$$CaO + H_2O \leftrightarrow Ca(OH)_2 \qquad \textbf{R 1-5}$$

The reactions of calcium under CO_2 or steam depend on the temperature range and the partial pressure of these two gases as highlighted by Shuai et al., [98] and shown in Figure 1-4. This graphic is divided in three regions. First, at temperatures < 500 °C and partial pressure of steam between 0.1 and 1 atm, CaO reacts with H_2O to form $Ca(OH)_2$. The dashed blue line represents the pressure where the reaction R 1-5 takes place at equilibrium, thus same number of CaO and $Ca(OH)_2$ co-exist.

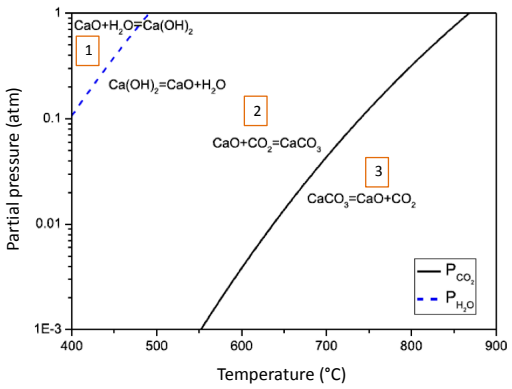

Figure 1-4. The equilibrium partial pressures of H_2O and CO_2 resulting from the decomposition of $Ca(OH)_2$ and $CaCO_3$ taken from [98].

In the second region, R 1-4 and reverse R 1-5 occur in a large range of temperature (400 – 850 °C) and partial pressure, thus calcium is in the forms CaO and $CaCO_3$ in different proportions. The black line separating region 1 from region 2 represents the equilibrium of reaction R 1-4, which indicates that the same content of CaO and $CaCO_3$ prevail.

Lastly, in the third region, from 550 to 900 °C and a wide partial pressure range, most of the $CaCO_3$ is decomposed in CaO and CO_2. In the same way as K, the release of Ca is higher at the early stage of gasification while at advanced char conversion the release is limited due to formation of silicate compounds [93].

In addition to K and Ca, other AAEMs follow transformation under CO_2 or steam gasification. Guizani et al., [85] studied the evolution of different AAEMs along the biomass gasification with CO_2 and H_2O. In this work the char was submitted to gasification until reaching different conversion degrees (0, 20, 50 and 70 %) and the content of AAEMs in the resulting char was analyzed. Their findings show that a much higher proportion of Si is released under CO_2 in comparison to steam gasification. On the other hand, at early stage of gasification Mg release seems to be the same for both oxidizing agents while at 70 % of char conversion, CO_2 gasification showed higher release of Mg. The oxidizing agent didn't show much influence in the transformation of Al, P, Mn, Fe and Zn.

The improvement of char properties by means of activation was assessed in this section. The principal advantages and disadvantages of the different activation processes are summarized in Figure 1-5.

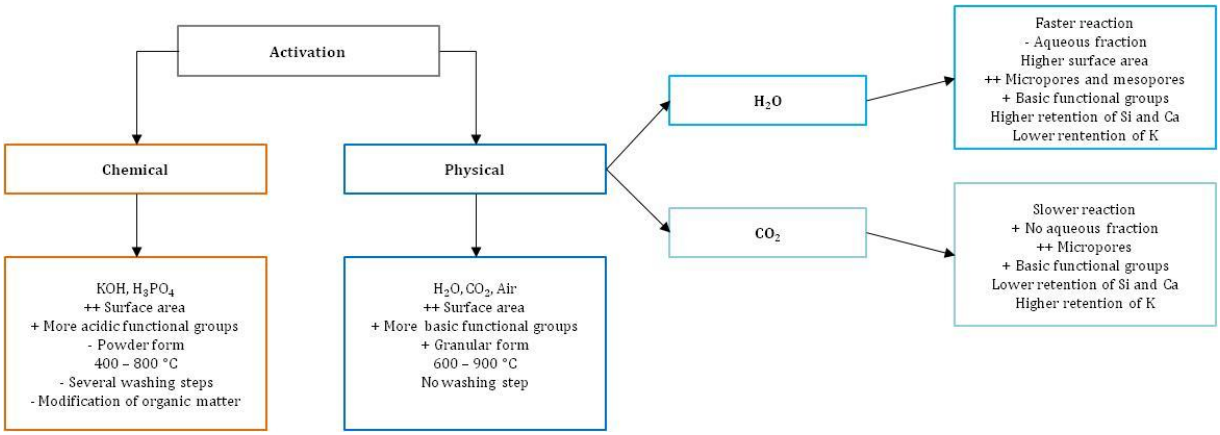

Figure 1-5. Advantages and disadvantages of chemical, physical, steam and CO_2 activation processes.

The chemical activation presents several disadvantages like, the obtained power AC, the several washing steps and modification of the inorganic content. It is important to mention that a powder AC is not suitable for gas-phase applications which is the intended use for the materials developed in this work. Therefore, in this study, physical activation is preferred since it allows the biomass conversion to be clean, straightforward avoiding additional stages with no alteration of the inorganic matter. The steam and CO_2 activations present different advantages mainly in terms of porosity development and retention of different AAEMs. These characteristics might improve or not the performance of the produced AC in certain applications.

1.6. Syngas

The gasification of biomass produces raw syngas which can be used in several applications [99]. The utilization of syngas varies from heat or power applications to a variety of synthetic fuels. The LHV of syngas is about 6 - 20 MJ/Nm^3 [100] thus it can be employed as fuel in different energy demanding processes. Syngas can be burned in traditional boilers or in more efficient energy conversion processes, such as gas turbines and engines. Syngas can also be used as fuel for electricity production by fuel cells. In addition, syngas serve as chemical precursor for the synthesis of chemicals and liquid fuels [45,101]. In fact, hydrogen production is the largest use of syngas. Hydrogen is mainly consumed for ammonia production, followed by refining and methanol production. Ammonia is the second largest synthetic chemical produced from syngas. Currently, the majority of methanol is synthesized from syngas. Methanol is also an important chemical intermediate used to produce a number of chemicals, including: formaldehyde, dimethyl ether, methyl tert-butyl ether, acetic acid, and olefins, to name a few. Finally, syngas is implemented in Fischer-Tropsch synthesis in order to produce diesel, gasoline, waxes and olefins [99,102].

1.6.1. Composition of syngas

Syngas is composed mainly of H_2, CO, CO_2, CH_4 and C_XH_Y [100,103] as presented in Table 1-11. In addition, syngas holds undesirable impurities composed of tars, nitrogen based compounds (NH_3, HCN, etc.), sulfur based compounds (H_2S, COS, etc.), hydrogen halides (HCl, HF, etc.), trace metals (Na, K, etc.) and particulate matter [57,104,105]. Tar is defined as all organic contaminants with a molecular weight larger than benzene thus tar overcomes a wide range of compounds including oxygenates, phenolic compounds and olefins, aromatic and polyaromatic hydrocarbons (PHA) [103,104,106]. Tar compounds can be classified into 5 categories as shown in Table 1-12. The class 1 refers to heavy tar that cannot be detected by the gas chromatography

(GC); class 2 are highly soluble water compounds; class 3 represents one-ring aromatics like ethylbenzene; class 4 and 5 are compounds that can condense at high temperature like naphthalene and pyrene.

Table 1-11. Composition of syngas from biomass gasification with steam [107]**.**

T (°C)	H_2 (%mol)	CO (%mol)	CO_2 (%mol)	CH_4 (%mol)	C_XH_Y (%mol)
700	28 ± 5	39 ± 5	14 ± 5	12 ± 3	3.5 ± 2
800	42 ± 5	30 ± 5	16 ± 8	8.5 ± 2	2.5 ± 2
900	45.5 ± 5	24.5 ± 5	19.5 ± 5	5.5 ± 3	1.5 ± 2

Table 1-12. Classification of tar components [57,103]**.**

Tar class	Class name	Property	Representative compounds
1	GC-undetectable	Very heavy tars, cannot be detected by GC. Can condensate at very high temperatures and low concentrations	Determined by subtracting the GC-detectable tar fraction from the total gravimetric tar
2	Heterocyclic	Tars containing hetero atoms; highly water-soluble compounds	Pyridine, phenol, cresols, quinoline, isoquinoline, dibenzophenol
3	Light aromatic (1 ring)	Usually light hydrocarbons with single ring	Toluene, ethylbenzene, xylenes, styrene
4	Light PAH compounds (2-3 rings)	2 and 3 rings compounds; can condense at relatively high concentrations and intermediate temperatures	Indene, naphthalene, methylnaphthalene, biphenyl, acenaphthalene, fluorene, phenanthrene, anthracene
5	Heavy PAH compounds (4-7 rings)	Larger than 3-ring, these components condense at high-temperatures at low concentrations	Fluoranthene, pyrene, chrysene, perylene, coronene

The composition of syngas is influenced by temperature of the oxidation process, type of gasifier, biomass composition and gasifying agent. It has been stated that syngas is richer in hydrogen at higher gasification temperatures while the content of other gases (CO, CH_4, C_XH_Y) decreases [107] as shown in Table 1-11. In addition, the gasifying agent have great influence in the syngas composition and its LHV (Table 1-13). According to these studies, using steam as oxidant agent enhances the H_2 content and LHV of syngas, however a large percentage of steam remains in the gas stream (11 – 61 %).

Tar concentration in syngas depends on the biomass, process conditions and type of gasifier. In general lower oxygen supply and lower temperature result in higher tar concentration [104]. Other contaminants originated from volatile organic and inorganic constituents in biomass (C, H, N, S, O, halogens and metals) are present in syngas at varying concentrations depending on the precursor composition and operating conditions of gasification. Nitrogen in biomass is converted to ammonia (NH_3), hydrogen cyanide (HCN), oxides of nitrogen (NO, NO_2, N_2O and

other NO_X) and nitrogen (N_2). Sulfur in the precursor is converted to hydrogen sulfide (H_2S) and other minor sulfur containing compounds. Halogens, like chlorine, and trace metals are released as hydrogen halides, such as hydrogen chloride (HCl), and as their respective salts by binding to metals in biomass such as alkali metals [104]. Particle matter can differ widely in composition depending on the feedstock and process. Inorganic compounds and residual solid carbon from biomass gasification constitute the bulk of the particulate matter, although bed material or catalysts can also be released. Inorganic particle matter includes alkali metals (potassium and sodium); alkaline earth metals (mostly calcium); silica (SiO_2); and other metals such as iron and magnesium [101]. Concentration of major syngas contaminants and the problems associated to each contaminant are presented in Table 1-14.

Table 1-13. Composition and LHV of syngas from biomass gasification with different gasifying agents [100,103].

Gasifying agent	Temperature (°C)	Gas product (vol.%)							LHV (MJ/Nm^3)
		H_2	CO	CO_2	CH_4	C_XH_Y	N_2	H_2O	
Air	780 - 830	5 - 16	10 - 22	9 - 19	2 - 6	0 - 3	42 - 62	11 - 34	3 - 6
Steam	750 - 780	38 - 56	17 - 32	13 - 17	7 - 12	2	0	52 - 60	8 – 9
Steam + O_2	785 - 830	14 - 32	43 - 52	14 - 36	6 - 8	3 - 4	0	38 - 61	8 - 10
Air	-	9 - 10	12 - 15	14 - 17	2 - 4	-	56 - 59	-	3 - 6
Oxygen	-	30 - 34	30 - 37	25 - 29	4 - 6	-	0	-	10 - 15
Steam or CO_2	-	24 - 50	30 - 45	10 - 19	5 - 12	-	0	-	12 - 20
Steam + O_2	-	45 - 51	13 - 25	15 - 20	1 - 4	-	0	-	7 - 10

The information that is not available in the consulted references is represented by the "– "symbol.

Table 1-14. Main impurities of syngas and associated problems adapted from [101,103–108].

Contaminant	Concentration	Problems
Tars	0.01 - 150 g/Nm^3	Fouling Catalyst deactivation Condensation at T < 400°C Metallic corrosion
NH_3	350 – 18000 ppmv	Catalyst deactivation Regulated pollutant if burned (NO_X)
HCl	1 – 500 ppmv	Catalyst deactivation Environmental pollution
H_2S	20 - 200 ppmv	Catalyst deactivation Acid corrosion of metals Regulated pollutant if burned (SO_2)
Particulate matter	100 - 8000 mg/Nm^3	Fouling Corrosion Erosion Catalyst deactivation

Each contaminant in syngas creates specific downstream hazards. The problems include rapid deactivation of catalysts which play a critical role in syngas conversion reactions as well as

corrosion and pipe blockages [101]. In fact, the deactivation of catalyst is a key problem since fuels and chemicals synthesis from syngas does not occur in the absence of an appropriate catalyst. Tars can condensate in pipes, filters or heat exchangers of downstream equipment and cause catalyst deactivation leading to collapse of the entire process [57,103,104]. The Fischer-Tropsch, methanol and ethanol synthesis are carried out at temperature < 400 °C. At this temperature tars can condensate which represents a risk for the process. Operation problems can be prevented or minimized by controlling the impurity levels in the syngas [99].

Table 1-15. Requirements of syngas upgrade according to each application [107]**.**

Compound	Motor	Gas turbine	Methanol Synthesis	Fischer Trospch
Tar	< 100 mg/Nm^3	< 5 mg/Nm^3	0.01 – 1 mg/Nm^3	0.1 mg/Nm^3
NH_3	< 70 ppm	< 1.5 ppm	< 0.1 ppm	0.02 ppm
HCl	< 6 ppm	< 0.6 ppm	< 0.06 ppm	< 0.01 ppm
H_2S	< 70 ppm	< 0.7 ppm	< 0.1 ppm	< 0.01 ppm
Particulate matter	< 50 mg/Nm^3	< 30 mg/Nm^3	< 0.02 mg/Nm^3	0
Alkali	< 1 mg/Nm^3	0.24 mg/Nm^3	0	≈ 0

Most downstream applications have very severe requirements of syngas purity with varying levels of upgrade demands depending on the application or emission standards (Table 1-15). Therefore, tar levels must be decreased in order to answer to the needs of downstream applications.

1.6.2. Syngas treatment technologies

The selection of the technology to treat syngas depends on the intended use of the gas. The energy in tar compounds represent 3 – 10 % of the raw material [109] therefore for energy applications it is preferred to convert tars into light gases such as H_2, CO and CH_4. However, the synthetic fuel production has strict standards of conditioning that are not feasible by means of tar conversion. Thus, these applications may require tar removal technologies in order to achieve the gas purity [101].

1.6.2.1. Thermal cracking

Thermal cracking of tars is achieved through high temperatures in order to break large hydrocarbons into lighter non-condensable gases. Usually thermal cracking of tar must be carried out at temperatures between 1100 and 1300 °C [101,104,110]. Tar decomposition was investigated by Nestler et al., [111] at temperatures between 700 and 1050 °C using naphthalene. Results showed that temperature has great influence in tar conversion. At 800°C no conversion of naphthalene was observed but, conversion was increased to 3 % at 850°C and

finally to 58 % at 1050 °C. Besides, at elevated temperature residual tar is transformed into secondary and tertiary tar components, which are more aromatic and difficult to degrade [108,112]. Thus, thermal cracking requires large energy inputs, long residence times and thermally resistant reactors which increase the cost of this method [111].

1.6.2.2. Non-thermal plasma

Plasma is generated at significantly higher temperatures than gasification (thermal plasma) or by high energy electron-molecule collisions (non-thermal plasmas). This highly excited atmosphere is full of free radicals, ions, and other reactive molecules which allows tar breakdown. Various types of non-thermal plasmas solutions are available, including pulsed corona, dielectric barrier discharges, DC corona discharges, RF plasma, and microwave plasma. Among these technologies, pulsed corona is the most common method. It has been reported that corona plasma is able to remove 90 – 95 % of naphthalene from syngas. The glid-arc plasma technology for tar decomposition has also been tested. It was found that less than 50% of tar was removed at 600 °C and at 800 °C, tar conversion was slightly higher [103]. These methods are effective, however their use is not extended since they are expensive, they have limited lifetime of the pulsed power devices, require high energy input and they are complex to operate [101].

1.6.2.3. Mechanical or physical methods

Mechanical or physical gas treatment solutions include scrubbers, spray and wash towers, rotating particle separators, adsorbing bed and other filters, cyclones and electrostatic precipitators [57,108]. These technologies remove tars employing absorption, adsorption and filtration as well as mechanical, physical and electrostatic separation. These methods are divided into two categories: dry and wet gas cleaning. Dry gas cleaning is usually carried out prior to gas cooling (T > 500 °C) and partly below 200 °C after gas cooling, whereas wet gas cleaning is used after gas cooling usually at room temperature [103]. Several tar removal technologies and their performances in tar reduction are presented in Table 1-16. In general, filters present good performance for tar removal, however tar deposited in the filter is difficult to clean leading to eventual plugging.

Wet gas cleaning approaches are more commonly used since tar removal by means of condensation is the least complicated way to remove tars. It has been reported that tar separation in a venturi scrubber used to purify syngas from a countercurrent rice husk gasifier showed 51 to 91 % conversion efficiency [108]. Even so, this system is fairly expensive besides, it removes tar from the syngas but energy in the tar is lost. Moreover, this method generates

contaminated streams which causes another waste treatment problem [104]. Other experiments have demonstrated that removal efficiency of a wet electrostatic precipitator (ESP) is about 40 to 70 % in different gasifiers. However, ESP present some disadvantages due to its large size and elevated cost making it suitable for large-scale operations only [103].

Table 1-16. Tar removal efficiency in various cleaning systems adapted from [103,108]**.**

Technology	Type	Temperature (°C)	Tar reduction (%)
Sand bed filter	Dry	10 - 20	50 - 97
Wash tower	Wet	50 - 60	10 - 25
Venturi scrubber	Wet	-	50 - 90
Rotational atomizer	Wet	< 100	-
Wet electrostatic precipitator	Wet	40 - 50	0 - 60
Fabric filter	Dry	130	0 - 50
Rotational particle separator	Dry	130	30 - 70
Fixed bed tar adsorber	Dry	80	50
Catalytic tar cracker	Dry	900	> 95

The information that is not available in the consulted references is represented by the "– "symbol.

1.6.2.4. Catalytic cracking

The catalytic cracking of tars employs lower temperatures than thermal cracking since catalysts weaken the activation energy of cracking reactions. The catalytic method is thermal integrated with the downstream applications and avoids higher cost by operating at lower temperature compared to thermal cracking. However, there are challenges to overcome such as the catalyst deactivation by poisoning or carbon deposition. The catalyst is poisoned when contaminants from the gas stream are adsorbed irreversibly onto the active sites. For instance, sulfur is known as a common poison of catalyst, in particular metal catalysts [101]. Several catalyst have been studied such as noble metal-based catalysts, zeolites, iron ores, alkali metals, calcinated rocks and nickel-based catalysts [57]. However, these superior cracking catalysts have not demonstrated long term sustainable activity or mechanical strength [101]. The advantages and disadvantages of some catalyst are presented in Table 1-17.

Char from pyrolysis could be recovered and used as cheaper catalysts (0.16 USD/kg) than commercial catalyst (10 – 100 USD/kg). Chars exhibit a wide range of physical and chemical properties which depend on operating conditions and biomass characteristics such as structure and mineral content. In conclusion, chars are potential catalyst which are worth to study considering their cost, availability and renewable character.

Table 1-17. Advantages and disadvantages of several catalysts for tar removal adapted from [57]**.**

Catalyst	Advantage	Disadvantage
Char	Abundant Sustainable (Production inside gasifier) High tar conversion compared to dolomite	Consumption because of gasification reactions Its properties are not fixed depending on biomass type and process conditions
Calcinated rocks	Abundant High tar conversion ≈ 95 % conversion with dolomite Often used as guard beds for expensive catalyst	Fragile materials and quickly eroded from fluidized beds
olivine	High erosion resistance	Lower catalytic activity than dolomite
clay minerals	Abundant Fewer disposal problems	Lower catalytic activity than dolomite Do not support high temperatures (800 - 850 °C) (lose pore structure)
Iron ores	Abundant	Rapidly deactivated in the absence of hydrogen Lower catalytic activity than dolomite
Alkali-metal-based	Production in the gasifier	Particle agglomeration at high temperatures Lower catalytic activity than dolomite
Activated alumina	High tar conversion compared to dolomite	Rapid deactivation by coke
Transition-metal-based	Able to achieve complete tar elimination at ≈ 900 °C Increase CO_2 and H_2 yield Higher tar reforming activity (Ni-based catalyst are 8-10 times more active than dolomite)	Rapid deactivation because of sulfur and high tar content in the feed Relatively expensive Relatively easy regenerated

Dolomite, $CaO \cdot MgO(CO_3)_2$, is well-known as an active catalyst for tar conversion which is usually implemented as a guard bed. Gusta et al., [113] studied different dolomites as catalyst for the decomposition of tars. Their results showed that the predominant components of dolomite are Ca and Mg, present in oxide forms (CaO and MgO) after calcination. The iron content was varied in the samples, ranging from 0.1 to 2.4 wt % Fe. In addition, the calcined dolomites had low surface areas, from ~8 to 22 m^2/g. The cleaning unit was feed with syngas coming from the gasifying unit. The experiments were carried out at 650 – 800 °C and thermal cracking increased from 28 to 55 % at these conditions. They concluded that the maximum tar conversion of 66 % was achieved at 750 °C using a Canadian dolomite with 0.9 wt % Fe.

Zhang et al., [114] studied the catalytic destruction of tar formed during gasification of biomass using different nickel-based catalysts treated with alkali in an effort to promote steam gasification of the coke that deposits on catalyst surfaces. The cleaning system included a guard bed of dolomite and a catalytic reactor was used to evaluate three commercial steam reforming catalysts. The experiments were carried out at 740 – 820 °C in a fixed-bed reactor and initial tar concentration of 10.4 g/Nm^3. All three metal catalysts proved effective in eliminating heavy tars (>99 % due to material performance and thermal cracking) and in increasing hydrogen

concentration by 6–11 vol% (dry basis). Results also showed that space velocity had little effect on gas composition whereas higher temperature improved hydrogen yield and reduced light hydrocarbons (CH_4 and C_2H_4), thus indicating that tar destruction is controlled by chemical kinetics.

Buchireddy et al., [115] used zeolites and nickel-supported zeolites to investigate their effectiveness in catalytic tar removal. All the experiments were performed using syngas (CO, H_2, CO_2, CH_4, N_2) as feed gas. These experiments were conducted at 750 °C with steam and a naphthalene concentration of 12 g/m^3. Nickel-supported zeolites showed higher activity (99.5%) towards naphthalene removal compared with zeolites. The superior activity of these materials was attributed to the activity of Ni and the acidic nature of zeolite support. The decrease in activity was associated with coke deposition and a loss of active surface area.

1.6.3. Tar removal using chars

The conversion of tars into light gases using chars involves several reactions in the solid and gas phases in addition to mass transfer phenomena. In this section, further discussion about the reaction pathway of tar conversion and the properties of char involved in tar removal will be addressed.

Abu El-Rub et al., [116] studied the potential of using biomass char as a catalyst for tar reduction. Biomass char is compared with other known catalysts used for tar conversion using naphthalene 40 g/N m^3. Tests were carried out in a fixed-bed reactor at a temperature range of 900 °C under atmospheric pressure. Two chars were studied, a commercial char and a pinewood pyrolyzed char at 500 °C. Chars were compared with calcined dolomite, olivine, biomass ash and commercial nickel catalyst. The conversion of naphthalene over these catalysts was carried out in CO_2 and steam atmosphere. Results showed that chars gave the highest naphthalene conversion among the low-cost catalysts used for tar removal. The efficiency of the different catalysts activity for naphthalene conversion at 900 °C was: nickel (100 %) > commercial char (99.6 %) > pinewood char (94.4 %) > biomass ash (73.7 %) > dolomite (61 %) > olivine (55 %) > silica sand (2 %).

Hervy et al. [117] prepared two chars by pyrolysis at 700 °C of : wood pallets (Char A), and food waste mixed with coagulation flocculation sludge (Char B). The resulting chars were tested at 650 °C in syngas catalytic cracking using ethylbenzene (40 g/Nm^3) as tar surrogate in the syngas stream (60 % N_2, 40 % CO). Results showed that ethylbenzene was converted into lighter gases proving reactivity of char samples. The highest ethylbenzene total conversion (71 wt.%) was

achieved with char prepared from the mixture of sludge and food waste (B) after 90 min of experiment. The higher activity of this sample was attributed to the mineral content composed of well dispersed oxide species of Ca and Al. Besides, slower deactivation by coke deposit of this char was explained by the presence of hydroxyapatite particles ($Ca_5(PO_4)_3(OH)$) embedded in the char matrix.

Burhenne and Aicher [118] studied the performance of chars from pyrolysis in the cracking of benzene. Chars were prepared by pyrolyzing spruce wood chips at 500 and 800 °C. Part of chars was activated with CO_2 at 800 °C. Benzene (4.5 g/m^3) was used as tar model and experiments were carried out at 850, 950 and 1050 °C under N_2 flow. Thermal cracking was 10 - 13 % at the temperature range of 850 – 950 °C. Conversion of benzene at 60 min of experiment was 39.3 and 8.8 % for pyrolyzed chars at 500 and 800 °C respectively. Activated samples showed higher catalytic activity displaying 73.2 - 85.3 % of benzene removal which didn't varied in the 850 - 950 °C temperature range. Activated samples showed 100 % of benzene conversion for about 15 min, then started to deactivate gradually and at 45 min the tar conversion was steady at 20 %. Deactivation of samples was caused by coke deposition decreasing microporous surface area. At 1050 °C benzene conversion was found to be mainly due to thermal cracking.

1.6.3.1. Reaction pathways of tar cracking

The main catalytic reactions involving tar (C_nH_m) conversion and other gas equilibrium reactions are listed in Table 1-18. The cracking of tars comprehends several decomposition and equilibrium reactions. The tar conversion reactions are kinetically limited therefore the use of catalysts makes it possible to increase the speed of these reactions. The cracking of tars generates the formation of small carbonaceous particles called "soot" or "coke" (R 1-6) and gases such as H_2, CH_4, CO and CO_2. These particles settle in the surface of materials blocking the pores mouth which ends deactivating the catalyst [105,117,118]. As it can be observed CO_2 and steam are involved in the reforming of tars to produce CO and H_2. In addition, CO_2, O_2, H_2 and H_2O can react with carbon particles to form CO, CO_2, CH_4 and H_2. Lastly, in presence of steam, CO reacts to favor the formation of H_2 and CO_2.

Table 1-18. Decomposition and equilibrium reactions for tar removal [45,57,104,107,110,119,120].

Thermal cracking	$C_nH_m \rightarrow C + C_xH_y + H_2 + CH_4 + CO + CO_2$	**R 1-6**
Hydrogen oxidation	$H_2 + \frac{1}{2}O_2 \rightarrow H_2O$	**R 1-7**
Methane oxidation	$CH_4 + O_2 \leftrightarrow CO_2 + 2H_2O$	**R 1-8**
Hydrocracking	$C_nH_m + \left(\frac{4n-m}{2}\right)H_2 \leftrightarrow nCH_4$	**R 1-9**
Boudouard	$C + CO_2 \rightarrow 2CO$	**R 1-10**
Dry reforming	$C_nH_m + nCO_2 \rightarrow 2nCO + \left(\frac{m}{2}\right)H_2$	**R 1-11**
Steam reforming	$C_nH_m + nH_2O \rightarrow nCO + \left(\frac{m}{2} + 2n\right)H_2$	**R 1-12**
Gasification with O_2	$C + \frac{1}{2}O_2 \rightarrow CO$	**R 1-13**
Combustion with O_2	$C + O_2 \rightarrow CO_2$	**R 1-14**
Gasification with steam	$C + H_2O \rightarrow CO + H_2$	**R 1-15**
Gasification with H_2	$C + 2H_2 \rightarrow CH_4$	**R 1-16**
Water gas shift reaction	$CO + H_2O \leftrightarrow H_2 + CO_2$	**R 1-17**
Methanation I	$CO + 3H_2 \rightarrow CH_4 + H_2O$	**R 1-18**
Methanation II	$CH_4 + H_2O \leftrightarrow CO + 3H_2$	**R 1-19**
Methanation III	$CO_2 + 4H_2 \leftrightarrow CH_4 + 2H_2O$	**R 1-20**
Water gas reaction	$C + 2H_2O \rightarrow CO_2 + 2H_2$	**R 1-21**

1.6.3.2. Properties of chars and AC that improve tar removal

In the review of Ravenni et al., [121] a series of studies where model compounds were used to predict the behavior of real tars upon contact with char surface were presented. This overview outlines the interactions between tar compounds and chars from pyrolysis and pyro-gasification processes or activated carbons according to their properties. It is highlighted that well dispersed AAEM and metals appear to be effective in forming active sites, when they are at accessible sites (micropores) on the surface. The difficulty to quantify the effect of oxygen functional groups is

mentioned, because at high temperature they are released and simultaneously created by carbon deposition. On the other hand, the BET surface area is presented as an important factor, together with the pore volume and the pore size distribution: the micropore volume and the total pore volume should be high, as active sites seem to be at the micropore scale. Therefore, in this section the properties of chars and activated carbons that are involved in the tar cracking are presented and discussed.

Porosity

Hervy et al. [107], studied the performance of pyrolysis chars and activated carbons for the conversion of ethylbenzene at 650 °C. Two pyrolysis chars were produced, one from wood pallets and another from food waste and coagulation flocculation sludge. The chars were produced through slow pyrolysis at 700 °C during 30 min with a heating rate of 22 °C/min in a semi-continuous horizontal screw reactor. Then chars were activated at 850 °C with steam for 80 min. The ethylbenzene removal experiments were carried out under 40 % of CO balanced with N_2 and ethylbenzene concentration of 40 g/Nm^3. The thermal cracking at these conditions 650 °C was around 38 %. The surface area of pyrolysis chars A and B was 50 m^2/g for the wood-char and 10 m^2/g for the sludge-char. The porosity of samples increased with activation to 625 and 221 m^2/g, respectively. The conversion of ethylbenzene due to materials properties and thermal cracking calculated at 85 min achieved by pyrolysis chars was 45 % for the wood-char and 71 % for the sludge-char. On the other hand, activated samples showed higher conversion of 77.3 and 85.8 % respectively. These results suggest that porosity plays an important role since higher porosity improved the tar conversion of the corresponding char.

In another study Hosokai et al., [122] studied the decomposition of benzene and naphthalene separately over a commercial charcoal at 700 – 900 °C. The inlet concentrations of aromatics were 7.5 – 15 g/Nm^3, steam was 0 – 15.5 vol% and H_2 was 0 –15.5 vol%. For the experiments, a fixed bed of charcoal with a height of 15 – 45 mm was placed in a vertical quartz tubular reactor with an inner diameter of 27 mm and heated under atmospheric N_2 flow. The charcoal, with an initial surface area of 740 m^2/g, was able to decompose naphthalene completely at 750 °C. Their results demonstrated that during benzene and naphthalene conversion over charcoal, the surface area and micropore volume decreases while the mesopore volume remains almost constant. This observation allowed them to conclude that micropores act as active sites for the tar decomposition causing loss of microporous volume, surface area and the activity of the char-coal. However, they mentioned that it is also probable that mesopores do not contribute to the tar conversion.

In the same way, Nestler et al., [111] investigated the efficiency of char from pyrolysis and AC in naphthalene removal from syngas. The wood char was produced by pyrolyzing spruce wood chips in a tubular batch reactor at 500 - 800 °C. Part of char was further activated with CO_2 at 800 °C. The surface areas of samples measured by N_2 adsorption was 267 - 310 m^2/g for pyrolysis chars and 563 – 593 m^2/g for activated carbons. The reactivity of materials for naphthalene cracking was investigated using a fixed-bed quartz reactor in a heated furnace with a constant inlet gas flow of naphthalene (0.57 g/Nm^3). They concluded that AC have high catalytic activity for naphthalene decomposition, whereas the non-activated char did not enhance the tar conversion since it has less micropores than AC. The efficiency of AC for the conversion of tar was found to be related to the amount of micropores with a pore diameter smaller than 0.7 nm. This result was attributed to the fact that pore diameters around the kinetic molecular diameter of the adsorbate are more reactive due to beneficial inter-molecular attraction forces. The carbon deposit was responsible for the deactivation of samples, where the micropores deactivate at a faster rate than mesopores.

The size and type of pores developed by the char are important parameters for its catalytic activity. According to literature, the presence of micropores is important for the tar conversion while mesopores reduce the deactivation by coke deposition.

Oxygen functional groups

It is known that the performance of ACs in tar cracking depends not only on the surface area but also on the surface chemistry. The exact role of oxygen groups on tar cracking reactions is not clearly understood yet. Some oxygen groups (OH, C-O and C = O) can interact with tars by hydrogen bonds [57]. In addition, the strong electron-donating ability of the hydroxyl group interacts with the aromatic rings which become π-electron rich systems. Thus, the aromatic rings form π–π* stacking interactions that offer a multilayer adsorption system. Other authors suggest that functional groups form some acidic centers that combine with polyaromatic rings (tars) having a negatively charged π electron. This interaction reduces the activation energy of tar cracking reactions [109].

In the study carried out by Hervy [107], the properties of two pyrolysis chars produced from wood pallets (A) and from food waste and coagulation flocculation sludge (B) were investigated and related to their performance of ethylbenzene conversion. The chars were produced through slow pyrolysis at 700 °C, then chars were activated at 850 °C with steam. Results suggested that the activity of B was mainly due to its high ash content and functional groups. It was stated that the quinone and pyrone groups, might promoted the oxidative dehydrogenation reactions of

ethylbenzene. In addition, it was mentioned that the efficiency of this sample was partly due to the hydroxyl groups which are important electron donors that can interact with aromatic rings.

Inorganic composition

According to literature, some mineral elements improve the reactivity of chars along gasification and reduce the tar yield of syngas. Among them, we find mainly potassium, magnesium, calcium and iron [89,117,123–125]. In fact, the reactivity of dolomite to remove tars is in the most part due to its composition of Ca (28 – 60 %), Mg (3 – 25 %) and a few Fe (0.1 – 2.4 %) since it has poor porosity (BET surface 8 – 22 m^2/g) [113] therefore the influence of pores is not significant. For some authors, the active form of calcium is lime (CaO) [98] which have diffused electron clouds that can overlap with the orbitals of the near molecules disturbing their stability and causing the fragmentation of the aromatic rings. Other authors have mentioned that calcium in the hydroxyapatite ($Ca_5(PO_4)_3(OH)$) [117] form, is involved in the conversion of tars. As far as potassium is concerned, it has also proved to decrease the tar levels. Knutsson et al., [126] stated that the formation of mixed Ca and K oxides changes the oxidation potential of the catalyst which increase the activity towards tar reduction.

Xie et al., [127] studied the influence of different additives such as alkali metal carbonates (Na_2CO_3 and K_2CO_3), alkaline earth metal oxides (CaO and MgO), transition metals (Ni and Fe_2O_3), natural ores (dolomite and olivine) and clays (kaoline and diatomite) in the reduction of tars. The results demonstrated that alkali metal carbonates, alkaline earth metal oxides, dolomite, olivine and transition metals mainly increased the yields of permanent gases (H_2, CO_2) and promoted the decomposition tars and light hydrocarbons (C_nH_m). On the other hand, clays don't seem to play an important role in the conversion reactions of tar and C_nH_m. They also concluded that CaO, MgO, Fe_2O_3, dolomite, and olivine also improve the water-gas shift reaction to further raise the yields of H_2 and CO_2.

In contrast, elements such as silica and phosphorous can inhibit calcium and potassium by forming silicates and phosphates according to Dupont and coworkers [124]. Therefore, they proposed the ratio K/(P + Si) as reference of reactivity (>1) or inhibitory behavior (<1) based on the composition of the catalyst. In addition of their melting temperature close to the temperature of gasification, certain mineral species such as calcium can also deactivate the catalyst by sintering [89,92]. Apart from the nature and quantity of mineral species present in the char, the size of the particles and their distribution on the surface of the solid are two determining properties for their catalytic activity. Well-dispersed particles on the surface of the char provide many active sites for cracking reactions, limit the risk of sintering and preserve the

porous structure of the solid by avoiding clogging of the pores by the presence of large mineral particles [89,117].

This section presented the problematic of syngas due to the presence of pollutants that limit its utilization as fuel or in the synthesis of chemicals. In addition, the composition of this gas was introduced and the syngas treatment technologies were presented. Finally, the properties of chars and AC that improve the tar removal were discussed. In the next section, the potential application of raw and activated chars in biogas cleaning will be discussed. In that sense, the composition of biogas is presented, the problems associated to different contaminants are introduced and the different technologies for the treatment of biogas are described.

1.7. Biogas

Under anaerobic conditions that means in absence of air, the microorganisms can degrade the fermentable organic carbon to produce biogas composed mainly of CH_4 and CO_2. At industrial scale the biogas is produced at sewage treatment plants (sludge fermentation stage), landfills, sites with industrial processing industry and digestion plants for agricultural organic wastes [128]. Biogas stands as good alternative in the developing field of renewable energies thanks to its methane content. It is expected that biogas worldwide use will be doubled from 14.5 gigawatts (GW) in 2012 to 29.5 GW in 2022 [129]. In addition primary production of biogas in Europe (including landfill and sewage gas) was estimated as 13.4 million tons of oil equivalents (Mtoe) in 2013 [130].

The production and valorization of biogas has the advantage of reducing CO_2 and CH_4 emission to the environment; besides it has several applications. Biogas can be valorized in several ways either cleaned or upgraded. The cleaning process requires biogas to be cooled immediately after production and cleaned for the content of hydrogen sulfide. Upgrading of biogas is required in order to increase the methane fraction of the gas (biomethane) and be able to inject it into the natural gas grid or use it as vehicle fuel as presented in Figure 1-6.

In addition, the CO_2 recovered after upgrading can be further used in other industrial applications, such as chemical synthesis [131,132]. The applications of biogas are listed by Holm-Nielsen as follows [133]:

- Production of heat and/or steam
- Electricity production with combined heat and power production
- Industrial energy source for heat, steam and/or electricity and cooling
- Upgraded and utilization as vehicle fuel

- Production of chemicals and/or proteins
- Upgrading and injection in the natural gas grids
- Fuel for fuel cells

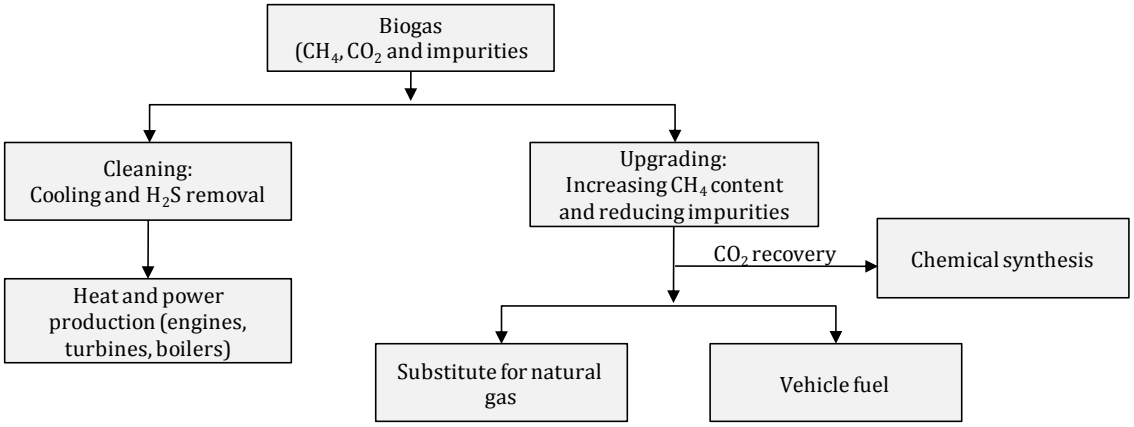

Figure 1-6. Applications of biogas.

1.7.1. Composition of biogas

Biogas main gases are methane (CH_4) and carbon dioxide (CO_2), however biogas holds detrimental compounds such as hydrogen sulfide (H_2S), ammonia (NH_3), steam, chlorine compounds, siloxanes, oxygen (O_2), volatile organic compounds (VOCs) and some heavy hydrocarbons. Their presence and concentration in biogas depend on the production method and the organic matter fed to the system (i.e., landfills, anaerobic fermentation of manure). The appearance of such pollutants is a major issue since they can be harmful to biogas thermo-catalytic conversion processes causing corrosion, erosion and fouling besides they cause negative environmental effects [134]. Typical composition of biogas is presented in Table 1-19.

Higher CH_4 content and LHV are obtained from anaerobic digesters (AD). Usually, less variation in the gas composition is obtained from AD since the organic matter nourished to landfill systems consists of all sorts of wastes including plastics. In the same way, it has been found that industrial wastes in landfill produce more benzene, toluene and organic silicon compounds in biogas [135]. Nitrogen and oxygen contents in gas from AD are usually low since biogas is produced in sealed tanks, avoiding contact with air. Landfill biogas can have higher nitrogen and oxygen contents since the extraction of the gas can cause a pressure decrease in the landfill system, which will result in air being sucked in [136].

Table 1-19. Typical composition of biogas from different production methods [129,131,136–138]**.**

Parameter	Units	Landfill gas	Biogas from AD
LHV	MJ/Nm^3	16	23
CH_4	% mol	35 - 65	50 - 80
CO_2	% mol	15 - 40	30 - 40
N_2	% mol	0 - 15	0 - 5
H_2	% mol	0 - 3	0
H_2O	% mol	1 - 5	1 - 5
O_2	% mol	0 - 10	0 - 1
H_2S	ppm	0 - 1000	0 - 4000
NH_3	ppm	0 - 5	0 - 100
Total Cl	mg/Nm^3	5	100
Siloxanes	mg/Nm^3	0 - 50	-
Heavy hydrocarbons	mg/m^3	0.6 - 287	0

Hydrogen sulfide is formed by bacteria that reduce sulfate present in the digester or landfill and during digestion of proteins containing sulfur. In landfill gas, hydrogen sulfide may also originate from gypsum (hydrated calcium sulfate) [136]. Some of VOCs such as aromatics, heterocyclic compounds, ketones, aliphatics, terpenes, siloxanes, alcohols and halogenated aliphatics can be found mainly in landfill gas [135,139]. The concentration of VOCs depends on the feed used for the gas production. For example: siloxanes can be found in products such as fire retardants, shampoos and deodorants. Thus, if these products are present in the substrate, siloxanes will be found in small amounts in the produced biogas [136].

Table 1-20. Main biogas impurities and associated problems [129,131,137,138,140]**.**

Impurity	Problems
CO_2	Reduction of calorific value
H_2O	Corrosion in compressors, gas storage tanks and engines due to reaction with H_2S, NH_3, and CO_2 to form acids Accumulation of water in pipes Condensation or freezing due to high pressure
O_2/air	Risk of explosion
H_2S	Cause corrosion with water Causes deactivation of catalyst Causes emission and health hazards due to SO_2 and SO_3 formation during to combustion. SO_2 and SO_3 are more toxic than H_2S
NH_3	Corrosive when dissolves in water leads to an increase in antiknock properties of engines Formation of N_{OX}
Total Cl	Corrosion in combustion engines
Dust	Clogging due to deposition in compressors and gas storage tanks
Heavy hydrocarbons	Corrosion in engines due to combustion
Siloxanes	Formation of SiO_2 and microcrystalline quartz due to combustion Deposition at spark plugs, valves, and cylinder heads abrading the surface

Contaminant in biogas cause several problems that limit its valorization. The biogas handbook [136]describes the associated problems to the main contaminant as follows, also summarized in Table 1-20:

- CO_2: Decreases the energy content in biogas therefore, if high volumetric energy content is required, the carbon dioxide should be removed. For other applications, such as power and heat generation, it does not cause problems. However, it can form carbonic acid with condensed water.
- Water: Causes corrosion in pipelines in the presence of carbon dioxide, due to formation of carbonic acid. Steam lowers the energy content of the gas and can affect energy valorization.
- H_2S: It can form sulfuric acid in combination with water and cause corrosion. In addition, the combustion of biogas containing hydrogen sulfide will lead to emissions of SO_2 formed during combustion. It is also important to mention that hydrogen sulfide is highly toxic for humans and can result in serious health danger.
- O_2/Air: Oxygen must be carefully controlled since flammable mixtures can be formed with methane in the biogas.
- NH_3: It is corrosive in combination with water leading to an increase in antiknock properties of engines. In addition, it can form N_{OX} during combustion [131].
- VOCs: During combustion, siloxanes form siloxane oxide which is insoluble and lead to unwanted depositions on combustion equipment causing damage to engines. Hydrogenated hydrocarbons can cause corrosion and acidification during combustion, due to the formation of acids.

Biogas can be employed for different energy services such as heat, combined heat and power (CHP) and transportation fuel as mentioned before. Biogas upgrading is not required when it is used in boilers or engines since quality requirements are mainly assessed by cleaning. However, other biogas applications such as injection in the natural gas grid or used as vehicle fuel have more strict specifications. For example, according to Table 1-21, the requirements of biogas as substitute of natural gas are more flexible than biogas for vehicle fuel since the first accepts methane content in the 70 – 98 % while the former demands higher methane purity (>96 %).

In the same way, vehicle fuel requires less H_2S and steam contents whereas the standard requirements of dust and VOCs are the same for both applications. Only higher ammonia content is accepted in biogas as vehicle fuel in comparison to the injection to the natural gas grid. Likewise, it has been stated that H_2S content higher than 1 ppm decreases the performance of solid oxide fuel cells (SOFC) [138]. Generally, upgrading technologies to increase methane content in biogas also eliminate unwanted compounds such as H_2S, NH_3, O_2/Air and siloxanes

[128]. However, to prevent corrosion and mechanical damage it is recommended to remove H_2S before upgrading [139]. The requirements of biogas quality to each application are presented in Table 1-21.

Table 1-21. Requirements of biogas upgrade according to each application [129,131,139]**.**

Compound	Gas heating (Boiler)	Kitchen Stove	Internal Engine (CHP)	Natural Gas Grid*	Vehicle fuel
CH_4	-	Heating value comparable to natural gas (37 MJ/m^3)	> 30 %	70 - 98 %	> 96 %
H_2S	< 250 ppm	< 10 ppm	< 1000 ppm	2 - 10 ppm	Removal required (5 ppm)
CO_2	No removal requirement (25 - 30 %)	No removal requirement (25 - 30 %)	No removal requirement (25 - 30 %)	Removal required (≤ 3 %)	Recommended (<4 %)
NH_3	-	-	-	< 3 ppm	< 20 ppm
Dust	-	-	-	< 5 ppm	< 5 ppm
Halogenated compounds	-	-	-	< 10 ppm	< 10 ppm
Organic silicon compounds	-	-	-	< 28 ppm	< 28 ppm
H_2O	No removal requirement (6 %)	No removal requirement (6 %)	Avoid condensation (<3 %)	Removal required (1 -8 %)	Removal required (< 3%)

** Biogas requirements for natural grid injection vary in each country; values set in France for natural gas were taken. The information that is not available in the consulted references is represented by the "– "symbol.*

1.7.2. Biogas treatment technologies

Technologies for upgrading biogas are summarized in Table 1-22. The treatment processes include several technologies such as water scrubbing, chemical or physical absorption, adsorption, membranes, cryogenic process, catalytic and biological process.

Table 1-22. Biogas treatment technologies [139]**.**

Process	Removed compounds	Comments
Water scrubbing	CO_2, sulfur compounds, water soluble VOC, ammonia	For organic silicon compounds removal, other technique is required. Pure water is not needed but water consumption is relatively high. Selective H_2S removal possible.
Chemical or physical absorption	CO_2, sulfur compounds, ammonia, halogenated compounds, organic silicon compounds	Higher cost of solvents and energy demand in regeneration phase (compared to water scrubbing)
PSA (Pressure Swing Adsorption)	CO_2, sulfur compounds, ammonia, halogenated compounds, organic silicon compounds	Adsorption capacity relatively low. Regeneration is not always possible.
Membranes	CO_2, organic silicon compounds	Low operation costs. More research is needed for economical evaluation of the process.
Cryogenic process	CO_2, sulfur compounds, ammonia, halogenated compounds, organic silicon compounds	O_2 and N_2 removal possible. More research is needed for economical evaluation of the process.
Cooling	Moisture, sulfur compounds, organic silicon compounds	Only partial removal of organic silicon compounds

Process	Removed compounds	Comments
Catalytic process	Organic silicon compounds, VOCs, sulfur compounds and acid gases produced during the oxidation process	Suitable for pre-treatment of biogas. More research is needed.
Biological removal	Sulfur compounds, VOCs, organic silicon compounds	Suitable for pre-treatment of biogas. Only partial removal of compounds. More research is needed.

Most of these techniques are able to remove sulfur compounds along with other impurities such VOCs, ammonia and siloxanes. These technologies are described in the present section and focus particularly on adsorption.

1.7.2.1. Absorption

This process relays on the solubility of various gas components in a liquid solvent. Hydrogen sulfide is a weak diprotic acid that is soluble in water with first and second dissociation constants equal to 7.2 and 13.9, respectively. In this process, the raw gas enters the absorption unit and meets the liquid in a counter-flow. There are two types of absorption: i) the physical which involves high pressure water scrubbing (HPWS) and organic physical scrubbing (OPS) and ii) the chemical which includes amine scrubbing (AS) and inorganic solvent scrubbing (ISS).

Physical absorption

High pressure water scrubbing is the most common technology used to separate CO_2 and H_2S from biogas and uses water as solvent. The process is based in Henry's law concept which states that the amount of dissolved gas is proportional to its partial pressure in the gas phase. The Henry's constant for H_2S and CO_2 in water at 20 °C are respectively 106E-3 and 36E-3 mol/Lbar while that of CH_4 is 25 times lower than CO_2. When the biogas has high concentration of H_2S, previous removal of H_2S is mandatory since it is difficult to regenerate H_2S from the solution and this reduces the capacity for CO_2 absorption. This technology is able to remove CO_2, water, soluble VOC and ammonia however, for organic silicon compounds other technique is required. In addition, it is no able to remove N_2 and O_2 [139]. Pure water is not needed but water consumption is relatively high. This technology have several disadvantages: i) the dissolved H_2S can cause corrosion problems; ii) it is expensive considering that high energy consumption is required during water regeneration and iii) the gases from the stripping process (the same that were removed from the biogas) are released or flared [129,131,141].

Caustic scrubbing using NaOH can be used to treat biogas in order to remove CO_2 and H_2S. The solution contacts the gas stream in a countercurrent flow in a packed or trayed column. The caustic solution in contact with CO_2 forms Na_2CO_3, thus the used stream cannot be regenerated

and must be discarded. This leads to a high consumption of caustic solution which represents an important disadvantage of the system. In addition, caustic solutions are considered hazardous wastes [141]. Organic physical scrubbing uses various organic solvents such as methanol (CH_3OH), N-methyl pyrrolidone (NMP), and polyethylene glycol ethers (PEG) instead of water. This technology is able to remove CO_2, H_2S, H_2O, O_2, N_2, and halogenated hydrocarbons. More energy is required for the solvent regeneration and the cost of the organic solvents is significantly higher than that for water [129].

Chemical absorption

Chemical absorption involves reversible reaction between molecules and solvent. The most common used solvents are amines which absorb acid gases like CO_2 and H_2S. When the concentration of CO_2 in biogas is low, chemical solvents are preferred over physical solvents. This process is able to remove CO_2, sulfur compounds, ammonia, halogenated compounds and organic silicon compounds [139]. The disadvantage of this technology is the energy consumption since high temperature is required to regenerate the chemical solvent although there are no methane losses [131]. If the raw biogas contains H_2S, it will be absorbed by the amine solution and higher temperature will be needed to regenerate the solution. Therefore, it is recommended to remove H_2S prior to the amine scrubbing process [129]. Another problem of this technology is the treatment of waste chemicals, corrosion, and contaminant build-up which makes the process more complicated [142,143].

1.7.2.2. Biofiltration

Biological based technologies as biofiltration have been developed for biogas treatment. The biofiltration unit consists of immobilized microorganisms in a packing material. The biogas stream flows through the filter bed where H_2S is transferred from the gas phase to the biofilm containing the microorganisms. The removal of H_2S from biogas is carried out by bacteria from the Thiobacillus and Sulfolobus family. These bacteria use H_2S as an energy source for growth and convert H_2S into elemental sulfur or sulfate through oxidation [144]. The biofiltration process requires strict operational conditions to control pressure, temperature and nutrients for bacteria. The disadvantage of this technology is that oxygen is required and if too much oxygen is injected it can lead to SO_4^{2-} generation and thus acidification of the system [142]. Consequently, strict handling must be taken in order to prevent the formation of explosives mixtures between CH_4 and O_2. In addition, depending on the intended application of biogas the traces of oxygen and nitrogen must be separated [136]. Other drawback is the additional

nutrients that are required for growing bacteria and the H_2S removal efficiency relays on the activity of bacteria [142].

1.7.2.3. Adsorption

The removal of H_2S from biogas by adsorption on AC is a well-known technique. The adsorbents must have the following characteristics: i) porosity ii) the surface of the adsorbent should be basic in order to attract acidic gases; iii) the pore distribution should enhance H_2S removal and avoid CH_4 adsorption and iv) it should have a good moisture removal capacity [129]. In addition, it has been demonstrated that adsorption can be a cost-effective technology at small scale [138] which could contribute to develop the decentralized energy production from biogas.

It seems that in the process of H_2S separation from biogas there are several parameters that play a critical role such us: porosity, surface chemistry and mineral content of the adsorbent. In the same way, oxygen and humidity contents of biogas might be involved, for that reason the role of these parameters will be discussed in this section.

Porosity of the adsorbent

Different authors agree that the microporosity developed by pores with diameters less than 2 nm plays an important role in the removal of H_2S [134,145,146]. Some authors state that materials with a high volume of micropores in the size range between 0.5 and 1 nm have better H_2S adsorption capacities [134]. This is due to the fact that physisorption of molecules is improved in pores with diameter close to the molecular size of the adsorbate [146]. In the work of Bandosz [147] the porosity of different AC was described in terms of relative microporosity which is the ratio of the volume of micropores to the total pore volume determined by the analysis of nitrogen adsorption/desorption isotherms. Values of relative microporosity closer to 1 indicate that the material is mainly microporous while values < 0.5 refers to mesoporosity. There is a correlation between the heat of adsorption and relative microporosity; the higher relative microporosity, the higher heat of adsorption. In dry conditions the physical adsorption in micropores is the most probable mechanism of the adsorption process.

Mineral content and surface chemistry

Mineral elements present in the materials not only influence the pH but also can play an important role in the adsorption of H_2S. Hervy et al., [148] tested two steam activated chars for the removal of H_2S (200 ppm) from nitrogen at 30 °C of temperature. These activated chars have very different properties: the first one has high surface area (625 m^2/g) and low ash content (2.5

%) composed of 42.2 % of CaO and 3.6 % of Fe_2O_3. The second one, with lower surface area (220 m^2/g) and higher ash content (59.4 %) composed of 34.3 % of CaO and 0.6 % of Fe_2O_3. Their experiments indicated that mineral species participated in the H_2S removal and Ca and Fe increased particularly the H_2S adsorption by promoting the formation of metal sulfide and metal sulfate species at the char surface. The characterization of materials demonstrated that the sample with higher ash content achieved the higher adsorption capacity (66.6 mg_{H2S}/g) in comparison to the activated char with lower inorganic fraction (13.0 mg_{H2S}/g). The efficiency of both materials is due to the influence of Ca and Fe which react with H_2S improving its removal as will be explained later.

In another study the comparison of raw AC with treated AC for the H_2S removal was carried out [146]. Two separated treatments were applied: oxidation at 200 °C and heat treatment in nitrogen at 900 °C. According to the authors, oxidation and heat treatments did not change the pore structure of AC. The adsorption experiments were carried out at 23 °C in a quartz reactor (38 cm long with 1 cm diameter) with a gas stream of 200 ppm of H_2S in N_2. The adsorbed H_2S in the raw AC was 2.65 mg_{H2S}/g whereas for the oxidized AC was 4.57 mg_{H2S}/g and 3.86 mg_{H2S}/g for the heat treated. Therefore, both treatments improved the adsorption capacity compared to the raw AC. Considering that the pore structure was not affected by the treatments they concluded that the change in the surface chemistry was responsible for the higher capacity. The oxidation increased the oxygen functional groups at the surface which might be one form of the active sites for H_2S adsorption. On the other hand, as stated by the authors, treatment at 900 °C decreased the surface oxygen containing functionalities leaving unsaturated carbon atoms at crystallite edges; these unsaturated sites are likely responsible for H_2S uptake. However, it is commonly believed that treatment at 900 °C under inert atmosphere leads to desorption of acidic functional groups [89] resulting in a basic material which justifies the improvement in the adsorption of H_2S.

The influence of Mg in the adsorption of H_2S has also been studied [149]. To do so MgO was impregnated in a granular AC. The resulting material was tested in H_2S removal from humidified air (80 % of relative humidity) at room temperature. The gas contained 10,000ppm of H_2S and it was passed through a column of granular AC (diameter 2.5 cm; bed height 15 cm). The experiments were stopped at 50 ppm of H_2S in the outlet stream. Mg was not detected in the virgin AC while it was calculated to be 1.2 % in the treated sample. Results showed that the adsorption capacity of virgin and treated sample was 53 and 275mg_{H2S}/g respectively. The performance of the sample was attributed to the ability to adsorb H_2S both physically and

chemically. It was concluded that the chemical adsorption mechanism involved the reaction of MgO with H_2S.

Adsorption mechanism

Humidity and some oxygen content can be found in biogas as described in Table 1-19, that is why it is not surprising that these parameters have been a subject of research for some authors. In the studies, humidity is provided either from the moisture of the biogas or from a preliminary stage of humidification of materials. According to Le Leuch et al., [150] in presence of humidity the H_2S removal mechanism is different. Humidity in biogas or from a pre-humidified char is condensed in the pore structure favoring the dissolution of H_2S in the water film. Polar groups present on the surface improve the adsorption of water molecules on the boundary surface. Then in the water film, H_2S is dissociated into HS^- and H^+ (R 1-24) if the pH is basic. HS- ions can be then oxidized to S or SO_2 in presence of oxygen (R 1-24 and R 1-25). It is important to mention that for some authors oxygen is adsorbed from the gas phase [150,151] while others refer to the oxygen from the surface functional groups [152,153]. Further oxidation leads to formation of SO_3 (R 1-27) while SO_3 in presence of water forms SO_4^{2-} (R 1-29).

$$H_2S_{gas} \leftrightarrow H_2S_{ads} \quad \textbf{R 1-22}$$

$$H_2S_{ads} \rightarrow H_2S_{ads-liq} \quad \textbf{R 1-23}$$

$$H_2S_{ads-liq} + H_2O \leftrightarrow HS^-_{ads} + H_3O^+ \quad \textbf{R 1-24}$$

$$HS^-_{ads} + C(O) \rightarrow S^*_{ads} + OH^- \quad \textbf{R 1-25}$$

$$HS^-_{ads} + 3C(O) \rightarrow SO_{2,ads} + OH^- \quad \textbf{R 1-26}$$

$$SO_{2,ads} + C(O) \rightarrow SO_{3,ads} \quad \textbf{R 1-27}$$

$$H^+ + OH^- \rightarrow H_2O \quad \textbf{R 1-28}$$

$$SO_{3,ads} + H_2O \rightarrow 2H^+ + SO_4^{2-} \quad \textbf{R 1-29}$$

Under dry conditions the adsorption-oxidation mechanism is simpler. Hydrogen sulfide on the surface of activated carbon is oxidized to elemental sulfur and/or sulfur dioxide according to the reactions R 1-30 and R 1-31 [147]. Deposited sulfur catalyzes the hydrogen sulfide oxidation and maximum activity is a function of the amount of sorbed sulfur by the activated carbon (R 1-32). This catalytic role of elemental sulfur in its own adsorption/oxidation process is only found under dry conditions.

$$H_2S_{gas} \leftrightarrow H_2S_{ads} \quad \textbf{R 1-30}$$

$$H_2S_{ads} + C(O) \rightarrow C(S^*_{ads}) + H_2O \quad \textbf{R 1-31}$$

$$C(S^*_{ads}) + H_2S_{ads} + C(O) \rightarrow C(SS^*_{ads}) + H_2O \rightarrow C(S_{8,ads}) \quad \textbf{R 1-32}$$

It seems that high relative humidity is needed in order to improve removal of H_2S. Le Leuch et al., [150] studied different AC in several conditions of relative humidity (10 – 90 %). Their results showed that adsorption capacity increases with higher relative humidity, however an excess of water flooding (RH > 60 %) decreases the adsorption from the gas phase on active carbon. They concluded that 60 % is the optimal relative humidity for an AC with 976m^2/g of surface area, mainly microporous (V_{micro}/V_{total} = 93 %) and pH_{pzc} = 9 [150].

Five carbonaceous adsorbents were studied by Bagreev et al., [154] for the removal of H_2S from humidified air (relative humidity of 80 % at 25 °C) containing 10,000 ppm of H_2S. The AC with higher adsorption capacity (0.608 g_{H2S}/g) contained calcium, iron and magnesium at levels of 0.7, 0.5 and 9.0 % respectively. The second material with high efficiency (0.201g_{H2S}/g) had high potassium content (3.5 %), both samples presented high surface areas (1110 and 779 m^2/g respectively). Their results suggested that in order to be adsorbed H_2S it has to be first oxidized. Different adsorption mechanisms described the oxidation pathway according to the inorganic element:

i) Iron oxides in a basic environment

$$Fe_2O_3 + 3H_2S \rightarrow FeS + FeS_2 + 3H_2O \quad \textbf{R 1-33}$$

$$Fe_2O_3 + 3H_2S \rightarrow Fe_2S_3 + 3H_2O \quad \textbf{R 1-34}$$

$$2Fe_2S_3 + 3O_2 \rightarrow 2Fe_2O_3 + 6S \quad \textbf{R 1-35}$$

ii) Calcium or magnesium oxides

$$CaO + H_2O \rightarrow Ca(OH)_2 \quad \textbf{R 1-5}$$

$$Ca(OH)_2 + 2H_2S \rightarrow Ca(HS)_2 + 2H_2O \quad \textbf{R 1-36}$$

$$Ca(HS)_2 + O_2 \rightarrow 2S + Ca(OH)_2 \quad \textbf{R 1-37}$$

They concluded that the amount of H_2S adsorbed and the extent of oxidation are governed by the surface pH and the dispersion of catalytic centers, part of such centers can be metals (iron and alkali and alkaline earth metals).

Other authors [149] have proposed H_2S adsorption mechanism involving substitution of O atoms by S as well as by metal supported addition mechanism. The O substitution pathway involves H_2O formation as indicated in R 1-38.

$$MgO + H_2S \rightarrow MgS + H_2O \quad \textbf{R 1-38}$$

$$Mg\_S + O_2 \rightarrow C + SO_2 \quad \textbf{R 1-39}$$

$$MgO + H_2S \rightarrow Mg\_S + HS \quad \textbf{R 1-40}$$

According to the consulted literature, there are several parameters influencing the adsorption of H_2S. The porosity of the material provides active sites for the adsorption (micropores) and it allows the access of the gas to the mineral species that can react with H_2S through different mechanisms. In that sense, the mineral composition of materials plays an important role since it improves the H_2S removal. Lastly, humidity and oxygen content in the gas stream can also influence the elimination of H_2S by enhancing the dissolution of H_2S in the water film and by oxidation of the acid gas.

1.8. Conclusion

This literature review allowed to determine the potential agricultural wastes available in France that can be used in the char production. The availability of buckwheat and millet wastes was highlighted, and their composition was presented. However, the references used in this literature review for the composition of these wastes are from studies dealing with subjects different that thermo-chemical conversion process from biomass wastes. In addition, the biomass conversion processes that leave a charred residue were reviewed. The characteristics of chars from slow pyrolysis were presented nevertheless, the comparison with chars from hydrothermal and pyro-gasification process was not included in this chapter. The characteristics of chemical and physical activation with either CO_2 or steam were discussed and summarized. The features of activated carbons prepared through CO_2 activation were presented however this information was not provided for activated carbons from steam activation. The potential valorization of chars from pyrolysis and activated chars is studied. This chapter explained that porosity, surface pH and mineral content of activated chars play an important role in the

cracking of tar compounds from syngas and the removal of H_2S from biogas. Tars and H_2S cause serious downstream problems that make difficult the utilization of biogas and syngas to produce energy or to synthesize chemicals without prior treatments. There is a lack of studies in the use of raw and activated chars for the cracking of light aromatics (main family of tars) other than benzene or toluene which is necessary for a better comprehension about the effectiveness of these materials. In addition, the influence of the oxidizing agent in activation on the properties of the resulting activated chars and its performance on tar cracking and H_2S removal has been barely studied. This literature review showed that there are few studies on the use of chars or activated carbons as catalysts for the cracking of ethylbenzene. Thus, this research aims to address this lack of data by exploring the purification efficiency of raw and activated chars prepared from different wastes for the cracking of ethylbenzene contained in syngas and removal of H_2S from biogas.

According to the information provided in this chapter, millet husks (MH) and buckwheat husks (BH) are selected based on their different chemical composition, besides there are locally available and they have been barely studied in the field of char production. A slow pyrolysis will be implemented in order to maximize the yield of chars from MH and BH. Then the properties of raw chars from pyrolysis are improved by means of physical activation which is similar to pyro-gasification. The physical activation with CO_2 or steam is preferred since it is an easier method than chemical activation with no additional steps and is environmentally friendly. The efficiency of raw and activated chars is studied in two potential applications: syngas and biogas cleaning. The role of the physical and chemical properties of chars is studied. In the same way, the influence of the composition of the gas (syngas and biogas) in the removal of tars and H_2S is investigated. Finally, an ultimate used after the implementation of raw and activated char in syngas and biogas cleaning is proposed according to the principles of circular economy.

Chapter 2. Materials and methods

Introduction

The properties of materials determine the application that suits the best according to their characteristics. In particular, chemical composition and textural structure influence the potential of each material to be used as adsorbent or catalyst. At the same time, properties are not only determined by the nature of the feedstock but also by the type of treatment they are submitted to and operation conditions. That is why it is important to establish which properties are important for a precise utilization in order to choose the right raw material, the accurate conversion process that must be followed and its operation conditions to obtain a product designed optimally for a specific purpose.

This chapter is divided in three sections. The first one provides information about the preparation of materials starting from pyrolysis followed by CO_2 and steam activation. Detail of operation conditions are also given. The second section comprehends description of characterization techniques that were implemented to study the properties of parent materials and final products. The methods that were employed intend to acquire deep knowledge about chemical and textural characteristics of samples. Finally, the third and last section of this chapter explains the experimental configuration of pilots that were applied to test performance of chars in different applications: as catalyst in syngas upgrading and as adsorbent in H_2S removal from biogas.

2.1. Preparation and activation of chars

2.1.1. Pyrolysis

As a remainder, millet husks (MH) and buckwheat husks (BH) were selected in order to produce char through slow pyrolysis considering the different composition and moisture (< 20%) which is adapted for processes such as pyrolysis. MH and BH were dried separately at 105 °C for at least 24h in order to remove moisture and then used to prepare raw chars by pyrolysis. Experimental configuration of pyrolysis is presented in Figure 2-1. The laboratory scale pilot was equipped with a semi-rotating quartz tube (Carbolite HTR 11/150) placed inside an

electrical furnace. Two thermocouples allowed following temperature at the wall of reactor and inside of it. Sweeping gas (nitrogen) was controlled by a valve and a flow meter. Gases from pyrolysis were driven out of the reactor and condensable fraction was recuperated in an oil collector which preceded an ice-cooled condenser. Outlet gas from pyrolysis was analyzed on line by gas micro-chromatography (SRA Instruments R 3000) composed of four modules working simultaneously by thermal conductivity detection. Analysis conditions are presented in Table 2-1.

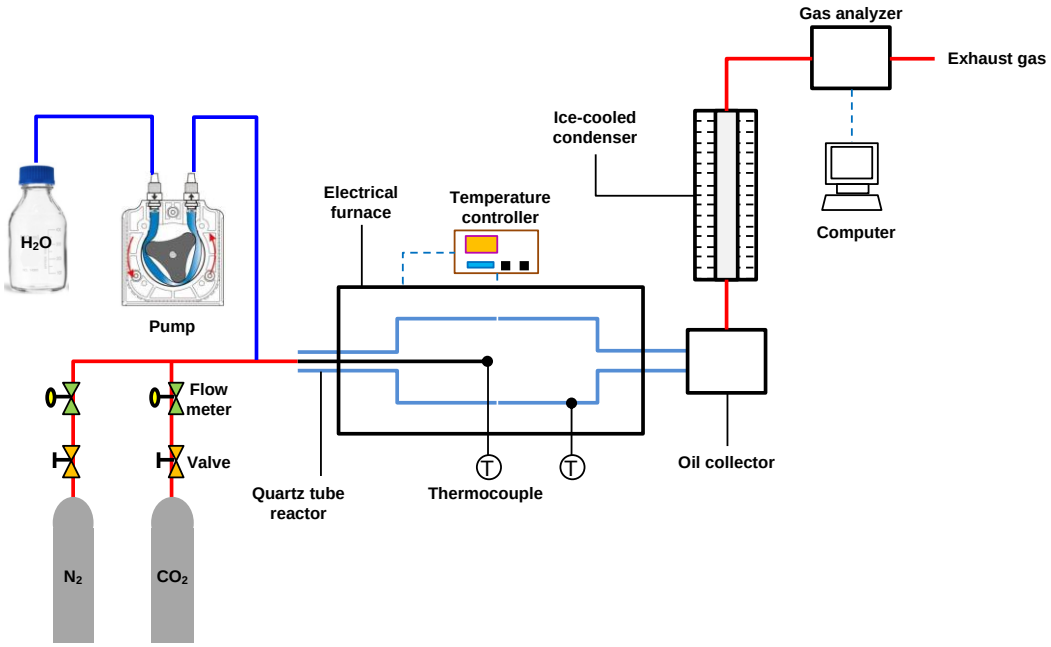

Figure 2-1. Experimental configuration of pyrolysis and activation pilot.

Table 2-1. Analysis conditions of micro-chromatography gas analyzer.

Parameter	**Module A**	**Module B**	**Module C**	**Module D**
Analyzed species	H_2, O_2, N_2, CH_4, CO	CO_2, H_2S, light hydrocarbons from C_2 to C_3	Hydrocarbons from C_4 to C_5	BTEX and organic solvent like ethylbenzene, benzene etc…
Column type	MS5A (molecular sieve)	PoraPLOT U (PPU)	Al_2O_3 (Alumina)	STABILWAX
Length	10 m	8 m	14 m	10 m
Temperature	90 °C	75 °C	130 °C	130 °C
Vector gas	Argon	Helium	Helium	Helium
Pressure	30 psi	27 psi	35 psi	27 psi

In order to transform biomass into chars by means of pyrolysis, 100 g of MH and BH were placed individually inside the quartz tube of 4.5 L of volume. It is important to mention that the proportion of mass load of biomass into the reactor shouldn't be normalized since it depends on the since and density of the feedstock. The system was purged by flushing with nitrogen (0.5 L /

min) until oxygen concentration at the outlet of the reactor was less than 5 vol.%. Then, as shown in Figure 2-2 the reactor was heated under N_2 flow of 0.75 NL/min at 10 °C/min until reaching 500 °C and kept at that temperature for 30 min. Nitrogen flow was set so as to have adequate time residence of sweeping gas and volatiles in the reactor in order to conduct slow pyrolysis of biomass according to the following equation where τ is gas residence time (min), *r* (m) and *l* (m) are the radio and the length of the quartz tube and *Q* (m^3/min) is the gas flow rate.

$$\tau = \frac{\pi r^2 l}{Q} \qquad \textbf{Eq. 2-1}$$

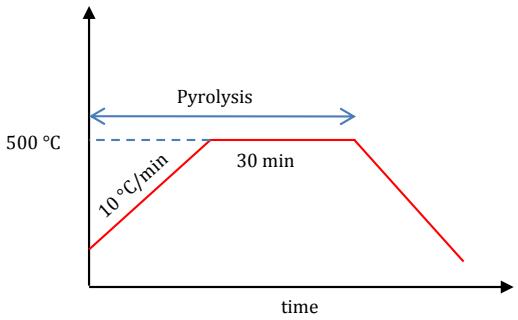

Figure 2-2. Temperature profile of pyrolysis.

Once pyrolysis was finished, the system was cooled down to room temperature under N_2 flow as well. Raw chars are denoted hereafter as MH-Char and BH-Char. Liquid fraction was collected and separated in a light and a heavier fraction (oil) that were both weighted. The oily phase was considered to measure its HHV and humidity since the lighter phase is mainly composed of water and has no energetic value. The measure of HHV is described in section 2.2.1.6. The yield of pyrolysis was calculated according to Eq. 2-2 where m_{Char} refers to the mass of char from pyrolysis and $m_{Biomass}$ denotes the mass of biomass loaded in the reactor. Gas chromatography was able to measure non-condensable gases such as H_2, O_2, N_2, CH_4, CO, CO_2, C_2H_4, C_2H_6, C_3H_8 and C_3H_6 in vol. %. The system performed a complete analysis every 3 min and the mass of each measured species (m_s) was evaluated by Eq. 2-3, where the interval of integration corresponds to the elapsing time of analysis, C_S represents the molar fraction of the detected species and m_s is its molecular weight, Q_{N2} is the nitrogen flow rate and C_{N2} is nitrogen molar fraction, V_m is the molar volume. The LHV of the gas phase was calculated according to Eq. 2-4 where n_i is the mol of gas species *"i"*, n_{gas} is the mol of produced gas and ρ_{gas} is the density of the gas phase. In the former equation P, R and T represent the pressure, ideal gas constant and temperature. Three batches of pyrolysis were prepared from each biomass waste.

$$Y_{Char}(\%) = \frac{m_{Char}}{m_{Biomass}} \times 100 \qquad \textbf{Eq. 2-2}$$

$$m_s = M_S \frac{\dot{Q}_{N2}}{V_m} \int_{t_0}^{tf} \frac{C_S}{C_{N2}} dt \qquad \textbf{Eq. 2-3}$$

$$LHV_{gas} = \frac{\sum LHV_i n_i}{n_{gas} V_m \rho_{gas} 1000} \qquad \textbf{Eq. 2-4}$$

2.1.2. CO_2 activation

Considering that pyrolysis chars will be implemented in tar cracking and hydrogen sulfide removal (gas phase applications), they must have some porosity that provides contact of the molecules in the gas phase with the active sites of the solid. Consequently, pyrolysis chars are submitted to activation aiming improve their textural properties, in particular to develop porosity. In order to choose activation conditions previous literature work was done and is summarized in Table 2-2.

Parameters such as inlet biomass, temperature of activation, initial mass of feedstock, activation time and CO_2:Char ratio were given particular attention. All reviewed papers use similar temperature of activation ranging between 800 and 900 °C. Activation time varied from 30 to 390 min achieving surface areas from 558 to 1700 m^2/g. Other parameter of concern was upper limit of CO_2 (70 vol.%) measured by the gas analyzer.

The pyrolysis of chars followed by their activation with CO_2 is named two-step activation and is described in Figure 2-3. According to this scheme two batchs of char are produced by pyrolysis of biomass under the conditions described in 2.1.1 , the chars are collected and then submitted to activation with CO_2. The condensed fraction is recovered and separated in two phases. The heavier phase is considered to measure HHV and humidity.

Considering the consulted references in Table 2-2, the two-step activation is carried out by loading 80 g of previously dried char into the rotating quartz tube reactor. The reactor was purged by using nitrogen at 0.5 L/min until oxygen concentration in the outlet stream was less than 5 vol.%. The system was heated at 10 °C/min under N_2 flow of 0.75 NL/min and activation temperature was fixed at 850 °C. At that point CO_2 was introduced in excess at 2.1 NL/min (70 vol.%) and N_2 was set at 0.9 NL/min (30 vol.%). Activation was maintained for 80 min, subsequently the reactor was cooled down under N_2 atmosphere to room temperature. No other chemicals were used in this process. Two batches of activated char were prepared from each char. The condensed fraction from the process is already recovered in pyrolysis (step 1); in the CO_2 activation stage (step 2) there is no generation of liquid phase.

Table 2-2. Literature review of biomass CO_2 activation conditions.

Biomass	Pyrolysis			CO_2 Activation					Ref
	Biomass initial mass (g)	Conditions	time (min)	Char initial mass (g)	Conditions	time (min)	Surface Area (m^2/g)	Total Volume (cm^3/g)	
Coconut shell	n.s	T = 600 °C Heating rate = 10 °C/min	120	30	T = 900 °C Heating rate = 50 °C/min CO_2 flow: 800 mL/min	240	1700	1,135	[68]
Wood waste (silver fir)	12.000	T = 600 °C	360	n.s	T = 800 °C CO_2 flow = 74 mL/min	390	815	0,45	[58]
Date stones	75	T = 700 - 900 °C Heating rate = 15 °C/min	n.s	n.s	T = 900 °C CO_2 flow = 250 mL/min	n.s	604	n.s	[155]
Oak	200	T = 500 °C	60	n.s	T = 900 °C CO_2 flow rate = 10 NL/min	n.s	1126	n.s	[87]
Date palm pits	10	T = 800 °C Heating rate = 20 °C/min	60	n.s	T = 1063 °C Heating rate = 20 °C/min CO_2 flow = 5.1 mL/min	68	980	0,61	[71]
Taixi anthracite	30	T = 700 °C Heating rate = 8 °C/min	40	n.s	CO_2 flow = 400 mL/min	68	1379	0,684	[156]
Peanut shells	40	T = 500 °C Heating rate = 10 °C/min	60	n.s	T = 900 °C CO_2 flow = 2500 mL/min	300	1060	0,802	[157]
Cocoa shell	35	T = 800 °C Heating rate = 15 °C/min	60	n.s	T = 850 °C	30	558	n.s	[158]
Olive-mill waste water	n.s	T = 350 °C Air flow = 300 mL/min	60	n.s	T = 840 °C CO_2 flow = 300 mL/min	n.s	1038	n.s	[73]
Pistachio-nut shells	10	T = 500°C N_2 flow = 150 mL/min Heating rate = 10 °C/min	120	n.s	T = 800°C Heating rate =10 °C/min CO_2 flow = 100 mL/min	120	1014	n.s	[159]

n.s: not specified

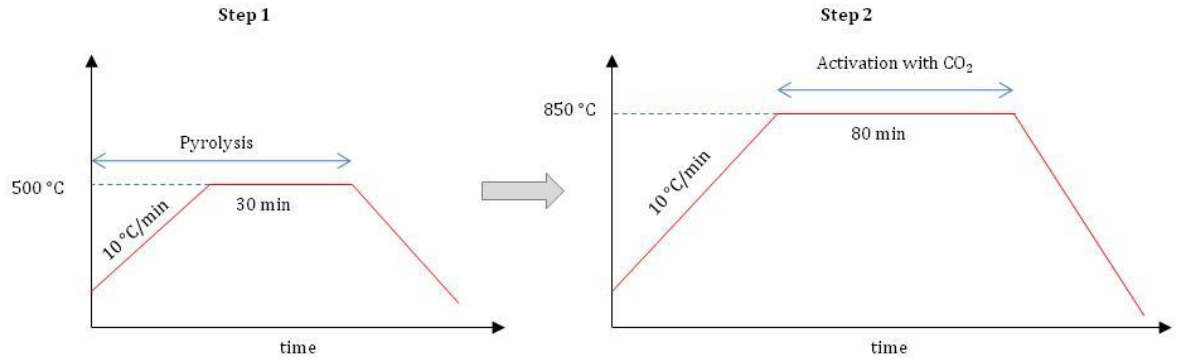

Figure 2-3. Description of two-step activation.

In parallel, one-step activation of the biomass was also carried out in order to compare the energy efficiency of the process with different biomass. Additionally, the two methods of activation allow comparing if activated chars are similar to chars from pyro-gasification process (one-step physical activation). One-step activation is well known as direct activation and is explained in Figure 2-4. In one-step activation, the biomass is pyrolyzed at 700°C for 30 min and immediately activated at 850 °C for 80 min. The higher temperature of pyrolysis in direct activation compared to 2-steps activation is justified with the purpose of improving the gas quality by increasing the H_2 and CH_4 formation which is favored at temperatures >500 °C as has been reported elsewhere [38,39]. The higher quality of the gas is supposed to increase its LHV allowing to recover more energy from this phase.

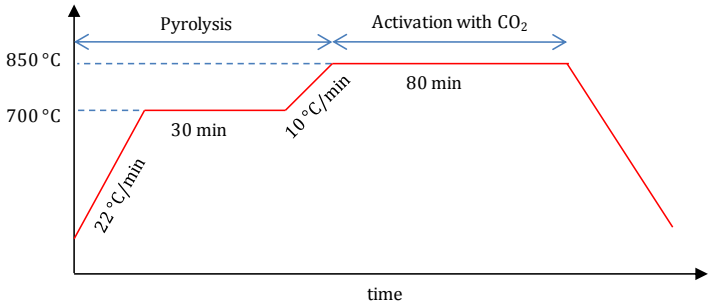

Figure 2-4. Description of one-step or direct activation with CO_2.

The one-step activation was conducted with 100 g of biomass previously dried. The purged reactor is heated at 22 °C/min under N_2 flow until 700 °C and held for 30 min. Then, temperature is raised at 10 °C/min until 850 °C, at that point CO_2 is introduced at 2.1 NL/min (70 vol.%) and N_2 is set at 0.9 NL/min (30 vol.%). Activation was maintained for 80 min, subsequently the reactor was cooled down under N_2 atmosphere to room temperature. Three baths of activated chars were prepared from each biomass. Activated chars are denoted hereafter MH-CO_2 and BH-CO_2.

2.1.3. Steam activation

Same configuration using rotating tube quartz reactor (Carbolite HTR 11/150) was used in steam activation (Figure 2-1). Operating conditions of steam activation are fixed according to activation temperature in CO_2 and previous work [160–164]. With these conditions several activated carbons have been prepared from different precursors such as sugar beet pulp, peanut hulls, millet stalks, cashew shells and rice husks. Surface areas varied from 325 to 1324 m^2/g according to the feedstock used.

100 g of MH and BH previously dried were loaded in the system. As presented in Figure 2-5 the unit was heated at 22 °C/min under N_2 flow at 0.91 NL/min until 700 °C, at that point temperature was maintained for 30 min in order to pyrolyse the raw material. Then temperature was raised to 850 °C at 10 °C/min and atmosphere was switched to H_2O. Steam was introduced into nitrogen flow using a peristaltic pump, at a concentration of 12 vol.% which was given by a water flow of 0.7 mL/min at room temperature. At the same time, Nitrogen was set at 0.53 NL/min (88 vol.%). After 80 min, reactor was cooled down under N_2 flow and activated chars denoted as MH-H_2O and BH-H_2O were collected.

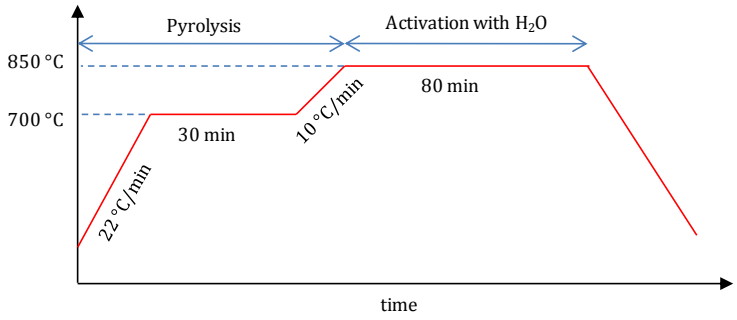

Figure 2-5. Description of one-step or direct activation with steam.

The condensed fraction was collected and separated in a light and a heavier fraction (oil) that were both weighted. The HHV and humidity of the oily phase were measured since the lighter phase is mainly composed of water and has no energetic value. Three batches of steam activated chars were prepared.

2.2. Characterization of chars and their parent materials

The characterization of materials is an important step of this work since the results from these analyses enable to relate the properties of biomass to chars and activated carbons. Therefore, biomass and its derived products were characterized as explained in Figure 2-6.

The TGA analysis allows to determine the biomass composition in terms of cellulose, hemicellulose and lignin contents; the ultimate or elemental analysis measures the CNHS-O composition; proximate analysis quantifies humidity, volatile matter, fixed carbon and ashes; the measure of HHV determine the energetic content of products; and the pHpzc establish if surface of materials are acidic or basic. In order to characterize the textural properties of materials, several analyses are employed at different porosity scale. The N_2 adsorption/desorption isotherms, Hg porosimetry and SEM analyses provide information about the porosity of samples at the micro, meso and macropore scale.

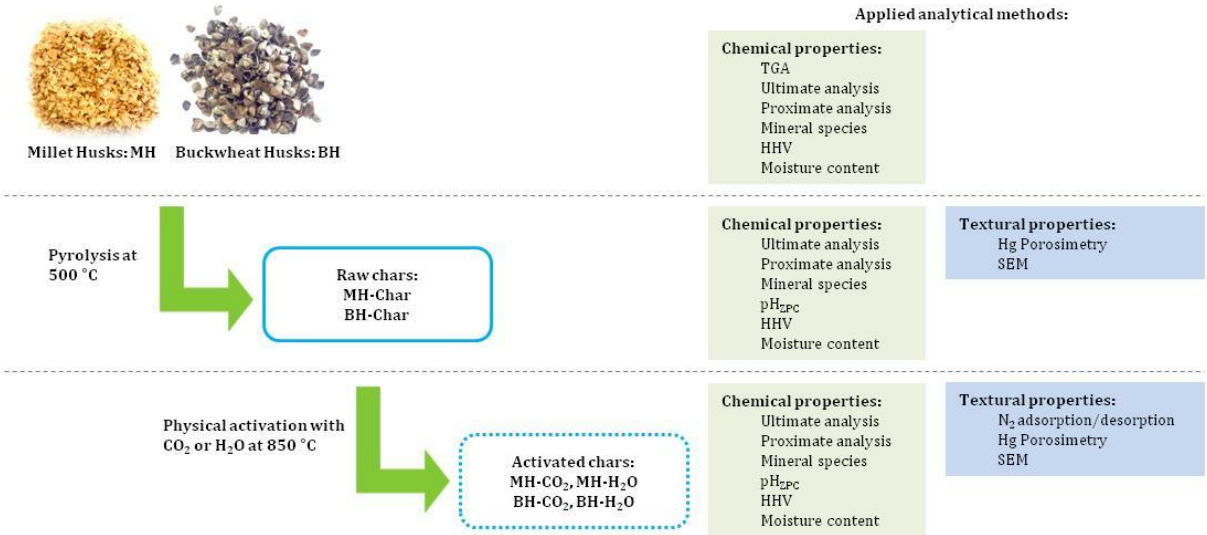

Figure 2-6. Analytical methods applied to each material in order to study its properties.

2.2.1. Chemical composition

The chemical features of materials are given by its organic and inorganic composition. The organic composition refers to the CHNS-O content, mineral species, cellulose, hemicellulose and lignin content. Consequently, the functional groups composed of CHNS-O establish the basic or acidic character of the samples as well as mineral species like carbonates are involved in the basic pH of the surface of materials. Therefore, the analyses carried out to characterize these properties are described in the present section.

2.2.1.1. Thermo gravimetrical analysis (TGA)

During a thermo-chemical conversion process such as pyrolysis of biomass, it is important to understand the evolution of thermal degradation for each constituent that stores chemical energy in biomass. In this respect, cellulose, hemicelluloses and lignin composition were determined since higher lignin content in the biomass enhances development of porosity in the activated char [165].

In TG - dTG analysis of lignocellulosic material two or three peaks usually appear which can be assigned to cellulose, lignin and hemicellulose [60,63,166] as illustrated in Figure 2-7a. Each constituent decomposes at different activation energy namely different temperature intervals depending on the biomass sample. First moisture is removed at 105 °C for 10 min, then when temperature rises up to 200 – 250 °C hemicellulose breaks down in this temperature range for 50 min. Meanwhile, weight lost between of 300 – 400 °C is related to decomposition of cellulose measured for 50 min. Finally, further weight decrease from 300 and 500 °C or even higher temperatures indicates the slow decomposition of the high weight molecule fractions of lignin

which was maintained for 90 min to ensure complete decomposition of this component. Therefore, material composition can be calculated by mass difference between the different ranges of temperature that correspond to each constituent as indicated in Figure 2-7b.

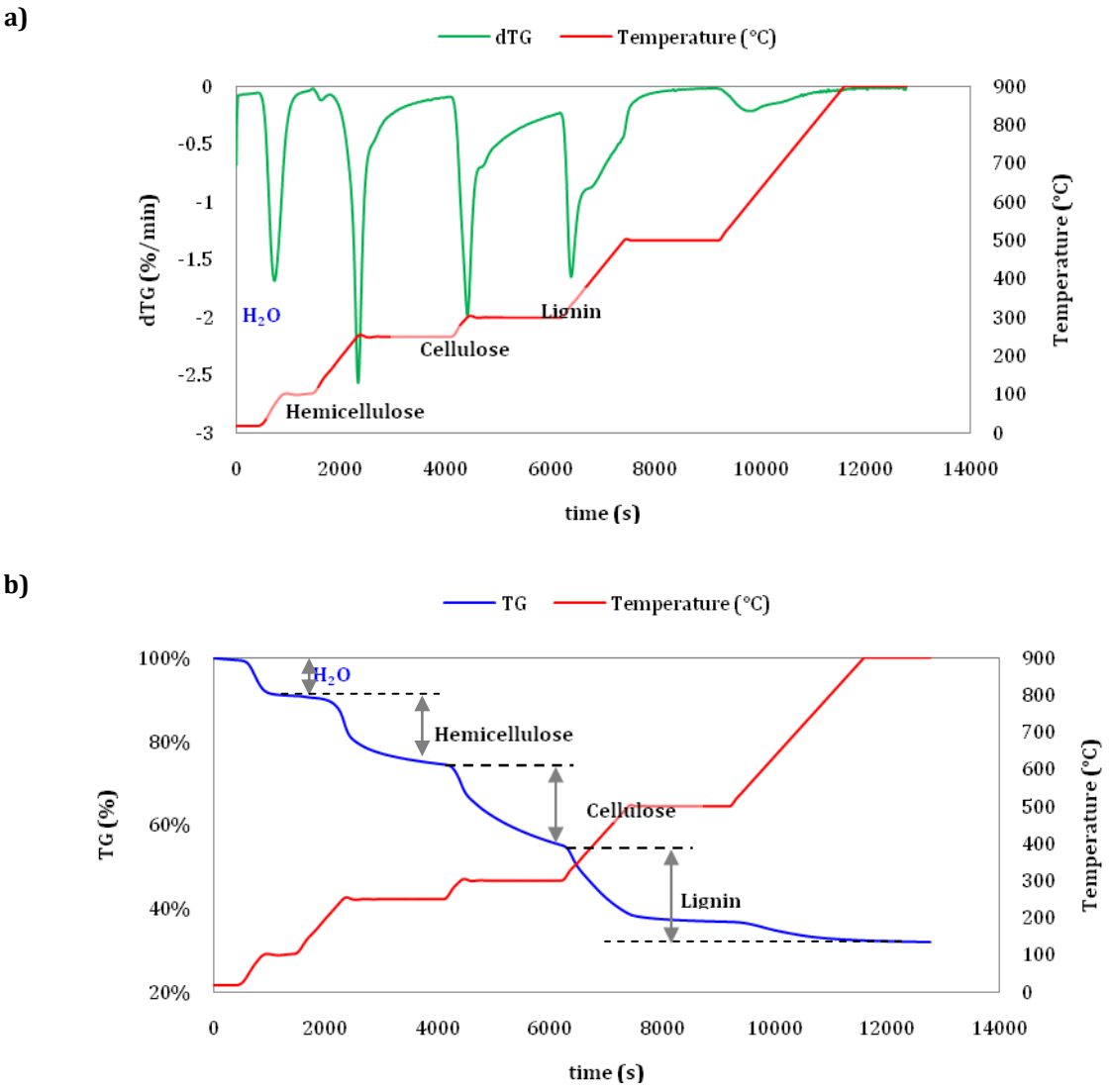

Figure 2-7. Determination of hemicellulose, cellulose and lignin from TG - dTG curves of buckwheat husks.

This technique was carried out in a SETSYS Evolution Thermo Gravimetric Analyzer (TGA). Biomass composition constituents were defined by continuously heating 20 - 40 mg of sample at 10 °C/min under nitrogen atmosphere. The analysis was considered complete when the sample reached constant weight. This analytical method was applied to biomass and its result serves not only to determine cellulose, hemicellulose and lignin content but to fix pyrolysis temperature as the point where carbonization process is completed and there is no further weight loss.

Experiments were carried out twice for each biomass; a blank test without sample was also performed to consider deviations of the crucible weight.

2.2.1.2. Ultimate analysis

Ultimate analysis also known as elemental analysis was performed on samples to determine C, H, N, S and O content using a Thermo Finnigan AE1112 Series Flash. This technique can be applied to biomass, char and bio-oil as well. All solid samples were dried at 105°C for 24h before the analysis. Experiments were carried out in the Thermo Finnigan EA 1112 Series Flash Elemental Analyzer. In order to carry out elemental analysis 0.5 to 1.0 mg of sample are place in a tin capsule (CHNS analysis) or silver (O analysis). For CHNS determination, flash combustion of the samples is performed at 920 ° C in oxygen. This combustion transforms the nitrogen, carbon, hydrogen and sulfur in the sample into nitrogen oxides, CO_2, H_2O, SO_2 and SO_3, respectively. A copper tube reduces the nitrogen oxides to N_2, and the sulfur trioxide (VI) SO_3 to SO_2. The gas mixture passes through a chromatographic column where various constituents (N_2, CO_2, H_2O and SO_2) are successively swept and detected at the outlet stream by a thermal conductivity detector [107]. Based in the calibration performed with reference substances (BBOT and sulfanilamide), content of C, H, N and S are calculated. For oxygen determination, the samples are pyrolyzed at 1000 ° C under helium. The different gaseous elements are separated on a molecular sieve chromatographic column and then analyzed by a thermal conductivity detector. From the same reference substances used for the CHNS quantification, oxygen content of the sample is determined. Ultimate analysis was performed in triplicate for all materials and oils.

2.2.1.3. Proximate analysis

The proximate analysis provides information about the moisture, volatile matter, ash content and fixed carbon determined by carrying out several steps [167]:

- Moisture content is determined as the weight loss at 105 °C until achieving constant weight. Moisture can also be measured by the Karl Fischer method. This technique is a chemical analysis procedure which is based on the oxidation of sulfur dioxide by iodine in a methanolic hydroxide solution according to the following reaction:

$$H_2O + I_2 + SO_2 + CH_3OH \rightarrow SO_4CH_3 + 2I \qquad \textbf{R 2-1}$$

  Therefore, a Karl Fischer solution containing iodine is added by volumetric titration until the first trace of excess iodine is present. Then, the volume of iodine spent is converted to water content considering that 1 mL of reagent there are 4.685 mg of H_2O. The advantage of this method is that it results in accurate water content whereas when

carrying out moisture determination by weight lost at 105 °C, mass decrease can be also related to release of volatiles. The Karl Fischer method was used to determine the moisture content of chars, activated carbons and oils from pyrolysis and activation. The analyses were performed twice for each sample.

- The volatile matter corresponds to the weight lost when the sample is heated under inert atmosphere from 105 to 900 °C according to D3175 ASTM until the stabilization of the weight.
- The ash content of biomass is determined by heating 10 g of the previously dried sample at 10 °C/min until 550 °C under air atmosphere according to ASTM D1102. This analysis was carried out in muffle furnace (Nabertherm P330) by triplicate. The analysis is stopped when the weight is stabilized.
- The ash fraction of chars and activated carbons is determined by heating 15 – 40 mg of material previously dried at 10 °C/min until 650 °C under air atmosphere according to D3174 ASTM Standard. This analysis was carried out in the SETSYS Evolution Thermo gravimetric Analyzer (TGA) by duplicate. The analysis is stopped when the weight is stabilized.
- Finally, fixed carbon is calculated by difference.

The proximate analysis was performed twice for all samples.

2.2.1.4. Mineral species

Interactions with minerals present in biomass are frequently reported to be reactive and therefore influence present activity during thermo-chemical conversion processes such as pyrolysis and pyro-gasification [36,86,117]. Since this property might influence pyrolysis of biomass, syngas and biogas purification, X-ray fluorescence technique was used to identify inorganic elements present in biomass, raw and activated chars. For that matter the X-ray fluorescence spectrometry (SHIMADZU EDX-500HS) was employed. This technique is a semi-quantitative method and the error percentage of this analysis is considered to be around 20 % for the main elements in ash composition.

This analytical method is based on the premise that when a sufficiently energetic x-ray beam interacts with an atom, an electron from the electron cloud can be torn off from the electronic layer to which it belongs with an energy E. The atom is then in a state of great instability. To find a stable state, an electron located on a higher energy level is likely to fill the free space by then emitting an electromagnetic radiation (X-ray photon) whose energy is characteristic of the chemical element [168].

Analyses were carried out under vacuum on the samples of the different materials: biomass, raw and activated chars. In the case of biomass (MH and BH) the analyses were executed employing ashes of each material that were obtained from 10 g of material in triplicate. Biomass were dried and then burned for 24 hours in a muffle furnace (Nabertherm P330) at 550 °C, temperature reached with a heating rate of 10 °C/min. This previous step was carried out in order to concentrate inorganic content of biomass. Meanwhile, analysis of raw and activated chars was performed using fresh materials since ash content is higher. The acquisition time of the analyses was 100 seconds. Every analysis was done in triplicate for each material considering the heterogeneity of biomass and chars.

2.2.1.5. pH of zero point charge (pH_{ZPC})

Determination of the surface pH of activated chars was carried out once by the point of zero charge method (ZPC) [107,161,169]. For that matter, 50 mL of 0.01 M NaCl solution was placed in several closed Erlenmeyer flasks. The solutions pH was adjusted between 2 and 12 using NaOH and HCl 0.1M solutions. Then, 0.15 g of char was added, and the final pH was measured after 5 days under agitation at room temperature. The pH_{pzc} was defined as the point where the curve pH_{final} vs $pH_{initial}$ crosses the line $pH_{final} = pH_{initial}$.

2.2.1.6. Higher Heating Value (HHV)

In order to carry out the energy balances of pyrolysis and activation, the Higher Heating Value (HHV) of materials and oils must be determined. The HHV is an important fuel property which defines the energy content of the fuel [17]. This analysis was performed at least twice for biomass, raw and activated chars and oils. HHV was measured experimentally using an oxygen PARR 6100 bomb calorimeter. This device burns the sample in the presence of oxygen inside a sealed container. The heat released from combustion is transferred to a mass of water that surrounds the container. For humid fuels, heating value must be corrected because a portion of the combustion heat is used to evaporate water in the biomass. Therefore, LHV is calculated from the measured HHV by subtracting the heat of vaporization of water in the products. A more accurate estimate of LHV can be obtained by including the heat released by the combustion of the hydrogen content of the biomass using Eq. 2-5 [170]:

$$LHV = HHV - M \times 2.260 - H \times 20.3 \qquad \textbf{Eq. 2-5}$$

where M is the moisture content (mass fraction) and H is Hydrogen content (mass fraction) from elemental analysis. If biomass is dried before the analysis, moisture content is zero. Therefore, final equation is as follows:

$$LHV = HHV - H \times 20.3 \qquad \text{Eq. 2-6}$$

2.2.2. Textural properties

During pyrolysis, the devolatilization process develops a rudimentary porosity in the char mainly at the macropore level whereas activation creates a more developed pore structure varying from micropores to macropores. Porosity is composed of pores with different pore sizes which are categorized according to IUPAC as follows [171]:

a) pores with widths exceeding about 50 nm are called macropores;
b) pores of widths between 2 nm and 50 nm are classified as mesopores;
c) pores with widths not exceeding about 2 nm are named micropores.

It has been stated that the inner pore configuration of chars is closely related to its pollutant removal capacity since it might influence distribution of active sites and transport of reactant molecules [109,147,172–174]. Thus, it is important to analyze such structure in terms of surface area, pore distribution and pore size. For that matter, techniques at different scales were used during this study. These methods include nitrogen gas sorption analysis, mercury porosimetry and Scanning Electron Microscopy (SEM). The volumetric technique based on nitrogen gas adsorption-desorption is not adapted to chars from pyrolysis with low surface area. For these materials, the quantity of gas adsorbed by the sample may be less than the amount of nitrogen introduced into the dead volume [171].

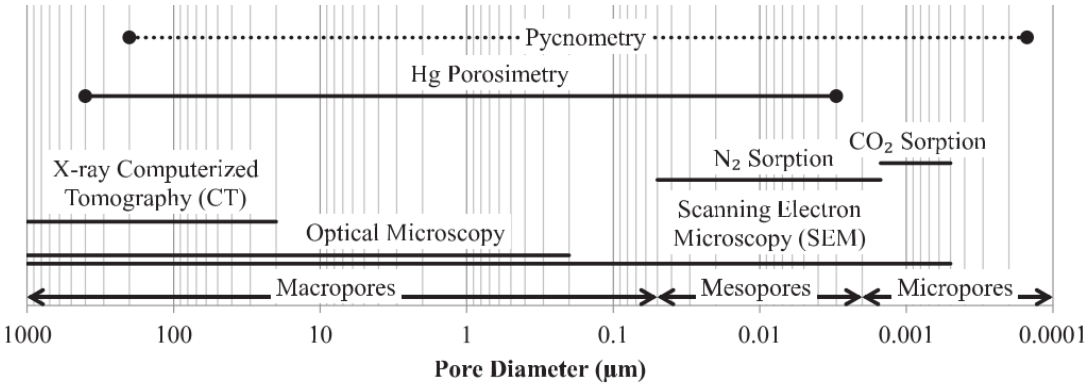

Figure 2-8. Pore size ranges and characterization techniques. Adapted from Brewer et al. [41].

According to Figure 2-8 there are more than a few techniques to study porous materials in relation to pore size. Thus, in order to study porous features of chars within the whole pore size range, it was necessary to couple characterization techniques so that they complement each other. Indeed, nitrogen adsorption with BET analysis is used to characterize pores in the micro and mesopore range (from ~0.4 nm to 50 nm). However, this method does not provide information about macropores which are present in char samples [32]. Therefore, SEM and

mercury porosimetry are applied to characterize porous structure at macropore level. The mercury porosimetry covers porosity in the 8 – 580,000 nm while SEM allows observing the surface of materials at the meso and macropore scale and a part or micropores.

2.2.2.1. Nitrogen adsorption – desorption

One of the methods to characterize porous structure, pore volume and surface area of porous materials is gas adsorption using nitrogen. This method developed by P.H. Emmett and S. Brunauer (1934) consists of injecting nitrogen at known pressure into a chamber of a given volume containing the sample which is kept under vacuum. During the test, sample is kept at constant temperature in a liquid nitrogen bath (at about 77K). For each nitrogen injection, the temperature and pressure of the system are recorded when the thermodynamic equilibrium is reached. The quantity of gas adsorbed by the sample corresponds to the sum of the differences between the quantity of adsorbate initially injected and the quantity of adsorbate remaining in the gas phase at the thermodynamic equilibrium. The set of equilibrium points (adsorbed quantity as a function of the nitrogen partial pressure) makes it possible to trace the adsorption isotherm. Adsorption-desorption analysis was held twice for activated chars. In this study, two equipment were used: Micromeritics ASAP 2020 and Micromeritics 3-FLEX. The equipment Micromeritics 3-FLEX can conduct a deeper degas thus the surface areas (BET) provided by this equipment can be slightly (~10 %) higher than those given by ASAP2020. This improved degassing also results in mesoporous volumes more accurate and higher than those provided by ASAP 2020. The nitrogen adsorption/desorption analyses were performed twice for each activated carbon.

Types of adsorption isotherms and hysteresis loops

Adsorption isotherms may be grouped into the six types as shown in Figure 2-9. Each type of isotherm is described below [175]. The reversible Type I isotherm is concave to the relative pressure axis. This type of isotherms is given by microporous solids with small external surfaces, the adsorption is limited by the accessible micropore volume rather than by the internal surface area.

Type II isotherm is particular of a non-porous or macroporous adsorbent. This curve represents unrestricted monolayer-multilayer adsorption. Point B, is often taken to indicate the stage at which monolayer coverage is complete and multilayer adsorption about to begin. Type III isotherms are not common. The reversible isotherm is convex to the relative pressure axis over its entire range. In such cases, adsorbent-adsorbate synergy plays an important role.

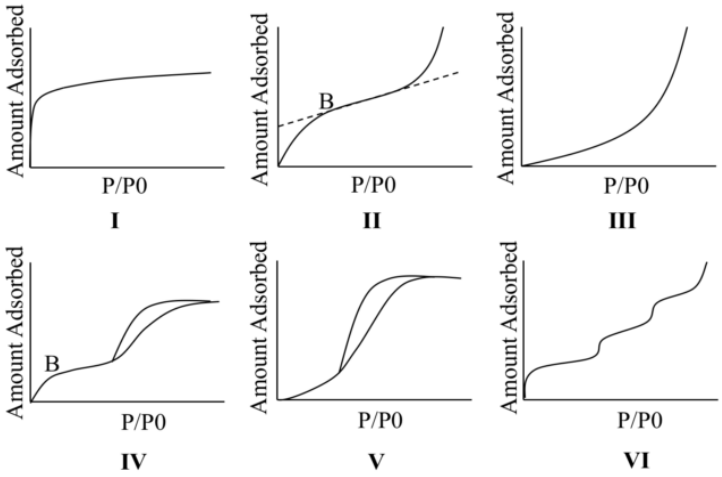

Figure 2-9. Types of adsorption isotherms found by nitrogen adsorption-desorption taken from [176]**.**

The feature most representative of the type IV isotherm is its hysteresis loop, which indicates capillary condensation at the mesopore level, and the limited uptake at relative pressure. At low relative pressure, the curve is associated to monolayer-multilayer adsorption since it follows the same path as the corresponding part of a type II isotherm. It is known that many mesoporous industrial adsorbents exhibit type IV isotherms.

The type V isotherm is rare; it is related to the type III isotherm considering that the adsorbent-adsorbate interaction is weak, however some porous adsorbents reveal this type of curve. Finally, type VI isotherm represents stepwise multilayer adsorption on a uniform non-porous surface [176].

Models used in nitrogen adsorption-desorption

BET method (surface area)

The BET model developed by Brunauer, Emmet and Teller in 1938, still remains the most diffuse tool to calculate surface area and porous volume of solids. This model is based on the principle of formation of multilayers but only the first layer of adsorbate molecules is attached to the solid surface by adsorbent-adsorbate adsorption forces. However, BET model has been criticized because real surfaces don't follow the postulation of the method. Currently BET model is the most applied to determine surface areas thus it can be taken as a reference method [176,177].

t-plot method (surface area, micropore and mesopore volume)

This method was developed in 1965 by DeBoer and coworkers and it establishes that for a macroporous solid material the adsorbed volume for unit surface against pressure results in a

single curve which is the same for every solid [177]. Thus, any deviation from the linear (non-porous solid) curve can be related to the presence of porosity. This method allows calculation of surface area and micropore and/or mesopore volume. It is recommended that a reference isotherm from a similar material to the sample is used. Indeed, when changing the reference isotherm both the slope and intercept of the curve change. In such a way, the disadvantage of this method is that a reference isotherm appropriate for all materials does not exist.

Horvath-Kavazoe method (micropore volume and micropore size distribution)

This model was developed by Horvath and Kavazoe in 1983 in which pore size is related to the relative pressure at which the pore is filled by the adsorbate. This model can be used in activated carbons however; it should be used carefully in ultramicroporous materials (D_p < 0.7 nm) since progressive filling of pores might be interpreted as a non-uniform size distribution [176,177].

BJH method (mesopore volume and mesopore size distribution)

In 1951 Barrett, Joyner and Halenda developed the BJH model which uses the desorption points of the isotherm to perform calculations in the mesopore region and cannot be applied to the microporous region. The principle of the method is that progressive adsorption reduces the free pore space available for capillary condensation due to multilayer adsorption. In order to employ this method, it is necessary to assume a geometric model usually cylindrical or slit shaped. The BJH method is still widely used by commercial instruments to calculate mesopore volume and mesopores size distribution [175–177].

Experimental procedure and analysis

Surface areas, microporous and mesoporous volumes of activated chars were measured by means of nitrogen adsorption / desorption at -196 °C using a Micromeritics ASAP2020 and Micromeritics 3-Flex volumetric apparatus. Prior to the measurements, samples must be degassed in other to remove species adsorbed in its surface. Degassing of materials is usually achieved by exposing the chars to a high vacuum at high temperature. However, outgassing at too elevated temperature or under ultra-high vacuum conditions (residual pressure < 1 μPa), may lead to changes in the surface composition, e.g. decomposition of hydroxides or carbonates, formation of surface defects or irreversible changes in texture. Therefore, outgassing temperature must be properly chosen considering the range over which the thermal gravimetric curve obtained in vacuum shows least possible slope [171,176]. In this study, samples were degassed under vacuum for 48 h at 350 °C using a heating rate of 10 °C/min.

Surface areas were determined by applying the BET theory. Volume and size distribution of micropores were calculated using the Horvath-Kavazoe model. The BJH model was applied to the desorption isotherm to determine mesopore volume. This characterization technique was carried out on all the activated carbons or activated chars. This technique is not suitable for chars resulting from pyrolysis with negligible porosity thus low surface area; therefore, they were analyzed by mercury porosimetry.

Lastly, the relative microporsity is defined as the percentage of micropores relative to the presence of mesopores and is calculated using Eq. 2-7 where V_{micro} and V_{meso} are the micro and mesoporous volumes respectively.

Relative microporosity $$R_{micro}(\%) = \frac{V_{micro}}{V_{meso} + V_{micro}}$$ **Eq. 2-7**

2.2.2.2. Mercury porosimetry

Mercury porosimetry makes it possible to characterize the porous structure of a material (surface area and pore size distribution) specifically for pore diameters larger than 8 nm, hence some mesopores and macropores. In this technique the sample cell is filled with mercury while the system is under reduced pressure. Then, pressure is increased slowly allowing mercury to penetrate pores in the sample or any void spaces between sample particles. One of the most important limitations of mercury porosimetry is that it measures the largest entrance towards a pore, but not its actual inner size. In addition, this technique cannot be used to analyze closed pores since the mercury has no way of entering into those pores (Figure 2-10).

According to literature, most of the pore volume of pyrolyzed chars is in macropore range, thus is not measured by nitrogen gas sorption analysis. According to literature [178,179] there are several parameters that can influence accuracy of data from mercury porosimetry analysis, among them are:

- Compressibility of mercury with increasing pressure
- Compressibility of the sample which can cause error in the measure of volume. Indeed, compressibility can vary from 10^{-9} to 10^{-11} m^2/N [178,180]. However, it can be higher in presence of open or closed pores.
- Retention of mercury after extrusion. This is due to the ink-bottle type pores or other shape pores with constricted “necks” since Washburn equation uses the diameter of the entrance of the pore and not the largest diameter of the pore.
- Considering cylindrical pore geometry might not represent the real porous shape of the sample.

- Assumption of constant contact angle between mercury and solid material.
- Pore breakdown when increasing pressure to force mercury into the pores.

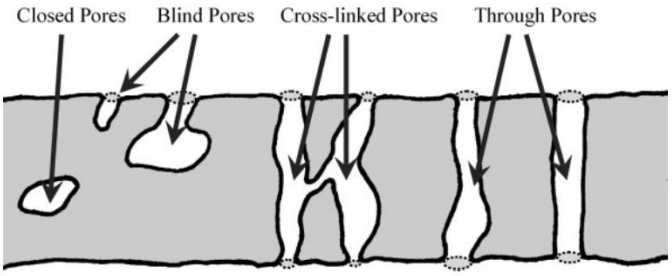

Figure 2-10. Schematic representation of pores types taken from [179].

Experimental procedure and analysis

Mercury porosimetry analysis was performed twice for raw and activated chars in a Micrometrics Autopore IV. Values of mercury surface tension and contact angle used in the software of the porosimeter were 0.485 N/m and 154.9°. Macropore volume (V_{ma}) was defined as the cumulative pore volume at pores sizes larger than 50 nm. Meanwhile mesopore volume (V_{me}) was calculated as the difference between cumulative volumes at 8 and 50 nm. Then cumulative pore volume of macro- and mesopores was derived as V_{ma} + V_{me}. Prior to analysis, samples were dried at 105 °C.

Pore distribution and porous volume

From experimental data obtained by mercury porosimetry, pore diameter is calculated as the amount of mercury that can be inserted into the pores of a sample in function of intrusion pressure according to Washburn equation [181]. Since mercury is a non-wetting liquid, pressure must be applied so it can penetrate into pores of the sample. The pore diameters D can be calculated from the applied pressure as illustrated by Eq. 2-8 where γ is mercury surface tension, θ is the contact angle between mercury and solid and P is the applied pressure. The smaller size of the pore, the greater the pressure to be applied to mercury.

$$D = \frac{-4\gamma \cos\theta}{P} \qquad \textbf{Eq. 2-8}$$

2.2.2.3. Scanning electron microscopy (SEM)

Scanning electron microscopy can be used to observe the surface and texture of materials. Coupled with a dispersive energy X-ray spectroscopy (EDX) microanalysis system, local

information about mineral species in the surface of the sample can be obtained. In this work, the SEM technique is used to examine external characteristics of materials as well as to observe the distribution of mineral species on the surface of chars. SEM images are the result of the interaction between an electron beam and the surface of a material radiating secondary electrons, backscattered electrons, X-rays, photons and heat. These secondary electrons return to the detector at different intensities depending on their orientation. The detection of backscattered electrons makes it possible to obtain a color contrast on the SEM images due to the difference in atomic number between the elements present. This method allows studying the spatial differences in chemical composition of a sample. Since mineral species are heavier elements than the carbon matrix, the first ones appear brighter than the carbon surface [107].

Experimental procedure

Chars were characterized by a ZISS DSM982 SEM equipped with a high-resolution Gemini column operating at a voltage of 10-15 kV. Before the analysis, chars were covered with a layer of 2-3 nm Au / Pd to ensure good electrical conductivity. Spatial chemical composition was observed by a dispersive energy X-ray spectroscopy (EDX) microanalysis system (Noran Voyager IV).

2.3. Experimental configuration of syngas and biogas treatment

With the aim of testing performance of chars in the treatment of syngas and biogas, a reactor was built in the laboratory in order to be able to use raw and activated chars in a fixed-bed allowing the gas stream to go through it. The fixed-bed column is a vertical cylinder in stainless steel (length: 15 cm; internal diameter: 2.15 cm) which is inserted inside an electrical furnace to control temperature.

Three thermocouples made it possible to measure the temperature at the heart of the bed as well as at the foot and at the reactor head. In addition, a plate with different gases was assembled with the aim of testing syngas and biogas with varying compositions. Pictures of reactor, furnace and plate gas are presented in Figure 2-11.

These elements compose the system used for syngas and biogas treatment. Different configurations were employed according to the gas used (syngas or biogas). Each configuration will be described in the following sections. Pressure sensors were placed upstream and downstream of the reactor in order to detect any leak during the tests. For safety reasons, the system was installed in a ventilated and closed room conceived for these experiments.

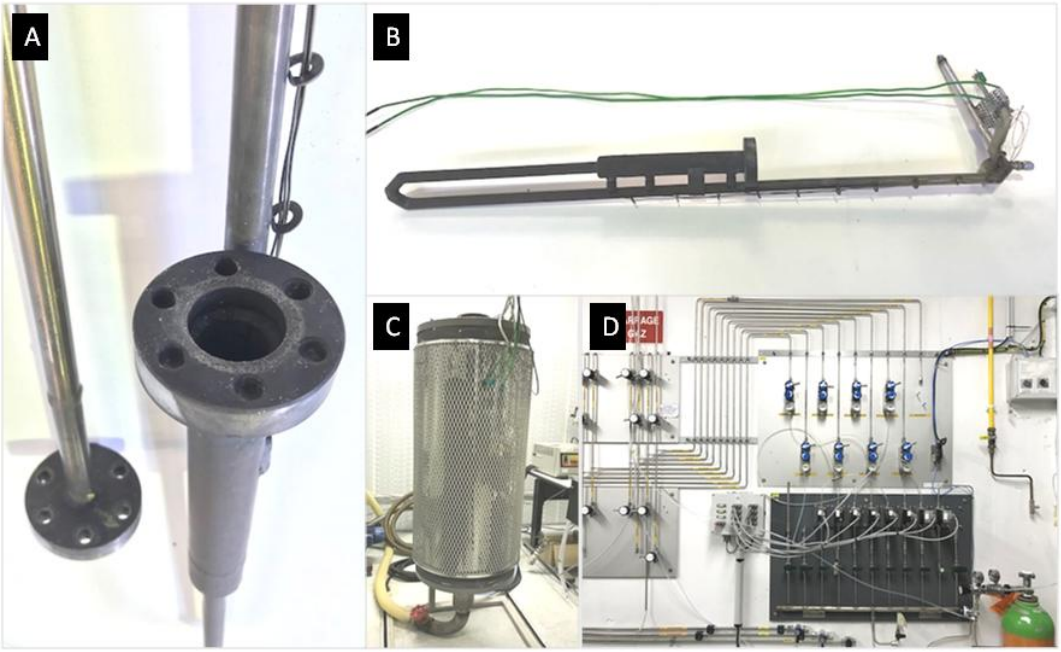

Figure 2-11. Main elements of experimental configuration of syngas and biogas tests. A) and B) Reactor, C) Electrical furnace, D) Gas plate.

2.3.1. Syngas upgrading

The experimental configuration assembled for syngas upgrading is presented in Figure 2-12. The gas plate allowed studying performance of chars with different compositions of syngas.

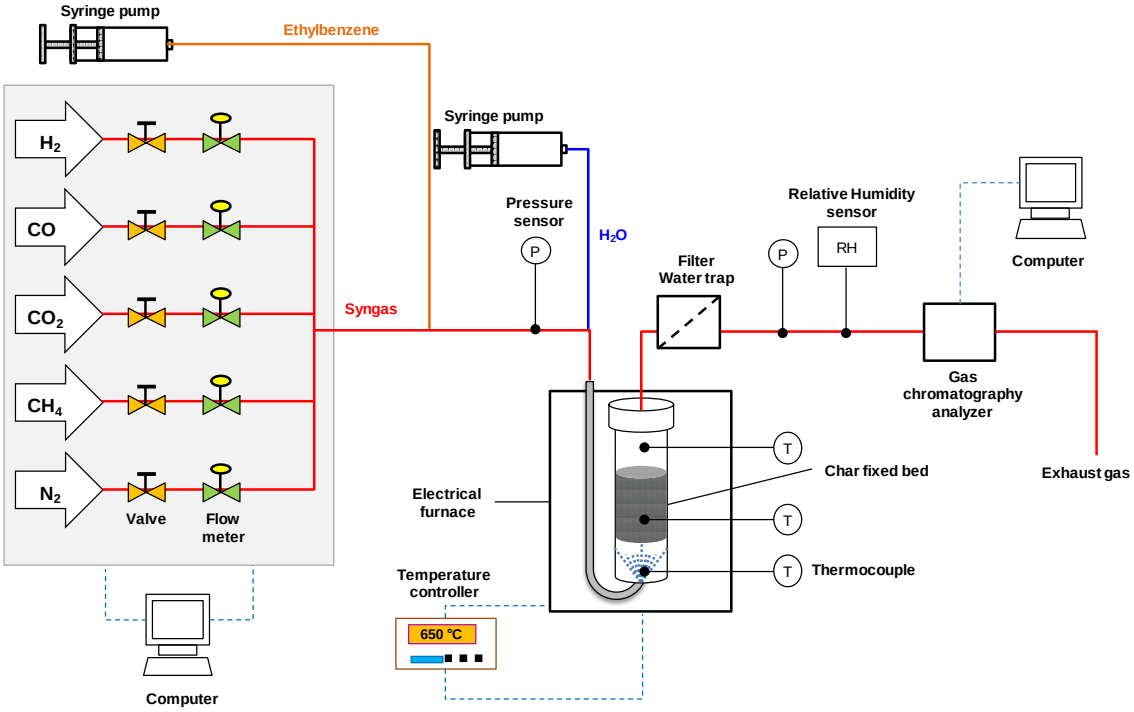

Figure 2-12. Experimental configuration of syngas tests.

The gas is preheated in the inlet tube (L: 1.02 m) of the reactor placed at the bottom of the column. Catalytic cracking of tars takes place during the passage of the ascending gas through the fixed-bed of char supported by a grid. An additional grid in the outlet of the reactor (upper part) was placed to prevent losing the granulated char. An upward flow was chosen to avoid settling of the catalytic bed favoring preferential paths. Outlet gas composition was measured on line with a gas chromatograph analyzer (SRA Instruments R3000). The gas analyzer was calibrated with ethylbenzene (C_8H_{10}) and typical tar components of different concentrations such as benzene (C_6H_6) and styrene (C_8H_8). This technique was able to measure non-condensable gases like N_2, H_2, CH_4, CO and CO_2. The system performed a complete analysis every 3 min, the mass of each measured species (ms) was evaluated according to Eq. 2-3. Analysis conditions of gas chromatography were presented in Table 2-1.

Tests were carried out at 650 °C since it is the average syngas outlet temperature of the gasification process [182] thus, additional energy is not required to heat the gas stream. It is worth noting that tar cracking is influenced by temperature and usually in the absence of catalyst tar conversion is carried out at higher temperatures [57,101,103]. Chars performance in syngas purification was tested using ethylbenzene (EB) as surrogate of one-ring aromatic hydrocarbons which make up to 66% of tar from biomass gasification [100,106]. Ethylbenzene at 40 g/Nm^3 was injected to the syngas with a syringe pump of 50 mL. It is worth mentioning that the selected tar concentration is within the range of typical syngas tar content (5 – 75 g/Nm^3). Likewise, steam was injected using a syringe pump of 50 mL. Three different matrices were implemented which are presented in Table 2-3.

Table 2-3. Composition of the different gaseous matrices that were studied for tar cracking.

Gas matrix	H_2 (vol.%)	CO (vol.%)	CO_2 (vol.%)	CH_4 (vol.%)	N_2 (vol.%)	H_2O (vol.%)	EB (g/Nm^3)
Simple	0	40	0	0	60	0	40
Dry syngas	23	17	15	11	34	0	40
Humid syngas	20	15	13	10	30	12	40

Experiments were started using a simple gas matrix composed of N_2 and CO in order to evaluate char's performance in ethylbenzene removal. Then a dry syngas composed of H_2, CO, CO_2, CH_4 and N_2 was implemented to examine the influence of gas species in tar cracking. Finally, a humid syngas with the same composition than the previous matrix adding H_2O was employed in order to observe the influence of steam in the ethylbenzene conversion.

Total gas flow rate was fixed in order to obtain a gas velocity in the column of 0.1 m/s. This speed is lower than those commonly encountered in fixed bed gas treatment (from 0.3 to 1 m/s), and aims to limit the pressure losses caused by the fixed-bed [107]. This flow rate was calculated according to prevailing conditions of pressure (1 atm) and temperature (650 °C) using Eq. 2-9:

$$Q_{gas} = u_0 \times s = u_0 \times \left(\frac{\pi d_i^2}{4}\right) \qquad \textbf{Eq. 2-9}$$

where Q_{gas} is the total flow rate, u_0 is the gas speed, s is the cross area of reactor and d_i is the internal diameter of the column. Based on the dimensions of the column and operational conditions, the calculated total flow rate resulted in 0.68 NL/min or 2.2 L/min at 650 °C which was the same for every syngas experiment. Gas flow rates (in NL/min) were controlled by mass flow meters.

The height of the fixed-bed of materials is selected in order to obtain residence times of the volatiles passing through catalyst bed close to those used by other authors (0.2 – 0.4 s) [103,115], as well as a duration of experimentation lower than 6 hours. Therefore, the height of the fixed-bed was 4 cm for all materials in order to work at constant bed volume. A blank test with an empty column was also carried out in order to determine the thermal cracking of ethylbenzene at 650 °C. Experiments were performed twice for activated chars, however raw chars were tested once since results were no different from ethylbenzene cracking with an empty column. Thermal cracking was evaluated three times in order to obtain representative figures. With the aim of studying possible reactions between the gas mixture and chars at 650 °C, blank tests with char in absence of EB were carried out.

Materials were dried in an oven at 105 °C before experiments in order to avoid reactions between the released steam and tars, and performing mass balances on the mass of the fixed-bed of char. The system was heated up under a nitrogen flow, then when the temperature was stable at 650 °C, a leak test was performed. Once the leak test was validated, different gas species were fed according to the composition of the gas mixture until reaching equilibrium state. Next, the syringe pump was started and drained into a glass container until the flow was constant. The cracking test began when the ethylbenzene flow was connected to the system. At the end of the test, the flow of ethylbenzene and furnace were stopped, and the system was purged using nitrogen flow until complete cooling of the reactor (T <60 ° C). Experiments were performed twice for activated chars and once for raw chars.

Performance of chars

The materials performance in the catalytic removal of tars is often presented as a percentage of converted tar which is the difference between inlet and outlet tar concentration, divided by the tar concentration in the inlet stream [111,116,118,172] as shown in Eq. 2-10.

$$Y_{EB}\,(\%) = \frac{EB_{in} - EB_{out}}{EB_{in}} \qquad \textbf{Eq. 2-10}$$

However, Eq. 2-10 has two limitations. The first one is that it does not allow to discriminate thermal cracking from performance of materials and the mass of the latter is not considered. In this study, a different approach was taken with the purpose of overcoming these limitations. Therefore, efficiency of materials was defined in terms of tar conversion (X_{tar}) calculated as grams of ethylbenzene cracked per gram of sample excluding thermal cracking according to Eq. 2-11 where C_0 is the inlet ethylbenzene concentration (g/Nm^3), C_t is outlet ethylbenzene concentration at time t (g/Nm^3), C^* is ethylbenzene thermally cracked at time t (g/Nm^3), Q_{gas} is the inlet total gas flow (Nm^3/min) and m_{char} is the initial mass of the char (g).

$$X_{tar} = \int_{t_0}^{t} \frac{C_0 - C_t - C^*}{m_{char}} Q_{gas} \qquad \textbf{Eq. 2-11}$$

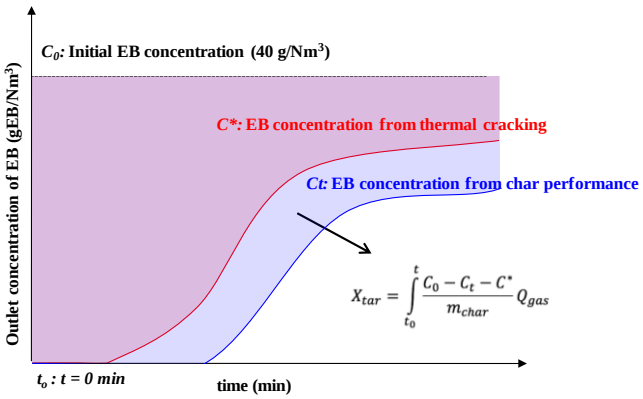

Figure 2-13. Calculation method of performance defined as tar conversion due to presence of chars.

The Figure 2-13 gives a graphical explanation of the above equation: the curve in red represents the thermal cracking and the blue breakthrough curve is the global tar cracking due to the thermal cracking and efficiency of a given material. The area between these 2 curves is proportional to the efficiency of materials.

2.3.2. Gasification of exhausted materials in syngas upgrading

The gasification of exhausted materials was implemented in order to perform a preliminary study of a potential final use for these materials after syngas treatment. Operational conditions were chosen according to literature. In general, temperature of gasification varies between 800 to 1500 °C [45] therefore 900 °C was selected with the intention to consume less electrical energy compared to other studies. Different oxidants can be used in gasification such as H_2O, CO_2, O_2 or air [120,124,183,184]. A mixture of H_2O and CO_2 was preferred considering the synergistic effect between steam and carbon dioxide on the gasification [95,96]. Therefore, composition of gasification atmosphere was 40 vol.% H_2O, 20 vol.% CO_2 and 40 vol.% N_2 according to the work of Gao and coworkers [96]. Initial mass of materials was 0.5 g in order to reduce time of experiments.

The gasification process can be evaluated in terms of syngas quality which is related to its composition, heating value [185], and possible impurities contained. It is important to mention that LHV and ash content should also be taken into consideration to choose the precursor of gasification. Indeed, high ash content in the precursor (41 – 46 wt.%) generates operational problems reducing life of gasifier. Besides, high ash content increases syngas cleaning cost and low carbon content weakens LHV of produced syngas [45]. According to this, MH-Char, MH-CO_2 and MH-H_2O are not suitable to be used in gasification since its high inorganic content represents difficulties to carry out oxidation of these chars. Consequently, only BH-CO_2 and BH-H_2O were submitted to gasification after deactivation in syngas upgrading.

Experimental procedure

BH-CO_2 and BH-H_2O were dried in an oven at 105 °C before carrying out the tests. Materials are first used in ethylbenzene conversion under a simple mixture (CO + N_2) at 650 °C until they reach a saturation state (deactivation). Then the reactor is heated up under a nitrogen flow until 900 °C. When temperature stabilizes the atmosphere was changed to H_2O + CO_2 following the above-mentioned composition. Steam was introduced to the system by means of a pump syringe of 50 mL. Production of syngas was followed by gas chromatography in real time. Gasification process was carried out until production of H_2 was close to zero. At the end of the test, furnace was cooled down under nitrogen flow (T <60 ° C) and remaining ashes were recovered. The gasification was performed once for BH-H_2O and twice for BH-CO_2 in order to check the reproducibility of this experiment.

2.3.3. H_2S removal from biogas

The experimental configuration assembled for H_2S removal from biogas is presented in Figure 2-14. The gas plate allowed studying capacity of chars with different compositions of biogas. The inlet of gas is placed at the bottom of the column and removal of H_2S takes place during the passage of the ascending gas through the fixed-bed of char. Outlet gas composition is measured on line with ProCeas analyzer which measures the concentration of H_2S, CH_4 and CO_2 in a giving stream by means of enhanced absorption spectroscopy. Its detection limit for H_2S is 10 ppb. This equipment is calibrated at its point of manufacture. In addition, gas chromatography was also implemented to follow N_2, CH_4 and CO_2.

Since biogas is usually produced at ambient temperature varying from 25 to 55 °C [130,186] tests were carried out at average temperature of 30 °C. In the case of biogas, performance of chars is related to the capacity of chars to adsorb H_2S. The tests were performed injecting 200 ppm of H_2S to the gas. It is worth mentioning that the selected H_2S concentration is within the range of typical biogas composition (0 – 4000 ppm) [129,131,137]. Three different matrices were implemented which are presented in Table 2-4.

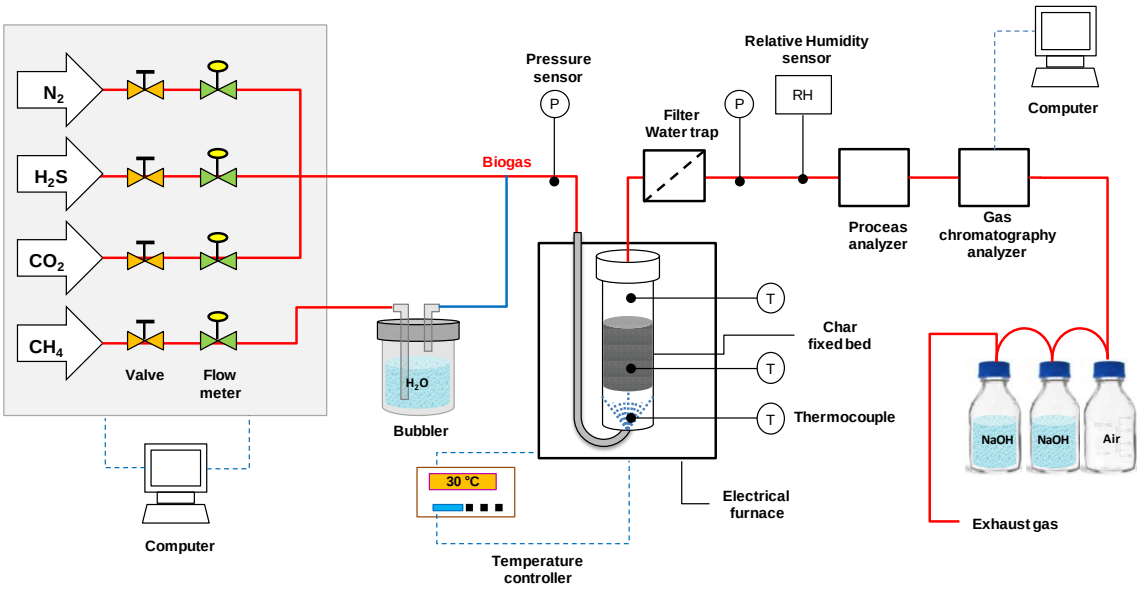

Figure 2-14. Experimental configuration of biogas tests.

Table 2-4. Composition of the different gas matrices that were studied for H_2S removal.

Gas matrix	N_2 (vol. %)	CH_4 (vol. %)	CO_2 (vol. %)	H_2O (vol. %)	H_2S (mg/m³)
Simple (H_2S + N_2)	99.9	0	0	0	200
Dry biogas	50	32	18	0	200
Humid biogas	50	30	16	4	200

Experiments were started using a simplified gas composed of N_2 and H_2S in order to evaluate capacity of chars for H_2S removal. Then a complex mixture of dry biogas composed of, CH_4, CO_2 and N_2 was applied to observe the influence of CH_4 and CO_2 in the adsorption capacity of materials. Finally, a humid biogas with the same composition than the previous mixture adding H_2O was employed in order to observe the influence of steam in the adsorption process. Steam was introduced to the system implementing a bubbler filled with water which humidified methane gas, later this stream was mixed with the other gases before entering the reactor as shown in Figure 2-14.

The system was also equipped with a H_2S trap in order to reduce sulfur hydroxide concentration in the downstream before going to the ventilation circuit. The system consisted on three bottles; the first one was empty in the case that upstream pressure drops. Then two bottles with 1M NaOH solutions served to decrease H_2S concentration according to the following reaction:

$$H_2S + 2NaOH \rightarrow Na_2S + 2H_2O \qquad \textbf{R 2-2}$$

The experiment was connected to a security system with automatic detection of H_2S in the room. The flow of gas Q_{gas} is calculated according to operating conditions of pressure (1 atm) and temperature (30 °C) using Eq. 2-9 resulting in 2.2 NL/min which was the same for every biogas experiment. Gas flow rates (in NL/min) were controlled by mass flow meters. At the same time, the volume of the fixed-bed was used to determine residence time by means of Eq. 2-12 where V_{bed} is the volume of the char fixed-bed, r is the radius of the column, Q_{gas} is the gas flow rate and τ is the residence time.

$$\tau = \frac{V_{bed}}{Q_{gas}} = \frac{\pi r^2 h}{Q_{gas}} \qquad \textbf{Eq. 2-12}$$

Chars fixed-bed height h was 4 cm for all materials in order to perform all experiments at constant bed volume. The residence time in an empty column is fixed at 0.4 s and corresponds to those implemented in industrial adsorbers (from 0.1 to 5 s) [187]. The residence time in a column filled with chars or ACs is probably longer and different for each material, however it is assumed that the difference is not significative and this time is not measured. As a result, the gas velocity in the column is 10 cm/s. This value is lower than the gas velocities encountered in industrial adsorption processes (generally 14 - 17 cm/s) [187]. A blank test was carried out with the intention of determining the response of the system to the H_2S concentration imposed at the beginning of the experiment. This blank test was carried out in an empty column under conditions identical to those used during the adsorption test.

Experiments were performed twice for activated chars, however raw char was tested once since performance of this materials was poor. Materials were dried in an oven at 105 °C before carrying out the tests with the purpose of study steam influence later and performing mass balances on the fixed-bed of char. The system was operated at 30 °C and air was swept out using N_2 in order to eliminate O_2 inside the reactor. At the desired temperature, leak test was performed before starting each experiment. The different gas species were fed according to the composition of the biogas matrix until reaching steady state. Next, H_2S gas at 200 ppm was introduced which was taken as $t = 0$ of the experiment. The adsorption tests were held until outlet concentration attained 200 ppm meaning that the involved material has reached its maximum capacity. At the end of the test, the flow of H_2S was stopped and the system was maintained under N_2 atmosphere, then char was recovered and weighted.

Determination of capacity of chars

Performance of materials was evaluated in terms of adsorption capacity (q_{ads}) calculated as the removal of H_2S (mg) per gram of char according to Eq. 2-13 where C_0 is the inlet H_2S concentration (ppm), C_t is outlet H_2S concentration at time t (ppm), 1.36 is the equivalence factor to convert concentration unities from ppm to mg/Nm^3, Q_{gas} is the inlet total gas flow (Nm^3/min) and m is the initial mass of the char (g). The inlet concentration of H_2S (C_0) was calculated from measured initial flow rates and H_2S bottle concentration as shown in Eq. 2-14 and Eq. 2-15 where C_{H2S} is the concentration of H_2S bottle, Q_{H2S} is the flow rate of H_2S, Q_{CH4} is the flow rate of CH_4, Q_{CO2} is the flow rate of CO_2, Q_{N2} is the flow rate of N_2 and Q_{gas} is the total flow rate of biogas.

$$q_{ads} = 1 - 1.36\frac{Q_{gas}}{m}\int_{t_0}^{ti} C_0 - C_i - C_{i-1} \qquad \textbf{Eq. 2-13}$$

$$C_0 = \frac{C_{H2S}Q_{H2S}}{Q_{gas}} \qquad \textbf{Eq. 2-14}$$

$$Q_{gas} = Q_{H2S} + Q_{CH4} + Q_{CO2} + Q_{N2} \qquad \textbf{Eq. 2-15}$$

The Figure 2-15 gives a graphical explanation of adsorption capacity calculation: the blue is the outlet concentration of H_2S. The light blue area is proportional to maximum adsorption capacity of materials.

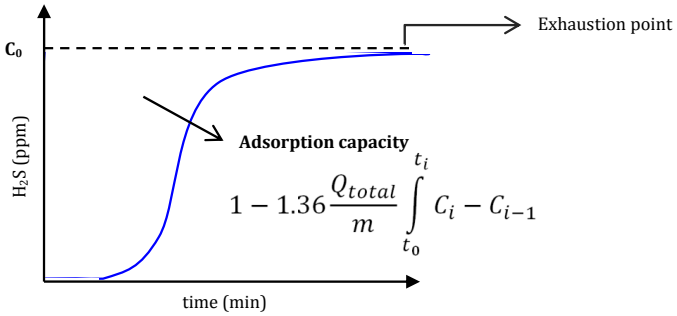

Figure 2-15. Calculation method of performance defined as adsorption capacity of materials.

This chapter explained the preparation of 8 materials, 2 chars from pyrolysis and 6 activated chars. In the same way, the characterization techniques employed to analyze their properties were presented and their implementation in different applications was described. The summary of the characterization analyses is presented in Table 2-5.

Table 2-5. Matrix of material characterization analyses.

Sample /Analysis	BH-Char	MH-Char	BH-CO_2 2-steps	BH-CO_2 1-steps	MH-CO_2 2-steps	MH-CO_2 1-steps	BH-H_2O	MH-H_2O
CHNS-O	√	√	√	√	√	√	√	√
Proximate Analysis	√	√	√	√	√	√	√	√
Ash composition	√	√	√	√	√	√	√	√
pH_{pzc}	√	√	√	√	√	-	√	√
HHV	√	√	√	√	√	√	√	√
N_2 adsorption	-	-	√	√	√	√	√	√
Hg Porosimetry	√	√	√	-	√	-	√	√
SEM	√	√	√	-	√	-	√	√

Likewise, the experiments carried out and the analyses to characterize the used materials are depicted in Table 2-6. To sum up, pyrolysis chars were only tested in simplified syngas to eliminate tars and simplified and humid biogas to remove H_2S. Activated chars prepared by 2-steps CO_2 activation and direct H_2O activation were tested in tar cracking and H_2S removal using different mixtures of syngas and biogas. The surface of exhausted activated chars from tar cracking in a simplified gas were analyzed by Hg porosimetry and SEM. On the other hand, activated chars saturated with sulfur compounds were analyzed by means of N_2 adsorption and thermos-gravimetric analysis.

Table 2-6. Matrix of experiments and post-experiments analyses of materials.

Sample /Analysis	BH-Char	MH-Char	BH-CO_2 2-steps	BH-CO_2 1-steps	MH-CO_2 2-steps	MH-CO_2 1-steps	BH-H_2O	MH-H_2O
EB + CO + N_2	√	√	√	-	√	-	√	√
Dry syngas	-	-	√	-	√	-	√	√
Humid syngas	-	-	√	-	√	-	√	√
H_2S + N_2	√	√	√	-	√	-	√	√
Dry biogas	-	-	√	-	√	-	√	√
Humid biogas	√	√	√	-	√	-	√	√
Hg Porosimetry	√	√	√	-	√	-	√	√
N_2 adsorption	-	-	√	-	√	-	√	√
SEM	-	-	√	-	√	-	√	√
TGA	-	-	√	-	√	-	√	√

2.4. Conclusion

This chapter presented the different production methods of materials, how to improve their properties and explained their implementation in different applications. Two agricultural wastes were studied: buckwheat husks and millet husks. These wastes were pyrolyzed separately at 500 °C. Two oxidizing agents were used to improve their properties and open up new possibilities of valorization: activation with either steam or CO_2. Both activations aimed at developing porosity in the surface of pyrolysis chars and concentrate their mineral elements. The analytical techniques used to characterize the physical and chemical properties of materials have been described. These chars are intended to be used as adsorbents and potential catalysts for the purification of biogas and syngas. The experimental configurations to test the efficiency of materials were presented and the methods to calculate their performance were explained.

Chapter 3. Material characterization

Introduction

The characterization of the biomass, the pyrolysis chars and the activated chars is necessary in order to define their properties and to understand their performance in syngas and biogas cleaning as far as chars are concerned. Therefore, this chapter presents the chemical and textural properties of pyrolysis chars and activated chars. In the same way, this chapter aims to explain the influence of the pyrolysis, the CO_2 and steam activation in the resulting features of materials. In that sense, the release of inorganic elements is clarified and the mineral species found in the surface of materials is described. Finally, the mass and energy balances of the processes are carried out with the purpose of evaluating the energy efficiency of the pyrolysis and activation. Different performance indicators are calculated to estimate the energy recovery from oil and gas phases and to assess the possibility of valorizing the solid phase (chars and activated carbons) as an energy vector or as material.

3.1. Biomass characterization

Different analysis techniques described in Chapter 2 were carried out in order to determine the chemical characteristics of the buckwheat husk (BH) and the millet husk (MH) (Table 3-1). Both biomasses were analyzed by triplicate and the average values with the corresponding deviation are presented.

The ultimate analysis of (BH) and (MH) are in agreement with the composition of agricultural wastes as presented in Chapter 1, Table 1-2. C and O are the major elements with 47.5 % and 44.1 % respectively in BH and 42.3 % and 39.3 % respectively in MH and sulfur has not been detected in both biomasses. If the sum of C, H, N and O percentages is close to 100 % due to the low ash content (2.6 %) in BH, the case of MH is rather different since the ash accounting for 12.2 % are mainly constituted of Si (9.5 %) and K (1.4 %).

Different thermo-gravimetric curves (Figure 3-1) are obtained from TGA analysis and the cellulose and hemicelluloses contents are quite similar for both biomasses. As it was explained in the previous chapter, the determination of cellulose, hemicellulose and lignin fractions in

biomasses is calculated based on the mass and the temperature profile. The values of cellulose and hemicelluloses are respectively 20.4 and 18.5 % for BH and 25.8 and 20.3 % for MH. However, the lignin in BH is relatively high (27.0 %) compared to MH (15.7 %) which explains the higher fixed carbon (18.1 %) in BH than in MH (13.3 %).

Table 3-1. Chemical characterization of dried biomass.

Analysis	Composition	BH	MH
Ultimate analysis (wt.%)	C	47.5 ± 0.6	42.3 ± 0.3
	H	5.8 ± 0.3	5.6 ± 0.1
	N	2.3 ± 0.8	0.7 ± 0.1
	S	n.d*	n.d*
	O	44.1 ± 1.1	39.3 ± 0.2
Thermo-gravimetric analysis (wt.%)	Cellulose	20.4 ± 0.1	25.8 ± 0.4
	Hemicellulose	18.5 ± 0.3	20.3 ± 1.3
	Lignin	27.0 ± 2.6	15.7 ± 0.5
Proximate analysis (wt.%)	Moisture	12.5 ± 0.1	9.4 ± 0.3
	Volatile matter	66.9 ± 0.6	65.1 ± 0.4
	Fixed carbon	18.1 ± 0.7	13.3 ± 0.3
	Ash	2.6 ± 0.1	12.2 ± 0.1
Main mineral composition (wt.%)	K	Trace	1.4 ± 0.1
	Ca	Trace	Trace
	P	Trace	Trace
	Si	n.d	9.5 ± 0.1
Bomb calorimeter (MJ/kg)	HHV	18.3 ± 0.2	17.7 ± 0.02

**n.d: non-detected.*

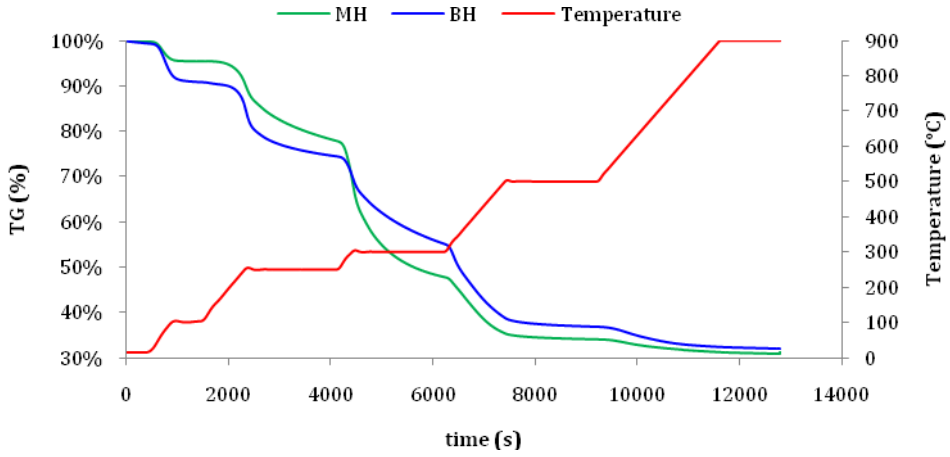

Figure 3-1. TGA analysis curves of BH and MH.

As it was shown in the first chapter, BH and MH are very different materials in terms of inorganic composition. According to Table 1-3 and Table 1-4 the main elements in BH decrease

as follows: K_2O > MgO > SiO_2 > CaO while MH is composed principally of SiO_2 > CaO > K_2O > Fe_2O_3 or expressed as elements by Si > Mg > Ca > K. The difference in composition of millet ash between references can be related to the variation in the grain due to location or it can be related to different analytical methods. In this study, the same main elements are found for BH and for MH being Si the main mineral which is in agreement with literature presented in Chapter 1 [24,30,31].

Finally the Higher Heating Values (HHV) of BH and MH are 18.3 and 17.7 MJ/kg which are common values for herbaceous biomass [170], however HHV of BH is higher than MH which is explained by the high ash content of the latter.

In conclusion, the main difference of these agricultural residues is their lignin content and inorganic distribution. These two features may probably affect their behavior during the pyrolysis and the activation and their future efficiency in terms of catalytic tar cracking and H_2S removal.

3.2. Pyrolysis

BH and MH have been previously dried at 105 °C and placed in a semi-rotating quartz tube under N_2 flow. The pyrolysis was executed at 10 °C/min and 500 °C (see Chapter 2). The raw chars denoted hereafter as BH-Char and MH-Char were collected and weighted. The yield of pyrolysis was calculated according to Eq. 2-2. The yields of BH-Char and MH-Char are 38.3 ± 0.3 % and 38.0 ± 0.1 % respectively. The similarity of both yields can be explained by the lignin and ash contents of each biomass: 27 % and 2.6 % in BH and 15.7 and 12.2 % in MH.

3.2.1. Chemical characterization

The characterization of raw chars is presented in Table 3-2. Both chars were analyzed by triplicate and the average values with respective deviation are presented. Only the analysis of the pH_{pzc} was conducted once. It can be noted that the slow pyrolysis significantly increases the carbon content in the resulting chars while decreasing hydrogen, and oxygen contents. This result is in agreement with literature since pyrolysis releases most of the non-carbon elements particularly H, O in the form of gases and tars [16]. It can be seen that BH-Char presents higher C (78.4 %), H (3.1 %), N (1.3 %) and O (15.5 %) than MH-Char as their precursors (BH and MH).

Table 3-2. Chemical characterization of chars from pyrolysis carried out at 500 °C.

Analysis	Composition	BH-Char	MH-Char
Ultimate analysis (wt.%)	C	78.4 ± 1.0	56.9 ± 0.3
	H	3.1 ± 0.1	2.5 ± 0.1
	N	1.3 ± 0.2	1.1 ± 0.1
	S	n.d*	n.d*
	O	15.5 ± 0.8	12.5 ± 0.6
Proximate analysis (wt.%)	Moisture	5.4 ± 0.1	3.2 ± 0.9
	Volatile matter	28.7 ± 0.6	6.2 ± 0.6
	Fixed carbon	60.2 ± 0.6	61.1 ± 1.1
	Ash	5.7 ± 0.1	29.6 ± 0.2
Main mineral composition (wt.%)	K	2.4 ± 0.1	4.8 ± 0.6
	Ca	1.5 ± 0.1	0.2 ± 0.1
	P	0.7 ± 0.1	0.9 ± 0.2
	Si	n.d*	21.6 ± 0.9
	Mg	0.8 ± 0.1	n.d*
Bomb calorimeter (MJ/kg)	HHV	28.1 ± 0.6	22.7 ± 0.2
Point of zero charge	pH_{pzc}	5.7	5.3

**n.d: non-detected*

As result of the thermo-conversion process, raw chars have increased ash content which is much higher in MH-Char (29.6 %) than in BH-Char (5.7 %) as their parent biomass. The value in MH-Char (29.6 %) is maybe overestimated since ash particles have always a mixed black and white color in spite of duplicates and longtime of combustion. This behavior might be explained considering that this char has high Si content which may form silicate with other elements preventing their release. During pyrolysis of biomass part of the inorganic content is also released from the solid phase. The release of mineral content can be calculated according to Eq. 3-1 where *Ash* represents the ash content (%) in the raw char and biomass respectively and Y_{Char} is the char yield from pyrolysis. Results show that the loss of mineral content in pyrolysis is 16.0 % for BH-Char and 7.8 % for MH-Char. Thus, the elevated content of silica in MH-Char and lower ash release of this sample might indicate that this mineral is more resistant to transformation at 500 °C than K, Ca, P and Mg.

$$Ash\ release\ (\%) = \left(1 - \frac{Ash_{Char}}{\frac{Ash_{Bio}}{Y_{Char}} \times 100}\right) \times 100 \qquad \textbf{Eq. 3-1}$$

As expected, the inorganic elements are more concentrated in pyrolysis chars than in the biomass. According to results, MH-Char has higher content of Si (21.6 %), K (4.8 %) and P (0.9

%) compared to BH-Char which presents lower K (2.4 %), higher Ca (1.5 %) and some Mg and P (0.8 and 0.7%). Regarding magnesium, BH and MH have not revealed traces even if the results found in the literature (Table 1-3 and Table 1-4) state that this element is the second most important among the mineral ones but a content of 0.8 % is detected in the BH-Char. The limitations of the equipment can also be explained this absence.

Consecutively to the pyrolysis, the HHV of BH-Char and MH-Char have increased to 28.1 and 22.7 MJ/Kg respectively and the highest value corresponds to the char with the lowest ash content. This latter is the major difference deduced from the proximate analysis.

The pH of chars was determined by the method of point of zero charge (pH_{PZC}), results are presented in Figure 3-2. According to the methodology, the pH_{PZC} is the point where the curves pH_{final} vs $pH_{initial}$ intercept the curve pH_{final} equal to $pH_{initial}$ (black line). Results show that the pH_{PZC} is 5.7 for BH-Char and 5.3 for MH-Char. This outcome suggests that at the surface of pyrolysis chars there are mainly acidic functional groups which is not surprising considering that acidic functional groups (carboxylic type, anhydride, etc) composed of O and H are released during pyrolysis at temperatures from 380 – 720 ° C [89]. Therefore, in the pyrolysis process carried out at 500 °C probably most of the acidic functional groups remain bonded to the carbonaceous matrix.

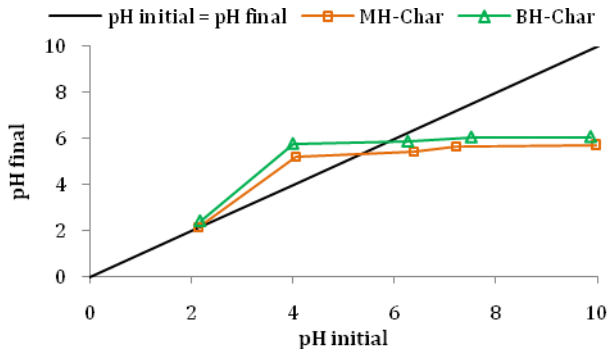

Figure 3-2. Point of zero charge pH of chars from pyrolysis carried out at 500 °C.

3.2.2. Textural characterization

Usually porosity of materials is determined by the well-known nitrogen adsorption technique which provides information about the BET surface are, volume of micropores (D_p <2 nm) and mesopores (2 nm < D_p < 50 nm). This method does not give information about macropores (D_p > 50 nm), thus data concerning this scale of porosity is rarely found in literature. Therefore, the porosity determination of pyrolysis chars reputed difficult by N_2 adsorption because of the lack of micropores and/or mesopores was measured by mercury intrusion porosimetry. This

technique is also able to determine the compressibility of materials at high pressure (usually higher than 10 MPa).

Results from mercury porosimetry analysis must be analyzed considering the compressibility of samples since this parameter can influence the calculation of pore volume. The samples were analyzed twice, thus the values presented in Table 3-3 correspond to the average and the standard deviation of two analyses.

The compressibility of pyrolysis chars observed in Figure 3-3 shows that the cumulative volume of BH-Char is almost constant as the $dV/dD_{Pore\ Volume}$ increase gradually with the pressure increase. In contrast, the cumulative volume of MH-Char initially increases until $dV/dD_{Pore\ Volume}$ of 0.0006 mL/g/nm. Then the cumulative volume increases while $dV/dD_{Pore\ Volume}$ is reduced to 0.0004 mL/g/nm with the pressure increase. After that, cumulative volume continues to augment until $dV/dD_{Pore\ Volume}$ of 0.0008 mL/g/nm which later ends at 0.0002 mL/g/nm for the highest cumulative volume (2.4 mL/g).

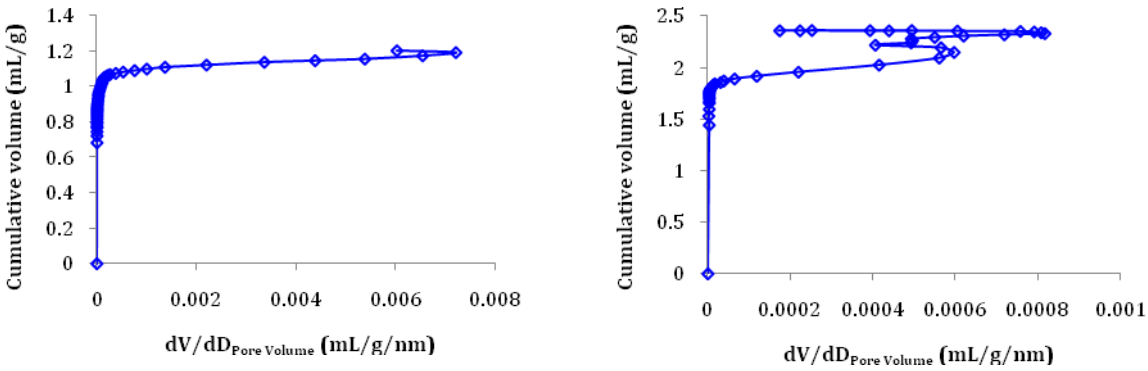

a) BH-Char **b) MH-Char**

Figure 3-3. Compressibility of chars during mercury porosimetry analysis: a) BH-Char and b) MH-Char.

The higher compressibility of MH-Char might be explained by its hollow cylindrical geometry resulting from pyrolysis process as shown in Figure 3-4. In contrast, this behavior was not evidenced in BH-Char which suggest that Si might be responsible for this outcome. Therefore, the pore structure of MH-Char might suffer some changes increasing the cumulative volume of mercury. In consequence, it is important to point out that results from MH-Char might be overestimated and must be carefully analyzed.

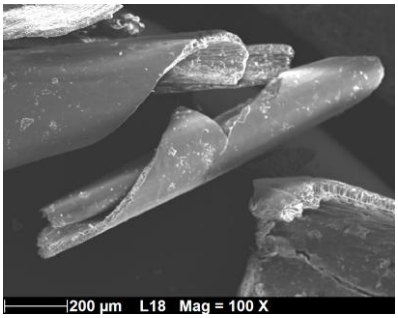

Figure 3-4. SEM image of MH-Char from pyrolysis at 500 °C.

According to Table 3-3, MH-Char presents higher porous volume which can be due to the deformation of this sample. It is observed that BH-Char has high porous volume (0.540 cm^3/g) composed of 21 % of mesopores (8 nm < D_p < 50nm) and 78 % of macropores (85000 nm < D_p). This result indicates that chars from pyrolysis are mainly macroporous as has been stated in the literature [32].

Table 3-3. Textural characterization of chars from pyrolysis carried out at 500 °C.

Analysis	Parameter	BH-Char	MH-Char
Mercury porosimetry	V_{Total} (cm^3/g)	0.540 ± 0.084	0.786 ± 0.062
	V_{Meso} (cm^3/g)	0.111 ± 0.012	0.022 ± 0.001
	V_{Macro} (cm^3/g)	0.421 ± 0.072	0.755 ± 0.062

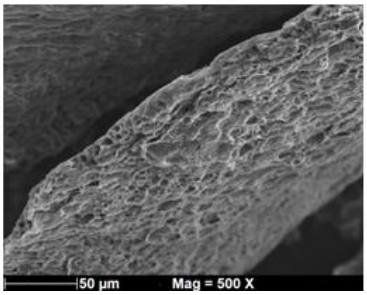

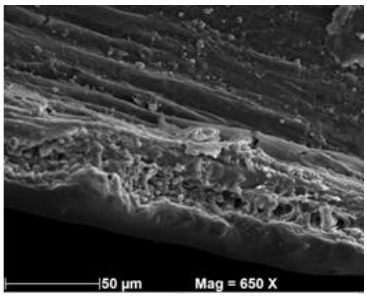

a) BH-Char **b) MH-Char**

Figure 3-5. SEM images of chars from pyrolysis: a) BH-Char, b) MH-Char.

The macro- and mesoporosity of materials was investigated by means of Scanning Electron Microscopy (SEM). The SEM images presented in Figure 3-5 show that apparently there is poor porosity in the surface of pyrolysis chars or that it is hindered by what seems to be organic matter (tars). However, it is important to mention that the geometry of samples makes it difficult to take the SEM images from the right angle. In addition, the conversion process affects the structure of the agricultural waste in particular for MH as mentioned before and indicated in Figure 3-6 where it can be observed that millet husks rolled during pyrolysis process.

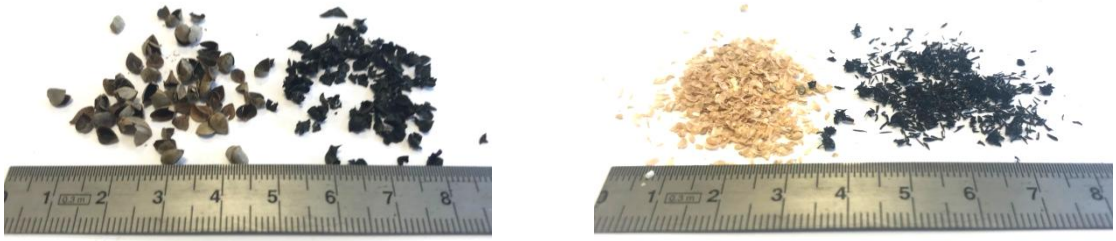

a) BH and BH-Char **b) MH and MH-Char**

Figure 3-6. Influence of pyrolysis at 500 °C in the geometry of biomass.

3.2.3. Mass and energy balances

The mass and energy balances of pyrolysis were calculated in order to determine the efficiency of the process in terms of energy recovery. The values presented in Table 3-4 correspond to the average value and standard deviation of 3 batch of pyrolysis for each biomass. As a remainder, char and oil were recovered after the process and weighted for the mass balance. The condensed phase was separated in a light and a heavier fraction and the former was considered to measure its HHV since the lighter phase is mainly composed of water and has no energetic value.

Table 3-4. Mass and energy balances of pyrolysis at 500 °C.

		BH-Char			MH-CHar		
		Mass fraction (wt.%)	**LHV (MJ/Kg)**	**Energy ($MJ/Kg_{Biomass}$)**	**Mass fraction (wt.%)**	**LHV (MJ/Kg)**	**Energy ($MJ/Kg_{Biomass}$)**
Inlet	Biomass	100	16.8 ± 0.2		100	17.1 ± 0.8	
	Electrical consumption	-	-	8.7	-	-	8.7
Outlet	Char	38.3 ± 0.3	27.5 ± 0.6	10.5 ± 0.1	38.0 ± 0.1	22.2 ± 0.2	8.45 ± 0.02
	Aqueous phase	13.5	0	0	15.2	0	0
	Oily phase	1.8	23.06 ± 0.25	0.4	5.9	10.02 ± 2.27	0.59
	Gas	25.2 ± 0.3	6.1 ± 0.1	1.5 ± 0.1	19.9 ± 0.6	8.0 ± 0.1	1.6 ± 0.1
Performance indicators:	**Target products:**	**Oil and gas**	**Char, oil and gas**		**Oil and gas**	**Char, oil and gas**	
	AEE*	**11.6 ± 0.2 %**	**74.3 ± 0.5 %**		**12.8 ± 0.4 %**	**62.1 ± 0.4 %**	
	AEE_{elec}**	**7.7 ± 0.1 %**	**49.0 ± 0.3 %**		**8.5 ± 0.2 %**	**41.1 ± 0.2 %**	
	NER***		**1.434 ± 0.010**			**1.218 ± 0.005**	

**AEE: apparent energy efficiency defined as the ratio of the energy content in the target products to the energy content of the raw biomass; **AEE_{elec}: takes into account the electrical consumption in the denominator; ***NER: Net energy produced in the process.*

The mass balances of the BH and MH pyrolysis are 78.8 and 79.0 % respectively. This is explained by the condensation of tars in pipes connecting the cold trap and the gas analyzer, in the same way, the volatilization of some compounds in the liquid phase is not considered in the calculation. According to literature, it seems that the mass loss can vary in the range 7.4 – 26 %

and is related to different factors[40]: i) unused biomass that remains in the pyrolyzer; ii) higher mass loss is found at lower temperature and slower heating rate (10 °C/min) as is the case of this work and iii) incomplete bio-oil recovery during collection.

The LHV of gas is calculated from the gas composition using the given Eq. 2-4. The composition of the gas from pyrolysis is depicted in Table 3-5 and was calculated taking N_2 as reference considering that it is non-reactive and thus it is not presented along with the other gases. The values given in Table 3-5 for the gas composition are cumulative. The pyrolysis gas is composed of H_2, CH_4, CO, CO_2 and C_XH_Y for both biomasses. The composition of the gas from BH pyrolysis is 1.8 % H_2, 11 % CH_4, 25 % CO, 57.7 % CO_2 and 5 % C_XH_Y. On the other hand, pyrolysis of MH results in 1.8 % H_2, 11 % CH_4, 31.6 % CO, 50 % CO_2 and 5.7 % C_XH_Y. Thus, gas from pyrolysis of BH presents higher CO_2 and lower CO and C_XH_Y contents in comparison to pyrolysis of MH.

Table 3-5. Gas composition from pyrolysis at 500 °C.

Biomass	H_2	CH_4	CO	CO_2	C_XH_Y
	mol%				
BH	1.84 ± 0.04	10.99 ± 0.25	24.94 ± 0.13	57.68 ± 0.29	4.56 ± 0.13
MH	1.79 ± 0.02	10.92 ± 0.04	31.64 ± 0.23	49.90 ± 0.26	5.74 ± 0.09

C_XH_Y: refers to C_2H_4 + C_2H_6 + C_3H_8 + C_3H_6.

The gas evolution from pyrolysis of biomasses at 500 °C is shown in Figure 3-7. It can be noticed that the CO and CO_2 production starts approximately at 200 °C, then around 350 °C the formation of CO_2 decreases and CO stabilizes. Overall, CO_2 remains the dominant gas during pyrolysis from the decomposition of cellulose and hemicellulose. On the other hand, the production of H_2, CH_4 and C_XH_Y start around 400 °C and stabilizes at the maximum temperature of the process. The low H_2 formation in both pyrolysis is attributed to low the temperature of the process since at higher temperature the H_2 content increases while CO and CO_2 decrease. This has been confirmed by other authors that have demonstrated that at higher temperatures (> 500°C), secondary pyrolysis reactions take place favoring the H_2 and CH_4 production for several biomass types [38,39].

With the purpose of comparing the energy efficiency of the process with each biomass, different indicators were calculated. The apparent energy efficiency (AEE) is defined as the ratio of the energy content in the target products to the energy content of the raw biomass; the indicator AEE_{elec} considers the electrical consumption in the denominator; and the Net Energy Ratio (NER) is the energy produced in the process. The electrical input (consumption) considered in AEE_{elec} and NER indicators is the electrical demand required to heat the system (reactor and gases)

which represents about 97 % while pyrolysis of MH and BH only represents 1.4 and 2.7 % of the total input (Annexe 2) respectively in function of the biomass.

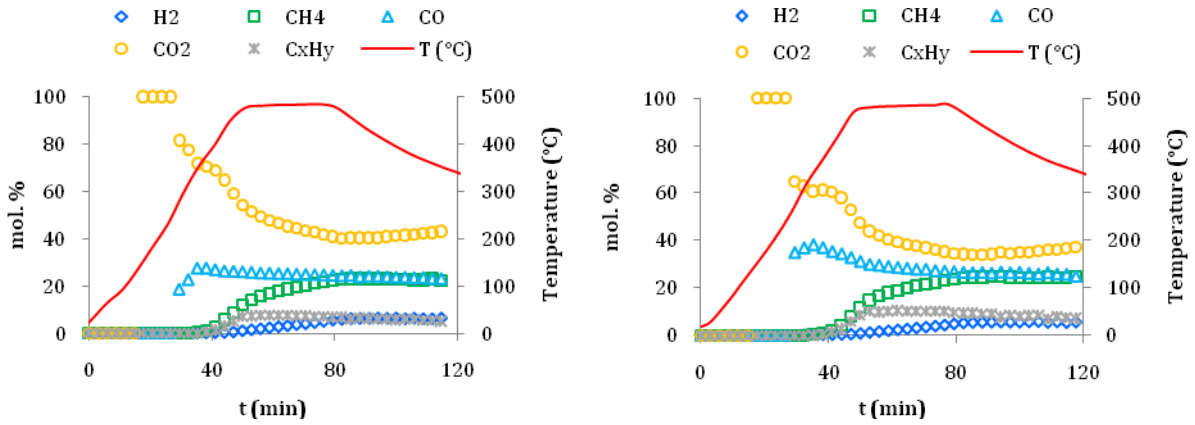

Figure 3-7. Gas composition from pyrolysis of a) BH and b) MH at 500 °C.

The AEE indicators for the pyrolysis of BH and MH suggest that the energy that can be recovered as oil and gas is respectively 11.6 % and 12.8 %. Pyrolysis of MH allows recovering slightly more energy than BH due to the higher yield of the oily phase (5.9 %). The gas percentage from pyrolysis of BH (25.2 %) is higher compared to MH (19.9 %), however the lower LHV of the first explained by the CO_2 content (57.68 %) decreases the AEE indicator. Regarding AEE_{elec} and taking oil and gas as target products, there is little difference between pyrolysis of BH and MH since the electrical consumption is the same for both processes (8.7 $MJ/kg_{Biomass}$). The higher value of AEE_{elec} in pyrolysis of MH is due to its higher oil fraction resulting from this process as mentioned before for AEE.

The low values of AEE (11.6 – 12.8 %) and AEE_{elec} (7.7 – 8.5 %) for the slow pyrolysis of both biomasses are attributed to the low temperature of the process. The LHV of the gas from BH and MH pyrolysis are 6.1 and 8.0 MJ/kg respectively (Table 3-4), these values are low however they are in agreement with other values (7.1 MJ/Kg) reported in the literature for the slow pyrolysis of rice straw at 500 °C [39]. The same authors also demonstrated that for the same biomass, the LHV of the gas varies from 4 to 11 MJ/Kg in function of temperature (300 – 700 °C). Moreover the degradation of lignin accounting for 27 % in BH, is high energy demanding since this molecule starts decomposing at 400 - 550 °C [22].

Results presented in Table 3-4 lead to conclude that if a material valorization of char is considered, then only gas and oil from pyrolysis are taken into account in the energy recovery, and the AEE and AEE_{elec} are low. Consequently, since most of the energy is hold in the char it is

necessary to consider the valorization of this product as an energy vector as well. In this way, it can be noticed that the efficiency of pyrolysis is much better according to AEE and AEE_{elec} which are 74.3 and 49.0 % for BH and 62.1 and 42.1 % for MH respectively. Other authors have also evaluated pyrolysis in terms of apparent energy efficiency indicators. In the work of Cao and Pawlowski [188] energy was produced from sewage sludge by means of slow pyrolysis at 400 – 550 °C. In this case, the target product is the bio-oil since apparently it is the main resulting phase (26 – 42 %) obtained by slow pyrolysis of this type of precursor according to the authors. The AEE obtained by the same calculation as the present work was 89.9 % which is higher than performance of pyrolysis of MH (62.1 %) and pyrolysis of BH (74.3 %).

The Net energy produced (NER) by the process which takes into account the energy contained in the char is considered to compare the efficiency of the processes. The NER indicator of BH and MH pyrolysis conducted at 500 °C are higher than 1 (1.43 and 1.22 respectively). Consequently, the energy hold by the char, the oily liquid phase and the gas is higher than the electrical energy required in both pyrolysis. It can be observed that pyrolysis of BH presents a lightly higher NER than MH pyrolysis. This result is due to the lower LHV of MH-Char (22.2 MK/kg) compared to BH-Char (27.5 MK/kg) caused by the high ash content of the first. Gaunt and Lehmann, [189] have reported higher NER from 2 to 7 dedicated to slow pyrolysis of switch grass or forage corn but in that case, the latent heat of the gas was recovered in order to decrease the electrical consumption and this has not been possible in our setup.

3.3. Activation with CO_2

Considering that pyrolysis chars will be implemented in tar cracking and hydrogen sulfide removal (gas phase applications) they must be porous. In order to create porosity at the surface of pyrolysis chars activation with $CO_2$was carried out. The activation with CO_2 was conducted by two different pathways: The first comprehends two steps described by Figure 2-3 in Chapter 2 and the second method is a one-step CO_2 activation or direct activation of the biomass explained in Figure 2-4. Two runs of 2-step activation of pyrolysis chars were carried out and three runs of 1-step activation of biomass were performed. The two methods allow comparing if activated chars are similar to chars from pyro-gasification process (one-step physical activation). The resulting activated carbons are denoted hereafter BH-CO_2 and MH-CO_2, 1-step for the direct activation and 2-step in the other case.

$$Y_{AC}(\%) = \frac{m_{AC}}{m_{Biomass}} \times 100 \qquad \text{Eq. 3-2}$$

The yields of activated carbons prepared by the 2 pathways of CO_2 activation are presented in Table 3-6. The yields of activated carbons are calculated using Eq. 3-2 where *m* is the mass or AC and biomass respectively. The yields are expressed from the biomass and are ranged between 23.5 - 25.5 % for BH and they are higher (28.9-30 %) for MH. As expected, they are lower than yields from pyrolysis (38 %). No significant difference is observed on the AC yields linked with the mode of activation. The slightly lower yield of activated carbons prepared through 1-step suggests that this method is able to release more matter from the solid phase.

Table 3-6. Yield of activated carbons and ash release in CO_2 activation at 850 °C.

Parameter	BH-CO_2 2-step	BH-CO_2 1-step	MH-CO_2 2-step	MH-CO_2 1-step
Y_{AC} (%)	25.5	23.5	30.0	28.9
Ash release (%)	22.5	6.0	12.7	-17.3

The ash release during pyrolysis and CO_2 activation was calculated according to Eq. 3-3 where *Ash* stands for ash content (%) of activated carbons and biomass correspondingly and Y_{AC} is the yield of materials. Regarding the two-step activation mode, the ash release is higher in BH-CO_2 (22.5 %) than in MH-CO_2 (12.7 %). Once again, the elevated content of silica in MH-CO_2 might indicate that this mineral is more resistant to release at 850 °C than K, Ca, P and Mg. The difference between the 2 modes of activation is more difficult to explain regarding the ash release. For the BH, it seems that more minerals are released when the chars cooled down and then re-heated to 850 °C. And as far as MH is concerned, the release leads to a negative value indicating that more matter are accounting for ash. The ash color is blackish and organic matter could remain in the ash fraction after the combustion, probably trapped by the silica after the particle deformation seen on Figure 3-5b.

$$Ash\ release\ (\%) = \left(1 - \frac{Ash_{AC}}{\frac{Ash_{Bio}}{Y_{AC}} \times 100}\right) \times 100 \qquad \text{Eq. 3-3}$$

The characterization, mass and energy balances of activated carbons prepared by both pathways were carried out in order to determine if there is a significant difference in the properties of materials and in the efficiency of the process.

3.3.1. Chemical characterization

The chemical characteristics of activated carbons are highly influenced by the precursor (Table 3-7). For most of the samples the characterization was performed by triplicate and results are presented as average values with corresponding standard deviation. The values that don't have standard deviation were analyzed once.

Table 3-7. Chemical characterization of CO_2 activated carbons.

Analysis	Sample	BH-CO_2 2-step	BH-CO_2 1-step	MH-CO_2 2-step	MH-CO_2 1-step
Ultimate analysis (wt.%)	C	83.3 ± 0.3	76.8 ± 0.3	53.7 ± 0.7	44.1 ± 0.7
	H	1.14 ± 0.04	0.5 ± 0.1	0.7 ± 0.2	0.6 ± 0.04
	N	1.50 ± 0.01	1.4 ± 0.4	0.81 ± 0.02	0.7 ± 0.03
	S	n.d	n.d	n.d	n.d
	O	8.4 ± 0.5	8.9 ± 0.3	6.0 ± 0.3	4.6
Proximate analysis (wt.%)	Moisture	0.9 ± 0.1	6.5	1.2 ± 0.1	3.4
	Volatile matter	29.1 ± 0.2	19.1	15.0	10.2
	Fixed carbon	62.2 ± 0.3	62.7	48.3	31.4
	Ash	7.9 ± 0.1	10.4 ± 0.1	35.5 ± 0.7	49.5 ± 0.3
Main mineral composition (wt.%)	K	3.1 ± 0.1	4.6 ± 0.1	5.8 ± 0.3	8.7 ± 0.1
	Ca	2.4 ± 0.1	3.0 ± 0.1	0.2 ± 0.1	0.3 ± 0.1
	P	0.8 ± 0.1	0.7 ± 0.1	1.8 ± 0.3	2.6 ± 0.1
	Si	n.d	n.d	26.9 ± 0.5	37.6 ± 0.1
	Mg	1.4 ± 0.1	2.3 ± 0.1	n.d	n.d
Bomb calorimeter (MJ/kg)	HHV	28.7 ± 0.2	29.0 ± 0.1	18.8 ± 0.5	17.7 ± 0.1
Point of zero charge	pH_{pzc}	11.9	12.0	9.7	-

n.d: non-detected.

It can be noticed that the carbon content of materials prepared through 1-step is rather lower than in 2-steps activation due to the higher yield of the former. The lower ash content is also related to the higher yield of activated carbon in 2-steps activation. The carbon content in BH and MH is associated to the C fraction of the corresponding activated carbon thus much higher C content is present in BH-CO_2 (76.8 – 83.3 %) than in MH-CO_2 (44.1 and 53.7 %). In the same way, higher H, N and O percentages are found in BH-CO_2 compared to MH-CO_2. The superior ash fraction and inorganic composition of MH-CO_2 are inherent characteristics of the parental biomass (MH). The higher C and lower ash content of BH-CO_2 provide the higher HHV (28.7 – 29.0 MJ/kg) of this material in comparison to MH-CO_2 (18.7 – 17.7 MJ/kg). No significant difference is found in terms of surface chemistry (pH) due to the volatilization of acidic groups caused by the physical activation at 850 °C as explained before and the presence of carbonates in activated carbons.

According to Figure 3-8, differences are found as result of activation process in comparison to chars from pyrolysis. The HHV and C content in BH-CO_2 appears to be constant compared to pyrolysis while ash content seems to slightly increase. The C content of MH-CO_2 decreases whereas the ash percentage increases and the HHV seem to slightly decrease as result of activation. In addition, it can be observed that all the pH_{PZC} of activated carbons are basic while the pH_{PZC} were acid in raw chars (Table 3-7).

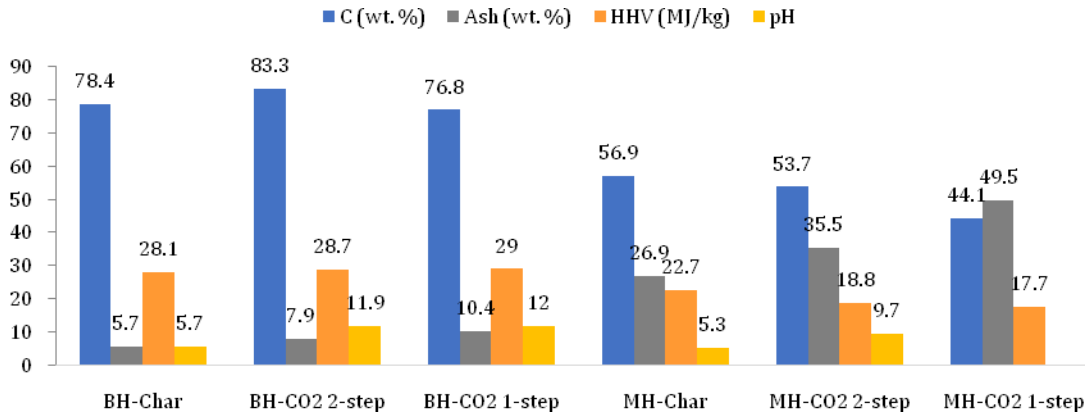

Figure 3-8. Influence of CO_2 activation at 850 °C in raw chars.

In order to compare the transformation of mineral elements, the theoretical concentration of each element "*i*" in activated carbons was calculated using Eq. 3-4 where the mass of each element in the raw char is represented by $m_{i,Char}$ (g) and m_{AC} refers to the mass of activated carbon (g). Then, the ratio measured concentration of each element "*i*" over the theoretical concentration is considered. It is important to have in mind that the ratio Measured/Theoretical must be interpreted as qualitative figures due to the deviation of the X-ray fluorescence analysis used to determine the ash composition of materials.

$$Theoretical\ i_{AC}(\%) = \frac{m_{i,Char}}{m_{AC}} \times 100 \qquad \textbf{Eq. 3-4}$$

Higher ratios indicate that most of the element *i* remains in the solid while lower values suggest that it is released. Results show that some elements are released while others seem to remain in the solid phase as indicated in Table 3-8 and Table 3-9. For example, in BH-CO_2 the release of P is higher than K whereas Ca and Mg appear to remain in the AC. In MH-CO_2 the release of elements seems to be rather low. This observation is justified by the fact that Si can forms silicates with Ca and K at high temperatures [190]. In the same way, it seems to be higher release in two-step CO_2 activation than in one-step as indicated by the higher ratios in the former for both biomasses.

Table 3-8. Ratio of measured elements over theoretical concentration in BH-CO_2.

BH-CO_2 2-steps			**BH-CO_2 1-step**		
Element	Theoretical (%)	Measured/Theoretical	Element	Theoretical (%)	Measured/Theoretical
K	3.8	0.8	K	3.9	1.2
Ca	2.4	1.0	Ca	2.4	1.2
P	1.1	0.7	P	1.1	0.6
Mg	1.3	1.1	Mg	1.3	1.8
Release decreases: P > K >			Release of P		

Table 3-9. Ratio of measured elements over theoretical concentration in MH-CO_2.

MH-CO_2 2-steps			**MH-CO_2 1-step**		
Element	Theoretical (%)	Measured/Theoretical	Element	Theoretical (%)	Measured/Theoretical
K	6.4	0.9	K	6.3	1.4
Ca	0.3	0.8	Ca	0.3	1.1
P	1.2	1.5	P	1.2	2.2
Si	28.7	0.9	Si	28.3	1.3
Release decreases: Ca > K and Si			Nearly no release of elements		

In conclusion, similar activated carbons in the case of BH-CO_2 are obtained by two or one-step CO_2 activation methods. The main difference between BH-CO_2 samples is the ash content which is slightly higher in 1-step pathway. In contrast, more difference is found in MH-CO_2 due to the elevated ash content through one-stage activation which is nearly 15 % higher. Consequently, the higher ash fraction affects the C content of the sample. Therefore, it seems that the pathway of activation influences the properties of resulting activated carbons depending on the inorganic composition of the precursor. This result is explained by several events: i) more carbon is released in one-step CO_2 activation which leads to the concentration of the ash fraction in the precursor; ii) calcium and potassium are released from BH-CO_2 but not from MH-CO_2 due to the Si content. Consequently, the higher carbon release in 1-step and nearly no transformation of elements causes more difference between prepared MH-CO_2 carbons by one or two-steps activation with CO_2.

3.3.2. Textural characterization

The activation process creates pores or empty spaces in the carbonaceous material. The degree of porosity can vary according to the characteristics of the feedstock. Therefore, the nitrogen gas adsorption analysis is conducted in order to compare the development of porosity for both precursors and activation methods. This technique is able to measure the surface area of activated chars and the porous volume at the micropore (D_p <2 nm) and mesopore scale (2 nm < D_p < 50 nm). The analyses were performed with two equipments Micromeritics ASAP 2020 and

3-FLEX. It is important to remind that the latter achieves lower pressure therefore it can perform a stronger degassing giving a more precise value of BET surface and mesoporous volume which are higher than those provided by ASAP 2020.

The results obtained from the nitrogen adsorption and mercury porosimetry analysis are summarized in Table 3-10. The averages values of two analyses are given with the corresponding standard deviation.

Table 3-10. Textural characterization of CO_2 activated carbons at 850 °C.

Analysis	Sample	BH-CO_2 2-step	BH-CO_2 1-step	MH-CO_2 2-step	MH-CO_2 1-step
	Analyzer	ASAP 2020	3-FLEX	ASAP 2020	3-FLEX
N_2 Adsorption/Desorption	V_{Total} (cm^3/g)	0.291 ± 0.011	0.339 ± 0.004	0.180 ± 0.003	0.187 ± 0.001
	V_{Micro} (cm^3/g)	0.261 ± 0.004	0.305 ± 0.005	0.147 ± 0.002	0.150 ± 0.001
	V_{Meso} (cm^3/g)	0.012 ± 0.010	0.055 ± 0.002	0.013 ± 0.001	0.056 ± 0.002
	BET Surface (m^2/g)	578 ± 4	612 ± 16	329 ± 6	312 ± 1
Mercury porosimetry	V_{Total} (cm^3/g)	0.555 ± 0.092	-	0.807 ± 0.054	-
	V_{Meso} (cm^3/g)	0.070 ± 0.004	-	0.029 ± 0.001	-
	V_{macro} (cm^3/g)	0.480 ± 0.088	-	0.770 ± 0.053	-

The nitrogen adsorption/desorption isotherms of samples are presented in Figure 3-9. The curves for all materials are of type I [175] as presented in Chapter 2 (Figure 2-9) which are typical of microporous materials. It can be seen that the behavior of the curves is in accordance with results presented in Table 3-10 since the samples that show higher adsorption are the ones with higher surface area.

As expected the activation process with CO_2 creates porosity in the surface of materials. It can be noticed that similar surface areas are obtained in one or two steps CO_2 activation as indicated by the N_2 adsorption analysis. The BET surface area and total pore volume of BH-CO_2 are close to 600 m^2/g and 0.3 cm^3/g respectively which are higher compared to MH-CO_2 (320 m^2/g and 0.18 cm^3/g). Therefore, it is possible to state that higher C content allows creating a higher degree of porosity.

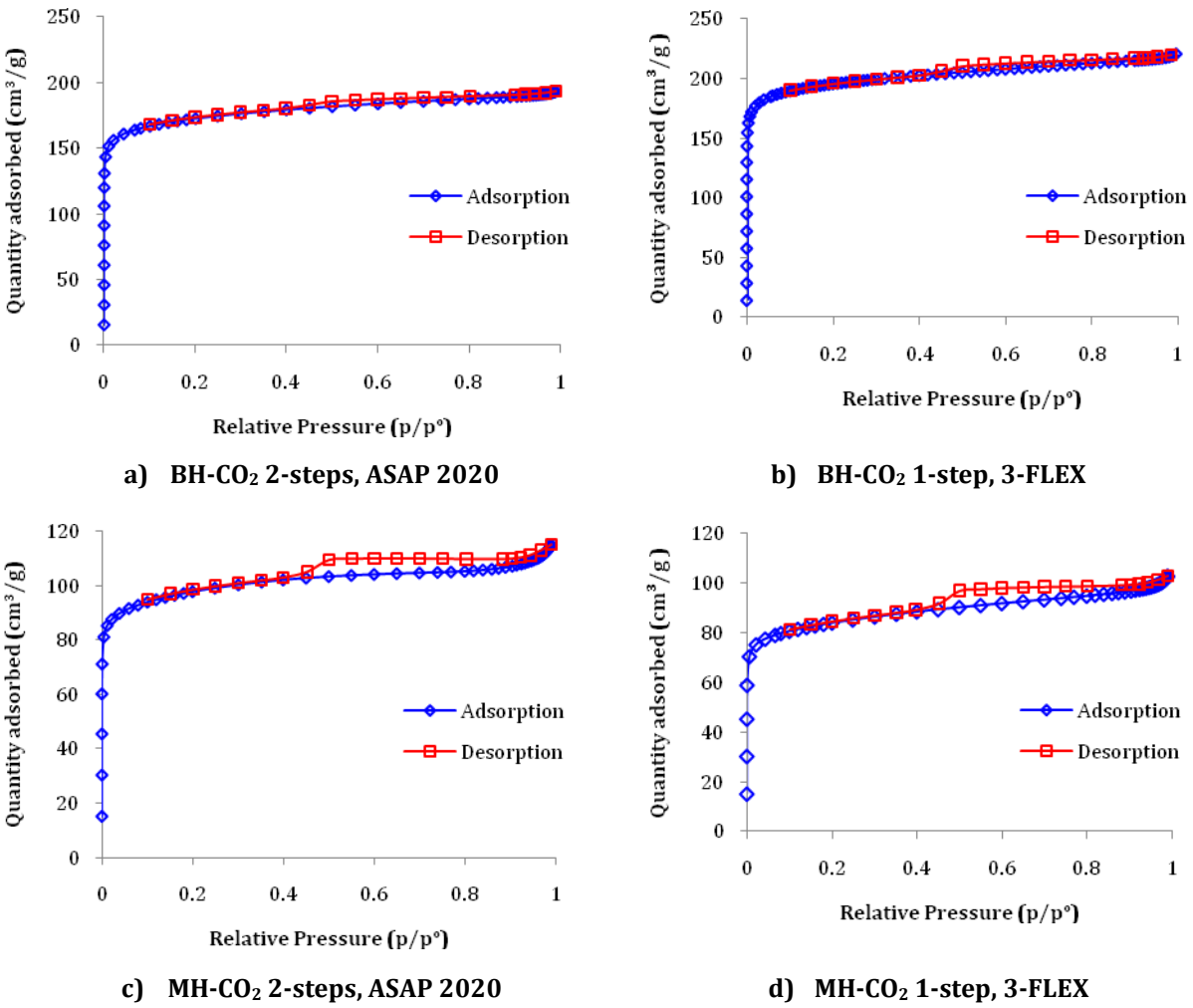

Figure 3-9. N_2 Adsorption/Desorption isotherms of a) BH-CO_2 2-steps, b) BH-CO_2 1-step, c) MH-CO_2 2-steps and d) MH-CO_2 1-step.

The pore distribution between micropores and mesopores is in agreement with the curves of type I attributed to microporous materials. The pore balance in BH-CO_2 2-steps is 96 % of micropores and 4 % of mesopores whereas the pore share from 1-step activation presents higher mesopores (15 %) and lower micropores (85 %). In contrast, MH-CO_2 from two-steps activation has 92 % of micropores and 8 % of mesopores whereas one-step method produces 73 % of micropores and 37 % of mesopores. The difference in the porosity distribution between samples prepared through 2 and 1-steps is in part related to the difference in the mesoporous volume provided by the equipment 3-FLEX. In spite of that, it seems that one-step activation creates slightly more mesopores than two-step activation. In the same way, it appears that CO_2 activation creates more micropores than mesopores.

Table 3-11. Pore distribution of activation carbons based on N_2 adsorption/desorption analysis.

Sample	BH-CO_2 2-step	BH-CO_2 1-step	MH-CO_2 2-step	MH-CO_2 1-step
Analyzer	**ASAP 2020**	**3-FLEX**	**ASAP 2020**	**3-FLEX**
Micropores (%)	96	85	92	73
Mesopores (%)	4	15	8	37

According to results from the mercury porosimetry analysis, MH-CO_2 presents high compressibility (Figure 3-10b) as its precursor (MH-Char), therefore porosity of this sample might be overestimated.

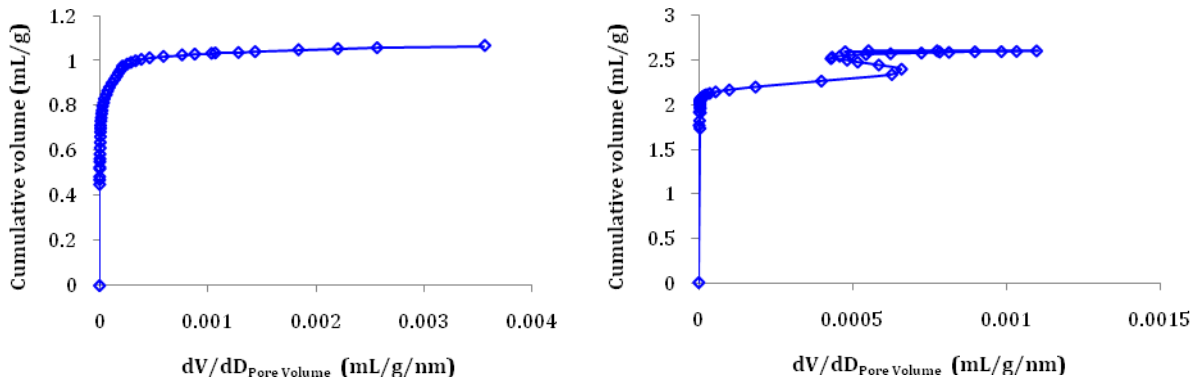

a) BH-CO_2 2-steps **b) MH-CO_2 2-steps**

Figure 3-10. Compressibility of activated chars during mercury porosimetry analysis: a) BH-CO_2 and b) MH-CO_2.

In addition, as was presented in Figure 3-6, millet husks were rolled during the pyrolysis and now they seem to have a cylindrical hollow geometry which enlarges the macroporous volume measured by mercury porosimetry. This can be appreciated in the SEM images shown in Figure 3-11 which present the porosity at macro and mesopore scale.

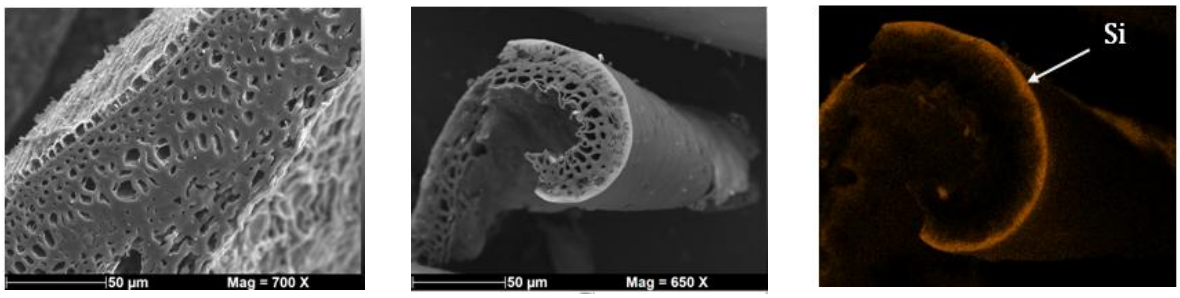

a) BH-CO_2 **b) MH-CO_2** **c) MH-CO_2**

Figure 3-11. SEM images of CO_2 activated carbons: a) BH-CO_2, b) MH-CO_2, c) EDX image of MH-CO_2.

The SEM images of activated carbons show that porosity was created compared to images from pyrolysis chars. In addition, the EDX image of MH-CO_2 shows that silica is well-dispersed in the

surface of the sample and this explains the lower porosity of MH-CO_2 compared to BH-CO_2 according to N_2 adsorption analysis. The layer of Si can explain the negative ash release of MH-CO_2 and nearly no transformation of minerals since this layer could act like a shield that prevents the release of Ca, K and P and even maybe char-particles as well.

As can be observed in Table 3-10, total porous volume (V_{Total}) measured by mercury porosimetry are higher than N_2 adsorption since in principle mercury porosimetry is capable of measuring pores in a wider range (Figure 2-8), whereas N_2 adsorption only captures micro- and mesopores [32]. The mesopore volume of both activated carbons is poor and is overestimated in mercury porosimetry in comparison to the N_2 adsorption. These two techniques are based on different assumptions with different molecules (N_2 and Hg) that can create some disparities especially at low ranges. In addition, the high pressure of mercury intrusion might be able to enter to pores covered with tars that are not available to N_2 gas. Results indicate that MH-CO_2 has higher porosity than its raw char (MH-Char) which might be related to higher compressibility of the first. On the other hand, BH-CO_2 has similar V_{Total} and V_{Macro} which suggest that CO_2 does not influence the macropores of the sample. However, the mesopore volume of BH-CO_2 is lower than BH-Char which is surprising.

The chemical composition of the initial biomass has a great impact on the final properties of activated chars. The high carbon and lignin contents of buckwheat husk allow obtaining a porous material that can be considered an activated carbon according to its carbon content between 77 to 83 % and S_{BET} between 580 and 610 m^2/g with more than 80 % of micropores. On the other hand, the high ash content of millet husk composed mainly of Si limits the conversion process and the resulting material has an elevated mineral content with low carbon fraction and porosity S_{BET} lower than 350 m^2/g, therefore this sample is denoted an activated char.

3.3.3. Mass and energy balance

In order to compare the efficiency of both methods with different biomass, mass and energy balances were calculated according to the limits established in Figure 3-12. To prepare one batch of AC more biomass is employed in 2-step activation in comparison to direct activation. This explains the higher mass fraction of AC obtained in 2-step activation for both feedstocks in the mass and energy balances presented in Table 3-12.

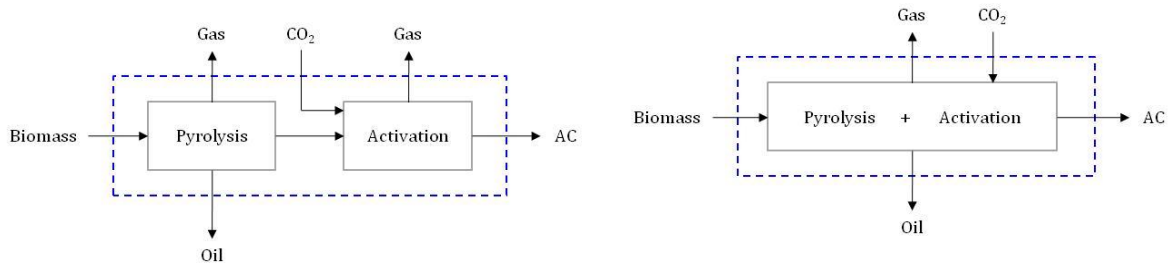

a) 2-steps activation **b) 1-step activation**

Figure 3-12. Limits of mass and energy balances of a) 2-steps and b) 1-step activations.

The 2-steps activation consumes 26 – 28 % more electrical energy in comparison to direct activation for both precursors. Moreover, the mass balances of direct activation are higher: 100 % and 77 % for BH and 88 % and 68 % for MH. As mentioned before, it is sometimes difficult to close the loop balance for several reasons as stated by other authors in literature [40]: i) unused biomass that remains in the reactor; ii) tars can get stuck in the pipes connecting the cold trap with the gas analyzer; iii) the volatilization of some compounds in the liquid phase; and iv) incomplete oil recovery during collection. It is important to keep this in mind since the efficiency indicators (AEE, AEE_{elec} and NER) are calculated based on the mass balance.

The gas production added to the excess of the activating gas lead to gas fractions ranged between 57 to 68 % for 2-steps activation and between 78 and 92 % for 1-step. No liquid phase is produced during the activation in the 2-step mode, the oil is produced during the pyrolysis stage and this explains the LHV of oil in Table 3-12 equal to Table 3-4. In the direct activations, the liquid phase represents only 0.7 - 0.8 %, the energy content is the highest in the gas phase with 1.42 - 2 $MJ/kg_{Biomass}$ followed by the activated chars with 0.9 to 1.7 $MJ/kg_{Biomass}$. In other words and considering the solid fraction (between 5 to 7 %), the energy content of activated chars is quite high.

It can be seen that when oil and gas are considered as energy vectors, the AEE and AEE_{elec} are very similar for 1 or 2-step activation. In the case of BH-CO_2 they are around 13 and 4 % whereas for MH-CO_2 the efficiency indicators are around 10 and 3 % respectively. This is due to the high fraction of CO_2 (70 %) that is fed to the reactor which decreases significantly the LHV of produced gas in the process. If the solid (AC) is considered to recover energy, performance indicators are higher in 2-step activation due to the higher production of AC. Overall, the NER indicator suggest that both pathways of activation have the similar efficiency.

Table 3-12. Mass and energy balances of CO_2 activation of char (2-Steps) and biomass (1-Step) at 850 °C.

		BH-CO_2 (2-step)			BH-CO_2 (1-step)			MH-CO_2 (2-step)			MH-CO_2 (1-step)		
		Mass fraction (wt.%)	LHV (MJ/Kg)	Energy ($MJ/Kg_{Biomass}$)	Mass fraction (wt.%)	LHV (MJ/Kg)	Energy ($MJ/Kg_{Biomass}$)	Mass fraction (wt.%)	LHV (MJ/Kg)	Energy ($MJ/Kg_{Biomass}$)	Mass fraction (wt.%)	LHV (MJ/Kg)	Energy ($MJ/Kg_{Biomass}$)
Inlet	Biomass	100	16.8 ± 0.2		100	16.8 ± 0.2		100	17.1 ± 0.8		100	17.1 ± 0.8	
	Electrical consumption			38.0	-	-	30.2	-	-	37.9	-	-	29.7
Outlet	AC	9.9 ± 0.4	28.3 ± 0.2	2.8 ± 0.1	5.7 ± 0.1	29.2 ± 0.6	1.7 ± 0.1	11.7 ± 0.4	18.7 ± 0.5	2.2 ± 0.1	7.0 ± 0.3	13.3	0.86 ± 0.03
	Aqueous phase	5.2	0	0	1.9	0	0	5.9	0	0.0	1.7	0	0
	Oily phase	0.7	23.06 ± 0.25	0.2	0.8	20.76 ± 0.12	0.2	2.3	10.02 ± 2.27	0.2	0.7	24.00 ± 1.42	0.2
	Gas	67.8 ± 3.2	2.9 ± 0.3	2.0 ± 0.2	91.6 ± 1.8	2.2 ± 0.1	2.0 ± 0.1	56.8 ± 5.3	2.6 ± 0.6	1.5 ± 0.2	78.2 ± 1.2	1.82 ± 0.03	1.42 ± 0.01
Performance indicators:	**Target products:**	**Oil and gas**	**AC, oil and gas**		**Oil and gas**	**AC, oil and gas**		**Oil and gas**	**AC, oil and gas**		**Oil and gas**	**AC, oil and gas**	
	AEE*	**12.8 ± 0.5 %**	**29.5 ± 0.8 %**		**13.1 ± 0.2 %**	**23.0 ± 0.2 %**		**9.8 ± 1.0 %**	**22.6 ± 1.2 %**		**9.35 ± 0.01 %**	**14.4 ± 0.2 %**	
	AEE elec**	**3.9 ± 0.2 %**	**9.0 ± 0.4 %**		**4.7 ± 0.1 %**	**8.2 ± 0.2 %**		**3.1 ± 0.5 %**	**7.0 ± 0.6 %**		**3.42 ± 0.02 %**	**5.3 ± 0.1 %**	
	NER***		**0.130 ± 0.013**		**-**	**0.128 ± 0.001**			**0.102 ± 0.009**		**-**	**0.083 ± 0.002**	

**AEE: apparent energy efficiency defined as the ratio of the energy content in the target products to the energy content of the raw biomass; **AEEelec: takes into account the electrical consumption in the denominator; ***NER: Net energy produced in the process.*

Table 3-13. Gas composition of CO_2 activation of char (2-Steps) and biomass (1-Step) at 850 °C.

Activated carbon	Steps	H_2	CH_4	CO	CO_2	C_xH_y
		mol%				
BH-CO_2	2-Step	5.06 ± 0.20	1.16 ± 0.07	24.18 ± 0.62	69.58 ± 0.35	0.02 ± 0.01
	1-Step	3.49 ± 0.10	1.46 ± 0.03	20.42 ± 0.41	74.52 ± 0.37	0.10 ± 0.05
MH-CO_2	2-Step	3.98 ± 0.16	0.86 ± 0.07	15.42 ±0.59	79.73 ± 0.82	0.01 ± 0.01
	1-Step	3.38 ± 0.08	1.48 ± 0.001	14.84 ± 0.21	80.03 ± 0.28	0.26 ± 0.01

a) BH-Char

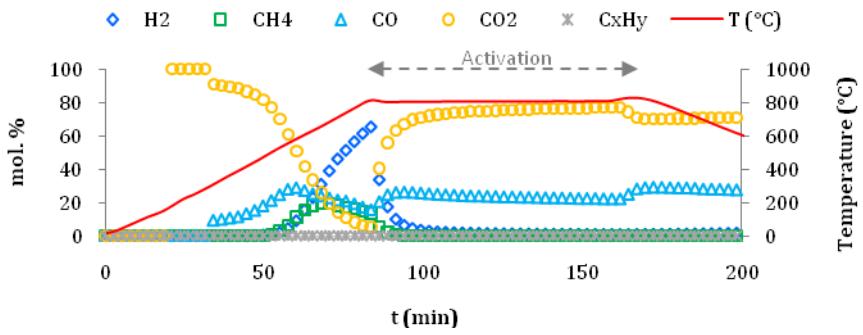

b) MH-Char

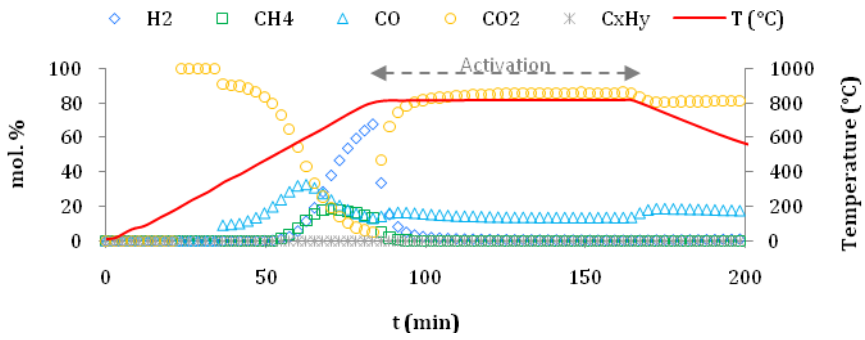

Figure 3-13. Gas composition from 2-steps CO_2 activation of a) BH-Char and b) MH-Char at 850 °C.

a) 1-step BH

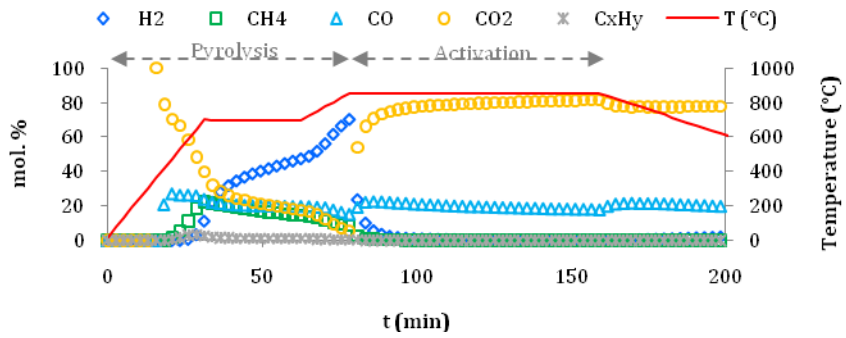

b) 1-step MH

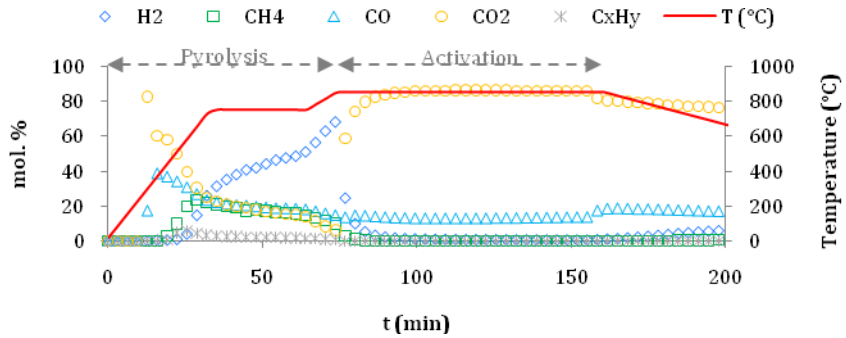

Figure 3-14. Gas composition from 1-step CO_2 activation of a) BH and b) MH at 850 °C.

The apparent energy efficiency (AEE) suggests that the energy that could be recovered as oil and gas from BH is higher than MH. The difference relays in the gas phase, as it can be noticed the

energy recovered as gas from BH-CO_2 is higher (2.0 $MJ/kg_{Biomass}$) than in the case of MH-CO_2 (1.4 - 1.5 $MJ/kg_{Biomass}$). This result is due to the higher gas fraction in BH-CO_2 (67.8 and 91.6 %) than in MH-CO_2 (56.8 and 78.2 %) as well as a slightly higher LHV of the first. The LHV of gas is calculated from the composition of the gas produced during the activation stage (Figure 3-13) for AC obtained through 2 steps. For materials from direct activation the LHV is calculated considering the gas produced in the whole process (pyrolysis + activation) related to Figure 3-14. The mentioned gas composition is presented in Table 3-13 as cumulative values. The resulting gas is composed of H_2, CH_4, CO, CO_2 and C_XH_Y, the high CO_2 content is due to the inlet of 70 % in the carrier gas for the activation process. In the same way, it can be observed that in 1-step activation the CO_2 content is higher (74.5 % in BH-CO_2 and 80.0 % in MH-CO_2) than in 2-steps (69.6 and 79.9 % respectively) since pyrolysis is carried out in the same process. The composition of the gas from BH-CO_2 is richer in H_2 (5.0; 3.5 %), CH_4 (1.1; 1.4 %) and CO (24.2; 20.4 %) and has lower CO_2 (69.6; 75.5 %) content in comparison to MH-CO_2 thus the LHV of the latter is lower.

When the electrical consumption is considered in AEE_{elec}, pyrolysis is more efficient than activation due to the high energy demand of the former. The electrical input (consumption) considered in AEE_{elec} is the electrical demand required to heat the system (reactor and gases) which represents about 99 % while the activation merely accounts for less than 1 % of the total input (Annexe 2). In the case of MH, there is more difference, the AEE from oil and gas in pyrolysis is 12.8 % whereas in activation these indicators represent are around 3.3 % of efficiency due to the lower fraction of bio-oil in activation which is explained by the deviation in the mass balance.

As shown in Figure 3-13 and Figure 3-14, the gas evolution in both activations is similar. The maximum formation of H_2 takes place at the highest temperature but starts to decrease as soon as CO_2 is introduced in the reactor (activation). This observation confirms that there is higher production of H_2 at higher temperatures under N_2 as mentioned previously. In both activations, it can be observed that formation of CH_4 starts at the same time as H_2, however the highest production takes place around 700 °C and then starts to decrease until being zero in the activation stage. It can be noticed that formation of CO takes place at early stage of the process around 300 – 400 °C and decreases as H_2 increases at temperatures < 850 °C. Then production of CO augments in the activation stage and remains the dominant gas after CO_2 most probably due to the Boudouard reaction (R 1-10). Therefore, the main difference in carrying out one or two steps activations is the higher CO_2 content produced during pyrolysis in direct activation of biomass (1-step).

Boudouard	$C + CO_2 \rightarrow 2CO$	**R 1-10**

Therefore, in order to be able to improve the energy recovery considering all products (AC, oil and gas) it is necessary to optimize the operating conditions of CO_2 activation and reduce the CO_2 inlet in a drastic amount. Overall, considering the net energy production (NER) pyrolysis process is much more efficient than CO_2 activation. Respective NER are in the range 1.22 - 1.43 for pyrolysis of MH and BH, 0.08 - 0.10 for MH activation and 0.13 for BH activation. These NER indicators are also very low since no energy recovery is made at the laboratory scale with the latent heat of the gas phase as it can be sometimes found in the literature [189].

It seems that the activation of pyrolysis chars (2-steps activation) and the direct activation comparable to pyro-gasification of biomass present very close energy efficiencies. Both processes display higher performance when the feedstock has low ash content as BH improving the energy that can be recovered from the products. This justifies that the activation with steam will be carried out in one step since it is straight forward. The interest of this work is to quantify energy indicators even if some uncertainties come up such as: loss in the mass balance, difficulties linked to characteristics of biomass (Si content in MH), deviations due to the heterogeneity of the products like the oily phase and deviations related to semi-quantitative analysis like X-ray fluorescence.

3.4. Activation with H_2O

The steam activation was implemented as the direct activation (1-step) of BH and MH independently. This process was carried out by loading BH and MH separately in the quartz tube under N_2 flow. The activation was executed at 850 °C by feeding the reactor with H_2O. Three batches of steam activation of both biomasses were performed. The resulting activated carbons are denoted hereafter BH-H_2O and MH-H_2O respectively. The characterizations of materials as well as the mass and energy balances of the processes have been carried out. The yields of steam activation are calculated according to Eq. 3-2. The yields of activated carbon based on the inlet biomass (Y_{AC}) are lower than those from CO_2 activation 29 % for MH-CO_2 1-step and 24 % for BH-CO_2 1-step, which suggests that more carbon has been released from the solid phase in presence of steam. In addition, it can be observed in that the yield of MH-H_2O (24 %) is higher than BH-H_2O (16 %) due to the elevated ash content of MH-H_2O.

Table 3-14. Yield of activated carbons and ash release in H_2O activation at 850 °C.

Parameter	BH-H_2O	MH-H_2O
Y_{AC} (%)	15.7	24.1
Ash release (%)	32.4	11.3

The release of mineral content was calculated using Eq. 3-3 resulting in 32.4 % for BH-H_2O and 11.3 % for MH-H_2O. The ash release is lower in MH-H_2O probably due to the presence of silica compared to BH-H_2O. The higher release of the inorganic fraction from BH-H_2O (32.4 %) compared to BH-CO_2 1-step (6.0 %) agrees with the lower yield of the first. In the case of MH-H_2O and MH-CO_2 1-step, it seems that there is more ash released from the first since the former appears to prevent the transformation of minerals as explained before. This result might be related to the higher surface areas of steam activated carbons, in other words, the mineral elements bonded to carbon particles might be released from the solid phase during the process of porosity development.

3.4.1. Chemical characterization

The chemical features of activated carbons are predisposed by the precursor (biomass) as indicated in Table 3-15. Most of the samples were analyzed by triplicate and are presented as average values with standard deviation. Single values are found from analysis performed once.

Table 3-15. Chemical characterization of H_2O activated carbons.

Analysis	**Composition**	**BH-H_2O**	**MH-H_2O**
Ultimate analysis (wt.%)	C	72.3 ± 1.9	51.1 ± 0.2
	H	0.9 ± 0.2	0.4 ± 0.1
	N	1.7 ± 0.2	0.5 ± 0.03
	S	n.d	n.d
	O	11.8 ± 0.6	2.7 ± 0.2
Proximate analysis (wt.%)	Moisture	6.3 ± 0.5	3.4
	Volatile matter	52.1 ± 0.8	10.2
	Fixed carbon	30.3 ± 1.1	41.4
	Ash	11.2 ± 0.2	44.9 ± 3.3
Main mineral composition (wt.%)	K	3.9 ± 0.2	9.4 ± 0.4
	Ca	3.4 ± 0.1	0.3 ± 0.1
	P	0.8 ± 0.1	2.1 ± 0.1
	Si	n.d	32.6 ± 0.6
	Mg	2.6 ± 0.1	n.d
Bomb calorimeter (MJ/kg)	HHV	27.7 ± 0.9	17.5 ± 0.01
Point of zero charge	pH_{pzc}	12.0	9.8

n.d: non-detected.

The higher C content in BH causes the superior C fraction of BH-H_2O (72.3 %) compared to MH-H_2O (51.1 %). Likewise, higher H, N and O contents are present in BH-H_2O in comparison to MH-H_2O. The larger ash content and inorganic composition of MH-H_2O are associated to the initial

MH. Consequently, the higher C and lower ash content of BH-H_2O provide a higher HHV (27.7 MJ/kg) than MH-H_2O (17.4 MJ/kg). The pH_{PZC} of BH-H_2O and MH-H_2O are 12 and 9.8 respectively which are comparable to those from CO_2 activation.

According to Figure 3-15, the steam activation process influences the chemical characteristics of raw chars. The C content of activated carbons decreases while the ash fraction increases which results in a lower HHV compared to pyrolysis chars. Consequently, the elements in the inorganic fraction are supposed to be more concentrated due to the higher ash content (Table 3-15).

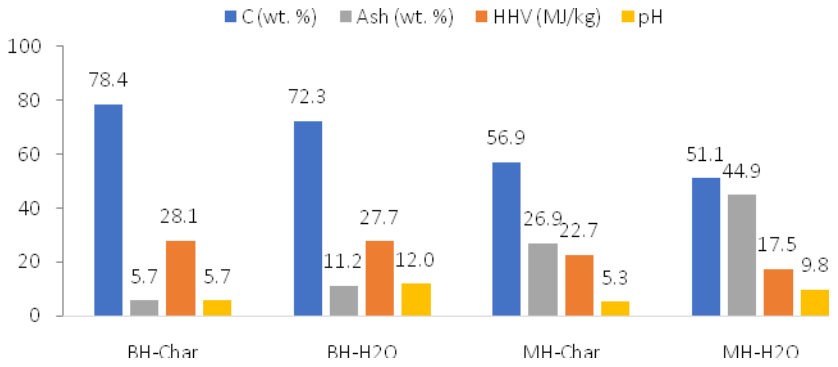

Figure 3-15. Influence of steam activation at 850 °C in raw chars.

The comparison of release between elements is performed as previously described in CO_2 activation. According to Table 3-16, in BH-H_2O the release of mineral elements decreases in the following order P > K > Ca: the phosphorus shows the tendency to be released in a higher degree than K and Ca while Mg remains in the solid phase in higher proportion. In the case of MH-H_2O there seems to be no release of the main elements (K, Ca and Si) due to formation of silicates [190], the 11.3 % of ash release presented in Table 3-14 must be related to the minor elements that compose the inorganic fraction and oxygen from the mineral species.

Table 3-16. Ratio of each measured elements over theoretical concentration in BH-H_2O and MH-H_2O.

BH-H_2O			MH-H_2O		
Element	Theoretical (%)	Measured/Theoretical	Element	Theoretical (%)	Measured/Theoretical
K	5.9	0.7	K	7.6	1.2
Ca	3.7	0.9	Ca	0.3	1.0
P	1.7	0.5	P	1.4	1.4
Si	-	-	Si	33.9	1.0
Mg	2.0	1.3	Mg	-	-
Release decreases: P > K > Ca			Poor release		

The similar content of K in AC prepared through 1-step 4.6 % in BH-CO_2 and 3.9 % in BH-H_2O might imply that oxidizing agent does not has any effect on the transformation of this mineral which is in agreement with Bai et al,. [92] who demonstrated that K release in gasification is not influenced by CO_2 or H_2O. However, other authors have established different trends. Hai-Bo et al., [93] found that the potassium release under CO_2 is similar to that under N_2 and Tchoffor et al., [91] stated that the release of potassium under H_2O is higher than in N_2. Both groups agreed that the potassium release seems to be mainly due to the release of K bonded to char particles.

As far as calcium is concerned, Bai et al. [92], demonstrated that calcium transformation depends on the activating agent and is more released during the CO_2 gasification. Moreover the Ca compounds can agglomerate and sinter resulting in clusters whereas they present homogeneous surface distribution under steam gasification [92,96].

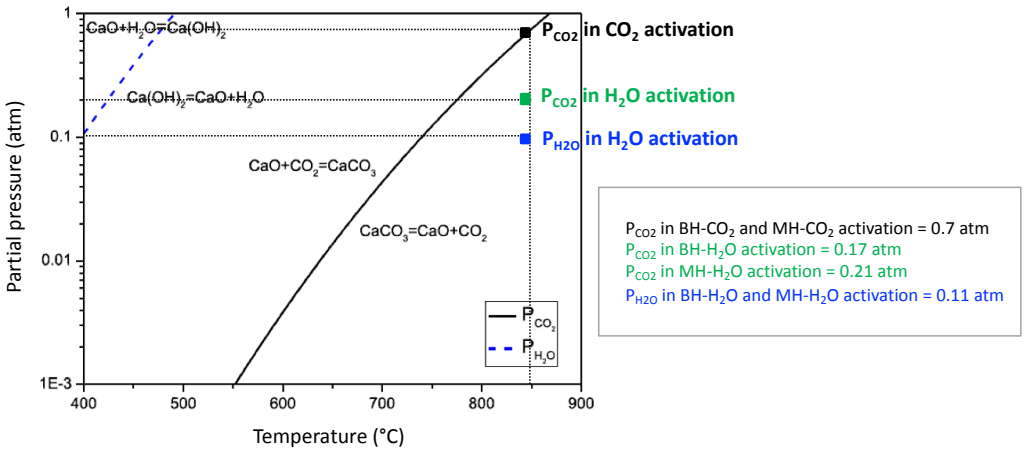

Figure 3-16. Reactions of $Ca(OH)_2$ and $CaCO_3$ in function of partial pressure of H_2O and CO_2 adapted from [98]**.**

The reactions of calcium compounds in function of the partial pressure of CO_2 and H_2O and temperature are presented in Figure 3-16. In this work, the activation under CO_2 of all materials at 850 °C is carried out with a partial pressure P_{CO2} around to 0.70 atm. Since the inlet of CO_2 is significant (70 %), there is no difference in partial pressure of CO_2 between activation of BH or MH. The partial pressures in steam activation are calculated based on the inlet of steam (12 %) and the cumulative gas composition previously presented in Table 3-19 and discussed later.

In steam activation, CO_2 is produced from the water gas shift reaction in different proportion for BH and MH. Therefore, at 850 °C the partial pressure of CO_2 in steam activation of BH is 0.17 atm while that of MH is 0.21 atm. Both pressures are very close and are represented by the green point in Figure 3-16 considering that the partial pressure is presented at logarithmic scale.

Therefore, calcium compounds in BH-CO_2 should be present as $CaCO_3$ and CaO forms corresponding to the equilibrium curve whereas calcium oxide CaO is the dominant species in BH-H_2O. The calcium compounds in MH-CO_2 and MH-H_2O should be in the same form as BH-CO_2 and BH-H_2O respectively. However, it is important to have in mind that the calcium content in MH-CO_2 and MH-H_2O is more than 10 times inferior to that of BH-CO_2 and BH-H_2O. Besides, calcium compounds are most probably trapped by silica in materials from MH therefore they are not available to react during their implementation in tar cracking and H_2S removal.

It appears that transformation of magnesium is not influenced by the oxidizing agent according to the Measured/Theoretical ratio which is 1.1-1.8 for activated carbons prepared from BH. In addition, phosphorus presents Measured/Theoretical ratio of 0.5-0.7 in activated carbons prepared from BH which suggest that this element is not influenced by the atmosphere of activation. However, results are different regarding release of P in MH-CO_2 (1.5; 2.2) and MH-H_2O (1.4). This can be related to the behavior of Si that seems to prevent the transformation of other elements. In the same way, the release of Si based on the Measured/Theoretical ratio (0.9 – 1.3) suggest that this element remains in the solid phase regardless the oxidizing agent which is not surprising considering that it can react with other elements to form silicates at high temperature. There is no a clear trend of release of K and Ca in MH-CO_2 and MH-H_2O since they can form silicate compounds with Si present in these materials.

3.4.2. Textural characterization

The textural characterization of steam activated carbons is presented in Table 3-17. The averages values of two analyses are given with the corresponding standard deviation. The nitrogen adsorption/desorption isotherms of BH-H_2O and MH-H_2O are presented in Figure 3-17. The curves for both materials are of type I [175] which are typical of microporous materials, however compared to isotherms of CO_2 activated carbons, steam activated carbons exhibit more adsorbed N_2 and a wider hysteresis loop indicating the presence of mesopores. The BET surface area and total pore volume of BH-H_2O are 997 m^2/g and 0.681 cm^3/g respectively which are higher compared to MH-H_2O (466 m^2/g and 0.278 cm^3/g).

The pore balance is 71 % of micropores and 29 % mesopores in BH-H_2O whereas the pore share is 83 % of micropores and 17 % of mesopores in MH-H_2O. Thus, it seems that the C content also benefits the creation of porosity at the mesopore scale.

Table 3-17. Textural characterization of H_2O activated carbons.

Analysis	Sample	BH-H_2O	MH-H_2O
	Analyzer	ASAP 2020	ASAP 2020
N_2 Adsorption /Desorption	V_{Total} (cm^3/g)	0.681 ± 0.136	0.278 ± 0.010
	V_{Micro} (cm^3/g)	0.419 ± 0.011	0.206 ± 0.011
	V_{Meso} (cm^3/g)	0.175 ± 0.083	0.043 ± 0.001
	BET Surface (m^2/g)	997 ± 81	466 ± 26
Mercury porosimetry	V_{Total} (cm^3/g)	0.938 ± 0.069	1.027 ± 0.064
	V_{Meso} (cm^3/g)	0.226 ± 0.006	0.031 ± 0.001
	V_{Macro} (cm^3/g)	0.688 ± 0.084	0.988 ± 0.064

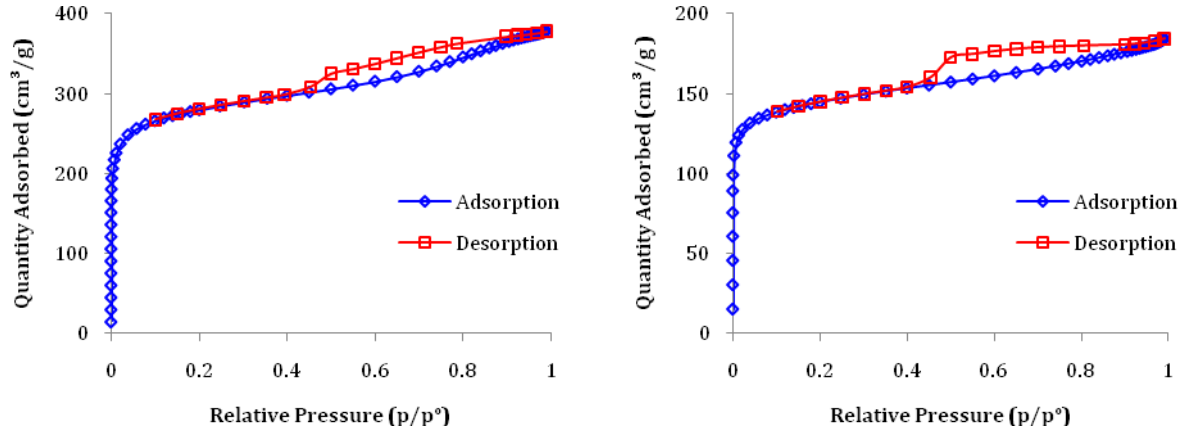

a) BH-H_2O, ASAP 2020 **b) MH-H_2O, ASAP 2020**

Figure 3-17. N_2 adsorption/desorption isotherms of a) BH-H_2O and b) MH-H_2O.

According to mercury porosimetry analysis (Figure 3-18), MH-H_2O also presents compressibility as MH-CO_2 and MH-Char.

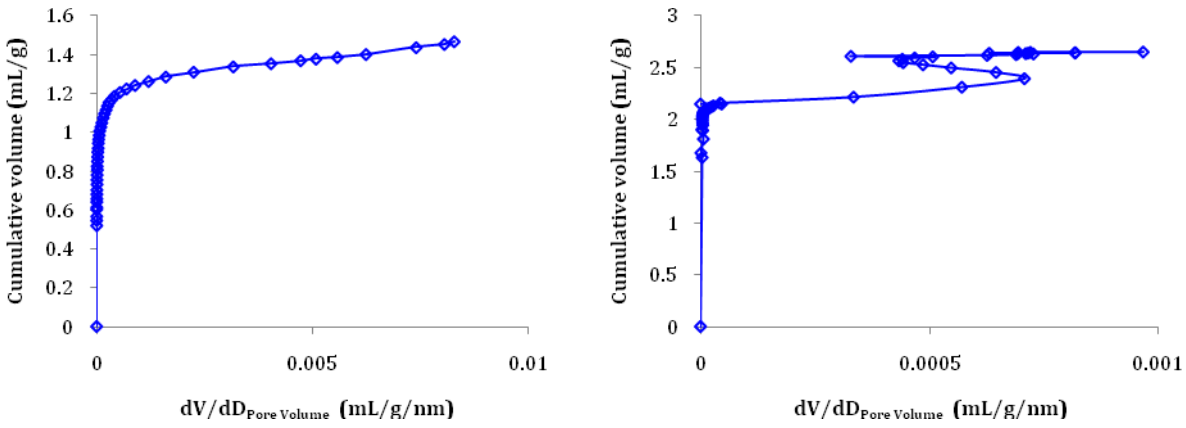

a) BH-H_2O **b) MH-H_2O**

Figure 3-18. Compressibility of activated chars during mercury porosimetry analysis: a) BH-H_2O and b) MH-H_2O.

Regarding Table 3-17, it can be noticed that the porous volume measured by mercury porosimetry of BH-H_2O and MH-H_2O are similar (0.9 – 1.0 cm^3/g) considering the deviation of results (0.06 cm^3/g). It is observed that steam activation provided BH-H_2O with high V_{Total} (0.938 cm^3/g) and V_{Macro} (0.688 cm^3/g). In the same way, the volume of mesopores (8 nm < Dp < 50 nm) of BH-$H_2$0 measured by mercury porosimetry (0.226 cm^3/g) is higher than N_2 adsorption (0.175 cm^3/g) corresponding to pores between 2 - 50 nm, however the difference is within the deviations of the latter (± 0.083 cm^3/g).

The porosity of samples at macro and mesopore level can be observed in Figure 3-19. According to the SEM images, pore are created inside MH and not at the surface therefore it seems that MH-H_2O has lower porosity than BH-H_2O probably due to the silica content of the first that reduces the pore development in the surface of this material.

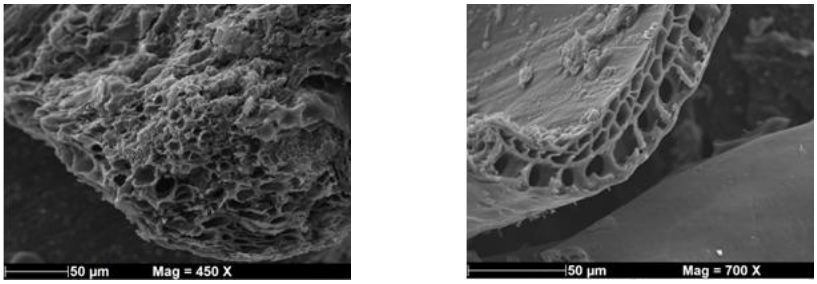

a) BH-H_2O **b) MH-H_2O**

Figure 3-19. SEM images of H_2O activated carbons: a) BH-H_2O, b) MH-H_2O.

The influence of oxidizing agent in activation is presented in Figure 3-20. It can be noticed that steam activation creates higher degree of porosity (higher surface area) compared to CO_2 activation. The superior porosity created by steam activation is due to easier diffusion of steam as explained by Ruiz-Fernández et al., [83] in the first chapter of this document. The higher surface area resulting from steam activation is in agreement with the work of other authors. Yang et al., [84] reported that the activation of walnut shells with H_2O or CO_2 under the same conditions led to activated carbons with higher surface area (771 m^2/g) and pore volume (V_{total} = 0.499 cm^3/g) with steam activation than CO_2 activation (552 m^2/g and 0.293 cm^3/g respectively).

The same trend was reported by Guizani et al., [85] in the gasification of chars with steam and CO_2. They demonstrated that for the same char conversion degree i.e. 50 %, H_2O-chars presented higher surface area (1225 m^2/g) and pore volume than CO_2-chars (842 m^2/g). In fact the work of Benedetti et al., [66] illustrates the similarities between chars from gasification and activated carbons in terms of formation mechanisms, carbon content and porosity. In fact, the physical

activation of biomass is comparable to pyro-gasification since both processes involve the thermo-chemical conversion of the feedstock starting with pyrolysis and followed by an activation stage or partial gasification. In addition, as result of these processes carbonaceous materials with high porosity and gas with similar composition and high LHV are obtained. In the work of Benedetti et al., [66] six chars from different gasification plants were characterized in terms of elemental and inorganic composition, ash content and porosity. The authors illustrated the similarities between some chars from gasification and activated carbons in terms of formation mechanisms, carbon content close to 80 % and varied porosity depending on the gasification technology.

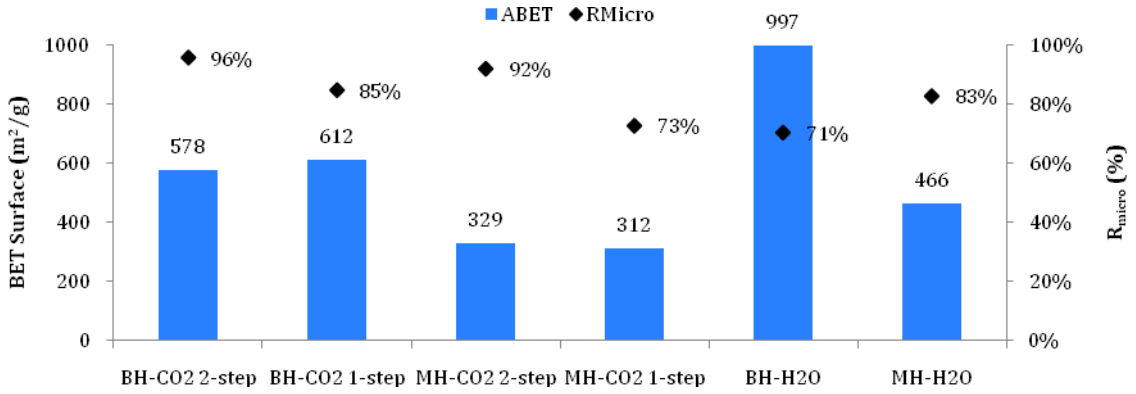

Figure 3-20. Relative microporosity and surface area of materials.

All samples were analyzed by Micromeretics ASAP 2020 except for BH-CO_2 1-step and MH-CO_2 1-step which were analyzed by Micromeretics 3-FLEX.

As shown by results, CO_2 activation creates more micropores in chars with low ash content achieving 85 % in BH-CO_2 compared to steam activation (71 % in BH-H_2O). Pyrolysis at high temperature (700 °C) might develop some mesoporosity which explains the lower microporosity of BH-CO_2 and MH-CO_2 obtained through direct activation. As mentioned before, the higher mesoporosity of samples prepared through 1-step is also in part due to the analyzer used for these samples (3-FLEX). Other authors have agreed that the CO_2 activation creates mainly microporosity while the steam activation results in a higher degree of mesoporosity [70] and that the mechanism of porosity development in this case consists in increasing the pore depth and the pore diameter [83].

3.4.3. Mass and energy balance

The mass and energy balances of steam activation were calculated in order to determine the efficiency of the process in terms of energy recovery (Table 3-18). The mass balances of steam

activations vary in the range 77.8 – 85.2 %, which is within the expected deviation considering that: i) unused feedstock remains in the reactor; ii) tars can get stuck in the pipes, iii) the volatilization of some compounds in the condensable phase; and iv) incomplete oil recovery. It is important to keep this in mind since the efficiency indicators (AEE, AEE_{elec} and NER) are calculated based on the mass balance.

Table 3-18. Mass and energy balances of H_2O activation at 850 °C.

		BH-H_2O			MH-H_2O		
		Mass fraction (wt.%)	**LHV (MJ/Kg)**	**Energy (MJ/$Kg_{Biomass}$)**	**Mass fraction (wt.%)**	**LHV (MJ/Kg)**	**Energy (MJ/$Kg_{Biomass}$)**
Inlet	Biomass	100	16.8 ± 0.2		100	17.1 ± 0.8	
	Electrical consumption	-	-	30.3	-	-	29.4
Outlet	AC	10.0 ± 0.4	27.5 ± 0.9	2.8 ± 0.1	15.3 ± 0.1	17.39 ± 0.01	2.7 ± 0.01
	Aqueous phase	23.9	0	0	22.5	0	0
	Oily phase	16.8	5.70 ± 0.01	1.0	3.0	23.7 ± 5.2	0.7
	Gas	34.5 ± 5.3	15.0 ± 0.4	5.2 ± 0.7	37.0 ± 0.6	14.3 ± 0.1	5.3 ± 0.1
Performance indicators:	**Target products**	**Oil and gas**	**AC, oil and gas**		**Oil and gas**	**AC, oil and gas**	
	AEE*	**36.6 ± 4.2 %**	**53.0 ± 4.0 %**		**34.9 ± 0.3 %**	**50.4 ± 0.3 %**	
	AEE elec**	**13.0 ± 1.5 %**	**18.9 ± 1.4 %**		**12.9 ± 0.1 %**	**18.6 ± 0.1 %**	
	NER***		**0.294 ± 0.022**			**0.294 ± 0.002**	

**AEE: apparent energy efficiency defined as the ratio of the energy content in the target products to the energy content of the raw biomass; **AEEelec: takes into account the electrical consumption in the denominator; ***NER: Net energy produced in the process.*

The apparent energy efficiency (AEE) suggests that the energy that can be recovered as oil and gas from steam activation is similar for both biomasses. This similarity is due to the comparable energy carried in both gases (14 – 15 $MJ/kg_{Biomass}$). In the same way, the higher mass fraction of MH-H_2O (15.3 %) than BH-H_2O (10.0 %) makes up for the lower LHV of the first (17.4 MJ/kg).

Table 3-19. Gas composition from H_2O activation at 850 °C.

Biomass	**H_2**	**CH_4**	**CO**	**CO_2**	**CxHy**
	mol %				
BH	52.4 ± 2.9	3.9 ± 1.4	24.6 ± 1.1	18.8 ± 1.7	0.4 ± 0.2
MH	45.4 ± 0.5	7.5 ± 0.3	21.9 ± 1.5	24.0 ± 0.6	1.2 ± 0.1

The LHV of gas resulting from the whole process (pyrolysis + activation) is calculated from the composition of the gas depicted in Table 3-19. The produced gas from steam activation is composed of H_2, CH_4, CO, CO_2 and C_XH_Y. It is important to mention that the gas does not contain steam since it was condensed before the outlet stream enters the gas analyzer. It can be noticed that, the gas from BH-H_2O is richer in H_2 (52.4 %) and CO (24.6 %) and has lower CO_2 (18.8 %) content in comparison to MH-H_2O thus the LHV of the latter is lower as shown in Table 3-18.

The profiles of gas from steam activation of BH and MH at 850 °C are presented in Figure 3-21. The production of H_2 riches its maximum (65 %) at the highest temperature and then stabilizes during the activation stage (60 %).

a) BH

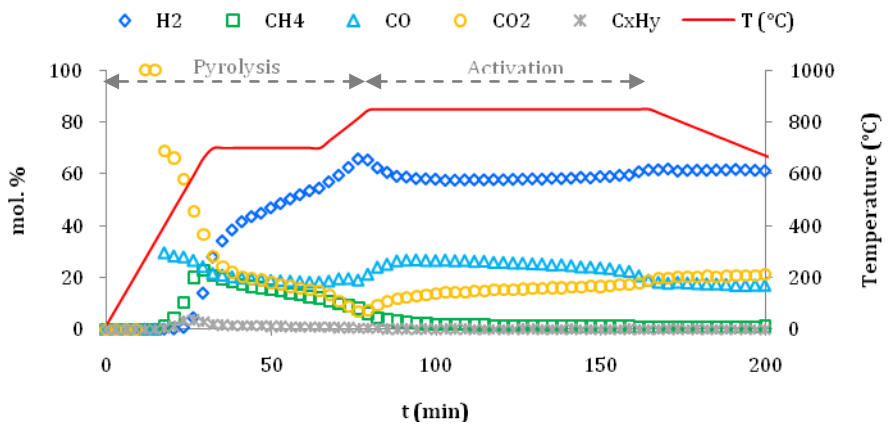

b) MH

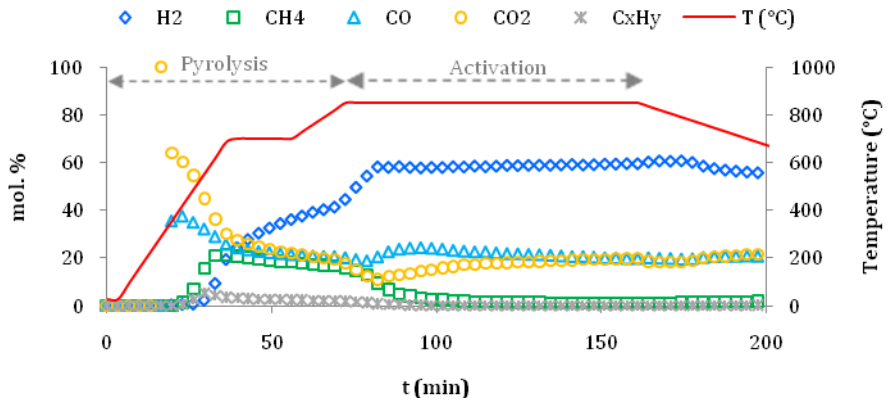

Figure 3-21. Gas composition steam activation of a) BH and b) MH at 850 °C.

It can be noted that H_2 is the dominant gas species through steam activation. On the other hand, CH_4 is mainly produced during pyrolysis while CO and CO_2 are produced during the whole process. It can be noted that production of CO and CO_2 start around 300 – 400 °C due to the decomposition of cellulose and hemicellulose and then decrease gradually until the end of pyrolysis. In the activation stage, formation of CO_2 is relatively constant varying from 23 to 26 %, while CO tends to increase from 10 to 19 %. The production of H_2, CO and CO_2 in the activation stage is explained according to the gasification with steam (R 1-15) and water gas shift reactions (R 1-17). It is worthwhile mentioning that MH-H_2O follows the same gas evolution as BH-H_2O.

Gasification with steam	$C + H_2O \rightarrow CO + H_2$	**R 1-15**
Water gas shift reaction	$CO + H_2O \leftrightarrow H_2 + CO_2$	**R 1-17**

If activated carbons are valorized as materials, energy recovery is made through oil and gas. In that sense, the recovered energy comes mainly from the gas as shown in Table 3-18 since the liquid phase is principally composed of water accounting for 58 % in BH activation and 88 % in the case of MH. The high water content is from steam generated in the pyrolysis stage and the steam employed in the activation step that is condensed in the cold trap. In addition, it is important to mention that the oily phase is heterogeneous and its LHV is variable.
If oil and gas are considered as energy vectors, steam activation is more efficient than pyrolysis since the apparent energy efficiency (AEE) of the process is 36.6 and 34.9 % for BH-H_2O and MH-H_2O respectively. This observation is also true if the electrical consumption required to heat the system (reactor and gases) is considered in AEE_{elec}. The electrical consumption to raise the temperature of the system represents about 99 % while the activation merely accounts for less than 1 % of the total input (Annexe 2).

The reason for the higher performance of steam activation is the high LHV (14 – 15MJ/kg) of the gas which allows recovering much of the energy consumed. However, if all products of steam activation are meant to be valorized as energy carries, the AEE are 53 and 50% for activation of BH and MH therefore, pyrolysis is preferred with AEE of 74 and 62 % justified by the higher mass fraction of char recovered in this process (38 %). This is also evidenced in the NER as the result of lower energy demand in pyrolysis. The net energy produced in steam activation can be improved if the heat of the gas is used in the process, thus modifications of the pilot should be made in order to incorporate this operation.

In the work of Dieme et al., [164] the production of several activated carbons from different feedstocks such as cashew shells, millet stalks and rice husks was studied. The operating conditions were similar to the ones used in the present work. The carbonization of raw materials was conducted under an inert atmosphere up to 850°C and then were activated with steam for 80 min. Mass and energy balances as well as efficiency indicators were calculated. If activated carbons were valorized as materials, the AEE indicators from activation of cashew shells, rice husks and millet stalks were 79.8 %, 30.1 % and 53.3 % respectively. On the other hand, if ACs were considered as energy vectors as well the NER ratios were 0.750, 0.284 and 0.416. The high performance of cashew shells activation compared to millet stalks and rice husks is due to the composition of materials. Cashew shells had the highest carbon content (54%) and the lowest ash fraction (4 %). In comparison to the present study, the lower efficiency of BH-H_2O and MH-H_2O activation is explained by the mass of water which is included in the calculations as an inlet of the process.

Lastly, steam activation (NER ~ 0.3) is more efficient than CO_2 activation (NER ~ 0.1) due to the steam condensation that improves the LHV of the gas in the first and the high CO_2 content in the gas from the latter. The condensation of steam allows separating the oxidizing agent from the gas phase avoiding to dilute the LHV of the former. In contrast, in activation with CO_2 it is not possible to separate the oxidizing agent which is fed in excess and this reduces the LHV of the gas considerably as mentioned before. Thus, condensing steam favors the energy efficiency of the process since the liquid phase has the lowest energy value even when activation is conducted with CO_2. Overall, the operation conditions of activation with CO_2 must be optimized in order to improve the energy recovery from this process.

The summary of CO_2 and steam activation processes and products are presented in Table 3-20 Table 3-21. Overall, the use of steam as activating agent is necessarily associated with a high aqueous fraction in the oil. However, this allows improving the LHV of the gas produced in this process. The use of steam also favors the H_2 content in the gas due to the water gas shift reaction. On the other hand, the advantage of using CO_2 as oxidizing agent is to have less water content in the liquid phase. Therefore, steam activation is a more efficient process in terms of energy recovery considering that the performance indicators AEE and NER are higher than those from CO_2 activation in spite of the lower mass balance (78 and 85 %) in comparison to CO2 activation (88 and 100 %). Thus, the inlet of CO_2 must be reduced and optimized in order to increase the LHV of the gas and be able to recover more energy from this process. It is evident that the activating agent has great influence in the properties of activated carbons.

Table 3-20. Comparison of CO_2 and steam activation process of BH and resulting products.

Parameter	BH: H_2O Activation	BH: CO_2 Activation
Mass balance	85 %	100 %
Oil	Oil with high water content due to condensation of steam LHV = 6 MJ/kg; Mass fraction of oil = 16 wt.%	Oil with lower water content LHV = 21 MJ/kg; Mass fraction = 0.8 wt.%
Gas	Higher H_2 and CO and lower CH_4 and CO_2 content resulting in higher LHV compared to CO_2 activation of BH LHV = 15 MJ/kg; Mass fraction = 34 wt.%	High CO_2 content and lower LHV compared to steam activation of BH LHV = 2.2 MJ/kg; Mass fraction = 92 wt.%
Activated carbon	Well dispersion of CaO as the dominant species. Lower release of Ca.	Same amount of CaO and $CaCO_3$ under the conditions of this study. Higher release of Ca.
	Higher surface area in comparison to CO_2 activation of BH	Lower surface area and higher relative microporosity compared to steam activation of BH
Energy performance	Higher energy efficiency due to higher H_2 content from water gas shift reaction and steam condensation. The processes must be optimized to improve the energy recovery compared to pyrolysis. AEE = 53 %; NER = 0.294	Lower energy efficiency due to the high content of CO_2 in the gas phase. The operating conditions of the process need to be optimized. Reducing the inlet of CO_2. AEE = 23 %; NER = 0.128

Table 3-21. Comparison of CO_2 and steam activation process of MH and resulting products.

Parameter	MH: H_2O Activation	MH: CO_2 Activation
Mass balance	78 %	88 %
Oil	Oil with high water content due to condensation of steam LHV = 24MJ/kg; Mass fraction of oil = 3 wt.%	Oil with lower water content LHV = 24 MJ/kg; Mass fraction = 0.7 wt.%
Gas	Higher H_2 and CO and lower CH_4 and CO_2 content resulting in higher LHV compared to CO_2 activation of MH LHV = 14 MJ/kg; Mass fraction = 37 wt.%	High CO_2 content and lower LHV compared to steam activation of MH LHV = 1.8 MJ/kg; Mass fraction = 78 wt.%
Activated carbon	Calcium compounds are probably in the form of calcium silicates. Most mineral elements seem to remain in the solid phase.	Calcium compounds are probably in the form of calcium silicates. Most mineral elements seem to remain in the solid phase.
	Higher surface area than CO_2 activation of MH	Lower surface area compared to steam activation of MH.
Energy performance	Higher efficiency than CO_2 activation, however, the processes must be optimized. AEE = 50 %; NER = 0.294	The lowest energy efficiency due to the low yield and LHV of the gas. AEE = 14 %; NER = 0.08

On one hand, steam activation produces activated carbons with higher porosity which includes micropores and mesopores. On the other hand, CO_2 activation seems to create higher relative microporosity, however if pyrolysis is carried out at higher temperature (700 °C) mesopores are generated as well reducing the percentage of micropores. In steam activation, calcium compounds are well dispersed and can be found as CaO if silicon is not present. In the former case, calcium will be rather found as silicates. In CO_2 activation, calcium is present as CaO and $CaCO_3$ which can be agglomerated and in presence of silica they can be trapped as silicates. It is important to mention that the fraction of K and Ca that reacts with Si to form silicates is unknown, therefore it is not possible to determine the fraction of Ca and K available to participate in solid-gas reactions.

3.5. Conclusion

The pyrolysis and activation of BH and MH have been carried out in order to valorize these agricultural wastes as energy vectors or materials. The resulting chars and activated carbons have been characterized in terms of chemical and textural properties with the intention of evaluating the influence of the parent biomass in the properties of pyrolysis chars and activated carbons. In addition, different methods of activation have been carried out: one and two-steps CO_2 activation and one-step steam activation. The influence of the oxidizing agent on the features of activated carbons was also analyzed. Finally, the mass and energy balances of the processes have been calculated aiming to evaluate the energy recovery depending on the type of process and material.

It was evidenced that the biomass has great influence in the properties of resulting chars and activated carbons. The higher C and lignin content of BH favors the LHV of the solid samples and the development of porosity at different pore scales. In contrast, the elevated ash fraction of MH results in lower LHV of the solid and less porosity according to N_2 adsorption analysis. It was observed that during pyrolysis of BH more ash is released than MH. The inorganic composition of raw chars is associated to the mineral elements present in biomass which are potassium, calcium, phosphorus and magnesium for BH-Char while MH-Char is composed of silica, potassium, calcium and phosphorus. There is high probability that MH and its derived materials have Mg according to literature, however this element cannot be well quantified by X-ray fluorescence. Finally, it was found than pyrolysis chars have more acidic functional groups in the surface than basic groups. In terms of porosity, it was evidenced that pyrolysis chars are mainly macroporous and that MH-Char and its derived activated carbons present high compressibility during the intrusion of mercury thus results of this sample might be overestimated.

The activation process modified the chemical and textural characteristics of pyrolysis chars. It seems that carrying out one or two-steps CO_2 activation influence the properties of activated carbons depending on the parent biomass. According to this study, CO_2 activation results in higher C and lower ash content than steam activation. It was observed that during one-step CO_2 activation of millet husk the silica seems to trap char particles inflating the ash content of this sample. The mineral release during CO_2 activation was lower than in steam activation due to the higher transformation of elements that are bonded to carbon during H_2O activation. In addition, the oxidizing agent influences the ash release and mineral species on the surface of activated carbons. In activation with CO_2, more Ca is released from BH-CO_2 and the calcium compounds remaining in the solid phase are found like CaO and $CaCO_3$ forms. Besides, Ca compounds are agglomerated thus they are not well-dispersed in the surface of activated carbon. In contrast, during steam activation less calcium is released from BH-H_2O and it is mostly present in the CaO form which is well dispersed in the surface. In the case of activation with either steam or CO_2 of MH and MH-Char, calcium compounds are most probable forming silicates. It appears that release of Mg, P and Si is not influenced by the oxidizing agent in activation. A less clear trend is observed with potassium which apparently is not influenced by the oxidizing agent.

The activation type also has significant influence in the porosity of activated carbons. Activation with CO_2 creates more micropores while steam activation develops micro- and mesopores, however if pyrolysis is carried out at elevated temperature mesopores can be created at this stage as well decreasing the relative microporosity of resulting AC. Additionally, H_2O-activated

carbons have higher surface area than samples activated with CO_2. The characteristics of the biomass are reflected in the properties of activated carbons. The higher carbon and lignin content of buckwheat husk allows creating higher porosity while the elevated ash content in millet husk mostly composed of silica reduces the creation of pores at the surface which explains the lower porosity of MH-CO_2 and MH-H_2O compared to BH-CO_2 and BH-H_2O respectively.

According to mass and energy balances, results from pyrolysis shows that the phase that carries most of the energy is the char thus it must be valorized as an energy vector as well as oil and gas. To do that, the char can be submitted to activation which is similar to gasification and the energy contained in the carbonaceous matrix will be transformed into syngas with higher LHV that can be used as energy or as precursor of synthesis of chemicals and fuels through the Fischer-trosph process. Then the gasified char or activated carbon which has higher porosity and more concentrated minerals can be implemented in other applications such as adsorbent, catalyst in the cleaning of syngas or it can be re-introduced in the gasifier in order to reduce tar formation according to the mineral composition of the char (more suitable for BH-materials). It was observed that the gas from steam activation has higher LHV than CO_2 activation; however the operating conditions of the latter can be optimized in order to increase the LHV of the gas improving the energy recovery from this process. In addition, modifications of the experimental configuration must be performed in order to recover the latent heat of the produced gas in the process and improve the energy recovery. The mass balances of activations don't affect the general conclusion since the method that allows to recover more energy is steam activation which presents lower mass balance (78 – 85 %) than CO_2 activation (88 – 100 %) due to the incomplete oil collection. This means that the energy efficiency of H_2O-activation can be superior if the mass balance of this method is higher.

The characteristics of the biomass don't seem to have significant influence in the energy recovery of pyrolysis and activations since the energy consumed in the carbonization and activation of biomass is low (< 3%) compared to the electrical input required to heat the reactor and gases.

Chapter 4. Syngas upgrading using chars

Introduction

As presented in Chapter 1, syngas from the gasification process is mainly composed of H_2, CO, CO_2, CH_4 and light hydrocarbons, it also contains impurities like particles, ammonia, soot and tars whose concentrations can vary from 5 to 75 g/Nm^3 depending on biomass and operating conditions of gasification process [104,106]. The tars have a negative impact in the potential applications of syngas since they can cause the fast deactivation of catalysts which play a critical role in syngas conversion reactions like Fischer-Tropsch [101]. Recently, chars have been reported to be promising materials to enhance the tar treatment as an adsorbent and/or catalyst based on the carbonaceous and mineral features [117,191]. However, the role of these properties is not well understood yet. In addition, there is a lack of studies on the use of raw and activated chars for cracking of light aromatic compounds other than benzene and toluene which does not allow evaluating the purification potential of these materials.

In this chapter, raw and activated chars have been implemented in a fixed-bed column whose temperature is maintained at 650 °C in order to investigate the catalytic decomposition of syngas tars. Ethylbenzene (EB) is chosen as surrogate of one-ring aromatic hydrocarbons, besides its decomposition into styrene and benzene allows studying other molecules in parallel. The purification efficiency of these different materials (chars and AC) is deduced from EB conversion profiles in comparison to thermal cracking whereas this is scarcely presented like this in the literature. Generally, the authors provide a total efficiency and they don't separate the material performance from the thermal cracking. Efficiency of chars is tested under different gas mixtures. First, a simple mixture composed of N_2, CO and EB is implemented in order to evaluate conversion of EB attributed only to properties of materials. Then, a dry complex mixture similar to syngas composed of H_2, CH_4, CO, CO_2, N_2 and EB is adopted in order to test selectivity of chars towards EB in presence of other gas species. Finally, steam is added to the complex mixture in order to study the impact of water in removal of EB. The experiments are carried in a fixed-bed of materials or with an empty column as shown in Figure 4-1.

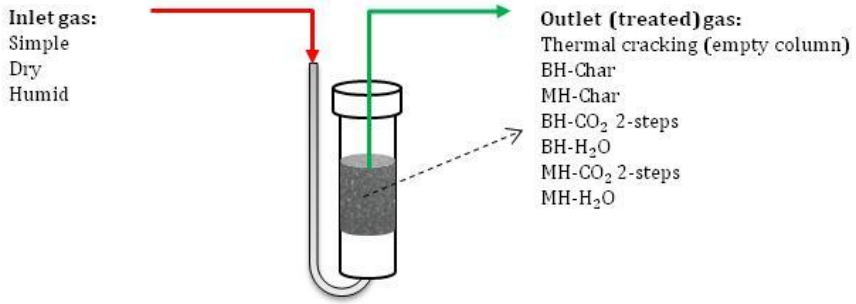

Figure 4-1. Description scheme to differentiate inlet and treated syngas.

The gas entering the column is named inlet gas and the outlet gas refers to the treated gas leaving the column filled with samples or thermal cracking with an empty column. For the experimental campaign, the samples selected from CO_2 activation were those prepared through 2-steps activation, thus BH-CO_2 2-steps and MH-CO_2 2-steps. This selection was made in order to compare the efficiency of materials with higher relative microporosity to those with more balanced distribution of porosity including a higher degree of mesoporisity (steam activated carbons).

Deactivation of chars is also investigated and defined as the time when conversion of ethylbenzene is no longer attributed to properties of materials but only to thermal cracking. Lastly, gasification of exhausted chars is studied with the aim of seeing if this can be an end life of chars. In this case, the purpose is to recover as much as possible energy from exhausted materials. Therefore, composition and quality (LHV) of syngas are taken as reference to determine the efficiency of the process.

4.1. Thermal cracking of ethylbenzene

Before studying the performance of chars, it is important to determine the degree of thermal decomposition of ethylbenzene at 650°C, which is the temperature chosen to conduct the catalytic tests of EB in presence of chars or AC. For all tests the EB concentration at the inlet of the column is 40 g/Nm^3. Thermal cracking was measured with an empty reactor for the three matrices of gas. The residence time in a column filled with chars or ACs is probably longer and different for each material, however it is assumed that the difference is not significative therefore this time is not measured. In addition, it is also believed that for a fixed-bed of 4 cm a slightly longer residence time does not influence EB. In order to determine the influence of the residence time in EB conversion, further experiments should be carried out increasing the bed height, nevertheless it should be noted that in this study the EB conversion is normalized to 1 g

of material. It is worth mentioning that composition of dry and humid syngas is representative of real syngas using different gasifying agents according to literature [100,103,107]. Gas flow was fixed in order to have a speed of 0.1 m/s inside the reactor at 650 °C.

The evolution of ethylbenzene concentration in the outlet stream of the column at 650 °C is shown in Figure 4-2. Note that concentration of ethylbenzene takes more than 40 min to reach its maximum value. This observation is justified by the dimensionless Reynolds number which was calculated for the three types of matrices and it was found that these gases follow a laminar flow with Reynolds equal to $4.0x10^{-3}$, $3.1x10^{-5}$ and $3.9x10^{-3}$ respectively due to the low velocity (0.1 m/s).

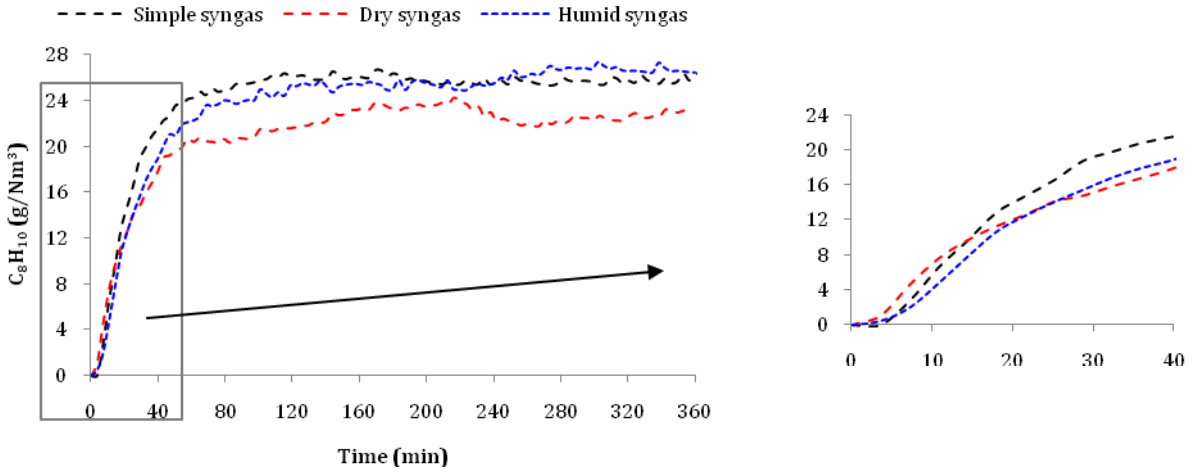

Figure 4-2. Thermal cracking in different syngas matrices at 650 °C, EB = 40 g/Nm³.

According to results, concentration of ethylbenzene starts raising at the same speed for all matrices, then after 20 min, the rate of increase in EB concentration is different for each type of gas mixture. The highest rate of EB concentration increase is accomplished with the simple mixture and the lowest with dry syngas suggesting that in the latter, conversion of EB is superior. Then at approximately 180 min, concentration of EB seems to stabilize around 23 - 26 g/Nm³ depending on the type of syngas. However, at 220 min thermal cracking in simple mixture remains constant whereas in dry syngas increases and in humid syngas it appears to decrease. This divergence of EB decomposition after 220 min might be linked to production of coke which can influence thermal cracking. Indeed, it seems that in presence of steam, the production of soot is more important. At the beginning of the test, there is no soot, then soot is formed over time. When their quantity is sufficient, the soot can impact the tar cracking reaction negatively.

Conversion of ethylbenzene including thermal cracking is calculated as the difference between inlet and outlet EB as usually presented in literature [111,116,118,172] according to Eq. 2-10.

$$Y_{EB}\,(\%) = \frac{EB_{in} - EB_{out}}{EB_{in}} \qquad \textbf{Eq. 2-10}$$

The total removal of ethylbenzene is calculated over 360 min for all matrices and thermal cracking conversion is 39 wt.%, 48 wt.% and 41 wt.% for simple mixture, dry and humid syngas respectively with 10 % of variation.

4.2. Calculation method

Performance of materials was evaluated in tar removal from different gas matrices containing ethylbenzene at a concentration of 40 g/Nm^3. All experimental tests are realized at 650 °C. Concentration of EB was measured at the downstream of the system with and without materials inside the column, which allows identifying the contribution of the thermal cracking and conversion attributable to the studied materials on the EB conversion. The efficiency giving by the following equation (Eq. 2-11) corresponds to the efficiency of the materials. The thermal cracking was determined and discussed in the previous section. As explained before, efficiency of samples (X_{tar}) is defined in terms of grams of ethylbenzene removed by gram of material.

$$X_{tar} = \frac{Q_{gas}}{m_i}\int_{t_0}^{t} C_0 - C_t - C^* \qquad \textbf{Eq. 2-11}$$

With C_0, C_t and C^* the EB concentration at the inlet, outlet and thermal cracking respectively. m_i is the mass of material used expressed in grams and Q_{gas} is the total flow of gas expressed in m^3/s.

4.3. Performance of raw and activated chars in simple mixture

4.3.1. Raw chars

The concentration of ethylbenzene in the outlet stream of the reactor filled of pyrolysis chars at 650 °C in function of time is depicted in Figure 4-3. According to this figure, ethylbenzene conversion over the raw chars MH-Char and BH-Char resulted in concentrations above those of thermal cracking in the outlet gas. This means that these materials are not active to remove EB from the gas; in addition, it is possible that they release or generate tars what explains that the EB concentration at the outlet is higher than the value obtained in the case of thermal cracking. This result has already been reported in the literature for cracking of naphthalene at initial

concentration of 0.57 g/Nm³ [111] and benzene 4.5 g/Nm³ [118] in nitrogen (simple mix) over wood chars from pyrolysis at different temperatures 850-1050 °C. In these studies the global conversion of the tar model with pyrolysis chars was the same or lower than the thermal cracking.

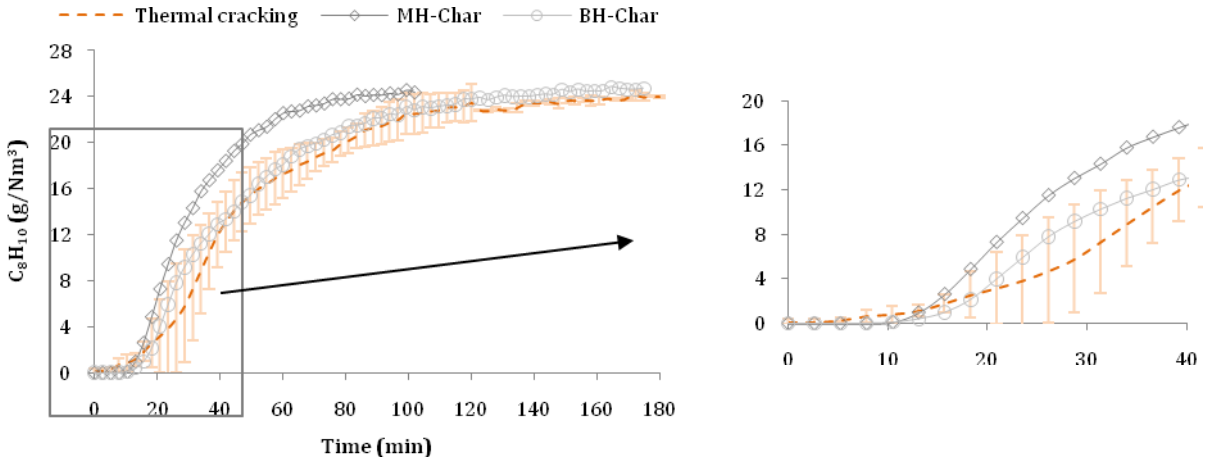

Figure 4-3. Concentration of EB in the outlet stream of the column filled with pyrolysis chars at 650 °C for a simple matrix and a concentration at the inlet of EB = 40 g/Nm³.

Curves from BH-Char and MH-Char are close to those of thermal cracking which implies that these samples lack of reactivity. Indeed according to the Figure 4-3, MH-Char and BH-Char start to lose their reactivity at 11 and 13 min respectively and at 15 and 20 min they are fully deactivated since ethylbenzene conversion is mainly due to thermal cracking. This is confirmed by the calculation of ethylbenzene removal by each sample which shows EB reduction efficiency lower than those obtained with the thermal cracking alone. Performance of materials is compared to thermal cracking in terms of EB conversion (Y_{EB}) and samples are compared between them in terms of X_{tar} which excludes the effect of thermal cracking and takes into account the mass of materials. Since the breakthrough curve of MH-Char was above thermal cracking the experiment was stopped at 100 min, therefore the balance of EB content in syngas is performed at this point to be able to compare to efficiency of BH-Char. According to Table 4-1, performance of pyrolysis chars is negative being -0.036 g_{EB}/g for BH-Char and -0.128 g_{EB}/g for MH-Char. This observation is evidenced also in Table 4-1 where it is shown that thermal cracking eliminates 49.4 % of EB while MH-Char and BH-Char achieve EB conversion of 66.0 and 58.4 % respectively which is close to cracking with an empty column.

Table 4-1. Removal of EB from simple matrix using pyrolysis chars at 650 °C for a simple matrix and EB = 40°C, balance calculated at 100 min.

t = 100 min	Thermal cracking	BH-Char	MH-Char
Y_{EB} (%)	62.9 ± 10	66.0	58.4
X_{tar} ($g_{EB}/g_{material}$)	-	-0.036	-0.128

The non-reactivity of pyrolysis chars can be explained by the limited porosity restricted to macropores which are too width to adsorb a molecule with a critical diameter close to 0.663 nm which correspond to the diameter of EB [192]. According to the literature, the pore diameters close to the molecular diameter of the adsorbate (micropores) are more reactive due to the beneficial intermolecular attraction forces [111]. In the same way, the deficient porosity of materials does not provide easy access to the mineral elements such as K (0.9 %), Ca (0.5 %) in BH-Char and K (4.5 %), Ca (0.2 %) in MH-Char, which are present in small quantities but probably involved in the conversion of ethylbenzene. Since pyrolysis of biomass was carried out at 500 °C, at this point formation of silicates and phosphates of calcium and potassium did not take place. In consequence, K and Ca are not inhibited by Si in MH-Char, however the low porosity makes them no available to participate in conversion of ethylbenzene.

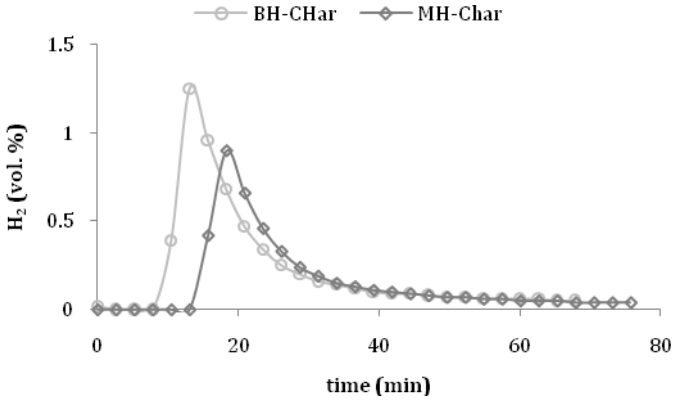

Figure 4-4. Hydrogen released from BH-Char and MH-Char at 650 °C under CO + N_2.

Another important observation is that MH-Char and BH-Char lost 24 and 30 % of their initial weight respectively during the experiment. Thus, transformation of these samples might take place which was verified by a blank test where the reactor was filled with MH-Char and BH-Char at 650 °C under syngas atmosphere (N_2, CO) without ethylbenzene (Figure 4-4). The blank test showed that hydrogen was released from chars to syngas. This could be the result of further pyrolysis or gasification of chars at higher temperature (650 °C) than the one used in the preparation process (500 °C).

Composition of gas resulting from tar cracking was calculated from experimental data, the balance was performed at 100 min for both samples and thermal cracking. The inlet and outlet gas composition are presented in Table 4-2 respectively. The decomposition of ethylbenzene results in formation of hydrogen (Trace), carbon monoxide (2 %), ethylene (C_2H_4) and ethane (C_2H_6). Results show that the same gas composition leaving the column is obtained for the empty column as well the reactor filled with pyrolysis chars. The tar reduction from 0.9 % to 0.4-0.6 %

is mainly attributed to thermal cracking. The difference in tar content from BH-Char (0.4 %) and MH-Char (0.6 %) is explained by the deviation of degradation of ethylbenzene due to temperature (Figure 4-3).

Table 4-2. Composition of inlet and treated simple mixture with pyrolysis chars at 650 °C, balance calculated at 100 min.

t = 100 min		H_2	CO	C_{2+} *	Tars**	N_2
		mol. %				
Inlet simple matrice		0	37	0	0.9	62
Outlet gas	Thermal cracking	Trace	39	Trace	0.6	60
	BH-Char	Trace	38	Trace	0.4	61
	MH-Char	Trace	39	Trace	0.6	61

**C_{2+}: refers to C_2H_4 + C_2H_6; **Tars: denotes remaining EB (C_8H_{10}) and other lighter tar molecules produced from EB conversion (C_6H_6 + C_8H_8).*

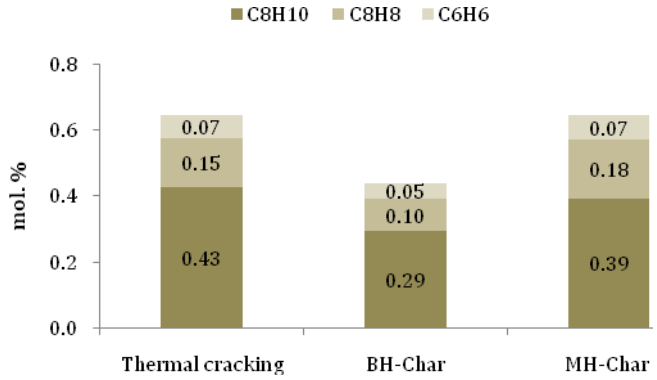

Figure 4-5. Tar composition in simple matrix treated with pyrolysis chars at 650 °C.

The tar composition of the gas leaving the column was determined from experimental data and is presented in Figure 4-5. More than half of total tar in the treated syngas is composed of remaining ethylbenzene (0.29 – 0.43 %). In addition, lighter tar compounds were formed from the fragmentation of ethylbenzene (C_8H_{10}). These compounds are mainly styrene (C_8H_8), which is formed in highest proportion followed by benzene (C_6H_6).

4.3.2. Activated chars

According to Figure 4-6, activation of chars increased their efficiency since the ethylbenzene concentration in the outlet gas is below the thermal cracking. This result suggests that increased porosity, concentrated mineral species and basic surface of activated chars (pH ~ 10 and 12) influences the catalytic properties of materials.

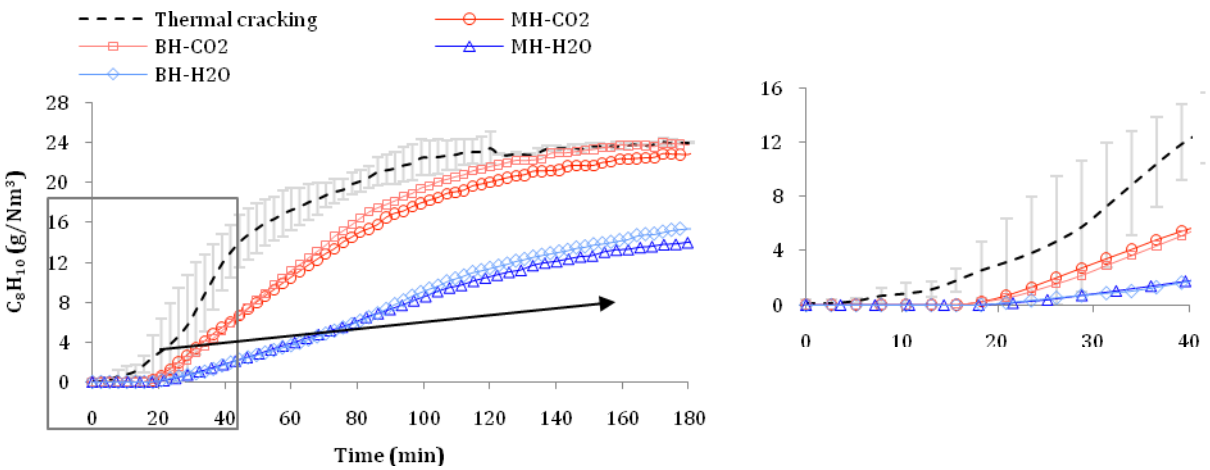

Figure 4-6. Concentration of EB in the outlet stream of the column filled with AC at 650 °C using a simple matrix and inlet concentration of EB of 40 g/Nm³.

With the column filled with either MH-CO_2 or BH-CO_2, ethylbenzene is fully cracked for 18 min, and then both samples start to deactivate completing full saturation at 180 min since outlet EB concentration is similar to thermal cracking. On the other hand, with MH-H_2O and BH-H_2O complete conversion of ethylbenzene is achieved for 22 min. After that point, concentration increases gradually and at 180 min of experiment ethylbenzene concentration in the outlet gas continues to be far below thermal cracking which means that both samples still present some reactivity. At this point, EB due to thermal cracking is 24 g/Nm³ whereas EB is found at 14 and 15.4 g/Nm³ in the stream leaving the column filled with MH-H_2O and BH-H_2O respectively.

Steam activated carbons show lower deactivation rate than CO_2 activated samples considering the rate of increase of EB concentration. Indeed at 180 min of test, the chars activated with CO_2 are saturated whereas the chars activated by steam show an efficiency of 25 and 21.5 % for MH-H_2O and BH-H_2O respectively. Note that there is a constant difference between CO_2 and steam activated carbons regarding increase of EB over time. This result might be due to the presence of mesopores in MH-H_2O (17 %) and BH-H_2O (29 %) that favor the mass transfer in the porous network and reduce deactivation rate compared to MH-CO_2 (8 %) and BH-CO_2 (4 %). Hosokai et al., [122] demonstrated that during benzene and naphthalene conversion over char-coal, the surface area and micropore volume decreases while the mesopore volume remains almost constant. This observation allowed them to conclude that micropores serve as active sites for the tar decomposition causing loss of microporous volume, surface area and the activity of the char-coal. It is also probable that mesopores do not contribute to the tar conversion, but they are responsible for the long-time stability of the char. It has been stated that microporous carbons exhibit high reaction rates at the beginning, but they achieve saturation very fast. In contrast,

mesoporous materials present more stable reactivity [118,193] which is the case of samples activated with steam.

The breakthrough curve of BH-CO_2 overlaps thermal cracking at 180 min, therefore it was chosen to calculate the EB removal from gas at this point to be able to compare all materials. BH-CO_2 and MH-CO_2 show EB cracking close to thermal cracking while steam activated chars present ~ 20 - 30% of additional efficiency. The efficiency attributed to materials properties is seen in the positive performance in terms of X_{tar} (Table 4-3).

Table 4-3. Removal of EB from simple matrix using activated chars at 650 °C and EB = 40 g/Nm³, balance calculated at 180 min.

t = 180 min	Thermal cracking	BH-CO_2	BH-H_2O	MH-CO_2	MH-H_2O
Y_{EB} (%)	53.6 ± 9.1	62.7 ± 3.1	81.1 ± 2.4	66.5 ± 8.2	82.1 ± 6.4
X_{tar} ($g_{EB}/g_{material}$)	-	0.200 ± 0.060	0.951 ± 0.153	0.139 ± 0.096	0.773 ± 0.094

The implementation of MH-CO_2 and BH-CO_2 resulted in lower removal of EB per gram of AC (0.139 and 0.200 g_{EB}/g respectively) compared to steam activated carbons: MH-H_2O (0.773 g_{EB}/g) and BH-H_2O (0.951 g_{EB}/g). The higher performance of MH-H_2O and BH-H_2O in comparison to MH-CO_2 and BH-CO_2 is due to the presence of mesopores that grant more resistance to deactivation by coke deposit as explained earlier.

In terms of X_{tar}, materials prepared from buckwheat husk, BH-CO_2 and BH-H_2O display improved performance compared to MH-CO_2 and MH-H_2O when the EB conversion is expressed in function of the mass of material used. This result is explained by the higher microporosity, presence of mesopores in steam activated samples and content of K, Ca and Mg in buckwheat husk. Content of potassium in BH-CO_2 (3.1 wt.%) and BH-H_2O (3.9 wt.%) is lower than in MH-CO_2 (5.8 wt.%) and MH-H_2O (9.4 wt.%). The ratio K/(Si + P) allows to determine the reactivity of the char/activated chars: if K/(Si + P) < 1 the silica and phosphorus have an inhibitory behavior whereas if K/(Si + P) > 1 the material shows reactivity in the tar cracking. Silica was not detected in BH-CO_2 and BH-H_2O, which explains that the ratios K/(Si + P) are higher than 1 for both samples. In contrast, MH-CO_2 and MH-H_2O present high content of silica therefore the catalytic activity of K and Ca is probably inhibited by the formation of silicates during the activation stage [86,190,194]. Knowing that, it seems that reactivity of activated chars prepared from millet is linked to the microporosity of these materials.

Calcium compounds are more concentrated in BH-CO_2 (2.4 %) and BH-H_2O (3.4 %), besides in these materials, magnesium was measured at 1.4 % and 2.6 % respectively, whereas in samples

from MH it was not detected. It was previously mentioned that the release of Ca is higher during activation under CO_2 than under steam which explains the higher concentration of calcium content in BH-H_2O. In the same way, lower yield of BH-H_2O justifies the higher concentration of Mg in this sample since Mg is not influenced by the oxidizing agent. It has been reported that calcium presents higher catalytic activity compared to potassium [86] and chars prepared from BH are richer in calcium. In addition, magnesium have also shown reactivity for tar elimination [105]. Therefore, the superior efficiency of BH-H_2O compared to BH-CO_2 might also be related to the K, Ca and Mg contents in the sample. In that sense, the higher Ca concentration with smaller particle size and good distribution in BH-H_2O compared to BH-CO_2 contributes to its capacity of ethylbenzene decomposition. The smaller size and good distribution of Ca enhances the interaction between this element and EB while agglomerated Ca is not or less available to react with the tar model. It should be noted that the role of porosity is also important since it not only contributes to conversion of tar but also improves mass transfer to the active sites containing Ca, Mg and K.

Considering that tar conversion into light hydrocarbons results in coke production [119] as shown in reaction R 1-6, it is expected that materials with superior performance (reactivity) present higher coke deposit which would be evidenced as weight gain .

Thermal cracking $C_nH_m \rightarrow C + C_xH_y + H_2 + CH_4 + CO + CO_2$ **R 1-6**

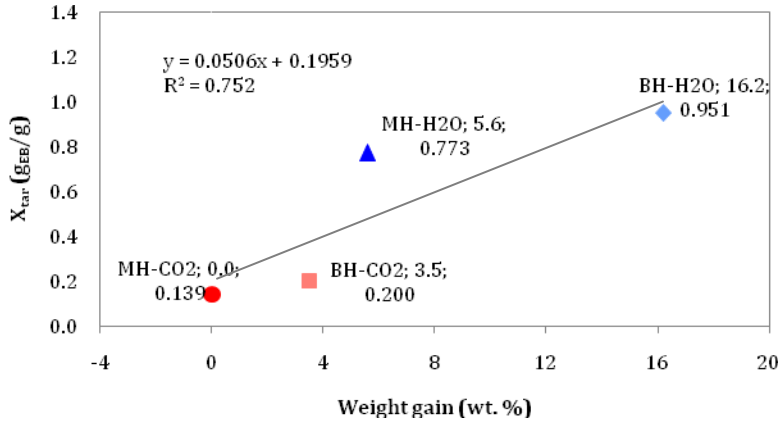

Figure 4-7. Weight gain of materials after EB cracking experiments vs performance of activated carbons in simple matrix at 650 °C.

According to Figure 4-7, there seems to be a tendency between performance and coke deposition in the surface of chars. Coke particles cover the active sites of activated carbons and blocks the pores, which leads to deactivation of the material. Note that MH-H_2O and BH-H_2O which have the highest performance also presented highest weight increase (5.6 and 16.2 %).

On the contrary, weight gain was not significant for MH-CO_2, this could be due to its low performance and the fact that part of coke remained in the reactor.

In the simplified matrix, the efficiency of materials is reflected in the composition of the treated gas as shown in Table 4-4. As result of thermal cracking, formation of H_2, CO and C_{2+} is evidenced while tar content is reduced from 0.9 to 0.7 %. The results show that some hydrogen is produced by thermal cracking and with the column filled with AC. In terms of tar content, MH-H_2O presents the lowest percentage, therefore tar composition must be analyzed in order to have better comprehension about this result.

Table 4-4. Composition of inlet and simple matrix treated with activated carbons at 650 °C, balance calculated at 180 min.

t = 180 min		H_2	CO	C_{2+}*	Tar**	N_2
		mol. %				
Inlet syngas		0	37	0	0.9	62
Outlet gas	Thermal cracking	Trace	39	Trace	0.7	60
	BH-CO_2	Trace	37	Trace	0.7	62
	BH-H_2O	Trace	37	Trace	0.6	62
	MH-CO_2	Trace	37	Trace	0.6	62
	MH-H_2O	Trace	38	0	0.4	61

*C_{2+}: refers to C_2H_4 + C_2H_6; **Tar: denotes remaining EB (C_8H_{10}) and other lighter tar molecules produced from EB conversion (C_6H_6 + C_8H_8).*

The tar composition of the treated syngas is presented in Figure 4-8 for all samples and thermal cracking. All materials present lower tar content than thermal cracking however BH-CO_2 presents slight inferior tar content. The reactivity of BH-CO_2 and MH-CO_2 results in similar tar composition while the tar distribution obtained with MH-H_2O and BH-H_2O is different, therefore the absence of mesopores also influences tar conversion, notably by impacting the distribution of cracking products.

According to Figure 4-8, gas from BH-H_2O and MH-H_2O present similar remaining ethylbenzene which is in agreement with EB conversion (Y_{EB}) presented previously (Table 4-3), 81.1% and 82.1 % respectively. However, activity of BH-H_2O decomposes ethylbenzene to other light tar compounds such as benzene and styrene in a higher extend than MH-H_2O which explains why the gas from the latter has the lowest tar content (0.4 %). This result suggests that CaO in BH-H_2O causes formation of lighter tar compounds from ethylbenzene while silica in MH-H_2O does not promote lighter tar formation. This result was also reported by Udomsirichakorn et al., [195], they analyzed the effect of CaO on tar yield and composition. To that end, silica sand and calcined limestone (CaO) were used as bed materials in the gasification with steam of sawdust of

pine wood at 650 °C and atmospheric pressure. The concentration of tar generated by the process was calculated and its composition was analyzed. The tar yield with the silica sand bed was 80 g/Nm^3 while that of CaO-bed was 30 g/Nm^3. Therefore, the authors concluded that CaO is involved in reforming tar into gas as evidenced by the decreased tar content with the addition of CaO. In addition, it was found that the use of in-bed CaO reduces the Class 1 tars (like EB) via rupturing and ring-opening reactions among the ring structures of Class 1 tars. As a result, formation of tar compounds occurs.

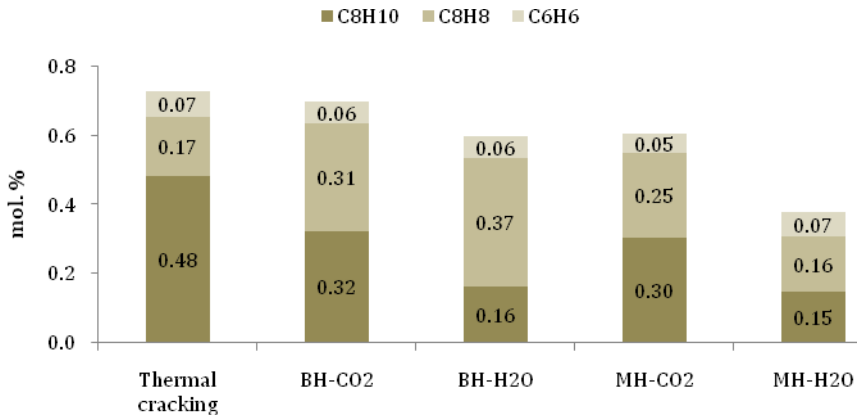

Figure 4-8. Tar composition in simple matrix treated with activated carbons at 650 °C.

The study of the EB conversion of materials with a simplified syngas avoiding the influence of the gas composition allow to conclude that the performance of materials decreases in the following order: BH-H_2O > MH-H_2O >> BH-CO_2 > MH-CO_2.

4.4. Performance of activated carbons in dry syngas

According to the results obtained with a simple matrix, the choice to study AC to remove EB from a complex matrix of syngas (H_2 + CH_4 + CO + CO_2 + N_2 + EB) was realized. Indeed, it does not seem relevant to continue with raw chars since they do not show successful results to crack EB from a simple matrix. The breakthrough curves of ethylbenzene concentration in the treated dry syngas using activated carbons are presented in Figure 4-9.

The same trend is observed with the dry syngas as it has been seen with the simple matrix: samples from steam activation show better capacity to remove EB than CO_2 activated carbons. The samples BH-H_2O and MH-H_2O show a slower deactivation rate than BH-CO_2 and MH-CO_2 due to pore distribution, notably due to the presence of mesopores as explained before. It is worth

mentioning than none of the samples reaches saturation or complete deactivation since at 200 min, the outlet concentration of EB is still lower than EB conversion due to thermal cracking (19 g/Nm^3) in a complex matrix such as a dry syngas. However, experiments are stopped at this point in order to compare performance of materials with those obtained in the simplified matrix. The concentration of ethylbenzene in the treated gas reaches between 13 and 14 g/Nm^3 by means of the column filled with MH-CO_2 and BH-CO_2 respectively against 20 and 24 g/Nm^3 in simple matrix, whereas MH-H_2O achieves 10.1 g/Nm^3 and BH-H_2O 7.6 g/Nm^3 against 14 and 15.4 g/Nm^3.

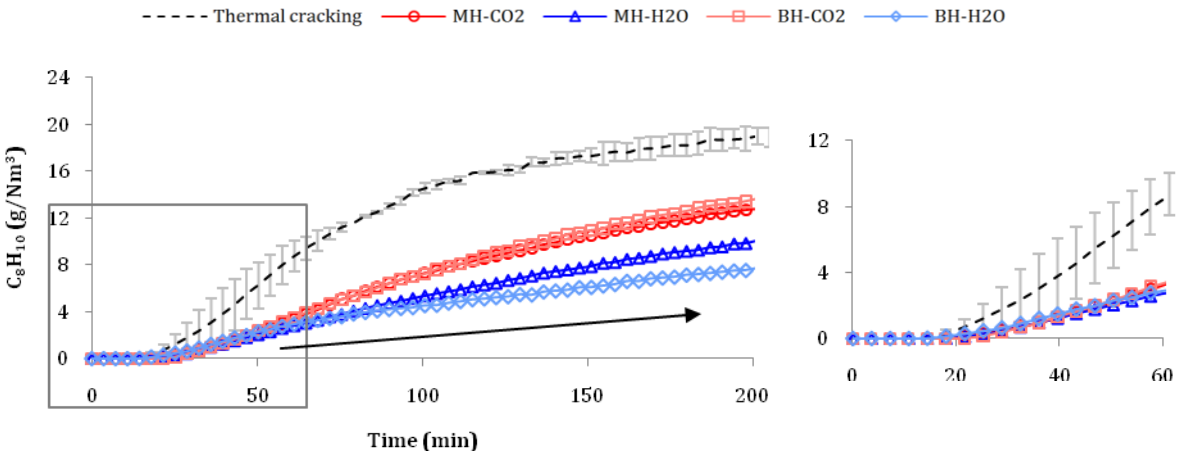

Figure 4-9. Concentration of EB in the outlet stream of the system at 650 °C using a dry syngas matrix.

As in the previous section, performance of materials is calculated at 180 min in terms of conversion of ethylbenzene (Y_{EB}) and X_{tar} which are depicted in Table 4-5.

Table 4-5. Removal of EB from dry syngas using activated carbons at 650 °C and EB = 40 g/Nm^3, balance calculated at 180 min.

t = 180 min	Thermal cracking	BH-CO_2	BH-H_2O	MH-CO_2	MH-H_2O
Y_{EB} (%)	72.1 ± 1.6	84.6 ± 0.1	90.4 ± 2.8	85.0 ± 4.1	88.6 ± 4.6
X_{tar} ($g_{EB}/g_{material}$)	-	0.377 ± 0.002	0.713 ± 0.036	0.213 ±0.072	0.370 ±0.099

All materials present 12.5 to 18.3 % additional ethylbenzene conversion compared to thermal cracking. In terms of X_{tar}, MH-CO_2 presents the lowest ethylbenzene removal (0.213 g_{EB}/g) which is explained by its lower porosity (BET surface of 329 m^2/g) composed of mainly of micropores and a ratio K/(Si + P) lower than 1. MH-H_2O and BH-CO_2 display improved performance in comparison to MH-CO_2. MH-CO_2 and BH-CO_2 have similar efficiency being 0.370 g_{EB}/g and 0.377 g_{EB}/g respectively, whereas with the simple matrix the efficiency of MH-H_2O is about 3

times better than that of BH-CO_2. However, this efficiency decreases with dry syngas, BH-H_2O presents the highest ethylbenzene removal (0.713 g_{EB}/g).

In dry syngas treatment, MH-CO_2 and BH-CO_2 samples increase their performance whereas MH-H_2O and BH-H_2O decrease theirs compared to simple matrix. This means that efficiency of materials is influenced by the syngas composition. In simplified matrix (CO + N_2 + EB), the reaction mechanism of EB conversion does not involve CO_2, since this gas is missing at the inlet and it is not produced during the cracking of EB. In contrast, dry syngas contains CO_2 which can influence the reaction pathway of ethylbenzene conversion considering that the gas composition determines the tar conversion pathway [172]. Indeed, the CO_2 content of dry syngas might promote the ethylbenzene conversion by means of dry reforming according to reaction R 1- 11. This reaction could explain why the thermal cracking is higher with dry syngas than simple matrix.

The efficiency of materials can also be influenced by their mineral content and form of oxides. As discussed in Chapter 3 calcium in activated carbons can be present as $CaCO_3$ and CaO which have different reactivity. It can be seen in Figure 4-10 that at the experiment conditions (650 °C and P_{CO2} = 0.14 atm), CaO in activated carbons reacts with CO_2 in the gas phase to form $CaCO_3$.

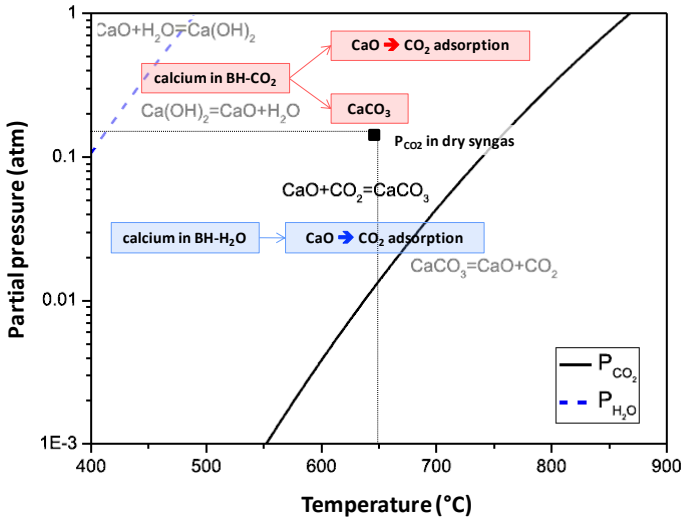

Figure 4-10. Reactivity of calcium oxides at 650 °C in function of partial pressure of CO_2 in dry syngas adapted from [98].

This is a well-known reaction in the industry where the CaO is used in many processes to remove carbon dioxide. Thus, neutralization of CO_2, contained by the dry syngas, competes with reforming of ethylbenzene (R 1-11) in dry syngas. It is important to remind that calcium in BH-

CO_2 is clustered which means that it is not available to react with CO_2 or that its reactivity is hindered to some degree.

In addition, due to the activation process, BH-CO_2 contains as much CaO as $CaCO_3$ while BH-H_2O contains mainly CaO in higher proportion. This explains why BH-H_2O is affected by the CaO content in a higher degree than BH-CO_2, and lower performance of BH-H_2O under dry syngas than that obtained with the simple matrix is observed.

Dry reforming $C_8H_{10} + 8CO_2 \rightarrow 16CO + 5H_2$ **R 1-11**

In contrast, MH-CO_2 and MH-H_2O are not influenced by calcium compounds since their concentration is very low and are probably trapped by silicates. These samples contain higher K content than BH-CO_2 and BH-H_2O; K is trapped by silicates present in high quantity in MH-CO_2 and MH-H_2O which inhibits the positive role of K in tar cracking. However, it is important to notice that the degree of inhibition is unknown. Thus, assuming that not all potassium is encapsulated by silica, it is plausible that remaining K reacts with CO_2 as well. The enhancement of CO_2 uptake on K-promoted catalysts has been demonstrated [196] and the amount of neutralized CO_2 increases with higher potassium loading. Consequently, performance of MH-CO_2 and MH-H_2O in dry syngas is affected by the K content due to the competition of CO_2 neutralization and dry reforming of EB. In particular, MH-H_2O is more influenced than MH-CO_2 since its K content is higher justifying the lower performance of the later.

In conclusion, efficiency of activated carbons in dry syngas in comparison to simple matrix increases for BH-CO_2 > MH-CO_2 whereas performance decreases for BH-H_2O > MH-H_2O which is explained by material properties (mineral elements) and parallel reactions involving CO_2: dry tar reforming (R 1-11) and CO_2 neutralization. In the same way that simple syngas, the reactivity of materials is related to weight gain caused by the coke deposition. This association is confirmed with dry syngas and is presented in Figure 4-11.

According to the graph, the highest weight increase is achieved in BH-H_2O which is also the material with best efficiency in terms of ethylbenzene removal per gram of activated carbon. It can be observed that the equation is similar to that of simplified syngas conserving the same range of magnitude. In addition, the correlation coefficient (R^2) is slightly higher (0.9) compared to simple gas (0.8).

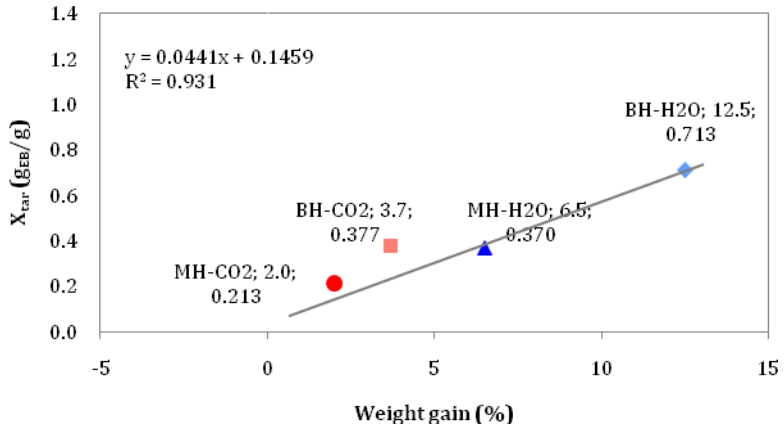

Figure 4-11. Weight gain of materials after EB cracking experiments vs performance of activated carbons in dry syngas at 650 °C.

The composition of the outlet gas (treated gas) is compared to the initial composition of dry syngas in Table 4-6. As it is expected, the gas composition does not change significantly since tar content represents only 1 % of the inlet syngas. It can be observed that in thermal cracking oxygen formation takes place accounting for 1 % and C_{2+} compounds are generated (Trace). In the same way, CO is increased by 3 %, CO_2 decreases by 2 % and tar content is reduced from 0.9 to 0.6 %. Activated chars further reduce the tar content than thermal cracking to reach about 0.3 % and 0.2 %. Results suggest that BH-CO_2 and BH-H_2O might promote the Boudouard reaction (R 1-10) which forms CO from CO_2 reaction with carbon. It is interesting to note that MH-CO_2 and MH-H_2O appear to promote formation of hydrogen (1 %) and that MH-H_2O presents the lowest tar content (0.2 %).

Boudouard reaction $C^* + CO_2 \rightarrow 2CO$ **R 1-10**

Table 4-6. Composition of inlet and dry syngas treated with activated carbons at 650 °C, balance calculated at 180 min.

t = 180 min		H_2	CH_4	O_2	CO	CO_2	C_{2+}*	Tar**	N_2
		mol. %							
Inlet syngas		21	11	0	17	14	0	0.9	35
Outlet gas	Thermal cracking	21	11	1	20	12	Trace	0.6	35
	BH-CO_2	21	11	1	20	11	Trace	0.3	35
	BH-H_2O	21	11	1	21	11	Trace	0.3	35
	MH-CO_2	22	11	1	18	12	Trace	0.3	35
	MH-H_2O	22	11	1	18	12	Trace	0.2	35

**C_{2+}: refers to C_2H_4 + C_2H_6; **Tar: denotes remaining EB (C_8H_{10}) and other lighter tar molecules produced from EB conversion (C_6H_6 + C_8H_8).*

The resulting tar composition from dry syngas treatment is described in Figure 4-12. Tar distribution shows that thermal cracking reduces ethylbenzene (C_8H_{10}) to 0.30 % which is

further decreased to 0.06 % with BH-H_2O and 0.07 % with MH-H_2O. In contrast, BH-CO_2 and MH-CO_2 reduce EB content to 0.10 %. It appears that MH-CO_2 and MH-H_2O form less tar compounds (0.17 and 0.15 %) in comparison to BH-CO_2 and BH-H_2O (0.18 and 0.20 %). Therefore, CaO in BH-H_2O promotes the highest conversion of ethylbenzene; however, it also achieves a superior formation of lighter tar compounds such as benzene and styrene that are easier to treat.

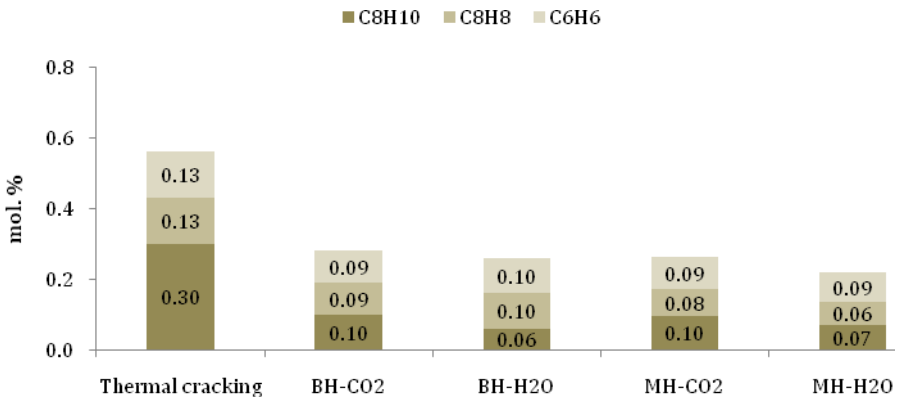

Figure 4-12. Tar composition in dry syngas treated with activated carbons at 650 °C.

4.5. Performance of raw and activated chars in humid syngas

Performance of activated carbons under humid syngas including steam (H_2 + CH_4 + CO + CO_2 + N_2 + EB + H_2O) was also tested; results are depicted in Figure 4-13. It can be seen that efficiency of activated carbons is similar at the beginning (t < 30 min) but then samples start to differentiate from each other.

As described in simple and dry syngas, the samples MH-CO_2 and BH-CO_2 display the same rate of deactivation. Under humid syngas, these materials lose almost full activity at 360 min since EB concentration at the leaving stream of the system (25 g/Nm^3) is close to resulting EB concentration from thermal cracking (26.4 g/Nm^3). On the other hand, MH-H_2O achieves 20.9 g/Nm^3 and BH-H_2O 17.2 g/Nm^3 at the downstream of the reactor. Therefore at 360 min the steam activated samples remain active and far from being fully saturated.

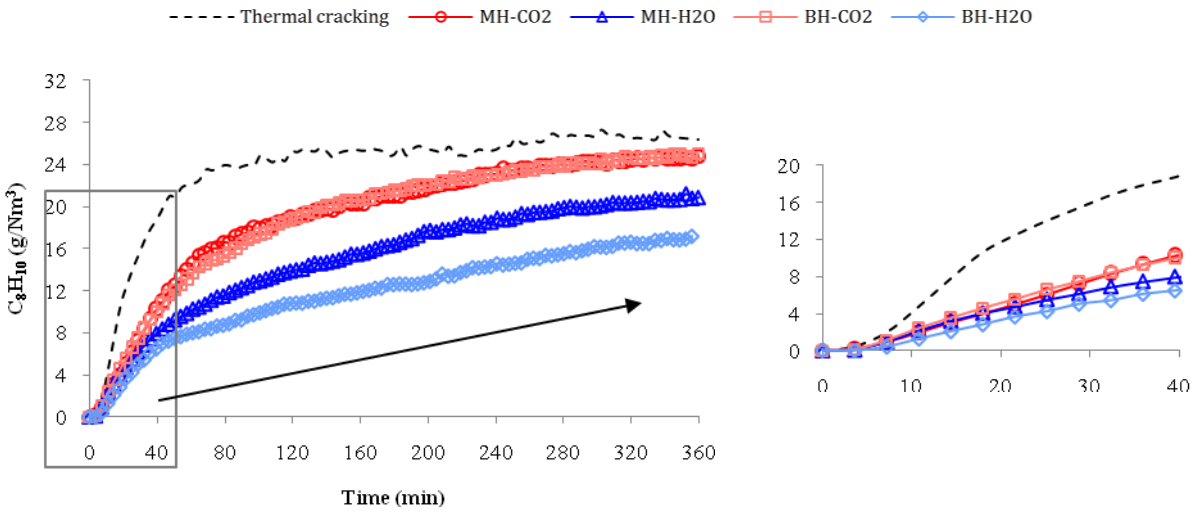

Figure 4-13. Concentration of EB in the outlet stream of the system at 650 °C using a humid syngas matrix.

In order to compare the results with those obtained with simple and dry syngas, performance of materials is calculated at 180 min in terms of conversion of ethylbenzene (%) and X_{tar} (g_{EB}/g) which are depicted in Table 4-7. All materials present between 15.5 to 31.6 % additional ethylbenzene conversion compared to thermal cracking. In terms of X_{tar}, ethylbenzene removal by BH-H_2O (1.246 g_{EB}/g) is 6.7 times higher than that from MH-CO_2 which showed the lowest removal of EB per gram of sample (0.186 g_{EB}/g). BH-CO_2 (0.449 g_{EB}/g) and MH-H_2O (0.514 g_{EB}/g) have similar performance as it was found in dry syngas.

Table 4-7. Removal of EB from humid syngas using activated carbons at 650 °C and EB = 40g/Nm³, balance calculated at 180 min.

t = 180 min	Thermal cracking	BH-CO_2	BH-H_2O	MH-CO_2	MH-H_2O
Y_{EB} (%)	46.8	62.8 ± 1.0	78.4 ± 7.2	62.3 ± 1.8	71.9 ± 2.7
X_{tar} ($g_{EB}/g_{material}$)	-	0.449 ± 0.018	1.246 ± 0.180	0.186 ± 0.147	0.514 ±0.048

The breakthrough curves of materials under dry and humid syngas are compared in Figure 4-14. Results show that under dry syngas, concentration of ethylbenzene in the treated gas is lower than in humid syngas for all materials; however performance of activated carbons is higher in humid syngas for almost all samples except for MH-CO_2. There are two possible explanations for this outcome. The first one is that thermal conversion of ethylbenzene in dry syngas is higher than in humid syngas reducing the cracking part due to materials. This is reinforced by the fact that in dry syngas the ethylbenzene concentration starts rising at 20 min while in humid syngas the breakthrough is almost instantaneous. This implies that the area between thermal cracking and curves of materials is larger in humid syngas leading to higher X_{tar}. The second reason could be the presence of steam in the matrix which prevents the deactivation of AC by soot formation

and their deposition on the material surface which is in agreement with the higher performance in terms of X_{tar}.

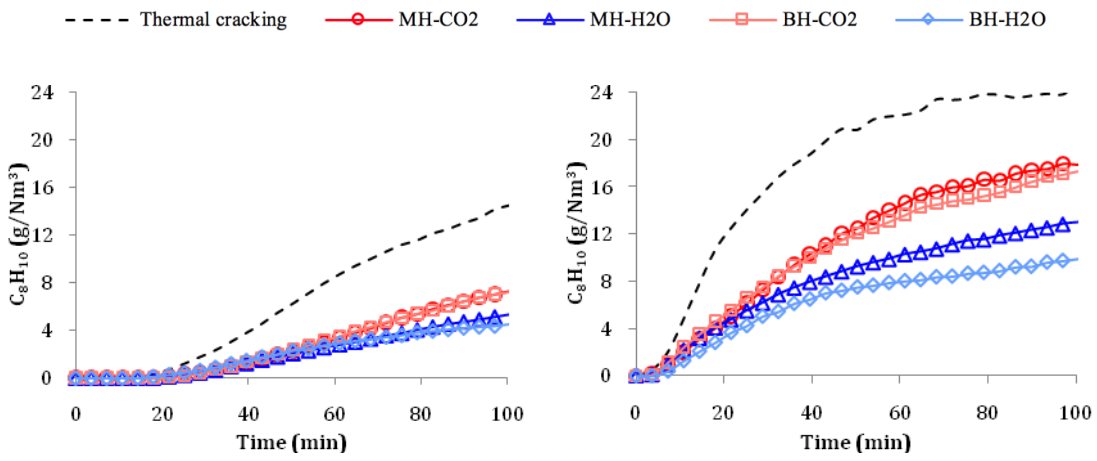

a) Dry syngas **b) Humid syngas**

Figure 4-14. Comparison of breakthrough curves of a) dry and b) humid syngas at 650 °C and EB = 40 g/Nm³.

The theoretical maximum capacity of BH-H_2O in humid syngas is calculated resulting in 2.9 g_{EB}/g, the details of calculation are presented in Annexe 3. The efficiency of this sample is higher to that from commercial catalysts. In the work of Coll et al., [106] a commercial catalyst ICI 46-1 with 15 % of nickel on alumina support, containing SiO, MgO, CaO, K_2O and Fe_2O_3, was tested in the treatment of biomass-derived syngas. The tar abatement was carried out by catalytic steam reforming using benzene as surrogate of tar molecules at 780 °C. Benzene was injected at 0.67 g/min. In this study, conversion was calculated as the fraction of the carbon contained in the organic feed that was converted to gas products (CO, CO and CH_4). The ICI 46-1 catalyst was able to convert 1.1 g_{org}/g_{cat}. However, thermal cracking is not differentiated by this method, which means that the efficiency given is not only due to the catalyst. Thus, the catalyst efficiency can be overestimated. In addition, the authors did not specify if this corresponds to the maximum efficiency.

The reactivity of materials is correlated to the weight gain produced by the coke deposition (Figure 4-15) as previously conducted for simplified and dry matrix. It can be noticed that the equation correlating the weight gain and the efficiency of materials is similar to the equations reported earlier and that the correlation coefficient is high (0.98). Therefore, the performance of materials is linked to coke formation from cracking of ethylbenzene.

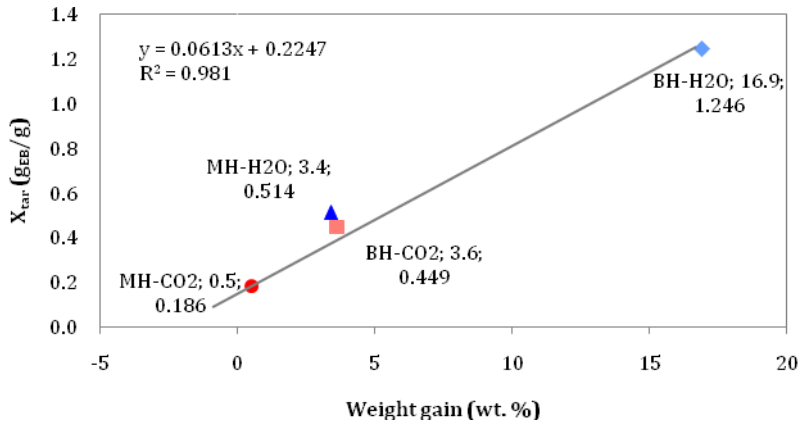

Figure 4-15. Weight gain of materials after EB cracking experiments vs performance of activated carbons in humid syngas at 650 °C.

The composition of the treated syngas is compared to the inlet composition of humid syngas in Table 4-8. It can be observed that as result of thermal cracking oxygen formation takes place accounting for 1 %. In the same way, H_2 increases by 2 %, CH_4 decreases in 1 %, CO is decreased by 2 %, steam is reduced by 2 % and tar content is reduced from 0.9 to 0.8 %. The materials promote further decrease of tar content to 0.5 and 0.6%. It appears that 1 % of additional H_2 is formed with BH-CO_2, BH-H_2O and MH-CO_2 and 2 % with MH-H_2O taking as reference thermal cracking. The steam consumed, higher content of hydrogen and lower percentage of CO in the outlet gas suggest that in humid syngas the water gas shift reaction (R 1-17) takes place during the gas treatment. It is interesting to note that MH-H_2O appear to favor higher hydrogen content (24 %), whereas BH-H_2O presents the lowest tar content (0.5 %). All materials have improved EB conversion compared to thermal cracking and BH-H_2O presents the highest tar.

Water gas shift reaction $CO + H_2O \leftrightarrow H_2 + CO_2$ **R 1-17**

Table 4-8. Composition of humid syngas treated with activated carbons at 650 °C, balance calculated at 180 min.

t = 180 min	H_2	CH_4	O_2	CO	CO_2	C_{2+} *	Tar **	N_2	H_2O
	mol. %								
Inlet syngas	20	10	0	14	13	0	0.9	31	12
Thermal cracking	22	9	1	12	13	Trace	0.8	31	10
BH-CO_2	23	10	1	14	12	Trace	0.6	31	8
BH-H_2O	23	10	1	14	13	Trace	0.5	31	8
MH-CO_2	23	10	1	14	13	Trace	0.6	31	8
MH-H_2O	24	10	1	13	12	Trace	0.6	31	8

**C_{2+}: refers to C_2H_4 + C_2H_6; **Tar: denotes remaining EB (C_8H_{10}) and other lighter tar molecules produced from EB conversion (C_6H_6 + C_8H_8).*

The resulting tar distribution from humid syngas treatment is given in Figure 4-16. BH-H_2O and MH-H_2O promotes further conversion of ethylbenzene (C_8H_{10}) to reach 0.14 and 0.19 % respectively. In contrast, BH-CO_2 and MH-CO_2 decrease EB content to 0.25 %, therefore more remaining EB is found in humid syngas treated with these latter samples. According to these results, when the total of tars decreases is because the concentration of EB is decreased. Indeed, for all materials the concentration of cracking products of EB is very similar from one another. This means that the different materials impact more the decomposition of EB than other products.

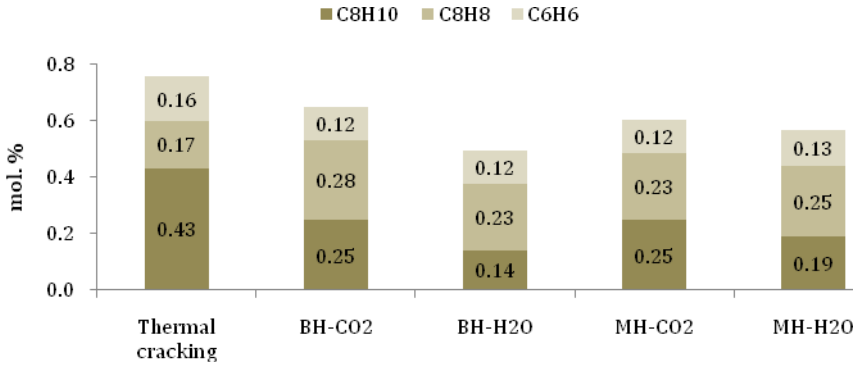

Figure 4-16. Tar composition in humid syngas treated with activated carbons at 650 °C.

Performance of materials in the different gas matrices is summarized in terms of X_{tar} at 180 min and is presented in Table 4-9. As explained before, in dry syngas MH-CO_2 and BH-CO_2 increased their efficiency whereas steam activated samples (MH-H_2O and BH-H_2O) decreased their performance taking as reference simple syngas. In contrast, with humid syngas efficiency of MH-CO_2 does not seem to be influenced, reactivity of MH-H_2O decreases while increases for BH-CO_2 and BH-H_2O. In view of this result, it appears that steam in humid syngas affects reactivity of activated carbons considering their composition, notably their mineral composition. This result implies that Ca, K and Mg species present stronger catalytic properties with steam than under dry gas which justifies the improved performance of BH-CO_2 and BH-H_2O.

Table 4-9. Performance of activated carbons under different syngas matrices at 180 min, T = 650°C and EB = 40 g/Nm³.

Sample	Simple matrix (Reference)	Dry syngas	Humid syngas
	CO + N_2 + EB	**H_2 + CO + CO_2 + CH_4 + N_2 + EB**	**H_2 + CO + CO_2 + CH_4 + N_2 + H_2O + EB**
Thermal cracking	**43.2%**	**51.8%**	**48.8%**
MH-CO_2	**X_{tar} = 0.139 ± 0.096 g_{EB}/g**	**X_{tar} = 0.213 ± 0.072 g_{EB}/g**	**X_{tar} = 0.186 ± 0.147 g_{EB}/g**
	Low surface area Mainly micropores High Si content K content	Dry reforming of EB No CO_2 adsorption	Steam + dry reforming CO_2 adsorption avoided Limited micropores
BH-CO_2	**X_{tar} = 0.200 ± 0.060 g_{EB}/g**	**X_{tar} = 0.377 ± 0.002 g_{EB}/g**	**X_{tar} = 0.449 ± 0.018 g_{EB}/g**
	Moderate surface area Mainly micropores Agglomeration of Ca compounds K and Mg content	Dry reforming of EB No CO_2 adsorption	Steam + dry reforming CO_2 adsorption avoided Limited micropores
MH-H_2O	**X_{tar} = 0.773 ± 0.094 g_{EB}/g**	**X_{tar} = 0.370 ± 0.099 g_{EB}/g**	**X_{tar} = 0.514 ± 0.048 g_{EB}/g**
	Moderate surface area Mesopores and micropores High Si content K content	Dry reforming of EB Adsorption of CO_2 by K Resistance to deactivation	Steam + dry reforming CO_2 adsorption avoided Resistance to deactivation
BH-H_2O	**X_{tar} = 0.951 ± 0.153 g_{EB}/g**	**X_{tar} = 0.713 ± 0.036 g_{EB}/g**	**X_{tar} = 1.246 ± 0.180 g_{EB}/g**
	Highest surface area Mesopores and micropores High content of well dispersed Ca compounds K and Mg content	Dry reforming of EB Adsorption of CO_2 by K and Ca Resistance to deactivation	Steam + dry reforming CO_2 adsorption avoided Resistance to deactivation Superior effect of Ca with steam

The difference in efficiency of materials in the treatment of dry and humid syngas indicates that the reaction pathway for the conversion of ethylbenzene is different in both cases compared to the reference experiment (simple matrix) and is influenced by the mineral composition of activated carbons. In consequence, it is believed that in humid syngas a different reaction pathway takes place perhaps involving the steam reforming reaction of ethylbenzene (R 1-12). This means that the reaction pathway in presence of steam might not involve CO_2 whereas this last is present in humid syngas. Dry reforming of ethylbenzene might also take place in a lesser extent considering that in this matrix the EB removal is higher, which suggest that the effect of competing reactions (CO_2 adsorption) is limited.

Steam reforming $$C_8H_{10} + 8H_2O \rightarrow 8CO + 13H_2$$ **R 1-12**

The campaign of experiments shows that the tar cracking is influenced by several parameters: the syngas composition, the surface area and the distribution of porosity, the mineral content and its distribution. In general, higher conversions of ethylbenzene are obtained in BH-H_2O and MH-H_2O, in particular the highest tar conversion is found with humid syngas treated by BH-H_2O. However, in all syngas matrices the lowest tar content including other tar compounds formed during the process is obtained with MH-H_2O.

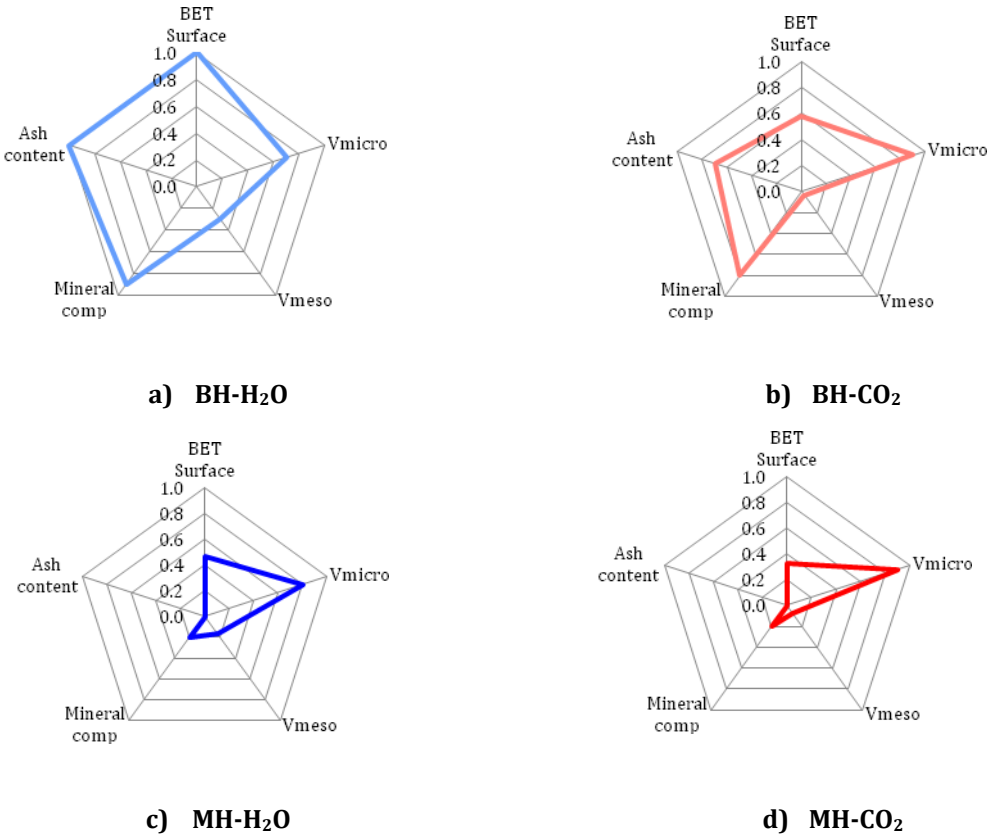

Figure 4-17. Comparison of properties of materials for their efficiency in EB cracking at 650 °C for all syngas matrices.

Radial graphs were made in order to compare properties of materials which are presented in Figure 4-17. In this figure, each property is normalized to the maximum value obtained on the studied materials allowing to visualize the main properties associated to the performance of each material. Ash content is considered as the ratio (Ca + K + Mg)/(Si + P) while mineral composition is expressed as the ratio (Ca + K + Mg)/Ash; V_{micro} and V_{meso} represent the percentage of micro and mesoporous volumes.

According to results from this graph, the percentage of micropores is a key property for all materials especially for MH-H_2O and MH-CO_2 since their surface BET is moderate and their mineral composition does not influence the decomposition of EB. The higher proportion of mesopores in BH-H_2O is important for the syngas cleaning however its role is not as relevant as that of micropores. In addition, the ash content and mineral composition of BH-H_2O and BH-CO_2 seem to play a crucial role in the degradation of tars at 650 °C.

This section allows to conclude that BH-H_2O presents the higher performance which is due to the synergy of porosity, micropores, mineral species and mesopores. The efficiency of BH-CO_2 is governed by the micropores and mineral species. However, the performance of MH-CO_2 and MH-

H_2O is mostly due to their micropores. The efficiency of materials can be affected by the syngas composition since CO_2 can react with the mineral species of some samples.

4.6. Deactivation of materials

Finally, the deactivation of materials is studied in order to have a better understanding of the interaction of materials with ethylbenzene. Heterogeneous conversion of EB molecules leads to formation of light gases and to a deposition of carbon on the surface of the samples better known as coke. To determine the influence of coke deposition in the pores of materials, mercury porosimetry was carried out in order to determine the change in porosity of samples after syngas treatment. This analysis was conducted for pyrolysis chars and activated carbons implemented in simple matrix (Table 4-10).

Table 4-10. Change in porous volume of samples after their implementation in simple syngas treatment at 650 °C and EB = 40 g/Nm³.

Parameter	BH-Char	BH-CO_2	BH-H_2O	MH-Char	MH-CO_2	MH-H_2O
ΔV_{Total} (%)	-64	-16	-16	7	-2	-12
ΔV_{Meso} (%)	-38	-21	-24	-17	0	-18
ΔV_{macro} (%)	-67	-15	-13	7	-2	-11

The symbol "Δ" refers to the change of the pore volume of materials after their implementation in tar cracking.

According to the results, the macro and mesoporous volume measured by the mercury porosimetry tends to decrease after the application of materials in syngas treatment which confirms the deactivation of samples by coke deposit. The macroscopic aspect of coke deposits on the activated carbon surface can be associated to an obstruction of the inner pores of the samples studied in this work. Therefore, a change on the material surface due to ethylbenzene cracking would be shown through scanning electron microscopy (SEM).

Considering saturation degree of MH-CO_2 and BH-CO_2 in simple gas, these samples are chosen to study the structural analysis via SEM since it is assumed that these materials suffered the most visible physical changes. The SEM image only allows determining macroscopic modifications on the surface of activated carbons. Figure 4-18 shows SEM images of MH-CO_2 and BH-CO_2 before a), c) and after b), d) EB cracking at 650 °C in simple matrix. The exhausted samples b) and d) shows that pores mouth are hindered by a layer of what seems to be organic matter. SEM images highlight that deactivation of samples is due to carbon deposition which ended blocking the pores on the surface.

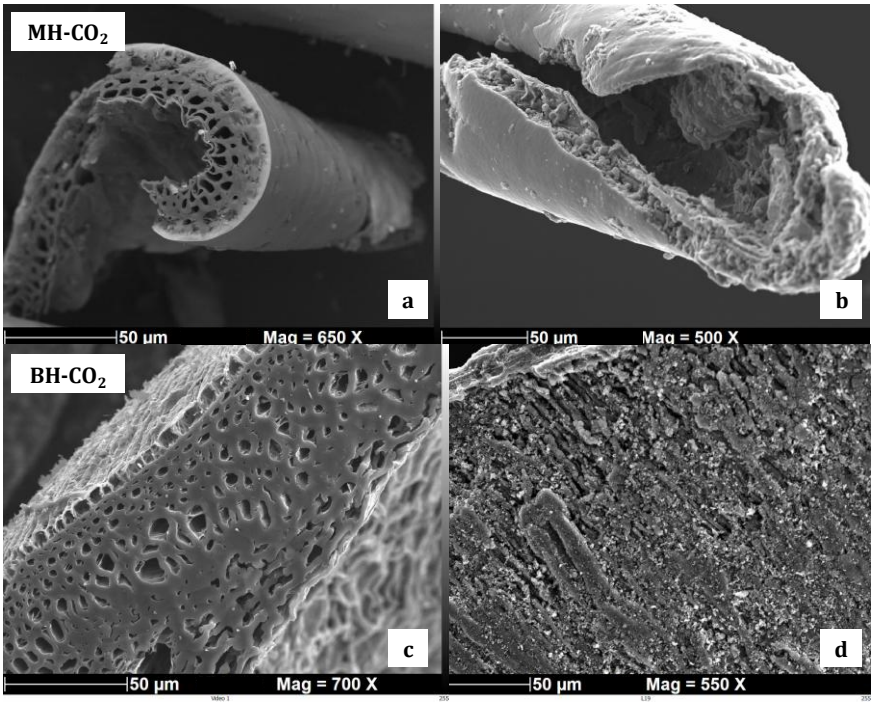

Figure 4-18. Comparison of fresh and exhausted MH-CO_2 and BH-CO_2 using SEM, a) and c) fresh samples; b) and d) exhausted samples.

The deactivation is defined as the loss of reactivity of materials which can be related to the decrease of the conversion rate of EB since the thermal cracking is constant. In order to determine the influence of gas composition, the deactivation rate is calculated as the first negative derivative of tar conversion according to Eq. 4-1. For this calculation it is necessary to use the EB conversion from both thermal cracking and materials (Y_{EB}) since the deactivation is associated to the coke deposition produced from degradation of EB due to temperature and attributed to AC. A deactivation rate close to zero indicates either that the samples are deactivated or that EB conversion is stable. Results are presented in Figure 4-19.

$$Deactivation\ rate = -\frac{dY_{EB}}{dt} \qquad \textbf{Eq. 4-1}$$

With the simple matrix, it is observed that deactivation rate is at its highest at 100 min for all materials. In this matrix, MH-CO_2 and BH-CO_2 suffered higher deactivation rate of 0.50 and 0.57 %/min, whereas for MH-H_2O and BH-H_2O deactivation rate is lower with 0.28 and 0.32 %/min respectively in the same time. This indicates that EB conversion in MH-CO_2 and BH-CO_2 happens mainly in the micropore range of porosity according to their relative microporosity (> 90 %) and the micropore volume is low thus the material undergoes a faster deactivation. After 100 min, deactivation rates start to decrease sharply being close to zero at 180 min for the microporous materials (MH-CO_2 and BH-CO_2). It is observed that MH-CO_2 and BH-CO_2 have lost most of their reactivity in the simplified matrix at 180 min as mentioned before.

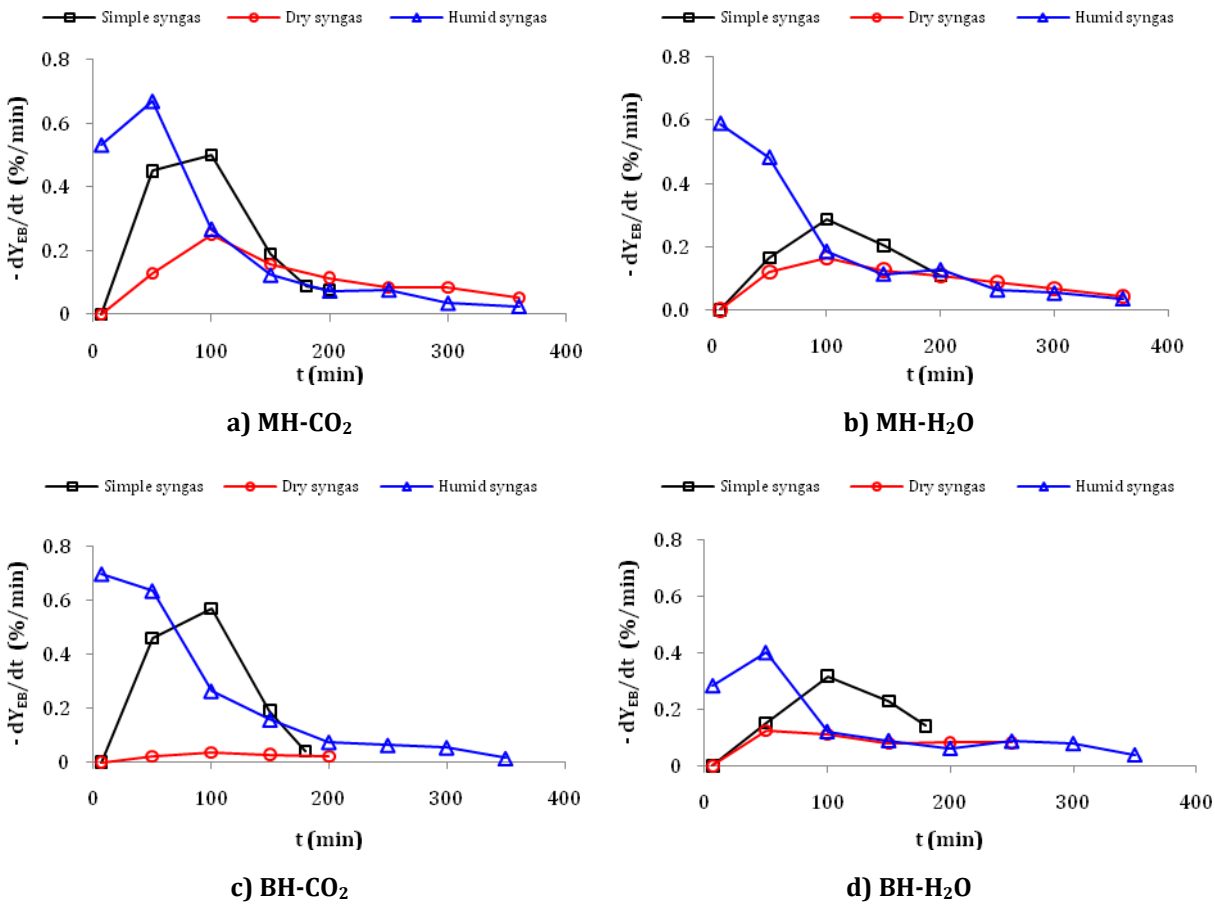

Figure 4-19. Deactivation rate of materials in different matrices of syngas at 650 °C and EB = 40 g/Nm³, a) MH-CO_2, b) MH-H_2O, c) BH-CO_2, d) BH-H_2O.

When other gas species like H_2, CH_4 and CO_2 are present in the syngas (dry syngas), the deactivation rate is slower. The highest deactivation rate in dry syngas takes place at 100 min reaching 0.27 %/min for MH-CO_2. The rate of deactivation of the samples decreases in the following order: MH-CO_2 > MH-H_2O > BH-H_2O > BH-CO_2. The higher degree of deactivation of MH-CO_2 is explained by its limited porosity: this is the activated carbon with the lowest surface area. The deactivation of MH-H_2O and BH-H_2O is slower due to their mesopores. This reduction in reactivity is justified by the coke formation from thermal cracking and the reaction with CO_2 in the case of BH-H_2O as described in the previous section. Lastly, BH-CO_2 presents the slowest and more constant deactivation rate of all samples in dry syngas; this is mainly due to a lesser neutralization of CO_2 with this sample.

According to Figure 4-19, steam contained in syngas impacts the deactivation rate of activated carbons. Indeed, the maximum rate of deactivation for all samples shifts in the first 50 min of the experiments varying from 0.40 %/min for BH-H_2O and from 0.70 %/min in the case of BH-CO_2. Results indicate that the conversion of EB might be faster in presence of steam, especially in the early minutes of experiment. In humid syngas, the deactivation rate of samples decreases in the

following order: BH-CO_2 > MH-CO_2 > MH-H_2O > BH-H_2O. The deactivation of materials seems faster for the microporous samples than the mesoporous ones as previously observed. Consequently, it appears that there is no competition between CO_2 and EB decomposition in presence of steam, dismissing loss in reactivity due to reaction with CO_2 in the active sites of BH-H_2O as is the case of dry syngas.

4.7. Gasification as ultimate use of chars

According to the principles of circular economy the end life of materials has to be considered. In that sense, used activated carbons should be recycled or reused in order to avoid any waste generation. Considering LHV of materials, it will be interesting to recover them for energy production; with this objective in mind two samples were selected to undergo gasification. In this section, a brief approach of gasification as end use of activated carbons is addressed.

Different criteria are important when gasification of chars is carried out: if the ash content is too high it can generate problems in the operation of the unit; in addition the inhibitory nature of some mineral species as presented in Chapter 1 must be considered. For example, it has been reported by some authors that the presence of Si decreases gas yield in char gasification [59]. Finally, the LHV of activated carbons must be considered for the energy recovery. Taking into account these different recommendations, MH-CO_2 and MH-H_2O are not eligible for gasification due to their low LHV and high ash content mainly composed by Si. On the contrary, BH-CO_2 and BH-H_2O meet all requirements mentioned before.

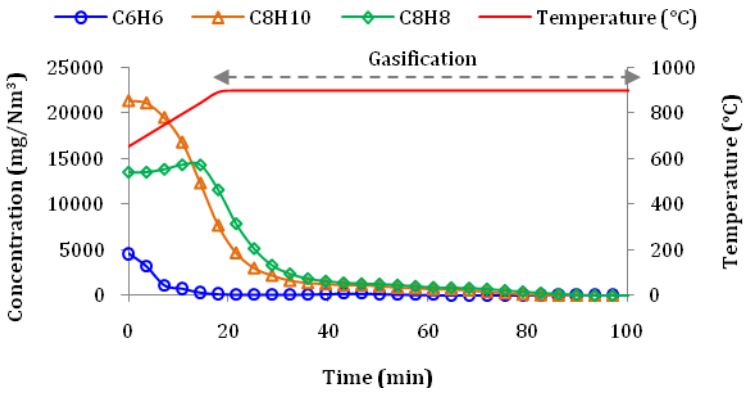

Figure 4-20. Tar compounds in produced gas from gasification of exhausted BH-CO_2 at 900 °C.

The Figure 4-20 shows the concentration of tar compounds (C_6H_6, C_8H_{10} and C_8H_8) in the outlet stream when the reactor is heated to 900 °C and during gasification. Results from this figure

indicate that the concentration of tar compounds decreases during gasification which suggests that these molecules are not adsorbed during syngas cleaning and then released by the sample during the increase of temperature to reach the gasification conditions. Thus, the observed tar concentration can be explained by some tar content remaining in the sampling line.The composition of the gas stream leaving the column is presented in Table 4-11.

Table 4-11. Syngas composition from gasification of exhausted activated carbons at 900 °C.

Sample	H_2	CO	CO_2	H_2O	Tar*
	mol. %				
BH-CO_2	17	15	54	14	0.22
BH-H_2O	39	10	37	14	0.08

**Tar: denotes tar compounds such as C_8H_{10} + C_6H_6 + C_8H_8.*

Gasification of BH-H_2O produces syngas with higher H_2 (39 %) and lower CO (10 %), CO_2 (37 %) and tars (0.08 %) contents compared to BH-CO_2. The ratio H_2/CO is 4 and 1 for BH-H_2O and BH-CO_2 respectively. In consequence, syngas produced from the gasification of exhausted BH-H_2O is useful in Fischer Tropsch process [21] since the ratio H_2/CO is higher than 2. This technology is fed with syngas rich in H_2 and CO and is able to synthesize waxes, olefins diesel and gasoline. The superior quality of syngas from gasification of the BH-H_2O might be explained by its mineral composition more riche in K, Mg and Ca, and less P. Indeed, higher content of calcium, magnesium and potassium increases the reactivity of the carbonaceous materials giving a gas with a higher hydrogen content and lower tar concentration; the syngas obtained presents better quality. This is due to the fact that these elements accelerate the water gas-shift reaction (R 1-17) increasing formation of H_2 in gas which has been reported in literature [98]. These authors studied the steam gasification of lignite at different temperatures (700 – 900 °C) and atmospheric pressure. Before gasification, the lignite was acid washed and $Ca(OH)_2$ was loaded on its surface. The Ca added was intended to be about 10 wt.% as a metal. It was found that the addition of $Ca(OH)_2$ reduce the tar yield by 62 – 77 %. The composition of the produced gas is similar to the syngas composition reported in the literature (Table 1-13), however the inlet of H_2O and CO_2 can be optimized in order to reduce the CO_2 content of the gas which should improve its quality in terms of H_2 and CO contents.

Mass and energy balances of gasification were performed as shown in Table 4-12. Mass balance of gasification of BH-CO_2 and BH-H_2O resulted in 72 and 92 wt.% respectively; the mass loss is certainly justified by the steam condensation in the water trap leaving the column (Figure 2-12) and deficiencies in the collection of ashes. The recovered energy is calculated as the percentage of the produced energy in the syngas to the inlet energy in ACs and calculated electrical

consumption (Annexe 4). According to results, it is possible to recover 4 times the inlet energy in the case of BH-CO_2 and 10 times in the case of BH-H_2O.

Table 4-12. Mass balance of gasification of exhausted samples.

		BH-CO_2				BH-H_2O			
		Mass (g)	**Mass fraction (%)**	**LHV (MJ/Kg)**	**Energy (MJ)**	**Mass (g)**	**Mass fraction (%)**	**LHV (MJ/Kg)**	**Energy (MJ)**
Inlet	Char	0.528	2.1	28.9	1.53E-02	0.535	1.9	27.5	1.47E-02
	H_2O	18.4	74.7	0	0	20.7	74.9	0	0
	CO_2	5.7	23.2	0	0	6.4	23.2	0	0
	Electrical input	-	-	-	3.30	-	-	-	3.30
	Total	*24.6*	100.0	-	*3.32*	*27.7*	100.0	-	*3.31*
Outlet	Ash	0.075	0.30	0	0	0.136	0.5	0	0
	Syngas	17.7	71.74	3.2	5.6E-02	25.3	91.6	**5.9**	1.5E-01
	Total	*17.8*	72.04	-	5.6E-02	*25.5*	92.1	-	1.5E-01
		Recovered energy (%)			2%	**Recovered energy (%)**			5%

Although both materials have similar LHV and are gasified under the same conditions, the LHV of obtained syngas from BH-H_2O is higher (5.9 MJ/kg) than that from BH-CO_2 (3.0 MJ/kg). These LHV are lower than those from steam activation (~15 MJ/kg) due to the remaining steam in the gas (14 %) as indicated in Table 4-11. On the other hand, the LHV of syngas from gasification of BH-CO_2 and BH-H_2O are 4 -5 MJ/Nm^3 which correspond to range of LHV reported in literature (Table 1-13) having a steam fraction of 11 - 34 %. Considering the global energy balance obtained in this study, steam activation gives better results due to the condensation of steam which increases the LHV of the gas.

The life end of materials prepared from millet husk is addressed in the next chapter considering that they are not available for use as soil conditioner or as precursor in gasification process.

4.8. Conclusions

This chapter focused in the application of raw and activated chars in tar removal from syngas. Ethylbenzene with a concentration of 40 g/Nm^3 was used as tar surrogate and different syngas matrices were studied starting from a simple one followed by more complex matrices.

Chars from pyrolysis (MH-Char and BH-Char) showed limited reactivity and were not able to increase tar removal further than thermal cracking. The lack of reactivity of these samples is

attributed to the absence of micropores which are developed in the activation stage. Therefore, no further experiments were carried out with these samples.

The performance of activated carbons was evaluated in different syngas matrices in order to determine the influence of syngas composition. To do so, efficiency of materials was first analyzed with a simplified syngas matrix that was taken as reference for the latter experiments. In addition, in this matrix the conversion of ethylbenzene is entirely attributed to performance of materials since apart from thermal cracking there are no side reactions such as dry and steam reforming of tars, the only parameters involved in this case are materials properties and thermal cracking. Results from this campaign of experiments suggested that porosity and mineral composition of materials are the main properties influencing degradation of EB. Indeed, BH-H_2O which is the sample with the highest surface area, superior Ca, Mg and K content and ratio K/(Si + P) > 1 resulted in the highest EB removal by gram of sample. MH-H_2O presented the second best performance thanks to mesopores that are more resistance to deactivation by coke deposit. This result indicates that the role of porosity is very important; it not only contributes to conversion of tar but also improves mass transfer to the active sites containing Ca, Mg and K. It was observed that microporous samples (MH-CO_2 and BH-CO_2) were deactivated first which explains that the materials with mesoporosity were more efficient. Indeed, mesopores allowed superior and more stable conversion of ethylbenzene in simplified syngas.

In dry syngas, the reaction pathway of tar conversion involves dry reforming with CO_2. The neutralization of CO_2 in samples containing Ca and K such as BH-H_2O and MH-H_2O, explains why these materials presented lower performance than in dry than in simple syngas. On the other hand, MH-CO_2 and BH-CO_2 increased their efficiency in comparison to simple syngas. In these samples, calcium compounds are not well dispersed but agglomerated in contrast to MH-H_2O and BH-H_2O. It is for this reason that reaction with CO_2 takes place in a lesser extend avoiding competition with dry reforming of ethylbenzene. In dry syngas, BH-H_2O presented the highest performance even though it was lower than in simple syngas for the reasons explained before. The global tar cracking (thermal and catalyst) is better in dry syngas. This is explained by the fact that the thermal cracking is more important in dry syngas than in others matrix with about 70 % of efficiency against about 50 % in simple matrix and humid syngas.

When the thermal cracking is subtracted at the global tar cracking, it was observed that steam in syngas has a favoring effect in tar cleaning since samples presented an improvement in efficiency except for MH-CO_2. It appears that steam in syngas inhibits the CO_2 reaction on the AC that take place in the tar conversion of dry syngas. The presence of steam in syngas seems to

determine the reaction pathway for the ethylbenzene conversion: steam probably involves reforming of tars, and steam reacts with carbon monoxide which increases the hydrogen content favoring the syngas quality.

Among the four samples used in this study, steam activated char from buckwheat husk (BH-H_2O) demonstrates the highest performance in all syngas matrices suggesting that surface area, ash content, mineral composition, micropore and mesopore presence are key properties in activated carbons that constitute the efficiency of this material in ethylbenzene conversion. These results must be temperate in terms of the production of by-products from EB cracking. Indeed, the calcium compounds present in this sample lead to formation of other tar components of lower molecular weight. In contrast, this effect is avoided in materials with much lower calcium and higher silica content (MH-CO_2 and MH-H_2O).

Deactivation rates of materials showed that in presence of steam conversion of ethylbenzene is faster, mostly in the first 50 min of experiment explaining the improvement in performance of most activated carbons. Meanwhile in dry syngas, degradation of ethylbenzene takes place at a slower rate. Deactivation of samples was critical for MH-CO_2 and BH-CO_2 due to their microporous character. In contrast, deactivation of MH-H_2O and BH-H_2O took place at a much slower rate. The faster rate of deactivation in humid syngas suggests that conversion of ethylbenzene is more rapid in this matrix than in simple and dry syngas.

The end-life of chars/activated carbons was briefly addressed, with notably the energy recovery from exhausted samples BH-CO_2 and BH-H_2O through a gasification process. The gas produced by gasification of exhausted BH-H_2O results in syngas with higher H_2 percentage and lower CO_2 content most probably due to its superior calcium content. The energy recovery from this material seems to be more interesting compared to BH-CO_2.

Chapter 5. H_2S removal from biogas using chars

Introduction

According to the biorefinery concept, the conversion of biomass into several product streams must be integrated with other technologies and processes. The pyro-gasification of biomass leads to production of syngas and a remaining carbonaceous material considered as a residue of the process which can be compared to activated carbon. In the context of a biorefinery, the integration of pyro-gasification and biogas production can be explored through the application of chars or activated carbons in the biogas cleaning. Therefore, considering that physical activation and pyro-gasification are similar processes, the implementation of activated carbons in the adsorption of H_2S from biogas is studied.

In order to identify the performance of chars activated carbons, breakthrough curves experiments are carried out with a simplified gas composed of H_2S balanced with nitrogen. Then, the impact of biogas composition on H_2S removal is studied under dry and humid conditions. The experiments were carried out until the saturation of materials. The exhausted activated carbons were characterized to determine in which measure the adsorption of H_2S modifies features of materials such as surface area, porous volume and pore distribution.

Lastly, the end life of materials is assed considering potential uses of exhausted samples. To do so, two important guidelines were considered. First, the ultimate use must be low energy consuming since H_2S removal is carried out at room conditions, thus disposal of spent materials shouldn't be more energy demanding that its main application. Second, it is imperative to avoid environmental concerns like generating more contamination due to the migration of sulfur compounds from exhausted materials to the environment. Accordingly, this study encompasses the integrity of whole the process, from the biomass conversion to the final use of its products as stated by the principles of circular economy.

Chapter 5. H_2S removal from biogas using chars

5.1. Calculation method

The adsorption capacity of materials was evaluated in H_2S removal from biogas at 30 °C and 200ppm of H_2S. Concentration of H_2S was measured at the downstream of the column in order to evaluate H_2S removal attributable to properties of materials such as porosity and presence of mineral species. The efficiency of samples is defined in terms of milligrams of H_2S removed by gram of material according to Eq. 2-13:

$$q_{ads} = 1 - 1.36\frac{Q_{total}}{m}\int_{t_0}^{t_i} C_i - C_{i-1} \qquad \textbf{Eq. 2-13}$$

where C is the concentration of H_2S (ppm), Q_{total} represents the total gas flow (Nm^3/min), m is the mass of char or AC (g) and *1.36* is the conversion factor from ppm to mg/Nm^3.

5.2. Performance of raw and activated chars in simple matrix (N_2 + H_2S)

The performance of activated carbons as hydrogen sulfide adsorbents was tested using the breakthrough capacity measurement procedures. The tests were carried out with a simple mixture N_2/H_2S, a dry and then a humidified biogas at 30 °C. Before all experiments, the materials were dried in an oven at 105 °C for at least 24 h. It is worth mentioning that composition of biogas used in this study is representative of real biogas according to literature [129,131,137,186,197]. Biogas is mainly composed of CH_4 and CO_2 and it usually has 4 – 5 mol. % of steam which gives a relative humidity of 27 %. In the present segment, performance of raw and activated chars under a simple mixture and more complex biogas matrices is explained. The operating conditions of the experiments are presented in Table 5-1.

Table 5-1. Operating conditions of H_2S removal at 30 °C.

Bed height (cm)	di (cm)	Qv (L/min)	τ (s)	Composition of gaseous matrices	H_2S (ppm)	Materials
4	2.15	2.18	0.4	N_2 + H_2S CH_4 (32 %), CO_2 (18 %), N_2 (50 %) + H_2S CH_4 (30 %), CO_2 (16 %), N_2 (50 %), H_2O (4 %) + H_2S	200	BH-Char, MH-Char, BH-CO_2, BH-H_2O, MH-CO_2, MH-H_2O

The breakthrough curves presented in Figure 5-1 show that performance of raw chars MH-Char and BH-Char in H_2S removal from biogas is limited.

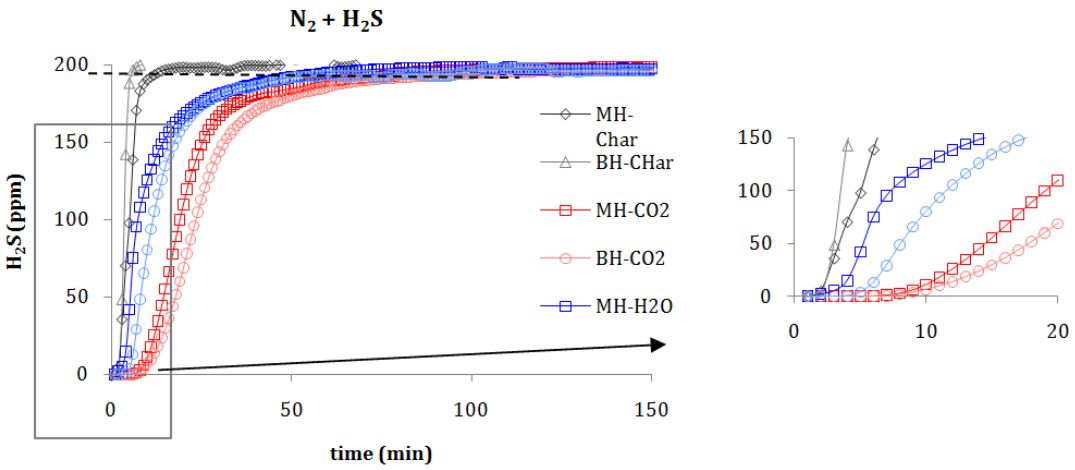

Figure 5-1. Breakthrough curves of materials at 30 °C in mixture of N_2 + H_2S.

The slope of the curves of these samples is sharp and they reach saturation in 5 and 10 min respectively. The lack of effectiveness of these materials is mainly related to the absence of porosity which is one of the properties that plays an important role in adsorption [145,198,199]. In the same way, both samples present acid surface, which means that these materials have more acid than basic functional groups. Therefore, the affinity of chars for acid gases like H_2S is poor. In the literature, different authors have shown that the surface chemistry influences adsorption of H_2S in activated carbons [145,146,152,200]. For example, the oxygen surface functionalities contribute to the oxidation and fixation of H_2S. The presence of basic functional groups which contain possible active sites allow to react with H_2S thanks to acid-base interactions since H_2S is an acid gas.

The activation of chars with steam or CO2 allowed to develop porosity and basic surface in all materials which is related to the increase of their H2S adsorption capacity. As shown in Figure 5-1 the slope in the breakthrough curves of these samples is moderate showing higher removal of H_2S in comparison to pyrolysis chars. The saturation time is longer for the CO_2 activated samples than for the steam activated ones. The samples MH-CO_2 and BH-CO_2 present saturation time of 120 and 150 min whereas MH-H_2O and BH-H_2O 100 min respectively. In consequence, less steep slopes and longer saturation times should result in higher performance.

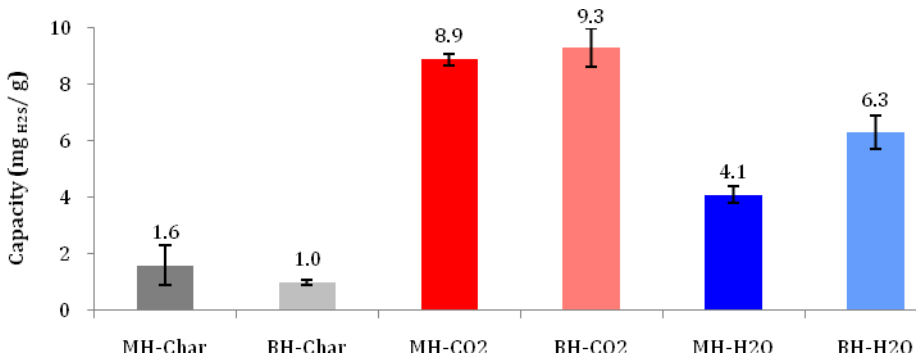

Figure 5-2. Adsorption capacity of materials at 30 °C in a mixture of N_2 + H_2S.

Adsorption capacity of materials was calculated from experimental data of breakthrough curves at the saturation time, results are depicted in Figure 5-2. Adsorption capacity of pyrolysis chars is poor as expected; the efficiencies are 1.6 and 1.0 mg_{H2S}/g for MH-Char and BH-Char respectively. Activated carbons present higher adsorption capacity, therefore developed porosity and basic pH play an important role in the adsorption of H_2S from biogas at room temperature. The highest removals of hydrogen sulfide at saturation point are achieved by MH-CO_2 and BH-CO_2 with 8.9 and 9.3 mg_{H2S}/g adsorption capacities. Less efficiency is displayed by MH-H_2O and BH-H_2O which reach 4.1 and 6.3 mg_{H2S}/g respectively. This result suggests that the activation type affects the adsorption capacity of materials. In this regard, CO_2 activation has better influence than steam activation. The main difference between activated carbons from CO_2 or steam activation is the distribution of porosity which suggests that samples with more micropores than mesopores improve the removal of H_2S from the gas mixture.

The adsorption capacities of the studied materials are lower than those reported in literature for physically activated carbons. In the work of Guo et al., [201] two activated carbons were used in the removal of H_2S. One AC was prepared from palm shell by CO_2 activation at 900°C for 2 h. The second sample was a coconut-shell-based commercial activated carbon obtained by steam activation. The palm shell activated carbon had BET surface area of 1072m^2/g, 0.26 cm^3/g of pore volume and 7.5% of ash content. The characteristics of the coconut shell activated carbon were 1183 m^2/g, 0.35 cm^3/g and 3.6% respectively. The dynamic adsorption of H_2S was conducted in a column (1 cm internal diameter and 20 cm long) filled with pre-dried samples operated with an updraft flow. The inlet stream to the column was composed of 2000 ppm of H_2S balanced with pure He gas. The experiments were carried out at room temperature and pressure of 1.0 bar. The runs were conducted until saturation, that is, when the outlet concentration

became equal to that of the inlet. The adsorption capacity of palm shell AC was 46 mg_{H2S}/g and that of coconut shell AC was 53mg_{H2S}/g. The elevated H_2S removal of these materials is partly probably due to the high BET surface areas, however the ash composition of materials was not specified and this property can influence the reaction mechanism with H_2S improving its adsorption. According to other authors, the ash-forming elements of palm shell are K > Ca > Na > Mg > Fe > Al [24]; on the other hand, coconut shell is composed of Si > K > Al > Fe > Mg [29] and as it was presented in Chapter 1, Fe, Ca and Mg improve the adsorption of H_2S. In the same way, the pH of materials and residence time of the gas in the column were not mentioned.

5.3. Influence of biogas composition

For the campaign of dry biogas experiments, only activated carbons are studied since pyrolysis chars proved to be poor sorbents in N2 + H2S. The breakthrough curves of activated carbons are depicted in Figure 5-3.

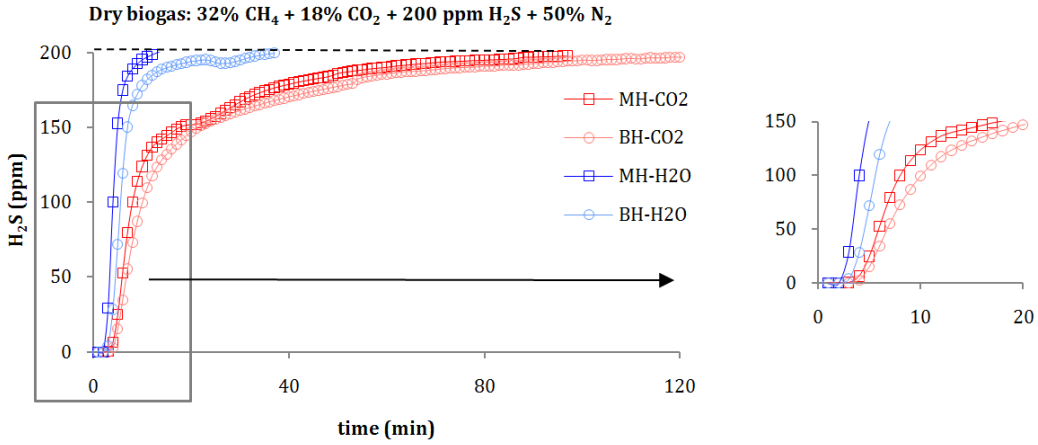

Figure 5-3. Breakthrough curves of materials at 30 °C in dry biogas.

The curves of these materials in dry biogas display more elevated slopes than in simple biogas. The steam activated carbons MH-H_2O and BH-H_2O, show a steeper slope compared to MH-CO_2 and BH-CO_2. In absence of CO_2 and CH_4 the H_2S concentration in the outlet gas at 10 min is 6.5 ppm for BH-CO_2, 11 ppm for MH-CO_2, 80 ppm for BH-H_20 and 125 ppm for MH-H_2O while in dry biogas these samples show 100, 124, 180 and 195 ppm of H_2S concentration at the same time respectively. In addition, in the simple mix the saturation time of MH-H_2O and BH-H_2O samples is 100 min, however in presence of CO_2 and CH_4 this time drops to less than 40 min. Conversely, MH-CO_2 and BH-CO_2 continue to exhibit longer hydrogen sulfide removal than the steam activated materials with 90 and 120 min

saturation time. Thus, results evidence that the adsorption capacity of activated carbons is influenced by the biogas composition.

The adsorption capacity of activated carbons is depicted in Figure 5-4. All samples exhibit less hydrogen sulfide removal however BH-CO_2 presents the smallest decrease of all samples. The decline in adsorption capacity of MH-H_2O is 4.1 times followed by 3.3 times for BH-H_2O, then 2.9 and 1.2 for MH-CO_2 and BH-CO_2 respectively. Therefore, BH-CO_2 continues to have the highest removal with 7.7 mg_{H2S}/g, followed by MH-CO_2 with 3.1 mg_{H2S}/g while BH-H_2O and MH-H_2O present poor adsorption. The fact that saturation time and adsorption capacity of samples are affected by the dry biogas suggest that CH_4 and CO_2 might compete with H_2S for the active sites of adsorption which is in agreement with other authors [137,151].

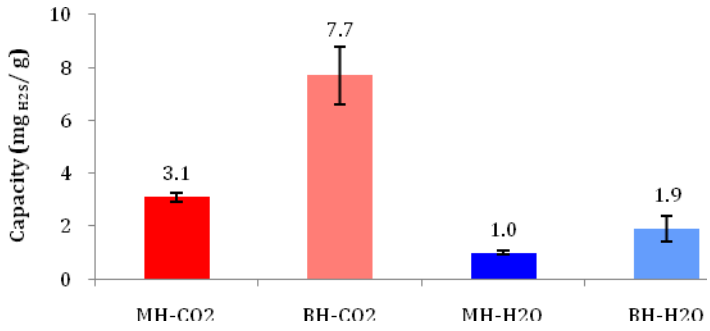

Figure 5-4. Adsorption capacity of materials at 30°C in dry biogas.

The adsorption capacity of samples is inferior to those reported in literature. Sitthikhankaew et al. [202], investigated the adsorption of H_2S from simulated biogas at 30 °C using a commercial activated carbon prepared from coconut shell. The biogas contained 3000 ppmv H_2S, 40 % CO_2, 2 % O_2 balanced with He and 70 % of relative humidity. The properties of the commercial sample were modified by steam activation at 900 °C for 1 h. The reactor (1.2 cm of internal diameter and 70 cm of length) was filled with 1 g of adsorbent. The experiments were carried out until saturation of materials. The raw commercial activated carbon had surface area of 1343 m^2/g, pore volume and pore size of 0.45 cm^3/g and 0.67 nm, respectively. After steam activation these features were modified to 1621 m^2/g, 0.60 cm^3/g and 0.75 nm. The adsorption capacity of the raw and modified samples were 13.8 and 27.6 mg_{H2S}/g respectively. The superior removal of these AC compared to BH-AC and MH-AC is due to the oxygen content of the gas which is adsorbed by the AC and influences the oxidation of H_2S to sulfur compounds, in the same way, the higher porosity partially contributes to improve the removal of H_2S. In this study, the ash

content and composition, surface pH and time residence of the gas in the column were not specified.

5.4. Influence of humidity

Activated carbons were tested to remove hydrogen sulfide from humid biogas. It is important to remember that before all experiments, materials were dried in an oven at 105 °C for 24 h minimum. The gas was humidified by implementing a bubbler filled with water which humidified methane gas at 27 % of relative humidity or 4 mol. %, then this stream was mixed with the other gases before entering the reactor. The breakthrough curves of materials are depicted in Figure 5-5.

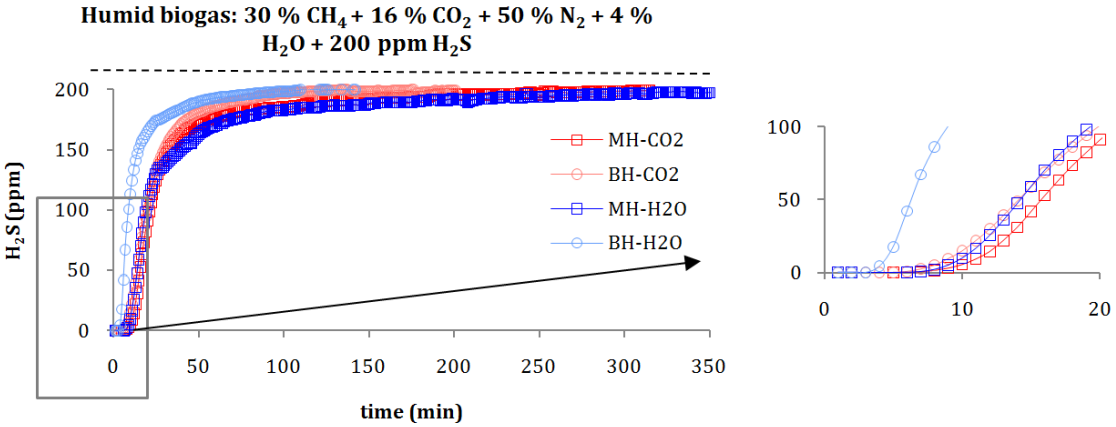

Figure 5-5. Breakthrough curves of materials at 30 °C in humid biogas.

All samples except BH-H_2O exhibit the same rate of increase in outlet concentration of H_2S. Thus, it seems that humidity impacts the adsorption of CO_2 and CH_4 contained in biogas. For example, the breakthrough time of materials to reach 5 % (10 ppm) of initial H_2S concentration is 5 min for BH-H_2O, 3 min for MH-H_2O, 9 min for MH-CO_2 and 11 min for BH-CO_2 whereas in dry biogas the breakthrough time is < 5min and in humid biogas is similar for all materials (around 10 min) except for BH-H_2O (5 min) as presented in Table 5-2.

Table 5-2. Breakthrough times of materials at 5 % of initial H_2S concentration.

Sample/ Matrix	Simple mix	Dry biogas	Humid biogas
	t (min)		
BH-H_2O	5	3	5
MH-H_2O	3	2	10
BH-CO_2	11	5	9
MH-CO_2	9	4	12

The slope of the breakthrough curves shows fair decrease in comparison to the previous dry biogas. The saturation time of the samples under humid biogas is 100, 150, 300 and 350 min for BH-H_2O, BH-CO_2, MH-CO_2 and MH-H_2O respectively. Therefore, the humidity of biogas has a beneficial effect in the adsorption of hydrogen sulfide.

The adsorption capacity of materials is presented in Figure 5-6. Test were carried out once with all materials except for BH-H_2O which was tested twice. The adsorption capacity of activated carbons is increased by humidity of in biogas. For instance, the adsorption capacity of MH-H_2O increases from 1 mg_{H2S}/g in dry biogas to 8.2 mg_{H2S}/g in humid conditions. In the same way, humidity improves the poor hydrogen sulfide removal of BH-H_2O from 1.9 to 6.2mg_{H2S}/g. The performance of MH-CO_2 doubles to 7.6 mg_{H2S}/g and BH-CO_2 presents adsorption of 7.9 mg_{H2S}/g. Therefore, it seems that humidity makes up for the possible competition of CH_4 and CO_2 with H_2S evidenced in dry biogas. This might be related to the solubility of the involved gases in water at 30°C, in fact H_2S has the highest solubility of 3 g/kg, followed by CO_2 (1.25 g/kg) and CH_4 (0.02 g/kg).

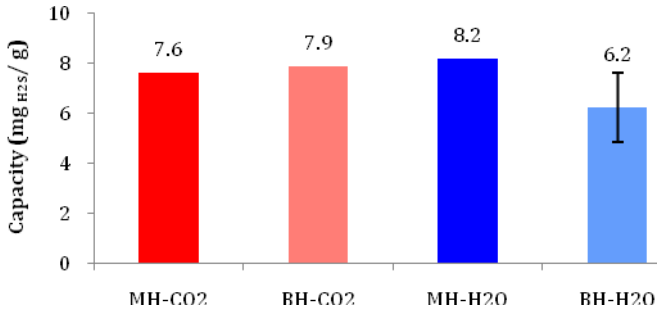

Figure 5-6. Adsorption capacity of materials at 30 °C in humid biogas.

The hydrogen sulfide removal by these samples is comparable to other activated carbons with similar characteristics found in literature. Hervy et al., [148] tested a steam activated carbon prepared from used wood pallets. The activation was carried out at 850 °C and the surface area of the sample was 625 m^2/g with 85 % of micropores, basic pH and low ash content (2.5%) composed mainly of CaO and K_2O. Adsorption tests were conducted at room temperature under N_2 with 200 ppm of H_2S. The residence time of the gas in the fixed-bed of was 1.2 s. It is important to mention that the activated carbon was not previously dried thus it contained some humidity inside the pore structure. The adsorption capacity reached at the saturation point (200 ppm) by the activated carbon was 13.0 mg_{H2S}/g.

5.5. Influence of materials properties

5.5.1. Influence of surface pH

Considering the influence of humidity of biogas in activated carbons and the fact that all materials present similar adsorption capacity regardless their properties, the raw chars are tested with humid biogas in order to determine their capacities under this condition. The breakthrough curves are shown in Figure 5-7.

It can be observed that the hydrogen sulfide concentration leaving the column increases very fast achieving 200 ppm in 4 minutes. The adsorption capacity of BH-Char and MH-Char are 0.54 and 0.95 mg_{H2S}/g respectively. Therefore, the beneficial effect of humidity is only seen with activated carbons which have basic pH, higher porosity and more concentrated mineral content. This result indicates that the adsorption mechanism comprises several stages and that humidity influences only part of them. In addition, porosity is required and mineral elements might be involved in the removal of H_2S.

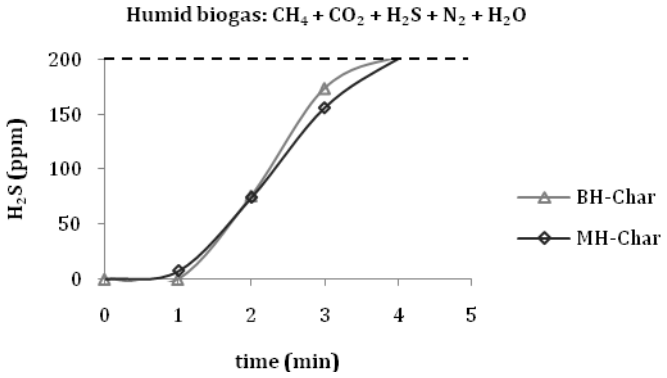

Figure 5-7. Breakthrough curves of chars at 30 °C in humid biogas.

5.5.2. Influence of porosity

In an effort to identify the surface features of activated carbons that do govern their performance, the H_2S adsorption capacities at saturation were compared to the structural parameters of samples such as surface area and pore volume. As presented in Chapter 3, surface area and pore volume of activated carbons decreases in the following order: BH-H_2O > BH-CO_2 > MH-H_2O > MH-CO_2. However, there is no direct correlation indicating that higher surfaces areas provide higher removal of hydrogen sulfide as indicated in Figure

5-8a. In view of the difference in performance due to different activation methods, the distribution of porosity in the activated carbons must be considered.

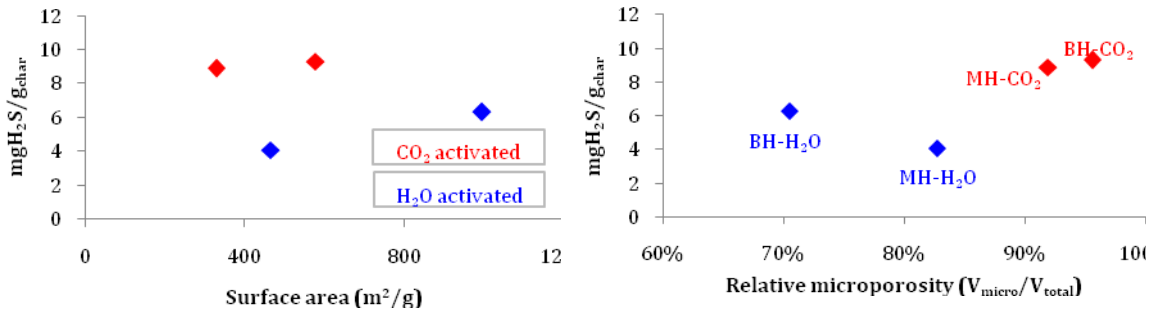

a) b)

Figure 5-8. Influence of porosity distribution in adsorption of H_2S from N_2 + H_2S at 30 °C.

As shown in Figure 5-8b, BH-CO_2 and MH-CO_2 which have high relative microporosity (> 90 %) display higher H_2S removal than materials with lower percentage of micropores (BH-H_2O and MH-H_2O). Thus, there seems to be a positive association between adsorption capacity and relative microporosity.

Similar results has been reported by Bandosz [147] who stated that there is a correlation between heat of adsorption and relative microporosity, which implies that the higher relative microporosity, the higher adsorption capacity. This theory is in agreement with the fact that pores of smaller size adsorb more molecules due to the superior adsorption potential exerted by their walls [146]. Therefore, the superior removal of hydrogen sulfide by CO_2 activated carbons is explained due to the higher share of micropores which exert stronger interaction than mesopores between H_2S and carbon.

The evolution of the textural properties of the materials can also provide information about the reaction mechanisms involved. For this reason, nitrogen adsorption analyzes of the exhausted samples were carried out. It is important to mention that materials are previously degassed at 30 °C under vacuum during 24 hours before the analysis. The textural properties and the adsorption capacities of materials are related in Table 5-3. It was not possible to analyze two samples: MH-CO_2 exhausted in dry biogas and MH-H_2O in humid biogas. The analysis of these samples didn't work probably due to the poor porosity of materials after H_2S removal.

It can be observed that in all exhausted materials porosity is reduced after H_2S removal from biogas. The reduction of the surface area (ΔS_{BET}) varies between 15 and 46 % which

is higher than the deviation from the analysis (1 – 8 %), thus the adsorption of H_2S impacts the porosity of activated carbons. In addition, the decrease of BET surface is in agreement with the decrease of microporous volume. Therefore, it seems that adsorption of H_2S takes places mainly in the smaller pores of materials or micropores.

Table 5-3. Textural properties of materials before and after biogas treatment with different gas composition.

Materials	Capacity (mg_{H2S}/g)	S_{BET} (m^2/g)	ΔS_{BET} (%)	V_{micro} (cm^3/g)*	ΔV_{micro} (%)	V_{meso} (cm^3/g)**
MH-CO_2 Fresh	-	329	-	0.174	-	0.013
MH-CO_2 N_2 + H_2S	8.9	279	-15	0.139	-20	0.041
MH-CO_2 Dry biogas	3.1	-	-	-	-	-
MH-CO_2 Humid biogas	7.6	250	-24	0.122	-30	0.052
BH-CO_2 Fresh	-	578	-	0.261	-	0.012
BH-CO_2 N_2 + H_2S	9.3	443	-23	0.219	-16	0.037
BH-CO_2 Dry biogas	7.7	431	-25	0.210	-20	0.067
BH-CO_2 Humid biogas	7.9	314	-46	0.154	-41	0.031
MH-H_2O Fresh	-	466	-	0.216	-	0.043
MH-H_2O N_2 + H_2S	4.1	378	-19	0.183	-15	0.088
MH-H_2O Dry biogas	1.0	367	-21	0.176	-19	0.085
MH-H_2O Humid biogas	8.2	-	-	-	-	-
BH-H_2O Fresh	-	997	-	0.419	-	0.175
BH-H_2O N_2 + H_2S	6.3	778	-22	0.376	-10	0.205
BH-H_2O Dry biogas	1.9	682	-32	0.334	-20	0.155
BH-H_2O Humid biogas	6.2	640	-36	0.309	-26	0.181

**V_{micro}: Calculated by the Horvath-Kawazoe model. **V_{meso}: Calculated by BJH model.*

Consequently, the deactivation of activated carbons in H_2S removal can be associated with the deposition of a sulfur layer on the carbon surface principally at the micropore scale which has also been seen by other authors [152]. There is no correlation between adsorption capacity of materials and the porosity decrease probably due to the adsorption of other gases such as CO_2 contained in biogas which competes with H_2S for the active sites of activated carbons. In general, mesoporous volume increases most likely attributable to the generation of new porosity by the adsorbed molecules like elemental sulfur or polysulfides. This is more pronounced for materials prepared from MH.

The influence of H_2S adsorption in the distribution of porosity of steam activated carbons is presented in Figure 5-9. The main peak at 0.6 nm in the fresh samples is decreased after H_2S removal from N_2 + H_2S and dry biogas in both materials. The pore size distribution for pore widths larger than 0.7 nm is not influenced by the gas cleaning. This means that

adsorption of hydrogen sulfide takes place mainly at the micropore scale at pore widths <1 nm which is in agreement with the diameter of H_2S (0.36 nm) [203]. The mesopores of the samples are not affected by the H_2S removal (data not shown).

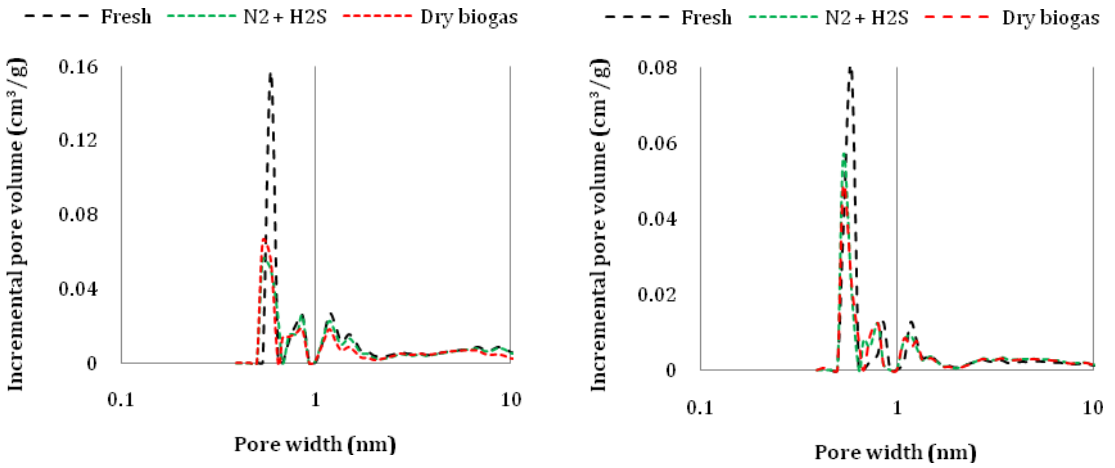

a) BH-H_2O **b) MH-H_2O**

Figure 5-9. Pore size distribution of steam activated carbons before and after H_2S adsorption.

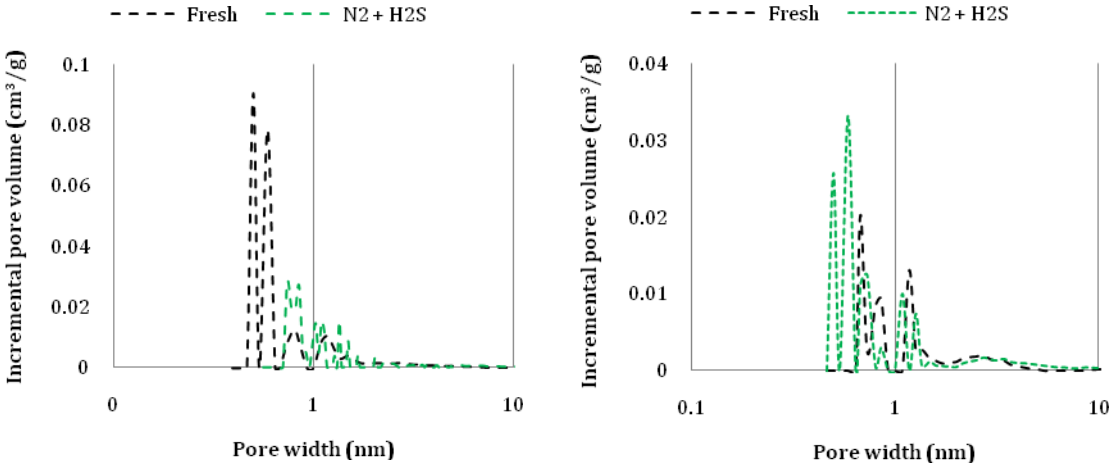

a) BH-CO_2 **b) MH-CO_2**

Figure 5-10. Pore size distribution of CO_2 activated carbons before and after H_2S adsorption.

The influence of H_2S adsorption in the distribution of porosity of CO_2 activated carbons is presented in Figure 5-10. It can be observed in that the H_2S removal influences the pore size distribution of activated carbons. For the fresh BH-CO_2 the pore distribution is bimodal with two peaks one at 0.5 nm and the second at 0.6 nm. These peaks disappear in the exhausted sample under N_2 + H_2S. The peaks of the fresh BH-CO_2 at 0.8 and 1.2 nm are

affected by the H_2S removal. In addition, it seems that H_2S adsorption has no influence on the mesopore distribution (2 – 50 nm) of the samples (data not shown).

On the other hand, the adsorption of hydrogen sulfide influences the pore size distribution of exhausted MH-CO_2. It seems that porosity is created at pore width smaller than 1.5 nm due to adsorption of H_2S in the simple mixture. However, it seems the pore size distribution is not affected in the mesopore range (data not shown). The results from BH-CO_2 and MH-CO_2 demonstrate that hydrogen sulfide removal has higher influence on the porosity of these materials which also present superior adsorption capacity than BH-H_2O and MH-H_2O.

In conclusion, the micropores with pore width smaller than 1 nm play an important role in the adsorption of H_2S. Therefore, the active sites of samples are principally the pores at small scale. In contrast, the function of the mesopores is no clear. In addition, the distribution of porosity is influenced according to the activation method. Lastly, the inorganic composition of materials seems to be a key parameter in the way the pores are affected by the H_2S removal.

5.5.3. Influence of mineral content

The inorganic fraction of materials studied in this work are composed of Ca, K, Mg, Si and P as presented in Chapter 3 and some of these mineral elements can influence the H_2S removal. In the work of Awe et al., [137] the activity of $CaCO_3$ in H_2S adsorption was studied in a three-phase reactor. This investigation demonstrated that carbonate-based sorbents are able to remove H_2S from air through acid-basic reactions and catalytic oxidation under humid conditions. Bagreev et al., [154] have also mentioned that of Ca, Fe, Mg and K are involved in the oxidation of H_2S and removal from humidified air (relative humidity of 80 % at 25 °C).

Consequently, it is possible that the inorganic content of BH-CO_2, MH-CO_2, BH-H_2O and MH-H_2O are implicated in the reaction pathway of H_2S removal from biogas. In order to verify this hypothesis different experiments and characterization analysis should be considered for future work. The influence of the inorganic fraction of materials can be studied by carrying out breakthrough curves experiments under the same conditions with either the residue of materials after combustion (ash) or acid-washed activated carbons which removes the ash content. In addition, further material characterization after H_2S

removal must be performed such as the analysis of the diffraction pattern with an X-ray diffractometer in the fresh and exhausted samples. The characteristic X-ray diffraction pattern provides a unique fingerprint of the crystals present in the sample which allows detecting the different forms of minerals species such as $CaCO_3$, CaO, CaS from the same element (Ca). Therefore, results can provide information about the interaction of mineral elements with hydrogen sulfide and the reaction mechanism. Fresh and exhausted activated carbons can also be analyzed by Raman spectroscopic technique. This analysis provides a structural fingerprint by which mineral species can be identified. Thus, the comparison of spectra before and after H_2S adsorption can elucidate if the mineral species are involved in the adsorption mechanism and react with H_2S forming new compounds. Likewise, X-ray Photoelectron Spectroscopy (XPS) can be carried out to obtain information about the composition and chemical state of activated carbons before and after H_2S removal from biogas.

Radial graphs were made in order to evaluate the main properties associated to the performance of each material which are presented in Figure 5-11. The properties of materials were normalized based on the maximum value obtained on the studied samples. In the figure, BET surface refers to the surface area; V_{micro} and V_{meso} are the percentage of micro and mesoporous volumes; Ca, Mg and K are the percentage of each element in the AC; and pH is the surface pH of materials.

It can be observed that the superior adsorption capacity of BH-CO_2 in dry conditions is due to its high percentage of micropores, basic pH, Mg and Ca content in a lesser extent. The efficiency of MH-CO_2 is related to its percentage of micropores and basic pH, on the other hand, its K content is probably forming silicates thus it is not able to react with H_2S. In the same way, the performance of MH-H_2O is mostly related to its basic pH and percentage of micropores since its K content is probably in the silicate form. Lastly, the adsorption capacity of BH-H_2O is in part due to its high surface area, basic pH, moderate micropores and Mg and Ca contents in a lesser extent; the mesopores don't influence the H_2S removal.

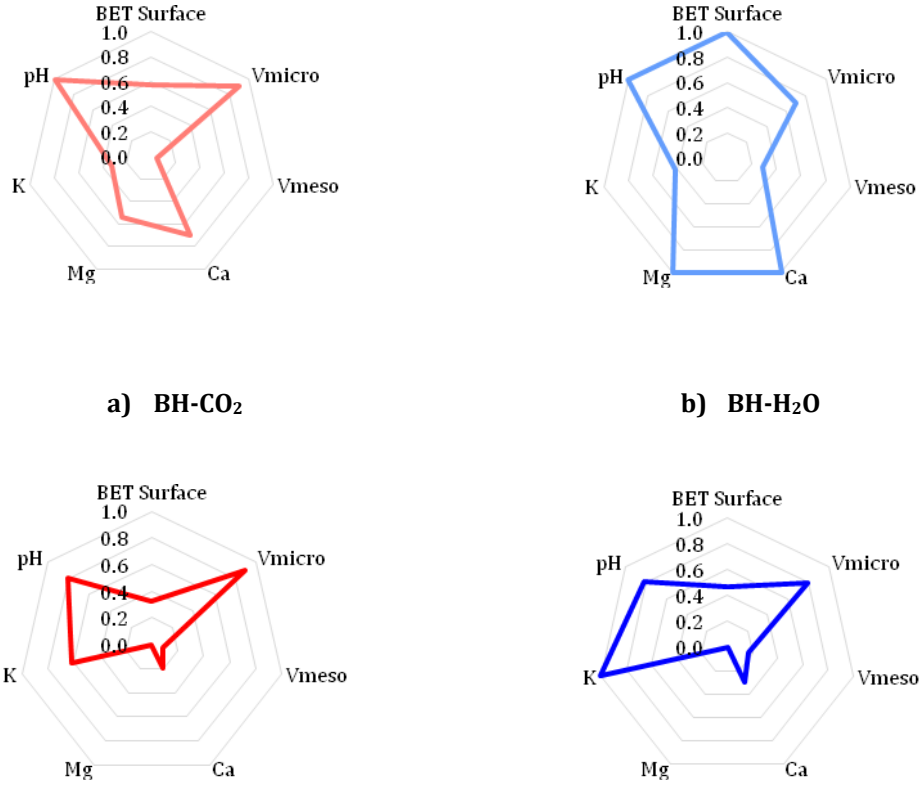

a) BH-CO_2 **b) BH-H_2O**

c) MH-CO_2 **d) MH-H_2O**

Figure 5-11. Influence of properties of materials in dry conditions.

5.6. Reaction pathway

In the previous section it was identified that distribution of porosity plays an important role in physisorption of H_2S however, porosity is not the only factor governing the removal of H_2S from biogas. The biogas composition can influence the removal of H_2S in link with activated carbons properties. Therefore, in order to get more insight of H_2S removal mechanism, the analysis of adsorbed sulfur compound must be assessed, for that end, it is possible to run a thermos-gravimetric analysis.

5.6.1. Reaction pathway

The removal of H_2S implies the adsorption of different sulfur compounds which involve several reaction pathways depending on the properties of the samples and the composition of the gas phase. In dry biogas the main reaction pathway involves the physical adsorption of hydrogen sulfide in the micropores and is controlled by the

intermolecular forces of the van der Waals type until reaching equilibrium between the activated carbon and the gas phase. This is illustrated in R 1-30 where the index "*gas*" denotes the gas phase and "*ads"* indicates the adsorbate phase. The physical adsorption is followed by the oxidative decomposition of H_2S on the surface of activated carbons as described in R 1-31 and R 1-32 [150]. In the present study, none of the gases contain oxygen therefore the oxidative decomposition of hydrogen sulfide involves the oxygen contained in the surface functional groups of activated carbons represented by *C(O)*. Deposited sulfur catalyzes the hydrogen sulfide oxidation and maximum activity is a function of the amount of sorbed sulfur by the activated carbon. This catalytic role of elemental sulfur in its own adsorption/oxidation process is only found under dry conditions. The main by-products of this mechanism of adsorption are elemental sulfur (S^*) and polysulfides (SS^*).

$$H_2S_{gas} \leftrightarrow H_2S_{ads} \qquad \textbf{R 1-30}$$

$$H_2S_{ads} + C(O) \rightarrow C(S^*_{ads}) + H_2O \qquad \textbf{R 1-31}$$

$$C(S^*_{ads}) + H_2S_{ads} + C(O) \rightarrow C(SS^*_{ads}) + H_2O \rightarrow C(S_{8,ads}) \qquad \textbf{R 1-32}$$

Under humid conditions, condensation of humidity in the pore structure of the AC enhances the adsorption capacity of materials due to the dissolution of H_2S into the pre-adsorbed water film. It is well known that surface of activated carbon is hydrophobic as result of a high degree of aromatization and the presence of graphene-like sheets. However, adsorption of water is enhanced by oxygen functional groups at the edges of graphene-like sheets and the number of polar groups on the surface of the activated carbon improves water adsorption [147]. The pKa constants of hydrogen sulfide are 7.2 and 13.9 for the first and second dissociation, respectively. The dissociation of hydrogen sulfide to HS^- depends not only on the amount of water adsorbed but also on the pH of the boundary surface. Activated carbons with basic pH promote the dissociation of H_2S to high concentrations of HS^- ions which are diffused in the water film. Then, HS-ions react with oxygen forming sulfur polymers [150]. The adsorption/oxidation pathway is described according to the following reactions where "*ads"* refers to the presence of molecules in the adsorbate phase:

$$H_2S_{gas} \leftrightarrow H_2S_{ads} \qquad \textbf{R 1-22}$$

$$H_2S_{ads} \rightarrow H_2S_{ads-liq} \qquad \textbf{R 1-23}$$

$$H_2S_{ads-liq} + H_2O \leftrightarrow HS^-_{ads} + H_3O^+ \quad \textbf{R 1-24}$$

$$HS^-_{ads} + C(O) \rightarrow S^*_{ads} + OH^- \quad \textbf{R 1-25}$$

$$HS^-_{ads} + 3C(O) \rightarrow SO_{2,ads} + OH^- \quad \textbf{R 1-26}$$

$$SO_{2,ads} + C(O) \rightarrow SO_{3,ads} \quad \textbf{R 1-27}$$

$$H^+ + OH^- \rightarrow H_2O \quad \textbf{R 1-28}$$

$$SO_{3,ads} + H_2O \rightarrow 2H^+ + SO_4^{2-} \quad \textbf{R 1-29}$$

It is important to mention that an excess of water (higher than 60 % of relative humidity) can decrease adsorption of activated carbons due to flooding as stated by Le Leuch et al., [150]. In addition, the catalytic effect of sulfur described in dry conditions is inhibited in the presence of water. The main by-products of this reaction pathway are sulfur oxides which is in agreement with results from TGA analysis.

Other authors have proposed different reactions involving calcium. In biogas containing CO_2, CaO and MgO are converted to carbonates and provide basic pH in the carbon surface favoring removal of H_2S. Bagreev et al., [154] proposed the reaction mechanism presented in R 1-5, R 1-36 and R 1-37. It can be noticed that reaction R 1-5 involves H_2O to form $Ca(OH)_2$ from CaO which then reacts with H_2S producing $Ca(HS)_2$ and H_2O. This mechanism is in agreement with desorbed sulfur compounds in the TGA analysis for the exhausted samples under humid conditions. In addition, this reaction pathway could explain the improvement of adsorption capacity of BH-H_2O in humid biogas.

$$CaO + H_2O \rightarrow Ca(OH)_2 \quad \textbf{R 1-5}$$

$$Ca(OH)_2 + 2H_2S \rightarrow Ca(HS)_2 + 2H_2O \quad \textbf{R 1-36}$$

$$Ca(HS)_2 + O_2 \rightarrow 2S + Ca(OH)_2 \quad \textbf{R 1-37}$$

Likewise, the adsorption mechanism of H_2S can involve Mg through the substitution of O atoms by S as well as by metal supported addition mechanism [149] as described in the following reactions:

$$MgO + H_2S \rightarrow MgS + H_2O \quad \textbf{R 5-1}$$

$$Mg\_S + O_2 \rightarrow C + SO_2 \quad \textbf{R 5-2}$$

$$MgO + H_2S \rightarrow Mg\_S + HS \quad \textbf{R 5-3}$$

5.7. Influence of fixed-bed height

The influence of the fixed-bed height was analyzed varying this parameter. To do so, the column is filled with sample BH-CO_2 to remove H_2S from humid biogas in the same condition as previous experiments, 200 ppm of H_2S at 30 °C. The fixed-bed height was increased from 4 cm to 8 and 12 cm. The breakthrough curves are presented in Figure 5-12.

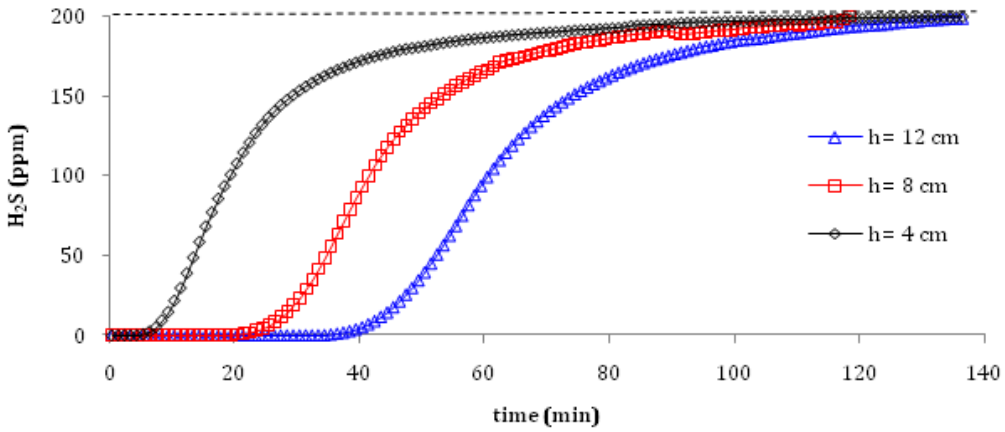

Figure 5-12. Influence of fixed-bed height using BH-CO_2 and humid biogas at 30 °C and inlet concentration of H_2S of 200 ppm.

It is observed that the increase of the volume of the fixed-bed amplifies the time of appearance of hydrogen sulfide in the outlet stream of the unit. When the fixed-bed height is 4 cm, H_2S is observed before 10 min while bed heights of 8 and 12 cm increase this time to 20 and 40 min respectively. The residence time of the gas in the fixed-bed of 4 cm is 0.4 s and increasing the height of the column to 8 and 12 cm augments the residence time to 0.8 and 1.2 s respectively. The H_2S removal with all heights of the fixed-bed is around 8 mg_{H2S}/g which means that this is the maximum adsorption capacity of this material and a higher initial H_2S concentration or bed height will not improve the H_2S removal. This result suggests that the removal mechanism with BH-CO_2 in humid biogas is governed mainly by the adsorption of molecules rather than their diffusion.

5.8. End life of materials

After exhausting activated carbons in H_2S adsorption, some authors have studied the feasibility of regeneration process in order to reuse this material. The regeneration of activated carbons requires elevated temperatures in order to achieve desorption of

pollutants. Bagreev et al., [204] studied the regeneration of spent activated carbons in H_2S adsorption from biogas. The process was carried out under air atmosphere at 300 °C. Hervy et al., [148] also explored the regeneration of saturated activated carbons at 750 °C during 1.5 h under nitrogen. However, the adsorption capacity is not always recovered and gases must be collected in order to prevent contamination. Consequently, the regeneration of exhausted activated carbons is not considered in this study.

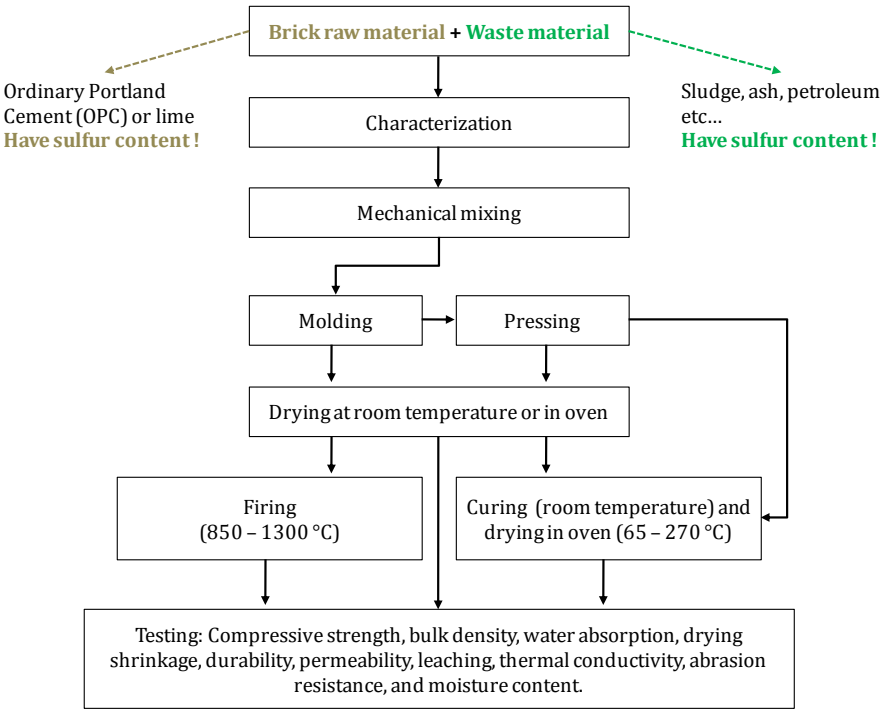

Figure 5-13. Methodology followed for manufacturing bricks from wastes adapted from [205,206]**.**

Currently, there is increasing interest of producing bricks from wastes in order to respond to the large demand of building materials and to deal with waste generation. Different wastes such as paper processing residues, cigarette butts, fly ash, textile effluent treatment plant sludge, plastic, sludge from industrial waste treatment plant, rice husk ash and petroleum effluent treatment plant sludge have been considered for this purpose [205]. In this application, wastes are used as additives which are mixed with the brick raw material, then the mix is characterized and used for the manufacturing of brick through different techniques such as firing and curing. Finally, the prepared bricks are tested in order to verify if they meet specific requirements as indicated in Figure 5-13. Although there is much research about bricks made from wastes materials that meet standard

requirements and various approved patents, the commercial application of these materials is very limited.

It should be pointed out that brick raw materials such as the Ordinary Portland Cement (OPC) have sulfur content in the form of SO_3 (2.4 %) [207] and wastes materials have varying sulfur content as well therefore the sulfur content of exhausted activated carbons in H_2S removal from biogas (< 1 %) should not be a limitation to consider this samples as potential waste material in brick manufacturing. However, during the conventional method of brick manufacture known as firing and carried out at high temperature (850 – 1300 °C), sulfur compounds from materials are released and cause new contamination. Besides, this process consumes large amounts of energy and releases greenhouse gases, thus this method raises important environmental concerns. The method of fabricating bricks through cementing (curing) is based on hydration reactions and is carried out at temperatures below 270 °C. Nevertheless, it is also energy demanding and leaves a carbon footprint [206].

Another method of producing bricks is through geopolymerization which relies on the chemical reaction of amorphous silica and alumina rich solids with an alkaline solution at ambient or slightly elevated temperatures. Advantages include abundant raw material sources, development of mechanical strength, durability, resistance to chemical attack and reduced energy consumption and greenhouse emissions, however the utilization of alkaline solutions induce extra costs [206]. This technique could be very interesting for spent activated carbons containing sulfur compounds since it has the ability to immobilize contaminants. Ahmari et al., [208] fabricated geopolymer bricks from mine tailings (MT) wastes that contain heavy metals dangerous for the air and underground water. The leaching analyses demonstrated that the heavy metals are effectively immobilized in the MT-based geopolymer bricks probably due to physical encapsulation. Therefore, geopolymerization is an interesting alternative to stabilize MT so that they can be used as construction materials. This study leads to believe that spent activated carbons in biogas treatment can be studied for the brick manufacturing by the geopolymerization technique limiting the release of sulfur compounds to the environment, however there are no studies exploring this option. Bearing in mind this limitation, it is not possible to affirm that bricks prepared from exhausted activated carbons meet standard requirements of building materials, nonetheless it is a potential alternative to consider for future investigations.

In that sense, two pathways are proposed for future work. On one hand, saturated BH-CO_2 and BH-H_2O can be studied in the brick fabrication due to their $CaCO_3$ and CaO content. The moderate temperatures of curing (65 – 270 °C) can minimize the release of sulfur compounds during the process. In addition, the resulting bricks are not expected to release sulfur compounds considering that temperatures higher than 300 °C are required according to regeneration process. The second via of investigation is to study all spent samples in the manufacture of bricks through geopolymerization. Besides, the release of sulfur compounds to the environment is avoided. In particular, MH-CO_2 and MH-H_2O are great candidates for this application due to their elevated silica content.

Another well-known alternatives for the end life of spent activated carbon resulting from its commercial and industrial use are: i) reactivation usually with steam, ii) disposal in landfill and iii) incineration or thermal destruction at cement kilns or waste-to-energy plants [209]. Usually, reactivation is less expensive than disposal and/or the purchase of fresh activated carbon. Landfilling is less costly than incineration and is preferred if the carbon is not suitable for reactivation, however, the sulfur compounds adsorbed on the carbon can leach out. Incineration is the most expensive of the three options but the one with the least potential liability since contaminants are destroyed in the process.

5.9. Conclusion

This chapter assessed the valorization of materials in biogas treatment aiming to remove H_2S, one of main contaminants that difficult the utilization of biogas. To do so, six materials were tested: two chars from pyrolysis and four activated carbons obtained by different methods. Breakthrough curve tests were carried out with different gas composition starting from a simplified mixture (N_2 + H_2S) to dry and humid biogas at room conditions.

It was observed that pyrolysis chars have poor adsorption capacity (< 1.6 mg_{H2S}/g) due to their limited porosity and acidic pH. The activation stage improves the adsorption capacity of raw chars achieving H_2S removal 8 times higher than pyrolysis chars. This study showed that the properties that govern hydrogen sulfide adsorption from biogas are pore size distribution and basic pH. Micropores are the active sites of materials where the physical adsorption of sulfur compounds takes place. In addition, CO_2 activation creates porosity composed principally of micropores favoring hydrogen sulfide removal while steam activation creates mesopores at higher proportion. The mineral species of activated carbons provide a basic pH which is necessary for the adsorption of acid gases such as

hydrogen sulfide. Further characterization of fresh and exhausted activated carbons must be carried out in order to determine more precisely the role of mineral species in hydrogen sulfide removal.

Results showed that the gas composition of biogas influences the adsorption capacity of materials. In simplified gas, the capacity of materials increases in the following order: MH-H_2O < BH-H_2O < MH-CO_2 < BH-CO_2. Materials displayed higher adsorption capacity under N_2 + H_2S than in dry biogas since other gases such as CO_2 and CH_4 can compete with hydrogen sulfide for the active sites. In humid conditions, the hydrogen sulfide removal achieved by activated carbons is similar for all samples indicating that humidity plays an important role in the adsorption mechanism of H_2S. The influence of humidity relies in the solubility of H_2S, CO_2 and CH_4 in the water film inside pores and since H_2S has the highest solubility, the humidity of biogas limits the competition with other gases (CO_2 and CH_4). However, the beneficial effect of humidity is not observed in pyrolysis chars proving that basic pH is required for the transfer of H_2S from the gas to the liquid phase.

Several reaction pathways take place in the adsorption of hydrogen sulfide from biogas. In dry conditions the physical adsorption and oxidation or chemisorption of H_2S leads to the storage of elemental sulfur and sulfur polysulfides whereas in humid conditions the formation of sulfur oxides and / or alkali sulfides is promoted in higher proportion. Since the H_2O content of biogas (4 – 5 mol. %) improves H_2S removal, a drying stage of the gas before treatment is not required however it can be a prerequisite after biogas cleaning depending on the target application. Parameters such as the relative humidity of the gas, particle size and moisture content of activated carbons should be studied to optimize the H_2S removal efficiency.

After exhausting activated carbons in H_2S elimination from biogas, materials can be considered as potential candidates for the brick manufactory. In order to minimize the release of sulfur compounds from the solid phase, two alternatives were identified for the end life of materials. Considering that exhausted samples contain sulfur compounds, the most suitable option for the end life of these materials is to use them as additives in the production of bricks through geopolymerization which is able to immobilize contaminants in an effective way. However, studies are necessary in order to establish if these exhausted activated carbons can meet the standard requirements of building materials such as compressive strength, water absorption and density among others.

Conclusions and future work

1. Conclusions

The thermo-chemical conversion of biomass is one of the key processes to develop energy systems not dependent of fossil fuels. These processes also deal with the managing of wastes since large amounts of residues can be processed through pyro-gasification and generates the possibility of valorizing wastes as stated by the principles of circular economy. Currently, the sub-product of pyrolysis and gasification of biomass known as char doesn't have many applications and is considered a waste which also limits the further development of thermo-chemical conversion process at industrial scale. Considering this limitation, this study aims to transform this residue into an added-value material by studying its properties and its potential use in different applications such as syngas and biogas treatment. In this section, the conclusions and perspectives for future work are presented.

Preparation of materials and energy efficiency of the processes

This study showed that the characteristics of biomass influence the features of pyrolysis chars. Precursors with high carbon and lignin content provide chars and activated carbons with high LHV and activated carbons with elevated porosity and while high ash contents decrease these properties of the resulting materials. In the same way, the inorganic composition and the activation method determine certain properties of resulting materials. During pyrolysis, the ash content increases while part of the ash-forming elements are released (<20 %) and the transformation of mineral elements depends on the composition of the inorganic content. In this sense, feedstock with high silica content like millet husk suffer less ash release compared to buckwheat husk where silica is not detected. In addition, chars from pyrolysis at 500 °C have poor porosity limited to macropores and present acidic surface.

The gasification or physical activation of chars modifies their chemical and textural characteristics. The CO_2 activation provides activated carbons with more carbon and less ash content compared to steam activation. In addition, activation with CO_2 results in materials with higher relative microporosity than activation with steam. It was observed that the activation agent, influence the transformation of mineral elements from the solid

phase. In activation with CO_2, more Ca is released and the calcium compounds remaining in the solid phase are found like CaO and $CaCO_3$ forms. Besides, Ca compounds are agglomerated thus they are not well-dispersed on the surface of activated carbon. In contrast, during steam activation less calcium is released, and it is mostly present in the CaO form which is well dispersed on the surface. In the same way, it appears that magnesium, potassium, phosphorus and silica are not influenced by the activating agent.

The selection of two biomasses and two activation types resulted in the production of six materials: two pyrolysis chars and four activated carbons. The sample BH-H_2O prepared from buckwheat husk through steam activation, presents the highest surface area (997 m^2/g), composed of 71 % of micropores. This sample presents Ca in the CaO form, K, Mg and P which provide its basic pH. BH-CO_2 samples have less surface area close to 600 m^2/g with more than 80 % of micropores. These activated carbons have similar inorganic composition, however in BH-CO_2 calcium is found in the $CaCO_3$ and CaO forms while CaO is the main species in BH-H_2O. Activated carbons prepared from millet husk, present lower porosity due to their high ash content. MH-H_2O has a surface area of 466 m^2/g with 83 % of micropores while the surface of MH-CO_2 samples are around 320 m^2/g composed of more micropores than mesopores. These materials have high content of silica accompanied with Ca, K and P.

The energy performance indicators show that slow pyrolysis presents the highest energy efficiency and the phase that carries most of the energy is the char thus it must be valorized as an energy vector. To accomplish that, the char can be submitted to physical activation or gasification in order to recover its energy as gas. Then the gasified char or activated carbon with higher porosity and more concentrated minerals can be implemented in biogas cleaning or it can be re-introduced in the gasifier depending on its composition in order to reduce tar formation in the process. The conditions of steam and CO_2 activation must be optimized in order to improve the LHV of the gas which can be valorized in other applications such as Fischer –Tropsh synthesis, with that mind the inlet of CO_2 must be drastically reduced.

Syngas upgrading

Chars from pyrolysis (MH-Char and BH-Char) showed limited reactivity attributed to the absence of micropores which are developed in the activation stage. Results from the simplified matrix suggested that porosity and mineral composition of materials are the

main properties influencing the degradation of ethylbenzene. BH-H_2O which is the sample with the highest surface area, superior Ca, K and Mg content and non-detectable silica resulted in the highest ethylbenzene removal (0.95 g_{EB}/g) by gram of sample. MH-H_2O presented the second-best performance (0.77 g_{EB}/g) thanks to mesopores that are more resistant to deactivation by coke deposit. However, the microporous samples (MH-CO_2 and BH-CO_2) were deactivated faster than steam activated samples.

In dry syngas, CO_2 is adsorbed reducing the performance of BH-H_2O and MH-H_2O. On the other hand, CO_2 does not compete with ethylbenzene for the active sites of MH-CO_2 and BH-CO_2 and their efficiency is increased in comparison to simple syngas. The thermal cracking is the highest in dry syngas however steam has a favoring effect in tar cleaning since most of the samples improved their efficiency except for MH-CO_2. The presence of steam probably involves reforming of tars, and steam reacts with carbon monoxide which increases the hydrogen content favoring the syngas quality. The activated carbon that presents the highest performance in all syngas matrices is BH-H_2O (0.7 – 2.9 g_{EB}/g) thanks to its surface area, micropores, mesopores and mineral composition that contribute to its efficiency in ethylbenzene conversion. The calcium compounds present in this sample lead to formation of lighter tar components whereas this effect is avoided with MH-CO_2 and MH-H_2O which have lower calcium and higher silica content. Deactivation rates of materials confirmed that saturation of MH-H_2O and BH-H_2O is slower than MH-CO_2 and BH-CO_2 due to their mesopores.

Biogas treatment

In the simplified matrix, chars from pyrolysis have poor H_2S adsorption capacity (< 1.6 mg_{H2S}/g) due to their limited porosity and acidic pH. The activation stage improves the adsorption capacity (4.1 – 9.3 mg_{H2S}/g) of materials achieving higher H_2S removal thanks to their developed porosity, pore size distribution and basic pH. Results showed that micropores are the active sites of materials where the physical adsorption of sulfur compounds takes place. The influence of the activation method is evidenced in the relative microporosity of BH-CO_2 and MH-CO_2 which favors hydrogen sulfide removal. Mineral species are important since they provide a basic pH which is necessary for the adsorption of acid gases such as hydrogen sulfide.

The gas composition of biogas influences the adsorption capacity of materials since activated carbons displayed higher adsorption capacity under N_2 + H_2S than in dry biogas

due to the competition of CO_2 and CH_4 with H_2S for the active sites. In humid biogas, the hydrogen sulfide removal is improved and the adsorption capacity is similar for all samples (6.2 – 8.2 mg_{H2S}/g) indicating that humidity plays an important role in the adsorption mechanism of H_2S. Steam in biogas condensates in the pores of activated carbons and the superior solubility of H_2S compared to CO_2 and CH_4, limits the competition of these gases for the active sites. However, the beneficial effect of humidity only takes place in materials with basic surface. Humidity of biogas influences the adsorption-oxidation mechanism of hydrogen sulfide in activated carbons. In dry biogas the physical adsorption and oxidation of H_2S leads to the storage of elemental sulfur and sulfur polysulfides whereas in humid conditions the formation of sulfur oxides and / or alkali sulfides takes place in a higher extend. The activated carbon with the highest adsorption capacity in all biogas matrices is BH-CO_2 (7.7 – 9.3 mg_{H2S}/g) attributed to its high surface area with high relative microporosity and mineral species that contribute to its efficiency in hydrogen sulfide removal.

Results from syngas and biogas cleaning lead to conclude that the activation method must be selected according to the intended application. In that sense, for biogas cleaning CO_2 activation is preferred in order to prepare materials with high relative microporosity while syngas cleaning requires activation carbons from steam activation with more mesopores that are resistant to the deactivation by coke deposit.

End life of materials

Considering the lower heating value of activated carbons, the exhausted materials in syngas cleaning are energy carriers whose energy can be recovered through gasification. Two materials were selected to explore this option: BH-CO_2 and BH-H_2O since their inorganic fraction is not composed of silica. The gasification of exhausted BH-H_2O was able to produce syngas with higher H_2 percentage and lower CO_2 content most probably due to its superior calcium content; therefore the energy recovery from this sample is more interesting compared to BH-CO_2. Exhausted MH-CO_2 and MH-H_2O in syngas cleaning, should be recovered as materials since their silica content limits the efficiency of their gasification; instead this high concentration of silica is desirable in materials used for construction purposes. With that in mind, further studies of MH-Char, MH-CO_2 and MH-H_2O as aggregates of building materials should be performed.

The ultimate use of materials has to be selected avoiding to generate environmental concerns. According to this principle, the final use of the spent activated carbons in H_2S removal from biogas has to be carefully chosen since these materials contain sulfur compounds toxic for the environment. Contaminated samples with sulfur compounds are potential candidates for the brick manufactory. Aiming to minimize the release of pollutants from the solid phase, two pathways were identified as ultimate use of these activated carbons. The brick fabrication technique depends on the composition of materials, for that reason BH-CO_2 and BH-H_2O can be studied as additives of bricks prepared through the curing method considering the calcium content of these samples. In the same way, regarding the elevated silica content of materials prepared from millet husks, their use in the production of bricks through geopolymerization should be investigated since this method is based on chemical reactions of amorphous silica and alumina rich solids with an alkaline solution. In addition, this method is interesting since it is able to immobilize contaminants in an effective way.

2. Perspectives

The physical activation or gasification process must be optimized in order to improve its energy efficiency. To do so, the inlet of the activating agents must be reduced in order to increase the lower heating value of products. The composition of the atmosphere in CO_2 activation should be modified reducing the percentage of CO_2 in a drastic proportion aiming to minimize the CO_2 content in the outlet syngas and avoiding the collapse of the LHV of the gas. However, with the objective of keeping or improving the surface area of the resulting activated carbon, this parameter must be followed. Likewise, steam should be reduced with the purpose of minimizing the water content of the liquid phase and be able to increase its energetic value. Another way of optimization is to combine steam and CO_2 as oxidizing agent, this way allows reducing the water content in the liquid phase and increasing the hydrogen content in the gas. In that sense, it is necessary to consider that the gasification of exhausted BH-H_2O was performed under 20 % of CO_2 and 40 % of steam balanced with nitrogen and the LHV of the syngas was 5.9 MJ/Kg due to the steam content of syngas (14 %). Therefore, for future work it is recommended to conserve the ratio H_2O:CO_2 equal to 2:1 and consider starring from H_2O of 6 %. Lastly, modifications of the pilot should be performed to facilitate the recovery of the latent heat of syngas and use it in the process to improve its energy efficiency.

The samples prepared through 1-step CO_2 activation were not tested in syngas or biogas cleaning. Therefore, it is interesting to determine the performance of these materials and compare them to their homologue activated carbons obtained through 2-steps activation. The aim of these experiments would be to verify if changes in carbon and ash content influence the performance of samples.

In the syngas cleaning experiments, it was observed that more coke production takes place with syngas containing steam; however it was not possible to quantify the coke formation. Thus, the influence of soot generation should be studied carrying out experiments using the TGA analysis in order to control the weight gain of the sample. The purpose of this campaign of experiments should be to relate performance of materials and coke production.

Further characterization of exhausted materials in syngas and biogas cleaning must be performed in order to determine more precisely the role of mineral species in the decomposition of ethylbenzene and the adsorption-oxidation of hydrogen sulfide. In this regard, additional analysis such as X-ray diffraction, Raman spectroscopy and X-ray Photoelectron Spectroscopy can be carried out to obtain information about the composition and chemical state of mineral elements in activated carbons before and after their use in syngas and biogas treatment. Conditions of biogas treatment should be optimized in order to improve the adsorption capacity of materials. Since the reaction mechanism is governed by the physical adsorption of H_2S, high diffusion of molecules must be ensured. Therefore, increasing the residence time of the gas in the fixed-bed should improve the adsorption capacity of activated carbons. This parameter and others such as relative humidity of the gas, particle size and moisture content of activated carbons must be studied to optimize the H_2S removal efficiency.

References

[1] IEA, World Energy Outlook 2007: China and India Insights, 2007. www.iea.org/Textbase/%5Cnhttp://www.iea.org/publications/freepublications/publication/weo_2007.pdf.

[2] C. national de L'industrie, Pyrolyse Et Gazeification , Energetique Et Le Developpement De L ' Economie Circulaire, (2015) 1–47. https://www.clubpyrogazeification.org/fr/ (accessed June 20, 2018).

[3] A.J. Marshall, P.F. Wu, S.H. Mun, C. Lalonde, Commercial application of pyrolysis technology in agriculture, Am. Soc. Agric. Biol. Eng. Annu. Int. Meet. 2014, ASABE 2014. 5 (2014) 3868–3886.

[4] P. Feng, W. Lin, P.A. Jensen, W. Song, L. Hao, K. Raffelt, K. Dam-Johansen, Entrained flow gasification of coal/bio-oil slurries, Energy. 111 (2016) 793–802. doi:10.1016/j.energy.2016.05.115.

[5] GLOBAL SYNGAS TECHNOLOGIES COUNCIL, (n.d.). https://www.globalsyngas.org/resources/the-gasification-industry/ (accessed September 4, 2018).

[6] European Commission, The role of waste-to-energy in the circular economy, 2017. http://ec.europa.eu/environment/waste/waste-to-energy.pdf.

[7] European Commission, Closing the loop - An EU action plan for the Circular Economy, 2015. https://ec.europa.eu/transparency/regdoc/rep/1/2015/EN/1-2015-614-EN-F1-1.PDF.

[8] European Environment Agency, Circular by design - Products in the circular economy, EEA Report, No. 6/2017, 2017. doi:10.2800/860754.

[9] H.-P. Schmidt, Journal of ecology, winegrowing and climate farming, Switz. First Eur. Ctry. to Off. Approv. Biochar. (2013). http://www.ithaka-journal.net/schweiz-bewilligt-pflanzenkohle-zur-bodenverbesserung?lang=en (accessed June 5, 2018).

[10] European Biochar Foundation (EBC), Guidelines for a Sustainable Production of Biochar, Eur. Biochar Found. (2016) 1–22. doi:10.13140/RG.2.1.4658.7043.

[11] K. Gell, J.W. van Groenigen, M.L. Cayuela, Residues of bioenergy production chains as soil amendments: Immediate and temporal phytotoxicity, J. Hazard. Mater. 186 (2011) 2017–2025. doi:10.1016/j.jhazmat.2010.12.105.

[12] W. Gwenzi, N. Chaukura, F.N.D. Mukome, S. Machado, B. Nyamasoka, Biochar production and applications in sub-Saharan Africa: Opportunities, constraints, risks and uncertainties, J. Environ. Manage. 150 (2015) 250–261.

doi:10.1016/j.jenvman.2014.11.027.

[13] K. Qian, A. Kumar, H. Zhang, D. Bellmer, R. Huhnke, Recent advances in utilization of biochar, Renew. Sustain. Energy Rev. 42 (2015) 1055–1064. doi:10.1016/j.rser.2014.10.074.

[14] IEA, IEA bioenergy Task 42 on biorefineries: co-production of fuels, chemicals, power and materials from biomass., 2007. https://www.iea-bioenergy.task42-biorefineries.com/en/ieabiorefinery.htm.

[15] F. Cherubini, The biorefinery concept: Using biomass instead of oil for producing energy and chemicals, Energy Convers. Manag. 51 (2010) 1412–1421. doi:10.1016/j.enconman.2010.01.015.

[16] M.A. Yahya, Z. Al-Qodah, C.W. Zanariah Ngah, Agricultural bio-waste materials as potential sustainable precursors used for activated carbon production: A review, Renew. Sustain. Energy Rev. 46 (2015) 218–235. doi:10.1016/j.rser.2015.02.051.

[17] C. S.a, P.P. Parikh, A unified correlation for estimating HHV of solid,liquid and gaseous fuels, Fuel. 81 (2002) 1051–1063. file://c/Documents and Settings/Administrador/Escritorio/Rogelio/2842-1-s2.0-S0016236101001314-main.pdf.

[18] K.M. Bryden, M.J. Hagge, Modeling the combined impact of moisture and char shrinkage on the pyrolysis of a biomass particle, Fuel. 82 (2003) 1633–1644. doi:10.1016/S0016-2361(03)00108-X.

[19] T. Kan, V. Strezov, T.J. Evans, Lignocellulosic biomass pyrolysis: A review of product properties and effects of pyrolysis parameters, Renew. Sustain. Energy Rev. 57 (2016) 1126–1140. doi:10.1016/j.rser.2015.12.185.

[20] D. Shen, W. Jin, J. Hu, R. Xiao, K. Luo, An overview on fast pyrolysis of the main constituents in lignocellulosic biomass to valued-added chemicals: Structures, pathways and interactions, Renew. Sustain. Energy Rev. 51 (2015) 761–774. doi:10.1016/j.rser.2015.06.054.

[21] M.I. Jahirul, M.G. Rasul, A.A. Chowdhury, N. Ashwath, Biofuels production through biomass pyrolysis- A technological review, Energies. 5 (2012) 4952–5001. doi:10.3390/en5124952.

[22] J.F. Saldarriaga, R. Aguado, A. Pablos, M. Amutio, M. Olazar, J. Bilbao, Fast characterization of biomass fuels by thermogravimetric analysis (TGA), Fuel. 140 (2015) 744–751. doi:10.1016/j.fuel.2014.10.024.

[23] J. Zou, H. Yang, Z. Zeng, C. Wu, P.T. Williams, H. Chen, Hydrogen production from pyrolysis catalytic reforming of cellulose in the presence of K alkali metal, Int. J. Hydrogen Energy. (2016). doi:10.1016/j.ijhydene.2016.04.207.

[24] K. Raveendran, A. Ganesh, K.C. Khilar, Influence of mineral matter on biomass pyrolysis characteristics, Fuel. 74 (1995) 1812–1822. doi:10.1016/0016-2361(95)80013-8.

[25] H. Hwang, S. Oh, I.-G. Choi, J.W. Choi, Catalytic effects of magnesium on the characteristics of fast pyrolysis products – Bio-oil, bio-char, and non-condensed pyrolytic gas fractions, J. Anal. Appl. Pyrolysis. 113 (2015) 27–34. doi:10.1016/j.jaap.2014.09.028.

[26] F. Nie, D. He, J. Guan, K. Zhang, T. Meng, Q. Zhang, The influence of abundant calcium oxide addition on oil sand pyrolysis, Fuel Process. Technol. 155 (2017) 216–224. doi:10.1016/j.fuproc.2016.06.020.

[27] D.M. Keown, G. Favas, J.I. Hayashi, C.Z. Li, Volatilisation of alkali and alkaline earth metallic species during the pyrolysis of biomass: Differences between sugar cane bagasse and cane trash, Bioresour. Technol. 96 (2005) 1570–1577. doi:10.1016/j.biortech.2004.12.014.

[28] D. Mourant, Z. Wang, M. He, X.S. Wang, M. Garcia-Perez, K. Ling, C.Z. Li, Mallee wood fast pyrolysis: Effects of alkali and alkaline earth metallic species on the yield and composition of bio-oil, Fuel. 90 (2011) 2915–2922. doi:10.1016/j.fuel.2011.04.033.

[29] J. Werther, M. Saenger, E.-U. Hartge, T. Ogada, Z. Siagi, Combustion of agricultural residues, Prog. Energy Combust. Sci. 26 (2000) 1–27. doi:10.1016/S0360-1285(99)00005-2.

[30] J.R. Ajayi, B.O. Rasheed, O.F. Mojirade, Exploratory assessment of strength characteristics of millet husk ash (MHA) blended cement laterized concrete, Adv. Appl. Sci. Res. 4 (2013) 452–457.

[31] L.A. Zemnukhova, E.D. Shkorina, G.A. Fedorishcheva, Composition of inorganic components of buckwheat husk and straw, Russ. J. Appl. Chem. 78 (2005) 324–328. doi:10.1007/s11167-005-0284-1.

[32] C.E. Brewer, V.J. Chuang, C.A. Masiello, H. Gonnermann, X. Gao, B. Dugan, L.E. Driver, P. Panzacchi, K. Zygourakis, C.A. Davies, New approaches to measuring biochar density and porosity, Biomass and Bioenergy. 66 (2014) 176–185. doi:10.1016/j.biombioe.2014.03.059.

[33] M. Patel, X. Zhang, A. Kumar, Techno-economic and life cycle assessment on lignocellulosic biomass thermochemical conversion technologies: A review, Renew. Sustain. Energy Rev. 53 (2016) 1486–1499. doi:10.1016/j.rser.2015.09.070.

[34] A. Sharma, V. Pareek, D. Zhang, Biomass pyrolysis—A review of modelling, process parameters and catalytic studies, Renew. Sustain. Energy Rev. 50 (2015) 1081–1096. doi:10.1016/j.rser.2015.04.193.

[35] C.R. Lohri, H.M. Rajabu, D.J. Sweeney, C. Zurbrügg, Char fuel production in developing countries – A review of urban biowaste carbonization, Renew. Sustain. Energy Rev. 59 (2016) 1514–1530. doi:10.1016/j.rser.2016.01.088.

[36] F.-X. Collard, J. Blin, A review on pyrolysis of biomass constituents: Mechanisms and composition of the products obtained from the conversion of cellulose, hemicelluloses and lignin, Renew. Sustain. Energy Rev. 38 (2014) 594–608. doi:10.1016/j.rser.2014.06.013.

[37] M. Tripathi, J.N. Sahu, P. Ganesan, Effect of process parameters on production of biochar from biomass waste through pyrolysis: A review, Renew. Sustain. Energy Rev. 55 (2016) 467–481. doi:10.1016/j.rser.2015.10.122.

[38] N. Gómez, J.G. Rosas, J. Cara, O. Martínez, J.A. Alburquerque, M.E. Sánchez, Slow pyrolysis of relevant biomasses in the Mediterranean basin. Part 1. Effect of temperature on process performance on a pilot scale, J. Clean. Prod. 120 (2016) 181–190. doi:10.1016/j.jclepro.2014.10.082.

[39] J. Park, Y. Lee, C. Ryu, Y.-K. Park, Slow pyrolysis of rice straw: Analysis of products properties, carbon and energy yields, Bioresour. Technol. 155 (2014) 63–70. doi:10.1016/j.biortech.2013.12.084.

[40] T. Imam, S. Capareda, Characterization of bio-oil, syn-gas and bio-char from switchgrass pyrolysis at various temperatures, J. Anal. Appl. Pyrolysis. 93 (2012) 170–177. doi:10.1016/j.jaap.2011.11.010.

[41] G. Chang, Y. Huang, J. Xie, H. Yang, H. Liu, X. Yin, C. Wu, The lignin pyrolysis composition and pyrolysis products of palm kernel shell, wheat straw, and pine sawdust, Energy Convers. Manag. 124 (2016) 587–597. doi:10.1016/j.enconman.2016.07.038.

[42] J.S. Cha, S.H. Park, S.-C. Jung, C. Ryu, J.-K. Jeon, M.-C. Shin, Y.-K. Park, Production and utilization of biochar: A review, J. Ind. Eng. Chem. (2016). doi:10.1016/j.jiec.2016.06.002.

[43] P. McKendry, Energy production from biomass (part 3): gasification technologies, Bioresour. Technol. 83 (2002) 55–63. doi:10.1016/S0960-8524(01)00120-1.

[44] M. Asadullah, Barriers of commercial power generation using biomass gasification gas: A review, Renew. Sustain. Energy Rev. 29 (2014) 201–215. doi:10.1016/j.rser.2013.08.074.

[45] P. Mondal, G.S. Dang, M.O. Garg, Syngas production through gasification and cleanup for downstream applications - Recent developments, Fuel Process. Technol. 92 (2011) 1395–1410. doi:10.1016/j.fuproc.2011.03.021.

[46] C. Kammann, A. Funke, Hydrothermal carbonization of biomass residuals : a

comparative review of the chemistry , processes and applications of wet and dry pyrolysis, Biofuels. 2 (2011) 71–106. doi:10.4155/bfs.10.81.

[47] H.A. Ruiz, R.M. Rodríguez-Jasso, B.D. Fernandes, A.A. Vicente, J.A. Teixeira, Hydrothermal processing, as an alternative for upgrading agriculture residues and marine biomass according to the biorefinery concept: A review, Renew. Sustain. Energy Rev. 21 (2013) 35–51. doi:10.1016/j.rser.2012.11.069.

[48] K. Tekin, S. Karagöz, S. Bektaş, A review of hydrothermal biomass processing, Renew. Sustain. Energy Rev. 40 (2014) 673–687. doi:10.1016/j.rser.2014.07.216.

[49] J. Akhtar, N.A.S. Amin, A review on process conditions for optimum bio-oil yield in hydrothermal liquefaction of biomass, Renew. Sustain. Energy Rev. 15 (2011) 1615–1624. doi:10.1016/j.rser.2010.11.054.

[50] A. Oasmaa, B. Van De Beld, P. Saari, D.C. Elliott, Y. Solantausta, Norms, standards, and legislation for fast pyrolysis bio-oils from lignocellulosic biomass, Energy and Fuels. 29 (2015) 2471–2484. doi:10.1021/acs.energyfuels.5b00026.

[51] H. Yang, J. Yao, G. Chen, W. Ma, B. Yan, Y. Qi, Overview of upgrading of pyrolysis oil of biomass, Energy Procedia. 61 (2014) 1306–1309. doi:10.1016/j.egypro.2014.11.1087.

[52] S. Sadaka, a. a. Boateng, Pyrolysis and Bio-Oil, Agric. Nat. Resour. (2009) 1–6. doi:FSA1052-PD-6-09N.

[53] A.K. Hossain, P.A. Davies, Pyrolysis liquids and gases as alternative fuels in internal combustion engines – A review, Renew. Sustain. Energy Rev. 21 (2013) 165–189. doi:10.1016/j.rser.2012.12.031.

[54] S.-J. Oh, G.-G. Choi, J.-S. Kim, Characteristics of bio-oil from the pyrolysis of palm kernel shell in a newly developed two-stage pyrolyzer, Energy. 113 (2016) 108–115. doi:10.1016/j.energy.2016.07.044.

[55] T. Chen, R. Liu, N.R. Scott, Characterization of energy carriers obtained from the pyrolysis of white ash, switchgrass and corn stover — Biochar, syngas and bio-oil, Fuel Process. Technol. 142 (2016) 124–134. doi:10.1016/j.fuproc.2015.09.034.

[56] W.T. Tsai, M.K. Lee, Y.M. Chang, Fast pyrolysis of rice husk: Product yields and compositions, Bioresour. Technol. 98 (2007) 22–28. doi:10.1016/j.biortech.2005.12.005.

[57] Y. Shen, J. Wang, X. Ge, M. Chen, By-products recycling for syngas cleanup in biomass pyrolysis – An overview, Renew. Sustain. Energy Rev. 59 (2016) 1246–1268. doi:10.1016/j.rser.2016.01.077.

[58] F. a. López, T. a. Centeno, I. García-Díaz, F.J. Alguacil, Textural and fuel characteristics of the chars produced by the pyrolysis of waste wood, and the

properties of activated carbons prepared from them, J. Anal. Appl. Pyrolysis. 104 (2013) 551–558. doi:10.1016/j.jaap.2013.05.014.

[59] J. Rizkiana, G. Guan, W.B. Widayatno, X. Hao, X. Li, W. Huang, A. Abudula, Promoting effect of various biomass ashes on the steam gasification of low-rank coal, Appl. Energy. 133 (2014) 282–288. doi:10.1016/j.apenergy.2014.07.091.

[60] J.A. Conesa, A. Domene, Biomasses pyrolysis and combustion kinetics through n-th order parallel reactions, Thermochim. Acta. 523 (2011) 176–181. doi:10.1016/j.tca.2011.05.021.

[61] J. Hayashi, A. Kazehaya, K. Muroyama, A.P. Watkinson, Preparation of activated carbon from lignin by chemical activation, Carbon N. Y. 38 (2000) 1873–1878. doi:10.1016/S0008-6223(00)00027-0.

[62] L. Wei, S. Xu, L. Zhang, H. Zhang, C. Liu, H. Zhu, S. Liu, Characteristics of fast pyrolysis of biomass in a free fall reactor, Fuel Process. Technol. 87 (2006) 863–871. doi:10.1016/j.fuproc.2006.06.002.

[63] B. Tiryaki, E. Yagmur, A. Banford, Z. Aktas, Comparison of activated carbon produced from natural biomass and equivalent chemical compositions, J. Anal. Appl. Pyrolysis. 105 (2014) 276–283. doi:10.1016/j.jaap.2013.11.014.

[64] S. You, Y.S. Ok, S.S. Chen, D.C.W. Tsang, E.E. Kwon, J. Lee, C.H. Wang, A critical review on sustainable biochar system through gasification: Energy and environmental applications, Bioresour. Technol. 246 (2017) 242–253. doi:10.1016/j.biortech.2017.06.177.

[65] European Biochar Foundation (EBC), Positive list of biomass feedstock approved for use in producing biochar, Eur. Biochar Found. (2013).

[66] V. Benedetti, F. Patuzzi, M. Baratieri, Characterization of char from biomass gasification and its similarities with activated carbon in adsorption applications 1 Introduction 2 Char as activated carbon, Appl. Energy. (2017) 1–8. doi:10.1016/j.apenergy.2017.08.076.

[67] J. Lee, X. Yang, S.-H. Cho, J.-K. Kim, S.S. Lee, D.C.W. Tsang, Y.S. Ok, E.E. Kwon, Pyrolysis process of agricultural waste using CO2 for waste management, energy recovery, and biochar fabrication, Appl. Energy. 185 (2017) 214–222. doi:10.1016/j.apenergy.2016.10.092.

[68] S. Guo, J. Peng, W. Li, K. Yang, L. Zhang, S. Zhang, H. Xia, Effects of CO2 activation on porous structures of coconut shell-based activated carbons, Appl. Surf. Sci. 255 (2009) 8443–8449. doi:10.1016/j.apsusc.2009.05.150.

[69] F. Rodríguez-Reinoso, M. Molina-Sabio, Activated carbons from lignocellulosic materials by chemical and/or physical activation: an overview, Carbon N. Y. 30

(1992) 1111–1118. doi:10.1016/0008-6223(92)90143-K.

[70] T. Yang, A.C. Lua, Characteristics of activated carbons prepared from pistachio-nut shells by potassium hydroxide activation, Microporous Mesoporous Mater. 63 (2003) 113–124. doi:10.1016/S1387-1811(03)00456-6.

[71] R. Suresh, A. Al Shoaibi, C. Srinivasakannan, A comparison of microstructure and adsorption characteristics of activated carbons by CO2 and H3PO4 activation from date palm pits, New Carbon Mater. 27 (2012) 344–351. doi:10.1016/S1872-5805(12)60020-1.

[72] M. Molina, F. Rodríguez, Role of chemical activation in the development of carbon porosity, Colloids Surfaces A Physicochem. Eng. Asp. 241 (2004) 15–25. doi:10.1016/j.colsurfa.2004.04.007.

[73] C. Moreno, F. Carrasco, M.V. López, M.A. Alvarez, Chemical and physical activation of olive-mill waste water to produce activated carbons, Carbon N. Y. 39 (2001) 1415–1420. doi:10.1016/S0008-6223(00)00268-2.

[74] H. Marsh, D.S. Yan, T.M. O'Grady, A. Wennerberg, Formation of active carbons from cokes using potassium hydroxide, Carbon N. Y. 22 (1984) 603–611. doi:10.1016/0008-6223(84)90096-4.

[75] V. Fierro, V. Torné-Fernández, A. Celzard, Kraft lignin as a precursor for microporous activated carbons prepared by impregnation with ortho-phosphoric acid: Synthesis and textural characterisation, Microporous Mesoporous Mater. 92 (2006) 243–250. doi:10.1016/j.micromeso.2006.01.013.

[76] J. Guo, A.C. Lua, Surface functional groups on oil-palm-shell adsorbents prepared by H3PO4and KOH activation and their effects on adsorptive capacity, Chem. Eng. Res. Des. 81 (2003) 585–590. doi:10.1205/026387603765444537.

[77] P. Nowicki, J. Kazmierczak, R. Pietrzak, Comparison of physicochemical and sorption properties of activated carbons prepared by physical and chemical activation of cherry stones, Powder Technol. 269 (2015) 312–319. doi:10.1016/j.powtec.2014.09.023.

[78] R. Bardestani, S. Kaliaguine, Steam activation and mild air oxidation of vacuum pyrolysis biochar, Biomass and Bioenergy. 108 (2018) 101–112. doi:10.1016/j.biombioe.2017.10.011.

[79] K. Yang, J. Peng, H. Xia, L. Zhang, C. Srinivasakannan, S. Guo, Textural characteristics of activated carbon by single step CO2 activation from coconut shells, J. Taiwan Inst. Chem. Eng. 41 (2010) 367–372. doi:10.1016/j.jtice.2009.09.004.

[80] M. Islam, M. Rouf, S. Fujimoto, T. Minowa, Preparation and characterization of activated carbon from bio-diesel by-products (Jatropha seedcake) by steam

activation, Bangladesh J. Sci. Ind. Res. 47 (2012) 257–264. doi:10.3329/bjsir.v47i3.13056.

[81] M. Shoaib, H.M. Al-Swaidan, Optimization and characterization of sliced activated carbon prepared from date palm tree fronds by physical activation, Biomass and Bioenergy. 73 (2015) 124–134. doi:http://dx.doi.org/10.1016/j.biombioe.2014.12.016.

[82] J. Ahmad, E. Cordioli, F. Patuzzi, D. Prando, M.J. Castaldi, M. Baratieri, Possible Utilization Pathways of Char from Biomass Thermochemical Conversion: Char as a Catalytic Filtering Medium for Tar Cracking, in: Eur. Biomass Conf. Exhib. Proc., 2016: p. 5. doi:10.5071/24theubce2016-2bo.2.3.

[83] M. Ruiz-Fernández, M. Alexandre-Franco, C. Fernández-González, V. Gómez-Serrano, Development of activated carbon from vine shoots by physical and chemical activation methods. Some insight into activation mechanisms, Adsorption. 17 (2011) 621–629. doi:10.1007/s10450-011-9347-1.

[84] L. Yang, T. Huang, X. Jiang, W. Jiang, Effect of steam and CO2 activation on characteristics and desulfurization performance of pyrolusite modified activated carbon, Adsorption. 22 (2016) 1099–1107. doi:10.1007/s10450-016-9832-7.

[85] C. Guizani, M. Jeguirim, R. Gadiou, F.J. Escudero Sanz, S. Salvador, Biomass char gasification by H2O, CO2and their mixture: Evolution of chemical, textural and structural properties of the chars, Energy. 112 (2016) 133–145. doi:10.1016/j.energy.2016.06.065.

[86] P. Lahijani, Z.A. Zainal, A.R. Mohamed, M. Mohammadi, CO2 gasification reactivity of biomass char: catalytic influence of alkali, alkaline earth and transition metal salts., Bioresour. Technol. 144 (2013) 288–95. doi:10.1016/j.biortech.2013.06.059.

[87] S.-H. Jung, J.-S. Kim, Production of biochars by intermediate pyrolysis and activated carbons from oak by three activation methods using CO2, J. Anal. Appl. Pyrolysis. 107 (2014) 116–122. doi:10.1016/j.jaap.2014.02.011.

[88] A. Bazan-Wozniak, P. Nowicki, R. Pietrzak, The influence of activation procedure on the physicochemical and sorption properties of activated carbons prepared from pistachio nutshells for removal of NO2 /H2S gases and dyes, J. Clean. Prod. 152 (2017) 211–222. doi:10.1016/j.jclepro.2017.03.114.

[89] N.B. Klinghoffer, M.J. Castaldi, A. Nzihou, Influence of char composition and inorganics on catalytic activity of char from biomass gasification, Fuel. 157 (2015) 37–47. doi:10.1016/j.fuel.2015.04.036.

[90] C. Guizani, F.J. Escudero Sanz, S. Salvador, The nature of the deposited carbon at methane cracking over a nickel loaded wood-char, Comptes Rendus Chim. 19

(2016) 423–432. doi:10.1016/j.crci.2015.10.009.

[91] P.A. Tchoffor, K.O. Davidsson, H. Thunman, Effects of steam on the release of potassium, chlorine, and sulfur during char conversion, investigated under dual-fluidized-bed gasification conditions, Energy and Fuels. 28 (2014) 6953–6965. doi:10.1021/ef501591m.

[92] Y. Bai, S. Zhu, K. Luo, M. Gao, L. Yan, F. Li, Coal char gasification in H2O/CO2 : Release of alkali and alkaline earth metallic species and their effects on reactivity, Appl. Therm. Eng. 112 (2017) 156–163. doi:10.1016/j.applthermaleng.2016.10.044.

[93] Z. Hai-bo, S. Qiang, W.U. Xing-yuan, Y.A.O. Qiang, Transformation of alkali and alkaline earth metallic species during pyrolysis and CO2 gasification of rice straw char, J. Fuel Chem. Technol. 46 (2018) 27–33. doi:10.1016/S1872-5813(18)30002-1.

[94] L. Wang, A. Moilanen, J. Lehtinen, J. Konttinen, B.G. Matas, Release of Potassium during Devolatilization of Spruce Bark, Energy Procedia. 105 (2017) 1295–1301. doi:10.1016/j.egypro.2017.03.463.

[95] D. Feng, Y. Zhao, Y. Zhang, H. Xu, L. Zhang, S. Sun, Catalytic mechanism of ion-exchanging alkali and alkaline earth metallic species on biochar reactivity during CO2/H2O gasification, Fuel. 212 (2018) 523–532. doi:10.1016/j.fuel.2017.10.045.

[96] M. Gao, Z. Yang, Y. Wang, Y. Bai, F. Li, K. Xie, Impact of calcium on the synergistic effect for the reactivity of coal char gasification in H2O/CO2 mixtures, Fuel. 189 (2017) 312–321. doi:10.1016/j.fuel.2016.10.100.

[97] N.H. Florin, A.T. Harris, Enhanced hydrogen production from biomass with in situ carbon dioxide capture using calcium oxide sorbents, Chem. Eng. Sci. 63 (2008) 287–316. doi:10.1016/j.ces.2007.09.011.

[98] C. Shuai, S. Hu, L. He, J. Xiang, L. Sun, S. Su, L. Jiang, Q. Chen, C. Xu, The synergistic effect of Ca(OH)2 on the process of lignite steam gasification to produce hydrogen-rich gas, Int. J. Hydrogen Energy. 39 (2014) 15506–15516. doi:10.1016/j.ijhydene.2014.07.111.

[99] P.L. Spath, D.C. Dayton, Preliminary Screening -- Technical and Economic Assessment of Synthesis Gas to Fuels and Chemicals with Emphasis on the Potential for Biomass-Derived Syngas, 2003. doi:10.2172/15006100.

[100] D. Prando, S. Shivananda Ail, D. Chiaramonti, M. Baratieri, S. Dasappa, Characterisation of the producer gas from an open top gasifier: Assessment of different tar analysis approaches, Fuel. 181 (2016) 566–572. doi:10.1016/j.fuel.2016.04.104.

[101] P.J. Woolcock, R.C. Brown, A review of cleaning technologies for biomass-derived syngas, Biomass and Bioenergy. 52 (2013) 54–84. doi:10.1016/j.biombioe.2013.02.036.

[102] A.S. Al-Rahbi, P.T. Williams, Hydrogen-rich syngas production and tar removal from biomass gasification using sacrificial tyre pyrolysis char, Appl. Energy. 190 (2017) 501–509. doi:10.1016/j.apenergy.2016.12.099.

[103] S. Anis, Z. a. Zainal, Tar reduction in biomass producer gas via mechanical, catalytic and thermal methods: A review, Renew. Sustain. Energy Rev. 15 (2011) 2355–2377. doi:10.1016/j.rser.2011.02.018.

[104] N. Abdoulmoumine, S. Adhikari, A. Kulkarni, S. Chattanathan, A review on biomass gasification syngas cleanup, Appl. Energy. 155 (2015) 294–307. doi:10.1016/j.apenergy.2015.05.095.

[105] Z.A. El-rub, E.A. Bramer, G. Brem, Review of Catalysts for Tar Elimination in Biomass Gasification, Ind. Eng. Chem. Res. 43 (2004) 6911–6919.

[106] R. Coll, J. Salvadó, X. Farriol, D. Montané, Steam reforming model compounds of biomass gasification tars: conversion at different operating conditions and tendency towards coke formation, Fuel Process. Technol. 74 (2001) 19–31. doi:10.1016/S0378-3820(01)00214-4.

[107] M. Hervy, Valorisation de chars issus de pyrogazéification de biomasses pour la purification du syngas : lien entre propriétés physico-chimiques et efficacité du traitement., Ecole Nationale Supérieur des Mines d'Albi-Carmaux, 2016.

[108] J. Han, H. Kim, The reduction and control technology of tar during biomass gasification/pyrolysis: An overview, Renew. Sustain. Energy Rev. 12 (2008) 397–416. doi:10.1016/j.rser.2006.07.015.

[109] F.-J. Wang, S. Zhang, Z.-D. Chen, C. Liu, Y.-G. Wang, Tar reforming using char as catalyst during pyrolysis and gasification of Shengli brown coal, J. Anal. Appl. Pyrolysis. 105 (2014) 269–275. doi:10.1016/j.jaap.2013.11.013.

[110] Y. Shen, K. Yoshikawa, Recent progresses in catalytic tar elimination during biomass gasification or pyrolysis—A review, Renew. Sustain. Energy Rev. 21 (2013) 371–392. doi:10.1016/j.rser.2012.12.062.

[111] F. Nestler, L. Burhenne, M.J. Amtenbrink, T. Aicher, Catalytic decomposition of biomass tars: The impact of wood char surface characteristics on the catalytic performance for naphthalene removal, Fuel Process. Technol. 145 (2016) 31–41. doi:10.1016/j.fuproc.2016.01.020.

[112] J. Park, Y. Lee, C. Ryu, Reduction of primary tar vapor from biomass by hot char particles in fixed bed gasification, Biomass and Bioenergy. 90 (2016) 114–121.

doi:10.1016/j.biombioe.2016.04.001.

[113] E. Gusta, A.K. Dalai, M.A. Uddin, E. Sasaoka, Catalytic decomposition of biomass tars with dolomites, Energy and Fuels. 23 (2009) 2264–2272. doi:10.1021/ef8009958.

[114] R. Zhang, R.C. Brown, A. Suby, K. Cummer, Catalytic destruction of tar in biomass derived producer gas, Energy Convers. Manag. 45 (2004) 995–1014. doi:10.1016/j.enconman.2003.08.016.

[115] P.R. Buchireddy, R.M. Bricka, J. Rodriguez, W. Holmes, Biomass gasification: Catalytic removal of tars over zeolites and nickel supported zeolites, Energy and Fuels. 24 (2010) 2707–2715. doi:10.1021/ef901529d.

[116] Z. Abu El-Rub, E.A. Bramer, G. Brem, Experimental comparison of biomass chars with other catalysts for tar reduction, Fuel. 87 (2008) 2243–2252. doi:10.1016/j.fuel.2008.01.004.

[117] M. Hervy, S. Berhanu, E. Weiss-Hortala, A. Chesnaud, C. Gérente, A. Villot, D. Pham Minh, A. Thorel, L. Le Coq, A. Nzihou, Multi-scale characterisation of chars mineral species for tar cracking, Fuel. 189 (2017) 88–97. doi:10.1016/j.fuel.2016.10.089.

[118] L. Burhenne, T. Aicher, Benzene removal over a fixed bed of wood char: The effect of pyrolysis temperature and activation with CO2 on the char reactivity, Fuel Process. Technol. 127 (2014) 140–148. doi:10.1016/j.fuproc.2014.05.034.

[119] D. Wang, W. Yuan, W. Ji, Char and char-supported nickel catalysts for secondary syngas cleanup and conditioning, Appl. Energy. 88 (2011) 1656–1663. doi:10.1016/j.apenergy.2010.11.041.

[120] D. Feng, Y. Zhao, Y. Zhang, Z. Zhang, L. Zhang, J. Gao, S. Sun, Synergetic effects of biochar structure and AAEM species on reactivity of H2O-activated biochar from cyclone air gasification, Int. J. Hydrogen Energy. 42 (2017) 16045–16053. doi:10.1016/j.ijhydene.2017.05.153.

[121] G. Ravenni, Z. Sárossy, J. Ahrenfeldt, U.B. Henriksen, Activity of chars and activated carbons for removal and decomposition of tar model compounds – A review, Renew. Sustain. Energy Rev. 94 (2018) 1044–1056. doi:10.1016/j.rser.2018.07.001.

[122] S. Hosokai, K. Kumabe, M. Ohshita, K. Norinaga, C.Z. Li, J. ichiro Hayashi, Mechanism of decomposition of aromatics over charcoal and necessary condition for maintaining its activity, Fuel. 87 (2008) 2914–2922. doi:10.1016/j.fuel.2008.04.019.

[123] Y. Huang, X. Yin, C. Wu, C. Wang, J. Xie, Z. Zhou, L. Ma, H. Li, Effects of metal catalysts on CO2gasification reactivity of biomass char, Biotechnol. Adv. 27 (2009) 568–572. doi:10.1016/j.biotechadv.2009.04.013.

[124] C. Dupont, S. Jacob, K.O. Marrakchy, C. Hognon, M. Grateau, F. Labalette, D. Da Silva Perez, How inorganic elements of biomass influence char steam gasification kinetics, Energy. 109 (2016) 430–435. doi:10.1016/j.energy.2016.04.094.

[125] G. Guan, M. Kaewpanha, X. Hao, Z. Wang, Y. Cheng, Y. Kasai, A. Abudula, Promoting effect of potassium addition to calcined scallop shell supported catalysts for the decomposition of tar derived from different biomass resources, Fuel. 109 (2013) 241–247. doi:10.1016/j.fuel.2012.11.074.

[126] P. Knutsson, V. Cantatore, M. Seemann, P.L. Tam, I. Panas, Role of potassium in the enhancement of the catalytic activity of calcium oxide towards tar reduction, Appl. Catal. B Environ. 229 (2018) 88–95. doi:10.1016/j.apcatb.2018.02.002.

[127] Y.R. Xie, L.H. Shen, J. Xiao, D.X. Xie, J. Zhu, Influences of additives on steam gasification of biomass. 1. pyrolysis procedure, Energy and Fuels. 23 (2009) 5199–5205. doi:10.1021/ef900459j.

[128] E. Ryckebosch, M. Drouillon, H. Vervaeren, Techniques for transformation of biogas to biomethane, Biomass and Bioenergy. 35 (2011) 1633–1645. doi:10.1016/j.biombioe.2011.02.033.

[129] I. Ullah Khan, M. Hafiz Dzarfan Othman, H. Hashim, T. Matsuura, A.F. Ismail, M. Rezaei-DashtArzhandi, I. Wan Azelee, Biogas as a renewable energy fuel – A review of biogas upgrading, utilisation and storage, Energy Convers. Manag. 150 (2017) 277–294. doi:10.1016/j.enconman.2017.08.035.

[130] O. Hijazi, S. Munro, B. Zerhusen, M. Effenberger, Review of life cycle assessment for biogas production in Europe, Renew. Sustain. Energy Rev. 54 (2016) 1291–1300. doi:10.1016/j.rser.2015.10.013.

[131] Q. Sun, H. Li, J. Yan, L. Liu, Z. Yu, X. Yu, Selection of appropriate biogas upgrading technology-a review of biogas cleaning, upgrading and utilisation, Renew. Sustain. Energy Rev. 51 (2015) 521–532. doi:10.1016/j.rser.2015.06.029.

[132] R. Kadam, N.L. Panwar, Recent advancement in biogas enrichment and its applications, Renew. Sustain. Energy Rev. 73 (2017) 892–903. doi:10.1016/j.rser.2017.01.167.

[133] J.B. Holm-Nielsen, T. Al Seadi, P. Oleskowicz-Popiel, The future of anaerobic digestion and biogas utilization, Bioresour. Technol. 100 (2009) 5478–5484. doi:10.1016/j.biortech.2008.12.046.

[134] N. Abatzoglou, S. Boivin, A review of biogas purification processes, Biofuels, Bioprod. Biorefining. 6 (2009) 246–256. doi:10.1002/bbb.

[135] S. Rasi, A. Veijanen, J. Rintala, Trace compounds of biogas from different biogas production plants, Energy. 32 (2007) 1375–1380.

doi:10.1016/j.energy.2006.10.018.

[136] A. Petersson, Biogas cleaning, Woodhead Publishing Limited, 2013. doi:10.1533/9780857097415.3.329.

[137] O.W. Awe, D.P. Minh, N. Lyczko, A. Nzihou, Y. Zhao, Laboratory-scale investigation of the removal of hydrogen sulfide from biogas and air using industrial waste-based sorbents, J. Environ. Chem. Eng. 5 (2017) 1809–1820. doi:10.1016/j.jece.2017.03.023.

[138] J.N. Kuhn, A.C. Elwell, N.H. Elsayed, B. Joseph, Requirements, techniques, and costs for contaminant removal from landfill gas, Waste Manag. 63 (2017) 246–256. doi:10.1016/j.wasman.2017.02.001.

[139] S. Rasi, J. Läntelä, J. Rintala, Trace compounds affecting biogas energy utilisation - A review, Energy Convers. Manag. 52 (2011) 3369–3375. doi:10.1016/j.enconman.2011.07.005.

[140] M. Ozekmekci, G. Salkic, M.F. Fellah, Use of zeolites for the removal of H2S: A mini-review, Fuel Process. Technol. 139 (2015) 49–60. doi:10.1016/j.fuproc.2015.08.015.

[141] S.A. Hosseinipour, M. Mehrpooya, Comparison of the biogas upgrading methods as a transportation fuel, Renew. Energy. 130 (2019) 641–655. doi:10.1016/j.renene.2018.06.089.

[142] Q. Zhao, E. Leonhardt, C. MacConnell, C. Frear, S. Chen, Purification Technologies for Biogas Generated by Anaerobic Digestion, Clim. Friendly Farming Improv. Carbon Footpr. Agric. Pacific Northwest. CSANR Res. Rep. 2010-00. (2010) 24.

[143] S.A. Hosseinipour, M. Mehrpooya, Comparison of the biogas upgrading methods as a transportation fuel, Renew. Energy. 130 (2019) 641–655. doi:10.1016/j.renene.2018.06.089.

[144] M. Ben Jaber, A. Couvert, A. Amrane, P. Le Cloirec, E. Dumont, Removal of hydrogen sulfide in air using cellular concrete waste: Biotic and abiotic filtrations, Chem. Eng. J. 319 (2017) 268–278. doi:10.1016/j.cej.2017.03.014.

[145] G. Monteleone, M. De Francesco, S. Galli, M. Marchetti, V. Naticchioni, Deep H2S removal from biogas for molten carbonate fuel cell (MCFC) systems, Chem. Eng. J. 173 (2011) 407–414. doi:10.1016/j.cej.2011.07.078.

[146] W. Feng, S. Kwon, E. Borguet, R. Vidic, Adsorption of Hydrogen Sulfide onto Activated Carbon Fibers: Effect of Pore Structure and Surface Chemistry, Environ. Sci. Technol. 39 (2005) 9744–9749. doi:10.1021/es0507158.

[147] T.J. Bandosz, On the adsorption/oxidation of hydrogen sulfide on activated carbons at ambient temperatures, J. Colloid Interface Sci. 246 (2002) 1–20.

doi:10.1006/jcis.2001.7952.

[148] M. Hervy, D. Pham Minh, C. Gérente, E. Weiss-Hortala, A. Nzihou, A. Villot, L. Le Coq, H2S removal from syngas using wastes pyrolysis chars, Chem. Eng. J. 334 (2018) 2179–2189. doi:10.1016/j.cej.2017.11.162.

[149] I.W. Siriwardane, R. Udangawa, R.M. de Silva, A.R. Kumarasinghe, R.G. Acres, A. Hettiarachchi, G.A.J. Amaratunga, K.M.N. de Silva, Synthesis and characterization of nano magnesium oxide impregnated granular activated carbon composite for H2S removal applications, Mater. Des. 136 (2017) 127–136. doi:10.1016/j.matdes.2017.09.034.

[150] L.M. Le Leuch, A. Subrenat, P. Le Cloirec, Hydrogen sulfide adsorption and oxidation onto activated carbon cloths: Applications to odorous gaseous emission treatments, Langmuir. 19 (2003) 10869–10877. doi:10.1021/la035163q.

[151] R. Sitthikhankaew, D. Chadwick, S. Assabumrungrat, N. Laosiripojana, Effects of humidity, O2, and CO2on H2S adsorption onto upgraded and KOH impregnated activated carbons, Fuel Process. Technol. 124 (2014) 249–257. doi:10.1016/j.fuproc.2014.03.010.

[152] D. V. Brazhnyk, Y.P. Zaitsev, I. V. Bacherikova, V.A. Zazhigalov, J. Stoch, A. Kowal, Oxidation of H2S on activated carbon KAU and influence of the surface state, Appl. Catal. B Environ. 70 (2007) 557–566. doi:10.1016/j.apcatb.2005.12.028.

[153] A. Bouzaza, A. Laplanche, S. Marsteau, Adsorption-oxidation of hydrogen sulfide on activated carbon fibers: Effect of the composition and the relative humidity of the gas phase, Chemosphere. 54 (2004) 481–488. doi:10.1016/j.chemosphere.2003.08.018.

[154] A. Bagreev, T.J. Bandosz, On the Mechanism of Hydrogen Sulfide Removal from Moist Air on Catalytic Carbonaceous Adsorbents, Ind. Eng. Chem. Res. 44 (2005) 530–538. doi:10.1021/ie049277o.

[155] M. Sekirifa, M. Hadj-Mahammed, S. Pallier, L. Baameur, D. Richard, A. Al-Dujaili, Preparation and characterization of activated carbon from date stones by physical activation with steam, J. Anal. Appl. Pyrolysis. 99 (2013) 155–160. doi:http://dx.doi.org/10.1016/j.jaap.2007.12.009.

[156] Y. Zhu, J. Gao, Y. Li, F. Sun, J. Gao, S. Wu, Y. Qin, Preparation of activated carbons for SO2 adsorption by CO2 and steam activation, J. Taiwan Inst. Chem. Eng. 43 (2011) 112–119. doi:10.1016/j.jtice.2011.06.009.

[157] M. Wu, Q. Guo, G. Fu, Preparation and characteristics of medicinal activated carbon powders by CO2 activation of peanut shells, Powder Technol. 247 (2013) 188–196. doi:10.1016/j.powtec.2013.07.013.

[158] F. Ahmad, W.M.A.W. Daud, M.A. Ahmad, R. Radzi, A.A. Azri, The effects of CO2 activation, on porosity and surface functional groups of cocoa (Theobroma cacao) – Shell based activated carbon, Environ. Chem. Eng. (2013) 378–388. doi:10.1016/j.cherd.2013.01.003.

[159] T. Yang, A.C. Lua, Characteristics of activated carbons prepared from pistachio-nut shells by physical activation, J. Colloid Interface Sci. 267 (2003) 408–417. doi:10.1016/S0021-9797(03)00689-1.

[160] J. Torres-Pérez, C. Gérente, Y. Andrès, Sustainable activated carbons from agricultural residues dedicated to antibiotic removal by adsorption, Chinese J. Chem. Eng. 20 (2012) 524–529. doi:10.1016/S1004-9541(11)60214-0.

[161] J. Torres-Perez, C. Gerente, Y. Andres, Conversion of agricultural residues into activated carbons for water purification: Application to arsenate removal, J. Environ. Sci. Heal. - Part A Toxic/Hazardous Subst. Environ. Eng. 47 (2012) 1173–1185. doi:10.1080/10934529.2012.668390.

[162] P. Lodeiro, S.M. Kwan, J.T. Perez, L.F. González, C. Gérente, Y. Andrès, G. McKay, Novel Fe loaded activated carbons with tailored properties for As(V) removal: Adsorption study correlated with carbon surface chemistry, Chem. Eng. J. 215–216 (2013) 105–112. doi:10.1016/j.cej.2012.11.052.

[163] M.M. Diémé, M. Hervy, S.N. Diop, C. Gérente, A. Villot, Y. Andres, C.K. Diawara, Sustainable Conversion of Agriculture and Food Waste into Activated Carbons Devoted to Fluoride Removal from Drinking Water in Senegal, Int. J. Chem. 8 (2015) 8. doi:10.5539/ijc.v8n1p8.

[164] M.M. Dieme, A. Villot, C. Gerente, Y. Andres, S.N. Diop, C.K. Diawara, Sustainable conversion of agriculture wastes into activated carbons: energy balance and arsenic removal from water, Environ. Technol. 3330 (2016) 1–8. doi:10.1080/09593330.2016.1193225.

[165] P.J.M. Suhas Carrott, M.M.L. Ribeiro Carrott, Lignin - from natural adsorbent to activated carbon: A review, Bioresour. Technol. 98 (2007) 2301–2312. doi:10.1016/j.biortech.2006.08.008.

[166] E. Yagmur, M.S. Tunc, A. Banford, Z. Aktas, Preparation of activated carbon from autohydrolysed mixed southern hardwood, J. Anal. Appl. Pyrolysis. 104 (2013) 470–478. doi:10.1016/j.jaap.2013.05.025.

[167] C. Analyses, Standard Test Methods for Proximate Analysis of Coal and Coke by Macro, Program. i (2012) 1–9. doi:10.1520/D7582.

[168] J. Despujols, Spectrométrie d ’ émission des rayons X . Fluorescence X, in: Tech. l’ingénieur, 2000: p. 18.

[169] P.C.C. Faria, J.J.M. Orfão, M.F.R. Pereira, Adsorption of anionic and cationic dyes on activated carbons with different surface chemistries., Water Res. 38 (2004) 2043–52. doi:10.1016/j.watres.2004.01.034.

[170] S. Sokhansanj, The Effect of Moisture on Heating Values, Biomass Energy Data B. (2011) 1–5. http://cta.ornl.gov/bedb.

[171] K.S.W. Sing, D.H. Everett, R. a. W. Haul, L. Moscou, R. a. Pierotti, J. Rouquérol, T. Siemieniewska, INTERNATIONAL UNION OF PURE COMMISSION ON COLLOID AND SURFACE CHEMISTRY INCLUDING CATALYSIS * REPORTING PHYSISORPTION DATA FOR GAS / SOLID SYSTEMS with Special Reference to the Determination of Surface Area and Porosity, Pure Appl. Chem. 54 (1985) 2201–2218. doi:10.1351/pac198557040603.

[172] Y. Zhang, W. Wu, S. Zhao, Y. Long, Y. Luo, Experimental study on pyrolysis tar removal over rice straw char and inner pore structure evolution of char, Fuel Process. Technol. 134 (2015) 333–344. doi:10.1016/j.fuproc.2015.01.047.

[173] R. Moliner, I. Suelves, M.J. Lázaro, O. Moreno, Thermocatalytic decomposition of methane over activated carbons: Influence of textural properties and surface chemistry, Int. J. Hydrogen Energy. 30 (2005) 293–300. doi:10.1016/j.ijhydene.2004.03.035.

[174] P. Gislon, S. Galli, G. Monteleone, Siloxanes removal from biogas by high surface area adsorbents, Waste Manag. 33 (2013) 2687–2693. doi:10.1016/j.wasman.2013.08.023.

[175] K.S.W. Sing, D.H. Everett, R. a. W. Haul, L. Moscou, R. a. Pierotti, J. Rouquérol, T. Siemieniewska, International union of pure commission on colloid and surface chemistry including catalysis* Reporting physisorption data for gas / solid systems with special reference to the determination of surface area and porosity, Pure Appl. Chem. 54 (1982) 2201–2218. doi:10.1351/pac198557040603.

[176] S. Sharifan, A comparative optimisation study of activated carbon production from hazelnut shells by thermal and microwave heating methods, Impezrial College London, 2013.

[177] G. Leofanti, M. Padovan, G. Tozzola, B. Venturelli, Surface area and pore texture of catalysts, Catal. Today. 41 (1998) 207–219. doi:10.1016/S0920-5861(98)00050-9.

[178] H.M. Rootare, A Review of Mercury Porosimetry, Adv. Exp. Tech. Powder Metall. (1970) 225–252. doi:10.1007/978-1-4615-8981-5_9.

[179] H. Giesche, Mercury porosimetry: A general (practical) overview, Part. Part. Syst. Charact. 23 (2006) 9–19. doi:10.1002/ppsc.200601009.

[180] Z. Li, D. Liu, Y. Cai, Y. Yao, H. Wang, Pore Structure and Compressibility of Coal

Matrix with Elevated Temperatures by Mercury Intrusion Porosimetry, Energy Explor. Exploit. 33 (2015) 809–826. doi:10.1260/0144-5987.33.6.809.

[181] E.W. Washburn, The dynamics of capillary flow, Phys. Rev. 17 (1921) 273–283. doi:10.1103/PhysRev.17.273.

[182] M. Shahbaz, S. yusup, A. Inayat, D.O. Patrick, M. Ammar, The influence of catalysts in biomass steam gasification and catalytic potential of coal bottom ash in biomass steam gasification: A review, Renew. Sustain. Energy Rev. 73 (2017) 468–476. doi:10.1016/j.rser.2017.01.153.

[183] C. Wu, V.L. Budarin, M. Wang, V. Sharifi, M.J. Gronnow, Y. Wu, J. Swithenbank, J.H. Clark, P.T. Williams, CO2 gasification of bio-char derived from conventional and microwave pyrolysis, Appl. Energy. 157 (2015) 533–539. doi:10.1016/j.apenergy.2015.04.075.

[184] I. Ahmed, A.K. Gupta, Syngas yield during pyrolysis and steam gasification of paper, Appl. Energy. 86 (2009) 1813–1821. doi:10.1016/j.apenergy.2009.01.025.

[185] N. Đurišić-Mladenović, B.D. Škrbić, A. Zabaniotou, Chemometric interpretation of different biomass gasification processes based on the syngas quality: Assessment of crude glycerol co-gasification with lignocellulosic biomass, Renew. Sustain. Energy Rev. 59 (2016) 649–661. doi:10.1016/j.rser.2016.01.002.

[186] E.I. Ohimain, S.C. Izah, A review of biogas production from palm oil mill effluents using different configurations of bioreactors, Renew. Sustain. Energy Rev. 70 (2017) 242–253. doi:10.1016/j.rser.2016.11.221.

[187] P. Le Cloirec, Adsorption en traitement de l ' air, Tech. l'ingénieur. 33 (2003) 1–13.

[188] Y. Cao, A. Pawłowski, Sewage sludge-to-energy approaches based on anaerobic digestion and pyrolysis: Brief overview and energy efficiency assessment, Renew. Sustain. Energy Rev. 16 (2012) 1657–1665. doi:10.1016/j.rser.2011.12.014.

[189] J.L. Gaunt, J. Lehmann, Energy balance and emissions associated with biochar sequestration and pyrolysis bioenergy production, Environ. Sci. Technol. 42 (2008) 4152–4158. doi:10.1021/es071361i.

[190] C. Dupont, S. Jacob, K.O. Marrakchy, C. Hognon, M. Grateau, F. Labalette, D. Da Silva Perez, How inorganic elements of biomass influence char steam gasification kinetics, Energy. 109 (2016) 430–435. doi:10.1016/j.energy.2016.04.094.

[191] A.N. M. Hervy, C. Gerente, A. Villot, L. Le-Coq, E. Weiss-Hortala, D. Pham Minh, Recycling of pyrolysis chars from food waste, wastewater treatment sludge and wood for the syngas purification, in: R.D.T. and A.S. J.W.C. Wong, M. Nelles (Ed.), Int. Conf. Solid Waste – Knowl. Transf. Sustain. Resour. Manag., 2015.

[192] M.M. Hossain, L. Atanda, N. Al-Yassir, S. Al-Khattaf, Kinetics modeling of

ethylbenzene dehydrogenation to styrene over a mesoporous alumina supported iron catalyst, Chem. Eng. J. 207–208 (2012) 308–321. doi:10.1016/j.cej.2012.06.108.

[193] C. (Charles) Xu, S. Hamilton, M. Ghosh, Hydro-treatment of Athabasca vacuum tower bottoms in supercritical toluene with microporous activated carbons and metal–carbon composite, Fuel. 88 (2009) 2097–2105. doi:10.1016/j.fuel.2009.05.020.

[194] L. Lundberg, P.A. Tchoffor, D. Pallarès, R. Johansson, H. Thunman, K. Davidsson, Influence of surrounding conditions and fuel size on the gasification rate of biomass char in a fluidized bed, Fuel Process. Technol. 144 (2016) 323–333. doi:10.1016/j.fuproc.2016.01.002.

[195] J. Udomsirichakorn, P. Basu, P.A. Salam, B. Acharya, Effect of CaO on tar reforming to hydrogen-enriched gas with in-process CO2 capture in a bubbling fluidized bed biomass steam gasifier, Int. J. Hydrogen Energy. 38 (2013) 14495–14504. doi:10.1016/j.ijhydene.2013.09.055.

[196] T. Osaki, T. Mori, Role of potassium in carbon-free CO2 reforming of methane on K-promoted Ni/Al2O3 catalysts, J. Catal. 204 (2001) 89–97. doi:10.1006/jcat.2001.3382.

[197] H.C. Shin, J.W. Park, K. Park, H.C. Song, Removal characteristics of trace compounds of landfill gas by activated carbon adsorption, Environ. Pollut. 119 (2002) 227–236. doi:10.1016/S0269-7491(01)00331-1.

[198] L. Barelli, G. Bidini, N. de Arespacochaga, L. Pérez, E. Sisani, Biogas use in high temperature fuel cells: Enhancement of KOH-KI activated carbon performance toward H2S removal, Int. J. Hydrogen Energy. 42 (2017) 10341–10353. doi:10.1016/j.ijhydene.2017.02.021.

[199] N. Mohamad Nor, L.C. Lau, K.T. Lee, A.R. Mohamed, Synthesis of activated carbon from lignocellulosic biomass and its applications in air pollution control—a review, J. Environ. Chem. Eng. 1 (2013) 658–666. doi:10.1016/j.jece.2013.09.017.

[200] T.J. Bandosz, Effect of pore structure and surface chemistry of virgin activated carbons on removal of hydrogen sulfide, Carbon N. Y. 37 (1999) 483–491. doi:10.1016/S0008-6223(98)00217-6.

[201] J. Guo, Y. Luo, A.C. Lua, R. an Chi, Y. lin Chen, X. ting Bao, S. xin Xiang, Adsorption of hydrogen sulphide (H2S) by activated carbons derived from oil-palm shell, Carbon N. Y. 45 (2007) 330–336. doi:10.1016/j.carbon.2006.09.016.

[202] R. Sitthikhankaew, S. Predapitakkun, R. Kiattikomol, S. Pumhiran, S. Assabumrungrat, N. Laosiripojana, Performance of commercial and modified

activated carbons for hydrogen sulfide removal from simulated biogas, 2011 IEEE 1st Conf. Clean Energy Technol. CET 2011. (2011) 135–139. doi:10.1109/CET.2011.6041474.

[203] G. Lei, C. Liu, H. Xie, F. Song, Separation of the hydrogen sulfide and methane mixture by the porous graphene membrane: Effect of the charges, Chem. Phys. Lett. 599 (2014) 127–132. doi:10.1016/j.cplett.2014.03.040.

[204] A. Bagreev, H. Rahman, T.J. Bandosz, Thermal regeneration of a spent activated carbon previously used as hydrogen sulfide adsorbent, Carbon N. Y. 39 (2001) 1319–1326. doi:10.1016/S0008-6223(00)00266-9.

[205] S.P. Raut, R. V. Ralegaonkar, S.A. Mandavgane, Development of sustainable construction material using industrial and agricultural solid waste: A review of waste-create bricks, Constr. Build. Mater. 25 (2011) 4037–4042. doi:10.1016/j.conbuildmat.2011.04.038.

[206] L. Zhang, Production of bricks from waste materials - A review, Constr. Build. Mater. 47 (2013) 643–655. doi:10.1016/j.conbuildmat.2013.05.043.

[207] N.M. Agyei, C.A. Strydom, J.H. Potgieter, The removal of phosphate ions from aqueous solution by fly ash, slag, ordinary Portland cement and related blends, Cem. Concr. Res. 33 (2003) 937. doi:10.1016/S0008-8846(02)01072-4.

[208] S. Ahmari, L. Zhang, Durability and leaching behavior of mine tailings-based geopolymer bricks, Constr. Build. Mater. 44 (2013) 743–750. doi:10.1016/j.conbuildmat.2013.03.075.

[209] P. Sciences, The Disposal of Activated Carbon from Chemical Agent Disposal Facilities, National Academy of Sciences, United States, 2009. doi:10.17226/12646.

List of Annexes

Annexe 1. Summary tables

Table 1. Summary of chemical characterization of biomasses and derived materials.

Analysis	Composition	BH	MH	BH-Char	MH-Char	BH-CO_2 2-step	BH-CO_2 1-step	MH-CO_2 2-step	MH-CO_2 1-step	BH-H_2O	MH-H_2O
Ultimate analysis (wt.%)	C	47.5 ± 0.6	42.3 ± 0.3	78.4 ± 1.0	56.9 ± 0.3	83.3 ± 0.3	76.8 ± 0.3	53.7 ± 0.7	44.1 ± 0.7	72.3 ± 1.9	51.1 ± 0.2
	H	5.8 ± 0.3	5.6 ± 0.1	3.1 ± 0.1	2.5 ± 0.1	1.14 ± 0.04	0.5 ± 0.1	0.7 ± 0.2	0.6 ± 0.04	0.9 ± 0.2	0.4 ± 0.1
	N	2.3 ± 0.8	0.7 ± 0.1	1.3 ± 0.2	1.1 ± 0.1	1.50 ± 0.01	1.4 ± 0.4	0.81 ± 0.02	0.7 ± 0.03	1.7 ± 0.2	0.5 ± 0.03
	S	n.d	n.d	n.d	n.d	n.d	n.d	n.d	n.d	n.d	n.d
	O	44.1 ± 1.1	39.3 ± 0.2	15.5 ± 0.8	12.5 ± 0.6	8.4 ± 0.5	8.9 ± 0.3	6.0 ± 0.3	4.6	11.8 ± 0.6	2.7 ± 0.2
Thermogravimetric analysis (wt.%)	Cellulose	20.4 ± 0.1	25.8 ± 0.4	*	*	*	*	*	*	*	*
	Hemicellulose	18.5 ± 0.3	20.3 ± 1.3	*	*	*	*	*	*	*	*
	Lignin	27.0 ± 2.6	15.7 ± 0.5	*	*	*	*	*	*	*	*
Proximate analysis (wt.%)	Moisture	12.5 ± 0.1	9.4 ± 0.3	5.4 ± 0.1	3.2 ± 0.9	0.9 ± 0.1	6.5	1.2 ± 0.1	3.4	6.3 ± 0.5	3.4
	Volatile matter	66.9 ± 0.6	65.1 ± 0.4	28.7 ± 0.6	6.2 ± 0.6	29.1 ± 0.2	19.1	15.0	10.2	52.1 ± 0.8	10.2
	Fixed carbon	18.1 ± 0.7	13.3 ± 0.3	60.2 ± 0.6	61.1 ± 1.1	62.2 ± 0.3	62.7	48.3	31.4	30.3 ± 1.1	41.4
	Ash	2.6 ± 0.0	12.2 ± 0.1	5.7 ± 0.1	29.6 ± 0.2	7.9 ± 0.1	10.4 ± 0.1	35.5 ± 0.7	49.5 ± 0.3	11.2 ± 0.2	44.9 ± 3.3
Main mineral composition (wt.%)	K	Trace	1.4 ± 0.1	2.4 ± 0.1	4.8 ± 0.6	3.1 ± 0.1	4.6 ± 0.1	5.8 ± 0.3	8.7 ± 0.1	3.9 ± 0.2	9.4 ± 0.4
	Ca	Trace	Trace	1.5 ± 0.1	0.2 ± 0.1	2.4 ± 0.1	3.0 ± 0.1	0.2 ± 0.1	0.3 ± 0.1	3.4 ± 0.1	0.3 ± 0.1
	P	Trace	Trace	0.7 ± 0.1	0.9 ± 0.2	0.8 ± 0.1	0.7 ± 0.1	1.8 ± 0.3	2.6 ± 0.1	0.8 ± 0.1	2.1 ± 0.1
	Si	n.d	9.5 ± 0.1	n.d	21.6 ± 0.9	n.d	n.d	26.9 ± 0.5	37.6 ± 0.1	n.d	32.6 ± 0.6
	Mg	n.d	n.d	0.8 ± 0.1	n.d	1.4 ± 0.1	2.3 ± 0.1	n.d	n.d	2.6 ± 0.1	n.d
Bomb calorimeter (MJ/kg)	HHV	18.3 ± 0.2	17.7 ± 0.02	28.1 ± 0.6	22.7 ± 0.2	28.7 ± 0.2	29.0 ± 0.1	18.8 ± 0.5	17.7 ± 0.1	27.7 ± 0.9	17.5 ± 0.01
Point of zero charge	pH_{pzc}	*	*	5.7	5.3	11.9	12.0	9.7	-	12.0	9.8

- Data not available
** Analysis not adapted for this material*
n.d: non-detected

Table 2. Summary of textural characterization of raw and activated chars.

Analysis	Parameter	BH-Char	MH-Char	BH-CO_2 2-step	BH-CO_2 1-step	MH-CO_2 2-step	MH-CO_2 1-step	BH-H_2O	MH-H_2O
N_2 Adsorption/Desorption	V_{Total} (cm^3/g)	*	*	0.291 ± 0.011	0.339 ± 0.004	0.180 ± 0.003	0.187 ± 0.001	0.681 ± 0.136	0.278 ± 0.010
	V_{Micro} (cm^3/g)	*	*	0.261 ± 0.004	0.305 ± 0.005	0.147 ± 0.002	0.150 ± 0.001	0.419 ± 0.011	0.206 ± 0.011
	V_{Meso} (cm^3/g)	*	*	0.012 ± 0.010	0.055 ± 0.002	0.013 ± 0.001	0.056 ± 0.002	0.175 ± 0.083	0.043 ± 0.001
	BET Surface (m^2/g)	*	*	578 ± 4	612 ± 16	329 ± 6	312 ± 1	997 ± 81	466 ± 26
Mercury porosimetry	V_{Total} (cm^3/g)	0.540 ± 0.084	0.786 ± 0.062	0.555 ± 0.092	-	0.807 ± 0.054	-	0.938 ± 0.069	1.027 ± 0.064
	V_{Meso} (cm^3/g)	0.111 ± 0.012	0.022 ± 0.001	0.070 ± 0.004	-	0.029 ± 0.001	-	0.226 ± 0.006	0.031 ± 0.001
	V_{macro} (cm^3/g)	0.421 ± 0.072	0.755 ± 0.062	0.480 ± 0.088	-	0.770 ± 0.053	-	0.688 ± 0.084	0.988 ± 0.064

- Data not available

** Analysis not adapted for this material*

Table 3. Summary of mass and energy balances of thermo-conversion processes of BH.

		BH-Char			BH-CO_2 (2-step)			BH-CO_2 (1-step)			BH-H_2O		
		Mass fraction (wt.%)	**LHV (MJ/Kg)**	**Energy ($MJ/Kg_{Biomass}$)**	**Mass fraction (wt.%)**	**LHV (MJ/Kg)**	**Energy ($MJ/Kg_{Biomass}$)**	**Mass fraction (wt.%)**	**LHV (MJ/Kg)**	**Energy ($MJ/Kg_{Biomass}$)**	**Mass fraction (wt.%)**	**LHV (MJ/Kg)**	**Energy ($MJ/Kg_{Biomass}$)**
Inlet	Biomass	100	16.8 ± 0.2		100	16.8 ± 0.2		100	16.8 ± 0.2		100	16.8 ± 0.2	
	Electrical consumption	-	-	8.7	-	-	38.0	-	-	30.2	-	-	30.3
Outlet	Char/AC	38.3 ± 0.3	27.5 ± 0.6	10.5 ± 0.1	9.9 ± 0.4	28.3 ± 0.2	2.8 ± 0.1	5.7 ± 0.1	29.2 ± 0.6	1.7 ± 0.1	10.0 ± 0.4	27.5 ± 0.9	2.8 ± 0.1
	Aqueous phase	13.5	0	0	5.2	0	0	1.9	0	0	23.9	0	0
	Oily phase	1.8	23.06 ± 0.25	0.4	0.7	23.06 ± 0.25	0.2	0.8	20.76 ± 0.12	0.2	16.8	5.70 ± 0.01	1.0
	Gas	25.2 ± 0.3	6.1 ± 0.1	1.5 ± 0.1	67.8 ± 3.2	2.9 ± 0.3	2.0 ± 0.2	91.6 ± 1.8	2.2 ± 0.1	2.0 ± 0.1	34.5 ± 5.3	15.0 ± 0.4	5.2 ± 0.7
Performance indicators:	**Target products for energy recovery:**	**Oil and gas**	**Char, oil and gas**		**Oil and gas**	**AC, oil and gas**		**Oil and gas**	**Char, oil and gas**		**Oil and gas**	**AC, oil and gas**	
	AEE*	**11.6 ± 0.2 %**	**74.3 ± 0.5 %**		**12.8 ± 0.5 %**	**29.5 ± 0.8 %**		**13.1 ± 0.2 %**	**23.0 ± 0.2 %**		**36.6 ± 4.2 %**	**53.0 ± 4.0 %**	
	AEE elec**	**7.7 ± 0.1 %**	**49.0 ± 0.3 %**		**3.9 ± 0.2 %**	**9.0 ± 0.4 %**		**4.7 ± 0.1 %**	**8.2 ± 0.2 %**		**13.0 ± 1.5 %**	**18.9 ± 1.4 %**	
	NER	**-**	**1.434 ± 0.010**		**-**	**0.130 ± 0.013**		**-**	**0.128 ± 0.001**		**-**	**0.294 ± 0.022**	

**AEE: apparent energy efficiency defined as the ratio of the energy content in the target products to the energy content of the raw biomass; **AEEelec: takes into account the electrical consumption in the denominator; ***NER: Net energy produced in the process.*

Table 4. Summary of mass and energy balances of thermo-conversion processes of MH.

		MH-Char			MH-CO_2 (2-step)			MH-CO_2 (1-step)			MH-H_2O		
		Mass fraction (wt.%)	**LHV (MJ/Kg)**	**Energy ($MJ/Kg_{Biomass}$)**	**Mass fraction (wt.%)**	**LHV (MJ/Kg)**	**Energy ($MJ/Kg_{Biomass}$)**	**Mass fraction (wt.%)**	**LHV (MJ/Kg)**	**Energy ($MJ/Kg_{Biomass}$)**	**Mass fraction (wt.%)**	**LHV (MJ/Kg)**	**Energy ($MJ/Kg_{Biomass}$)**
Inlet	Biomass	100	17.1 ± 0.8		100	17.1 ± 0.8		100	17.1 ± 0.8		100	17.1 ± 0.8	
	Electrical consumption	-	-	8.7	-	-	37.9	-	-	29.7	-	-	29.4
Outlet	Char/AC	38.0 ± 0.1	22.2 ± 0.2	8.45 ± 0.02	11.7 ± 0.4	18.7 ± 0.5	2.2 ± 0.1	7.0 ± 0.3	13.3	0.86 ± 0.03	15.3 ± 0.1	17.39 ± 0.01	2.7 ± 0.01
	Aqueous phase	15.2	0	0	5.9	0	0.0	1.7	0	0	22.5	0	0
	Oily phase	5.9	10.02 ± 2.27	0.59	2.3	10.02 ± 2.27	0.2	0.7	24.00 ± 1.42	0.2	3.0	23.7 ± 5.2	0.7
	Gas	19.9 ± 0.6	8.0 ± 0.1	1.6 ± 0.1	56.8 ± 5.3	2.6 ± 0.6	1.5 ± 0.2	78.2 ± 1.2	1.82 ± 0.03	1.42 ± 0.01	37.0 ± 0.6	14.3 ± 0.1	5.3 ± 0.1
Performance indicators:	**Target products for energy recovery:**	**Oil and gas**	**Char, oil and gas**		**Oil and gas**	**Char, oil and gas**		**Oil and gas**	**Char, oil and gas**		**Oil and gas**	**AC, oil and gas**	
	AEE**	**12.8 ± 0.4 %**	**62.1 ± 0.4 %**		**9.8 ± 1.0 %**	**22.6 ± 1.2 %**		**9.35 ± 0.01 %**	**14.4 ± 0.2 %**		**34.9 ± 0.3 %**	**50.4 ± 0.3 %**	
	AEE elec	**8.5 ± 0.2 %**	**41.1 ± 0.2 %**		**3.1 ± 0.5 %**	**7.0 ± 0.6 %**		**3.42 ± 0.02 %**	**5.3 ± 0.1 %**		**12.9 ± 0.1 %**	**18.6 ± 0.1 %**	
	NER	**-**	**1.218 ± 0.005**		**-**	**0.102 ± 0.009**		**-**	**0.083 ± 0.002**		**-**	**0.294 ± 0.002**	

**AEE: apparent energy efficiency defined as the ratio of the energy content in the target products to the energy content of the raw biomass; **AEEelec: takes into account the electrical consumption in the denominator; ***NER: Net energy produced in the proces*

Annexe 2. Calculation of energy consumption in pyrolysis and activation (quartz reactor)

The calculations of electrical consumption of pyrolysis and activations were carried out with a thermodynamic approach, considering the energy demand and energy loss. The calculation of energy consumption was achieved in several steps as follows:

1) Heating the quartz tube

Heating the quartz reactor up to the desired temperature uses an amount of energy calculated as $mC_p\Delta T$, with m being the weight of the reactor (experimentally measured), Cp the specific heat capacity and ΔT the temperature increase. The specific heat value of quartz was obtained from Hemingway (1987) cited by Sharifan [176] varying between 742.1 and 1167.5 J/Kg.K within the temperature range of 15 - 927 °C.

2) Heating and carbonization of biomass (Pyrolysis)

The energy consumed to heat and pyrolyze the biomass was calculated from the DSC curves obtained by the TGA analysis of raw materials. The DSC curves provide information about the heat exchange (power in miliwatts) consumed or produced throughout the carbonization of biomass under nitrogen (Figure 1 and Figure 2).

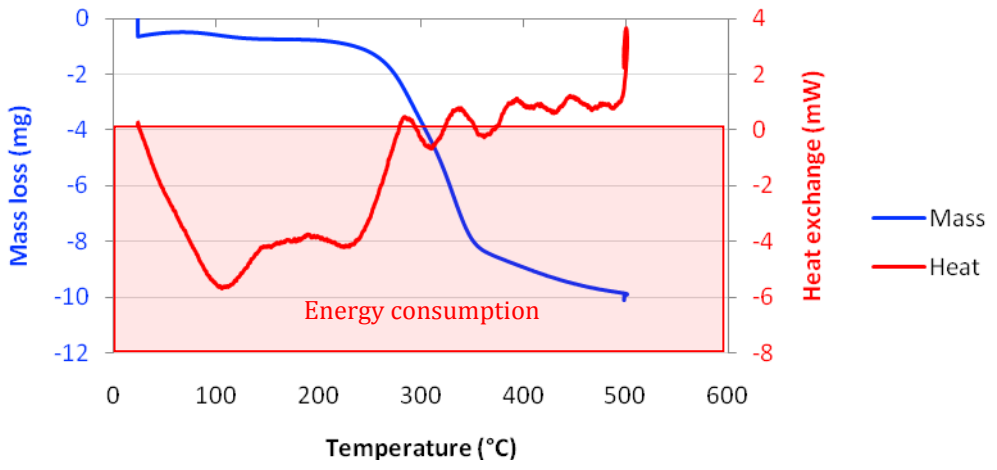

Figure 1. TGA curves of MH carbonization at 500 °C.

The mass loss is represented in the left axis and the heat exchange is represented in the right axis.

It should be noted that the negative heat value is the heat provided by the machine (red zone) and not the sample. This means that according to Figure 1, between 20 to ≈ 290ºC energy was consumed in the carbonization of MH, whereas in pyrolysis of BH (Figure 2) energy is consumed during the whole process except in the 330 – 360 °C temperature range. The energy consumption in pyrolysis of BH at 500 °C is due to the decomposition of lignin in this biomass. The ratio of lignin content in BH (27.0 %) to MH (15.7 %) is 1.7 which is proportional to the energy consumed in the carbonization stage of 100 g of each biomass, in fact the energy consumption BH/MH = 1.7.

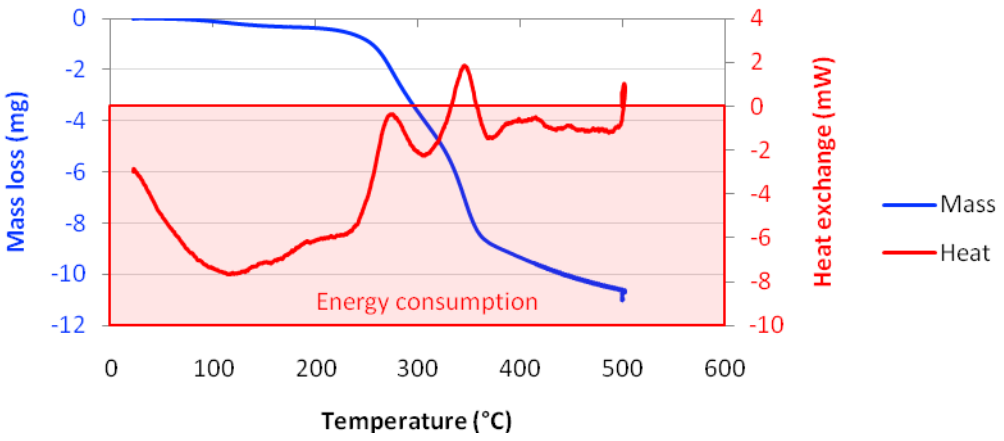

Figure 2. TGA curves of BH carbonization at 500 °C.

The mass loss is represented in the left axis and the heat exchange is represented in the right axis.

3) Heating, carbonization and direct activation of biomass

In direct activation of biomass, pyrolysis is carried out at 700 °C and the energy demand of the carbonization is obtained from the TGA analysis as in 2). The curves are presented in Figure 3 and Figure 4.

As presented in Chapter 3, the gas composition showed that the reactions taking place in CO_2 and steam activation are:

CO_2 activation:	$C + CO_2 \rightarrow 2CO$	ΔH (1123 K) = 11.45 kJ/mol
H_2O activation:	$C + H_2O \rightarrow CO + H_2$	ΔH (1123 K) = 19.06 kJ/mol
	$CO + H_2O \rightarrow H_2 + CO_2$	ΔH (1123 K) = 7.61 kJ/mol

Consequently, for the calculation of activation energy was carried out considering the total enthalpy of each activation method (CO_2 or H_2O) and the moles produced of H_2, CO and CO_2 respectively.

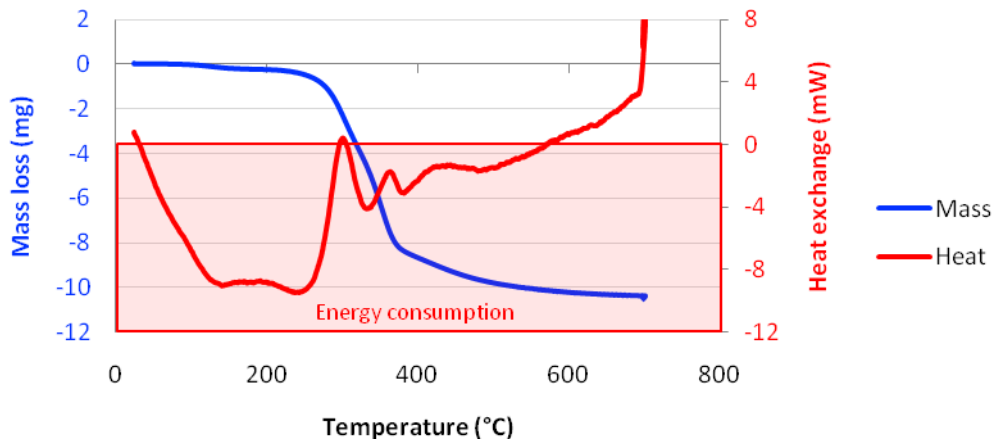

Figure 3. TGA curves of MH carbonization at 700 °C.

The mass loss is represented in the left axis and the heat exchange is represented in the right axis.

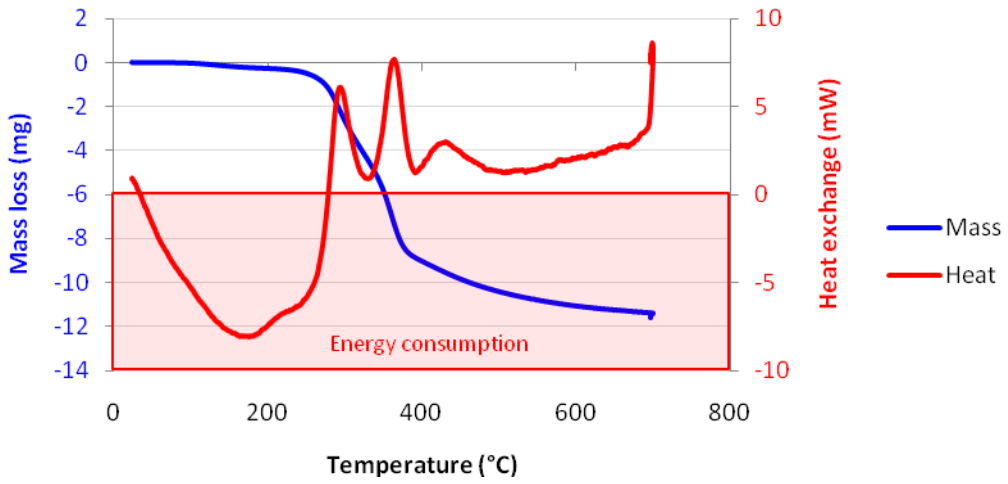

Figure 4. TGA curves of BH carbonization at 700 °C.

The mass loss is represented in the left axis and the heat exchange is represented in the right axis.

4) Heating the gases

Heating N_2:

The nitrogen is at room temperature before entering the reactor. Some energy is used to heat this gas while entering the system. For the calculation of energy consumed to heat up nitrogen, the specific heat and density of N_2 were required at different temperatures. By implementing this information (Table 5) in $mCp\Delta T$ the energy input to raise the temperature was calculated in two steps: (i) while ramping from ambient temperature to the final activation temperature, and (ii) during the dwell time.

Table 5. Specific heat and density of nitrogen at different temperatures (www.nist.gov/).

T (K)	300	400	500	600	700	800	900	1000	1100	1200
C_P (J/mol.K)	29.12	29.25	29.58	30.1	30.76	31.44	32.09	32.69	33.24	33.72
ρ (kg/m^3)	0.91	0.682	0.545	0.454	0.389	0.341	0.303	0.273	0.248	0.227

Heating H_2O:

Energy is required to heat and evaporate water, in addition, the energy used to raise the temperature of the steam to the activation temperature must be considered. These calculations were carried out in three steps; initially increasing temperature from 20 to 100 °C (liquid phase), the specific heat was used in $mCp\Delta T$ for the energy required to increase the temperature of water by 80 °C. Secondly, water vaporization with the enthalpy of 40.657 KJ/mol (Marsh, 1987) cited by Sharifan [176] and finally heating steam from 100 °C up to the activation temperature (Table 6).

Table 6. Specific heat of steam at different temperatures (www.nist.gov).

T (K)	500	700	900	1100	1200
C_P (J/mol.K)	35.22	37.5	40	41.52	43.75

5) Heat loss through insulation

The dimensions of the electrical furnace are presented in Figure 5. The furnace box was covered with thick layers of insulation material (ceramic fiber) where the reactor is placed. The heating elements are installed within the insulation walls.

A large fraction of the energy consumed in the electrical furnace is lost through the walls. It was assumed that the temperature inside walls of insulation is at the desired process temperature. The external steel cover was at ~ 40 °C. The heat transfer mechanism can be resembled to electrical resistances in a circuit.

The thermal resistance can be calculated for the insulation as R=L/S.K, where L is the insulation thickness, S is the surface area of insulation plates and K is the thermal conductivity of insulation. The surface area considered in the calculation is presented Figure 6.

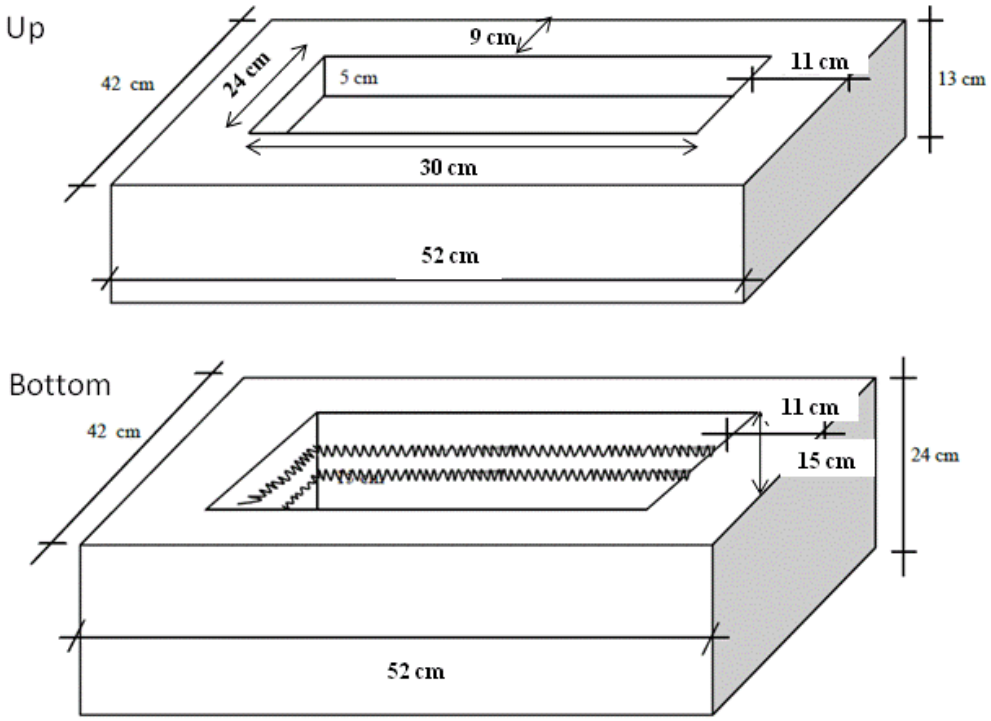

Figure 5. Dimensions of horizontal furnace used in pyrolysis and activations, adapted from Sharifan [176].

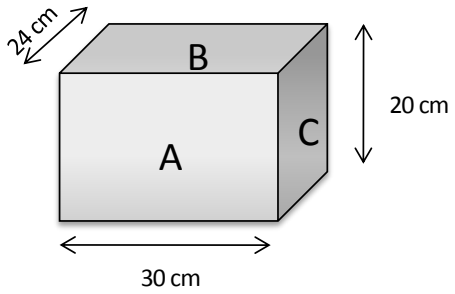

Figure 6. Surface area for the calculation of heat lost through insulation.

The thermal resistivity of the metal cover was considered negligible here; therefore the inside and outside temperature of the metal cover was assumed to be similar. The thermal conductivity of the insulation walls (ceramic fiber) is taken from a commercial provider (THERMOST THERMTECH CO. LTD) presented in Table 7. The heat flux through insulation walls can be expressed as $q = \frac{T_2 - T_1}{R}$.

Table 7. Thermal conductivity of ceramic fiber.

T (°C)	400	600	800
K (W/m.K)	0.08	0.13	0.20

Results from the calculation of energy consumption are presented in Table 8, Table 9 and Table 10 for pyrolysis and activations.

Table 8. Energy consumption in pyrolysis of MH and BH at 500 °C.

PYROLYSIS 500°C	MH-Char		BH-Char	
	Energy (MJ)	**%**	**Energy (MJ)**	**%**
Heating quartz reactor	0.82	29%	0.82	28%
Heating and carbonization of biomass	0.040	1.4%	0.080	2.7%
Heating gas (N_2)	0.018	0.6%	0.018	0.6%
Heat lost through insulation	2.002	69%	2.002	69%
TOTAL	*2.881*	*100%*	*2.921*	*100%*

Table 9. Energy consumption in activation of MH at 850 °C.

ACTIVATION OF MH AT 850°C	1-step MH-CO_2		MH-H_2O	
	Energy (MJ)	**%**	**Energy (MJ)**	**%**
Heating quartz reactor	1.21	12.9%	1.21	11%
Activation Energy	0.012	0.1%	0.041	0.4%
Heating and carbonization of biomass	0.075	0.8%	0.080	0.8%
Heating gas (N_2/CO_2/H_2O)	0.128	1.4%	1.331	13%
Heat lost through insulation	7.926	84.8%	7.926	75%
TOTAL	*9.346*	*100%*	*10.583*	*100%*

Table 10. Energy consumption in activation of BH at 850 °C.

ACTIVATION OF BH AT 850°C	1-step BH-CO_2		BH-H_2O	
	Energy (MJ)	**%**	**Energy (MJ)**	**%**
Heating quartz reactor	1.21	13%	1.21	11%
Activation Energy	0.021	0.2%	0.049	0.5%
Heating and carbonization of biomass	0.013	0.1%	0.015	0.1%
Heating gas (N_2/CO_2/H_2O)	0.128	1%	1.331	13%
Heat lost through insulation	7.926	85%	7.926	75%
TOTAL	*9.293*	*100%*	*10.526*	*100%*

Annexe 3. Calculation method of maximum capacity of BH-H_2O for EB removal from humid syngas

As can be noticed in Figure 7, the EB concentration in the treated gas increases linearly from t = 50 min to t = 360 min. In view of this behavior, this data is expressed as a linear equation with a correlation coefficient of 0.98 as presented in Figure 8 The obtained equation was used to calculate the EB concentration at t > 360 min. In addition, it was assumed that thermal cracking is constant at t longer than 360 min which reduced the initial EB concentration from 40 to 26g/Nm^3. Results are presented in Figure 9. These two assumptions allowed calculating the maximum capacity of BH-H_2O in terms of X_{tar}. It was found that BH-H_2O is saturated at 620 min since at this point the EB concentration is the same as thermal cracking. The maximum efficiency of the sample is found to be 2.9 g_{EB}/g.

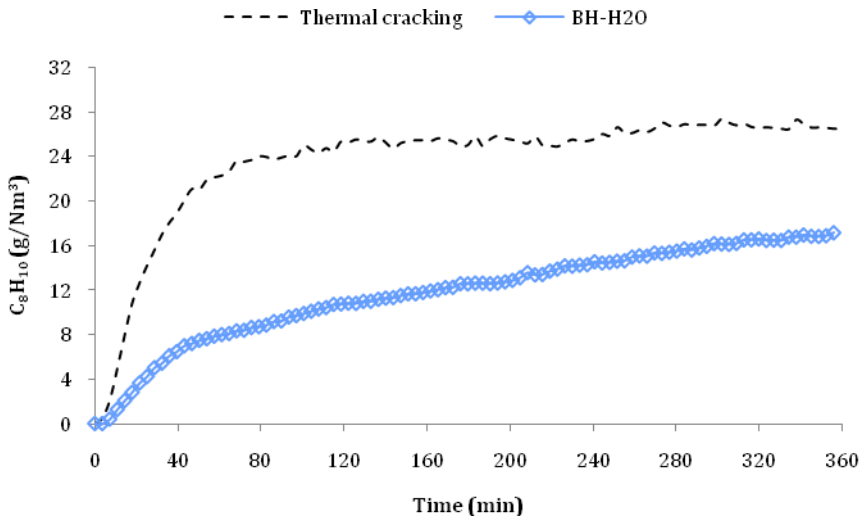

Figure 7. Humid syngas cleaning with BH-H_2O at 650 °C and EB at 40 g/Nm3.

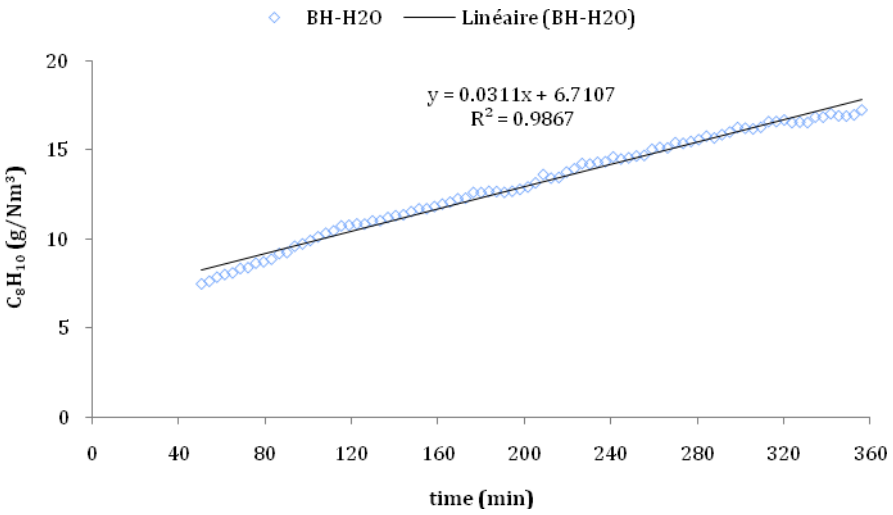

Figure 8. Linear representation of EB concentration in the treated syngas from 50 to 360 min.

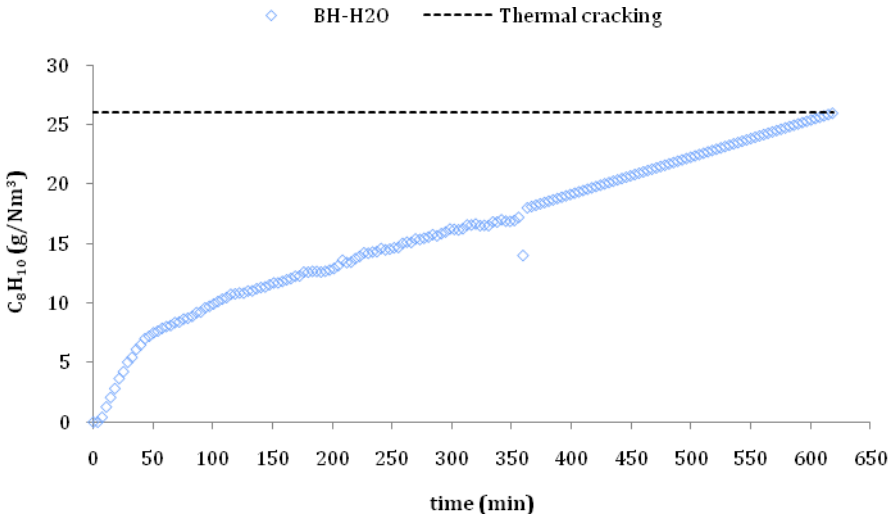

Figure 9. Calculated EB concentration at t longer than 360 min.

Annexe 4. Calculation of energy consumption in gasification of exhausted materials (vertical furnace)

The calculation of electrical consumption of the gasification process was carried out with a thermodynamic approach, considering the energy demand and energy loss. The calculation of energy consumption was achieved in several steps as follows:

1) Heating the column

Heating the quartz reactor up to the desired temperature uses an amount of energy calculated as $mCp\Delta T$, with m being the weight of the reactor (experimentally measured), C_P the specific heat capacity and ΔT the temperature increase. The specific heat value of stainless steel was used (C_P = 510 J/kg.K).

2) Heating furnace atmosphere (air)

The air is at room temperature before entering the reactor. Some energy is used to heat this gas while passing through the open system. For the calculation of energy consumed to raise the temperature of air, the specific heat (C_P = 32.47 J/mol.K) of air was required. By implementing this information in $mCp\Delta T$ the energy input to elevate the temperature was calculated.

3) Heat consumed in gasification

Considering that activation is a partial gasification and since the oxidizing agent is a mix of steam and CO2, the reactions that are assumed to take place in this stage are the same as in activation:

$C + CO_2 \rightarrow 2CO$	ΔH (1123 K) = 11.45 kJ/mol
$C + H_2O \rightarrow CO + H_2$	ΔH (1123 K) = 19.06 kJ/mol
$CO + H_2O \rightarrow H_2 + CO2$	ΔH (1123 K) = 7.61 kJ/mol

Then, according to the total mol production of CO + H_2, the heat consumed in the gasification stage was computed.

4) Heating the oxidizing agent (N_2 + H_2O + CO_2)

Some energy is used to heat the gases that enter the system. For the calculation of energy consumed to heat up these gases, the specific heats were required. By implementing this information in $mC_p\Delta T$ the energy input to raise the temperature was calculated in two steps: (i) while ramping from ambient temperature to the gasification temperature, and (ii) during the dwell time as explained before in Annexe 3.

5) Heat lost through insulation

The dimensions of the electrical furnace are presented in Figure 10. It is assumed that inside the vertical furnace, the reactor is covered with insulation material (ceramic fiber) of height equal to 0.15 m and thickness of 0.0285 m.

A large fraction of the energy consumed in the electrical furnace is lost. It was assumed that the temperature inside walls of insulation is at the desired process temperature. The external steel cover was at ~ 40 °C. The heat transfer mechanism can be resembled to electrical resistances in a circuit. The thermal resistance can be calculated for the insulation as $R=L/S.K$, where L is the insulation thickness, S is the surface area of insulation plates and K is the thermal conductivity of insulation.

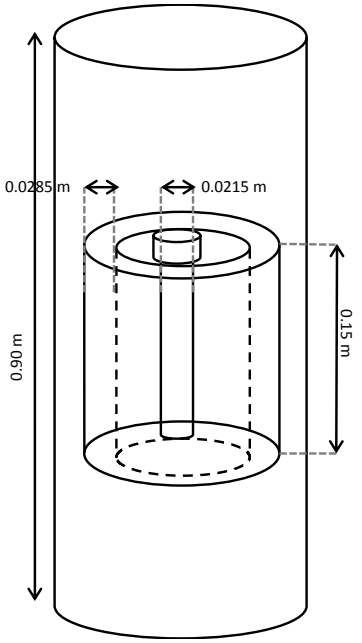

Figure 10. Dimensions of the vertical furnace used in gasification of exhausted samples.

The thermal resistivity of the metal cover was considered negligible here; therefore the inside and outside temperature of the metal cover was assumed to be similar. The thermal conductivity of the insulation walls (ceramic fiber) was presented previously (Table 7). The heat flux through insulation walls can be expressed as $q = \frac{T_2 - T_1}{R}$; results from the calculation of energy consumption are presented in Table 11:

Table 11. Energy consumption in gasification of exhausted BH-H_2O and BH-CO_2 at 900 °C.

GASIFICATION 900°C	BH-H_2O	BH-CO_2	%
	Energy (MJ)	Energy (MJ)	
Gasification energy	2.44E-05	8.77E-06	0.00%
Heating column	0.9	0.9	27%
Heating air	0.0029	0.0029	0.1%
Heating gas (N_2/CO_2/H_2O)	0.028	0.028	0.8%
Heat lost through insulation	2.4	2.4	72%
TOTAL	3.3	3.3	100%

As indicated by results, 3.3 MJ are consumed in the process in order to raise to temperature of the column and oxidizing agent.

Annexe 5. Résumé en français

Valorisation énergétique et matière de chars issus de biomasses résiduelles

Introduction

La conversion thermochimique de la biomasse est l'un des processus clés pour permettre le développement de vecteurs énergétiques alternatifs aux combustibles fossiles. Il existe différents procédés de conversion thermochimique tels que la pyro-gazéification qui peut s'adapter à une large éventail de biomasses résiduelles sèches dans des quantités relativement importantes. Ceci peut être une voie en vue de diminuer et valoriser la quantité de déchets produits à partir de biomasse comme le stipulent les principes de l'économie circulaire. Actuellement, un des sous-produits issus de la pyrolyse et/ou de la gazéification de la biomasse, connu sous le nom de char, n'a pas d'applications identifiées. Il en résulte qu'actuellement, il est considéré comme un déchet. Cet aspect est point limitant au développement des procédés de conversion thermochimique à l'échelle industrielle. Compte tenu de cette limitation, le projet de thèse avait pour objectif d'étudier la possibilité de valoriser ce résidu en un matériau à valeur ajoutée via l'étude de ses propriétés physico-chimiques et son utilisation potentielle dans différentes applications telles que le traitement du gaz de synthèse et du biogaz.

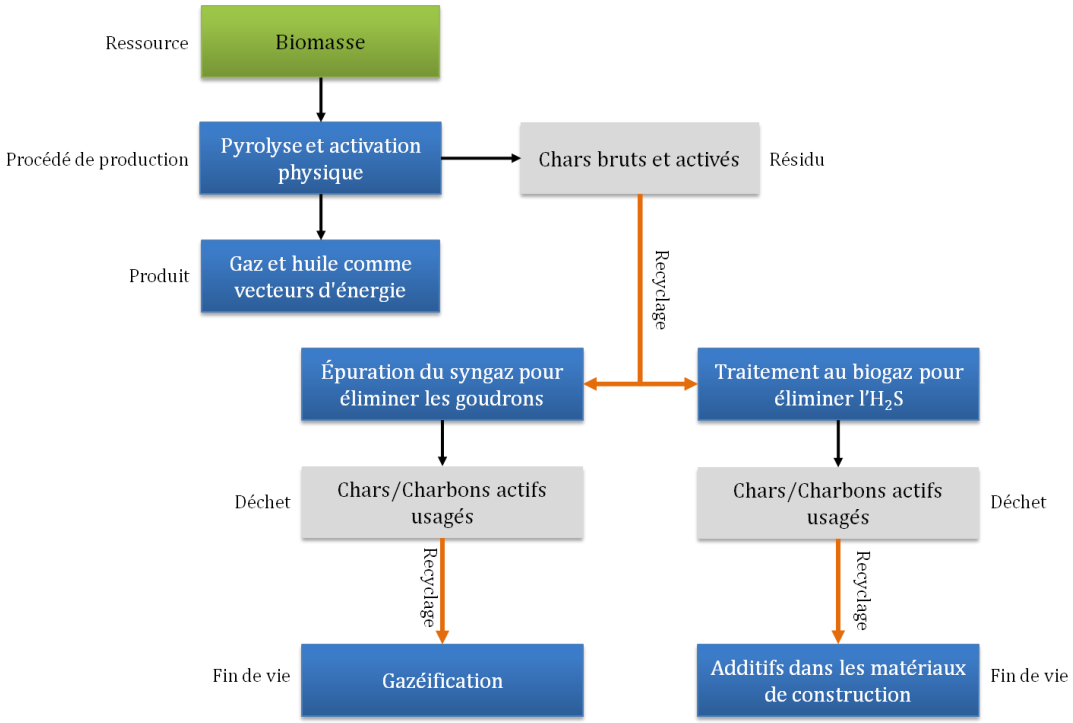

Figure 0-1. Schéma résumé du projet de thèse mettant en évidence les grandes étapes.

La Figure 0-1 résume le projet de thèse. Deux biomasses, les écales de millet (MH en anglais) et les écales de sarrasin (BH) ont été sélectionnées sur la base de leurs compositions chimiques

différentes, leurs disponibilités locales et sur le fait que ces biomasses ont été peu étudiées dans la littérature. Elles ont été utilisées pour produire des chars par pyrolyse, puis ont été activées soit avec du CO_2 soit de la vapeur d'eau afin d'obtenir des charbons actifs. Une fois les matériaux produits et leurs propriétés identifiées, deux voies de valorisation ont été envisagées : l'épuration de syngaz et le traitement de biogaz afin d'éliminer respectivement les goudrons et l'H_2S. Finalement, une étude prospective a été réalisée afin d'identifier le devenir ultime des matériaux usagés.

Matériels et méthodes

Deux chars sont produits par pyrolyse lente à 500 °C dans le but de maximiser leurs rendements. Les chars de pyrolyse sont nommés par rapport à la biomasse entrante : MH-Char et BH-Char. Puis, une activation physique conduite soit avec du CO_2 soit avec H_2O à 850 °C est réalisée afin d'améliorer les propriétés physico-chimique des chars. Deux agents oxydants différents ont été choisis afin d'étudier leurs impacts sur les propriétés du matériau obtenu. L'activation au CO_2 est réalisée en une ou deux étapes, tandis que l'activation à la vapeur d'eau est conduite en une seule étape. Les matériaux résultant de l'activation sont nommés sur la base du type d'activation et de la biomasse : MH-CO_2, MH-H_2O, BH-CO_2 et BH-H_2O. Les bilans matières et énergies sont réalisés afin de comparer l'efficacité énergétique des différents procédés mis en œuvre. Les matériaux produits sont caractérisés aussi bien d'un point de vue chimique que physique afin de pouvoir les comparer les uns au autres et d'identifier les liens entre leurs efficacités vis-à-vis d'un polluant donné et leurs propriétés physico-chimiques. La mise en œuvre des matériaux en épuration de syngaz et de biogaz se fait par un lit fixe constitué des chars bruts ou activés. Différentes compositions de syngaz et de biogaz sont utilisées afin d'étudier leurs influences sur l'efficacité des matériaux élaborés.

L'éthylbenzène (EB) est choisie pour représenter les goudrons vue que ce composé fait partie de la famille d'aromatiques légers, une des principales familles de goudrons. L'efficacité des matériaux pour le craquage EB est étudiée à 650 °C avec une concentration initiale d'EB de 40 g/Nm^3, un lit fixe d'une hauteur de 4 cm, diamètre de 2.15 cm et différentes compositions du gaz (Tableau 1) à une vitesse de 0.10 m/s. Concernant le biogaz, les performances des chars bruts et activés pour l'adsorption d'H_2S sont étudiées à température ambiante, avec une concentration initiale d'H_2S de 200 ppm, une hauteur de lit fixe de 4, 8 et 12 cm et différentes compositions du gaz (Tableau 2).

Tableau 1. Composition des différentes matrices de syngaz étudiées à 650 °C au travers d'un lit fixe de 4 cm.

Syngaz	H_2 (vol.%)	CO (vol.%)	CO_2 (vol.%)	CH_4 (vol.%)	N_2 (vol.%)	H_2O (vol.%)	EB (g/Nm^3)
Simplifié	0	40	0	0	60	0	40
Sec	23	17	15	11	34	0	40
Humide	20	15	13	10	30	12	40

Tableau 2. Composition des différentes matrices du biogaz étudiées à 30 °C et conditions expérimentales mises en œuvre.

Biogaz	CH_4 (vol.%)	CO_2 (vol.%)	N_2 (vol.%)	H_2O (vol.%)	H_2S (ppm)	Hauteur de lit (cm)	Température (°C)
Simplifié	0	0	100	0	200	4	30
Sec	32	18	50	0	200	4	30
Humide	30	16	50	4	200	4, 8, 12	30

Production des matériaux et bilans énergétiques des procédés de pyrolyses et d'activations

Cette étude a montré que les caractéristiques de la biomasse influencent les propriétés des chars de pyrolyse. Les écales de sarrasin contiennent un fort taux de carbone (47.5 %) et de lignine (27 %), il en résulte des chars et des charbons actifs avec un pouvoir calorique élevé (28 - 29 MJ/kg). Ces deux éléments favorisent le développement de la porosité dans les charbons actifs. A contrario, les écales de millet présentent une teneur élevée en cendres (12.2 %) qui a pour conséquence de limiter le développement de la porosité dans le cas des chars activés et le pouvoir calorique dans le cas de chars bruts et activés (17.5 – 22.7 MJ/kg). La composition inorganique et le procédé d'activation déterminent certaines propriétés des matériaux résultants. Lors de la pyrolyse, la teneur en cendres dans la phase solide augmente, bien qu'une partie des éléments inorganiques (<20 %) peuvent se retrouver dans la phase gazeuse. Ceci dépend de la composition minérale, de leur forme chimique ainsi que de la température à laquelle est conduite la pyrolyse. Les chars de pyrolyse ont une faible porosité, principalement constituée de macropores (diamètre de pore D_p > 50 nm) et ils présentent une surface acide (pH < 6).

La gazéification partielle ou l'activation physique des chars modifient les propriétés chimiques et texturales. L'activation au CO_2 permet d'obtenir des charbons actifs avec une teneur en carbone plus élevée et un taux de cendres inferieur à ceux obtenus avec une activation à la vapeur d'eau. L'activation au CO_2 produit des matériaux ayant une microporosité relative plus importante comparée à celles obtenues sous activation à la vapeur d'eau. Il a été observé que l'agent d'activation influence également la libération des éléments minéraux de la phase solide à la phase gazeuse. Lors de l'activation au CO_2, plus de calcium est libéré et les composés calciques restant dans la phase solide se retrouvent sous les formes CaO et $CaCO_3$. Les composés de calcium restant dans la phase solide sont agglomérés et ils ne sont pas dispersés de façon homogène à la surface du charbon actif. Par contre, lors de l'activation à la vapeur d'eau, une quantité moindre de calcium est libérée. Il est principalement présent sous la forme de CaO, dispersée de manière homogène à la surface du solide. Concernant les autres principaux éléments inorganiques contenus dans ces biomasses que sont le magnésium, le potassium, le phosphore et la silice, il semble que leur répartition ne soit pas influencée par l'agent d'activation.

Le charbon actif BH-H_2O préparé à partir des écales de sarrasin par activation à la vapeur d'eau présente la surface spécifique la plus élevée (997 m^2/g), composée de 71 % de micropores. Cet échantillon contient du calcium sous la forme CaO, du potassium, du magnésium et du phosphore qui donnent son pH basique. Les charbons actifs BH-CO_2 préparés en deux ou en une seule étape ont une surface inférieure à 600 m^2/g avec plus de 80 % de micropores. Les

charbons actifs préparés à partir des écales de millet présentent une porosité plus faible en raison de leurs teneurs élevées en cendres et de leurs faibles taux de lignine. MH-H_2O a une surface spécifique de 466 m^2/g avec 83 % de micropores tandis que la surface spécifique des échantillons de MH-CO_2 est d'environ 320 m^2/g composée de plus de micropores (>70 %) que de mésopores. Ces matériaux ont une teneur élevée en silice associée à une teneur plus faible de calcium, potassium et phosphore.

Les indicateurs de performance énergétique montrent que la pyrolyse lente présente le bilan énergétique le plus intéressant et que la phase qui contient la plus grande partie de l'énergie est le char (79 – 85 %). Ceci signifie que le char doit être valorisé en tant que vecteur énergétique. Pour ce faire, le char de pyrolyse peut être soumis à une activation physique ou à une gazéification afin de récupérer son énergie sous la forme de gaz. Puis, le char gazéifié qui dans certain cas peut être assimilé à un charbon actif dû aux caractéristiques physico-chimiques qu'il présente (porosité élevée et taux de carbone) peut être utilisé dans des filières d'épuration de gaz. Dans le cadre de cette étude, il a été choisi de mettre en œuvre les matériaux élaborés dans l'épuration du biogaz et du syngas afin de réduire respectivement H_2S et les goudrons.

Épuration du syngaz

Les chars de pyrolyse (MH-Char et BH-Char) ont montré une réactivité limitée attribuée à l'absence de micropores développés au stade de l'activation. Les résultats de la matrice simplifiée (N_2 + CO + EB) suggèrent que la porosité et la composition minérale des matériaux sont les principales propriétés influençant la dégradation de l'éthylbenzène. BH-H_2O, qui est l'échantillon présentant la plus grande surface spécifique, ainsi qu'une teneur en calcium, magnésium et potassium supérieures et un taux de silice non détectable, a permis d'obtenir l'élimination la plus élevée d'éthylbenzène (0.95 g_{EB}/g) par gramme d'échantillon. La seconde meilleure performance est obtenue par MH-H_2O (0.77 g_{EB}/g) due à la présence importante de mésopores qui semblent être plus résistants à la désactivation par dépôt de suie. Les échantillons microporeux (MH-CO_2 et BH-CO_2) obtenus par activation au CO_2 ont été désactivés plus rapidement que les matériaux activés à la vapeur d'eau.

Lors de l'épuration du syngaz sec, le CO_2 est neutralisé par BH-H_2O et MH-H_2O, ce qui réduit leurs performances vis à vis du craquage de l'éthylbenzène. Ce phénomène n'a pas été observé avec MH-CO_2 et de BH-CO_2 qui affichent une efficacité supérieure par rapport au syngaz simplifié. Le craquage thermique est le plus élevé dans un syngaz sec, mais la vapeur d'eau présente dans le syngaz humide a un effet favorable sur la décomposition des goudrons. Avec le syngaz humide, la plupart des échantillons étudiés ont amélioré leur efficacité, sauf pour le MH-CO_2. La présence de vapeur d'eau implique probablement le reformage des goudrons ; la vapeur d'eau réagit avec le monoxyde de carbone, ce qui augmente la teneur en hydrogène en favorisant la qualité du syngaz. Le charbon actif le plus performant quelle que soit la matrice de syngaz étudiée est BH-H_2O avec une performance de 0.7 –2.9 g_{EB}/g. Ceci s'explique par sa surface spécifique importante, sa répartition micropores/ mésopores et sa composition minérale qui contribuent à son efficacité dans la conversion de l'éthylbenzène. Il est à noter que la présence de calcium dans cet échantillon entraîne la formation de goudrons plus légers, alors que cet effet n'est pas observé avec MH-CO_2 et MH-H_2O présentant une teneur en calcium plus faible et une teneur en silice plus élevée. La désactivation des matériaux a confirmé que la saturation de MH-

H_2O et de BH-H_2O est plus lente que celle de MH-CO_2 et de BH-CO_2 ce qui peut être expliqué par la faible présence de mesopores dans ces échantillons principalement microporeux.

Purification du biogaz

Dans la matrice simplifiée de biogaz (N_2/H_2S), les chars de pyrolyse ont une faible capacité d'adsorption d'H_2S (<1.6 mg_{H2S}/g) en raison de leur porosité limitée et de leur pH acide. L'étape d'activation améliore la capacité d'adsorption (4.1 – 9.3 mg_{H2S}/g) des matériaux permettant une élimination plus élevée de H_2S due principalement à leurs porosités développées ainsi qu'à la distribution entre méso et micropores et à leurs pHs basiques. Les résultats ont montré que les micropores sont les sites actifs de ces matériaux ; ils permettent l'adsorption physique des composés soufrés. L'influence de la méthode d'activation est mise en évidence au travers de la microporosité relative du BH-CO_2 et du MH-CO_2 qui favorise l'élimination du sulfure d'hydrogène. La présence d'espèces minérales est importante car elles contribuent à l'obtention d'un pH basique, qui favorise les réactions acido-basiques avec H_2S.

La composition gazeuse du biogaz influence fortement la capacité d'adsorption des matériaux : les charbons actifs ont présenté une capacité d'adsorption plus élevée avec une matrice simple et une compétition entre CO_2, CH_4 et H_2S se met en place sur les sites actifs avec la matrice complexe sèche. Concernant le biogaz humide, l'élimination du sulfure d'hydrogène est améliorée et la capacité d'adsorption est similaire pour tous les matériaux (6.2 – 8.2 mg_{H2S}/g), ce qui indique que l'humidité joue un rôle important dans le mécanisme d'adsorption du H_2S. L'humidité relative du biogaz est condensée à l'intérieur des pores de charbons actifs ou les gazes sont solubilisées dans la phase liquide suivie d'une adsorption dans les sites actifs. L'effet de l'humidité est notamment due a solubilité supérieure du H_2S par rapport au CO_2 et au CH_4 limitent d'abord l'absorption des gazez et puis la compétition de ces gazes pour les sites actifs. Il est à noter que l'effet bénéfique de l'humidité n'a lieu que dans les matériaux à surface basique. L'humidité du biogaz influence le mécanisme d'adsorption-oxydation de l'H_2S dans les charbons actifs. Dans le biogaz sec, l'adsorption physique et l'oxydation de l'H_2S entraînent la rétention de soufre élémentaire et de polysulfures de soufre alors que, dans des conditions humides, la formation d'oxydes de soufre et / ou de sulfures alcalins ($Ca(HS)_2$, $Ca(OH)_2$, MgS) se produit plus largement. Le charbon actif ayant la capacité d'adsorption la plus élevée dans toutes les matrices de biogaz est BH-CO_2 avec une capacité de 7.7 – 9.3 mg_{H2S}/g. Cette efficacité peut être attribuée à sa grande surface spécifique qui présente une microporosité relative élevée et des éléments minéraux tels que le calcium, le magnésium et le potassium contribuant à son efficacité dans l'élimination du sulfure d'hydrogène.

Les résultats de purification du gaz de synthèse et du biogaz permettent de conclure que la méthode d'activation doit être sélectionnée en fonction de l'application envisagée. En ce sens, pour l'épuration du biogaz, il est préférable d'avoir recours à une activation au CO_2 afin d'élaborer des matériaux présentant une microporosité relative élevée, alors que l'épuration du gaz de synthèse nécessite des charbons actifs obtenus via une activation à la vapeur d'eau qui permettra de développer davantage les mésopores.

Fin de vie des matériaux

Les charbons actifs usagés dans l'épuration du syngaz ont un pouvoir calorifique assez élevé ce qui permet d'envisager une valorisation énergétique via une gazéification. Deux matériaux ont été sélectionnés pour explorer cette option : BH-CO_2 et BH-H_2O grâce à l'absence de silice dans leur fraction inorganique. La gazéification de BH-H_2O usagé a produit un syngaz ayant un pourcentage de H_2 plus élevé et une teneur en CO_2 inférieure au syngas produit à partir de BH-CO_2. Ceci est certainement du à sa teneur supérieure en calcium. La récupération d'énergie de cet échantillon est donc plus intéressante que celle du BH-CO_2. Le MH-CO_2 et le MH-H_2O usagés après l'épuration du syngaz doivent être récupérés car leurs teneurs en silice limitent leur utilisation en gazéification. Par contre, cette concentration élevée en silice pourrait être mise à profit dans les matériaux de construction. Dans cette optique, des études supplémentaires sur MH-Char, MH-CO_2 et MH-H_2O en tant qu'agrégats de matériaux de construction pourraient être réalisées afin de déterminer si il est possible de les incorporer dans des matériaux de construction et à quelle hauteur.

La fin de vie des matériaux doit être identifiée avec l'objectif de minimiser l'impact environnemental de ces derniers. Selon ce principe, l'utilisation finale des charbons actifs usagés dans l'élimination du H_2S contenu dans le biogaz doivent être soigneusement conduite car ces matériaux contiennent des composés soufrés toxiques pour l'environnement. Les échantillons contaminés contenant des composés soufrés pourraient être des candidats pour la manufacture de briques.

Annexe 6. Catalytic decomposition of ethylbenzene over chars prepared from buckwheat husk: The influence of physic activation in char performance

Pyrolysis chars and physically activated carbons prepared from buckwheat husks for catalytic purification of syngas

PENA Jenny, VILLOT Audrey*, GERENTE Claire

IMT Atlantique, GEPEA UMR CNRS 6144, UBL, 4 rue A. Kastler, CS 20722, 44307 Nantes Cedex 03, France

Corresponding author: Audrey.villot@imt-atlantique.fr

Abstract

This paper investigated the impact of oxidizing agent used during the physical activation of pyrolysis chars on the activated carbons and their efficiency in the tar cracking. The materials are produced from buckwheat husk, which is a French local biomass. A slow pyrolysis has been chosen to favor the production of raw chars. Then, activated chars are prepared by a physical activation under steam or CO_2. The produced materials are physical and chemical characterized before being implemented in a fixed bed. The efficiency of materials to remove tars from syngas was studied for that ethylbenzene (EB) was chosen as tar surrogate. The purification efficiency of the chars and AC is deduced from EB conversion profiles in comparison to thermal cracking. The nature of the oxidizing agent impact the porosity and the mineral composition of the AC produced: the CO_2 activation gives ACs with more carbon and less ash content. This is due to the fact that oxidizing agent impacts the volatilization of mineral element, particularly the Ca and the Mg. CO_2 activation results also in a higher relative microporosity (89 %) than steam activation (61 %) which itself gives the higher surface area. The pyrolysis char has not demonstrated any interest in the EB catalytic cracking whereas the ACs have highlighted higher performances. This is due to their porosity which is more developed and their higher ash content. BH-H_2O, which presents the higher porosity, has developed a better catalytic effect and was more resistant to the deactivation.

Key words: Activated carbon, chars, physical activation, pyrolysis, tar cracking.

Highlights

- Oxidizing agent impact the activated carbon features and its reactivity
- Steam physical activation of pyrolysis char is better than CO_2 to crack the tars
- Surface area and mineral composition are key properties to crack the tars
- Porosity is characterized by both mercury porosimetry and nitrogen gas sorption

1. Introduction

The pyro-gasification of biomass and residue appears as among the more promising conversion routes to produce a gaseous energy carrier named syngas which is mainly constituted of H_2 and CO. The pyro-gasification process is a thermochemical reaction which occurred between the biomass and an oxidant (air, steam, oxygen or carbon dioxide) at elevated temperature (700-1000°C). During this process, the solid biomass is converted in three phases: syngas, oil and a solid carbonaceous residue named char. Four steps are needed to achieve pyro-gasification: drying, pyrolysis, gasification and finally, reforming of the pyrolysis chars and condensable gases. During pyrolysis, biomass is decomposed at moderate temperatures (<700°C) under reducing atmosphere into three phases: gas, liquid products (bio-oil) and solid residues called bio-chars. Bio-chars represent 15–30 wt% of the initial biomass weight and contain about 25% of the initial recoverable energy. It is important to specified that char (gasification char) and bio-char (or pyrolysis char) are two different materials, with similar but not the same features.

Indeed, according to the European Certificate of Biochar, bio-char is defined as char produced from organic wastes through a pyrolysis process. Pyrolysis chars is a non porous carbonaceous materials which contained a variable part of mineral compounds initially contained in the biomass. Then, during the gasification, the carbonaceous substances are converted into syngas in the presence of an oxidizing agent at a temperature contained between 700 and 1000 °C. Similarly to the pyrolysis phase, the gasification gives three phases: syngas, tars and char; their amount and properties strictly depends on the initial composition of the feedstocks, the oxydising agent and the operating conditions. In this case, the char can exhibited a certain porosity as shown by some authors [1,2].

Syngas produced from pyro-gasification could be converted in energy (heat and/or electricity) through conversion process (gas engines, gas turbines, fuel cells, etc.) or used as precursor in the production of liquid fuel through the Fischer-Tropsch reaction or chemicals [3]. However, syngas should be purified before to be used in order to remove impurities originally contained in solid fuels (sulphur, chlorine, nitrogen compounds, etc.), particles (inorganics elements and soots), and pollutants generated by incomplete gasification as tars [4]. The presence of tars in syngas is the major issue limiting the development of pyro-gasification. Indeed, tar can condense at moderate temperature (350°C) thus fouling the equipment downstream of the gasifier or deactivate the catalysts used in the syngas upgrading process. Tar is a complex mixture of condensable aromatic and oxygenated hydrocarbons having a molecule weight higher than benzene (78 g/mol) [3], and are divided in five classes depending on their properties. Light tars are the main class generated by pyro-gasification of biomass. Their concentration can vary between 5 and 200 g/Nm3 of syngas [3]. Tar removal from syngas are widely studied and several methods have been developed [4–8]: physical treatment (electrostatic precipitator, inertial separation, wet and dry scrubbing), plasma cracking, thermal cracking and catalytic cracking. Among this method, the catalytic cracking presents several advantages: high reaction rate, the increase of syngas yield and purity, and the used at moderate temperatures [9–11]. Until now, the catalysts used suffer from rapid deactivation by coking [12], and elevated production cost. Knowing that the cost of the syngas cleaning represents over 25 % of the total investment and production costs of the biomass to liquid conversion [13]. Thus, the development of low-cost and eco-friendly catalysts can be a solution to reduce the cost of the syngas cleaning process.

Recently, chars have been reported to be promising materials to enhance tar clean-up as an adsorbent and/or catalyst based on the carbonaceous and mineral features [14,15]. Thus the implementation of chars in tar treatment seems to be an interesting approach. Previous studies reported that four main characteristics of the chars determined their activity even if their role remains not clear: the porous structures, the presence of O-containing groups on the char surface, the structure of the carbonaceous matrix, and the active sites formed by the inherent alkaline (Na, K) and alkaline earth (Mg, Ca) species (AAEM) distributed on the char matrix [16]. Taking into account of the main characteristics impacting the char activity and knowing that the nature of the oxidizing agent has an impact on the features of activated carbon (AC), in this study we chosen to study the impact of the oxidizing agent (steam and CO2) on the char features and on their activity in the tar cracking.

This paper aims to studying is to produced different materials (chars and activated chars) from buckwheat husk (BH), which is a French local biomass. Recently, the buckwheat production has augmented in 25 % from 2014 to 2016 which is explained by the increasing interest in food science given that it contributes to vegan or gluten-free diets. In spite of its increasing production, buckwheat has been barely studied in the literature. Lazdovica et al. [17] investigated the influence of buckwheat and wheat straw composition on yield of pyrolysis gases. A slow pyrolysis has been chosen to favor the production of raw chars. Then, in order to see the impact of the porosity and the oxidizing agent on the activated char activity, activated chars are prepared by a physical activation under steam or CO_2. Physical activation is more

environmental friendly than chemical one. From mass and energy balances the energy efficiency of this reaction is evaluated by the way on net energy ratio. The produced materials are physical and chemical characterized before being implemented in a fixed bed. The efficiency of materials to remove tars from syngas was studied for that ethylbenzene (EB) was chosen as surrogate of one-ring aromatic hydrocarbons, besides its decomposition into styrene, benzene and toluene allowed us to study other molecules in parallel. The purification efficiency of these different materials (chars and AC) is deduced from EB conversion profiles in comparison to thermal cracking. This global approach from the pyrolysis of raw biomass to the syngas purification in a fixed bed coupled with the energy efficiency of pyrolysis and activation processes is original and provides relevant information on the evaluation of decentralized energy production chains in a perspective of energy transition and circular economy.

2. Materials and methods

2.1. Chars preparation

2.2. Pyrolysis

100 g of BH previously dried at 105 °C were placed in a semi-rotating quartz tube under N_2 flow of 0.75 NL/min. The reactor was heated at 10 °C/min until 500 °C and kept at that temperature for 30 min. Afterwards, the system was cooled down to room temperature. The raw char denoted hereafter as BH-Char and the condensable phase were collected and weighted. The condensable gases (steam, light tars) are removed by a cold trap close to 0 °C before the gases are analyzed by the GC. The pyrolysis gas was analyzed by on line gas micro-chromatography (SRA Instruments R 3000) equipped with a thermal conductivity detector. This technique was able to measure the non-condensable gases such as H_2, O_2, N_2, CH_4, CO, CO_2, C_2H_4, C_2H_6, C_3H_8 and C_3H_6. The system performed a complete analysis every 3 min, the mass of each measured gaseous species *(m_s)* was evaluated by the given expression [18]:

$$m_s = M_S \frac{Q_{N2}}{V_m} \int_{t0}^{tf} \frac{C_S}{C_{N2}} dt \qquad (1)$$

where the interval of integration corresponds to the elapsing time of analysis, C_S represents the molar fraction of the detected species and M_s is its molecular weight, Q_{N2} is the nitrogen flow rate and C_{N2} is nitrogen molar fraction, V_m is the molar volume. The pyrolysis has been repeated at least 3 times and the average yield in char is close to 38.3 %.

2.3. Direct physical activation

100 g of BH previously dried were loaded in the quartz tube. The unit was heated at 22 °C/min under a N_2 flow at 0.91 NL/min until 700 °C and maintained at this temperature during 30 min. Then the reactor was heated at 10 °C/min until the temperature of activation (850 °C) and held for 80 min. In the case of steam activation, the atmosphere was switched to H_2O at 0.7 mL/min (12 vol.%) and N_2 was set at 0.53 NL/min (88 vol.%). After 80 min, the reactor was cooled down under N_2 flow. These conditions have been optimized based on our previous work [19–23]. The activation with CO_2 was carried out under the same conditions, with a CO_2 introduction at 850°C; CO_2 flow is 2.1 NL/min (70 vol.%) and those of N_2 was set at 0.9 NL/min (30 vol.%). The atmosphere composition in CO_2 activation was fixed according to the literature [24]. The activated chars were denoted as BH-H_2O and BH-CO_2 respectively. All the by-products from activations (activated chars, gas and condensable phases) were collected, weighted and, analyzed. The activations have been repeated at least 2 times and the average yield in activated carbon is close to 16.5 % for steam and 23.5 % for CO_2.

2.4. Characterization of materials

2.4.1. Chemical composition

The materials were characterized in terms of organic and inorganic composition. The ultimate analysis was performed on dried samples to determine C, H, N, S and O contents using a Thermo Finnigan AE1112 Series Flash. The proximate analysis was carried out by a SETSYS Evolution Thermogravimetric Analyzer (TGA) in order to determine the volatile matter (ASTM D3175) and the ash content in biomass and chars (ASTM D1102 and ASTM D3174 respectively). The fixed carbon was calculated by difference. The thermogravimetric (TGA) analyze was also used to determine the lignocellulosic materials distribution content in BH. For that, 40 mg of biomass were heated at 10 °C/min from room temperature to 900 °C under nitrogen atmosphere implementing different temperature steps of 50 min which are caracteristic of lignocellulosic substrates decomposition: 250°C for hemicelluloses, 300°c for cellulose and 500°C for lignin [25–27]. The inorganic composition of raw materials was analyzed by the X-ray fluorescence spectrometry (SHIMADZU EDX-500HS) with a semi-quantitative method. The error percentage of this analysis is considered to be around 20 % for the main elements in ash composition. The higher heating value (HHV) of the materials was measured experimentally using an oxygen PARR 6100 bomb calorimeter. All the above-mentioned analyses were performed three times for each sample. Finally the determination of the surface pH of chars and activated chars was carried out once by the point of zero charge method (PZC) adapted from [20].

2.4.2. Textural properties

The porosity of chars was measured by the adsorption/desorption of nitrogen at -196 °C (Micromeritics ASAP 2020). The samples were previously degassed under vacuum at 350 °C for 48 hours. The surface area was determined using the Brunauer-Emmet-Tellet (BET) model, while the mesoporous (2 < pore diameters < 50 nm) and microporous volumes (pore diameters < 2 nm) were calculated by the BJH and Horvath Kawazoe methods respectively. To complete the porosity characterization, the mercury porosimetry (Micrometrics Autopore IV 9500) was carried out; this analyze allows characterizing the macroporosity of the materials (pore diameters > 50 nm) and a part of the mesoporosity between 8 to 50 nm. The surface tension and the contact angle between the mercury and the carbon used were 0.485 N/m and 154.9° respectively. The macropore volume (V_{Macro}), measured was calculated as the cumulative pore volume at pores sizes larger than 50 nm. Meanwhile, the mesopore volume (V_{Meso}), measured by mercury porosimetry, was deduced as the difference between cumulative volumes at pore diameters between 8 and 50 nm. From the results obtained with the mercury porosimetry, the real density (ρ_{real}) was calculated according to Eq. (2). For both analysis, the samples were dried at 105 °C and each material was analyzed twice.

$$\rho_{real} = \frac{m_{sample}}{V_{sample} - V_{Pores}} \qquad (2)$$

2.5. Mass and energy balances

The mass and energy balances of pyrolysis and activation protocols have been determined by collecting and weighting the solid and the condensable phases. The condensable phase was constituted of an aqueous and an oily fraction. These two fractions were easily settleable and they have been weighted and characterized separately. The lower heating values (LHV) have been deduced from the HHV and the ultimate analysis; they have been reported for the biomass, the raw and activated chars, and the oily phase. Regarding the gas phase, an average LHV was calculated based on the gas composition since the mass of each gas was given by Equation (1) using the nitrogen flow as the reference gas. The energy performance was evaluated by determining the Net Energy Ratio (NER) which is calculated according the equation (3) where W represents the weight fraction (wt.%) and E refers to electric consumption (MJ) of the process. The NER corresponds to the energy hold in the by-products of the process compared to the input electrical energy. If it is higher than 1, the energy hold in the by-products is higher than

the electrical consumption. This means that the energy recovery of BH by-products contributes to a global positive balance under the considered process. If the ratio is lesser than 1, then the considered process is not optimized in terms of energy recovery.

$$NER = \frac{W_{oil}LHV_{oil} + W_{gas}LHV_{gas} + W_{solid}LHV_{solid}}{E} \quad (3)$$

2.6. Syngas treatment

A fixed-bed column (length: 4 cm; internal diameter: 2.15 cm) was set up inside an electrical furnace in order to control the temperature (Figure 6-1). Tests were carried out at 650 °C in a simple gaseous matrix composed of 60 % N_2 and 40 % CO since these conditions correspond to a typical temperature in a gasification process [28], then with a syngaz matrix. The performance of chars and activated chars was evaluated using ethylbenzene (EB) as tar surrogate at 40 g/Nm^3 which is within the range of tar concentration in a syngas (5-200 g/Nm^3) [3]. The outlet gas composition was measured on line with a gas chromatograph analyzer (SRA Instruments R 3000). The gas analyzer was calibrated with ethylbenzene (C_8H_{10}) and three other typical tars components, which are benzene (C_6H_6), toluene (C_7H_8) and styrene (C_8H_8). The mass of each measured species (m_s) was evaluated according to Equation (1). The total flow rate was fixed in order to obtain a gas velocity in the column of 0.1 m/s. Since the gas velocity was kept constant as well as the height bed, the residence time of the gas in empty column was 0.41 s at 650°C. A blank test without sample was also carried out in order to determine the thermal cracking of ethylbenzene at 650 °C. The experiments were performed once with the raw char since the results were no different from the blank test and twice with the activated chars. The thermal cracking was evaluated three times in order to obtain representative curves. The results are presented as the mean values and the bars correspond to the standard deviation.

The materials performance in the catalytic removal of tars is often presented as a percentage of converted tar which is the difference between inlet and outlet tar concentration, divided by the tar concentration in the inlet stream [10,29–31]. However, this expression has two limitations. It does not discriminate the thermal cracking from the catalytic cracking onto the studied materials and the mass of these latter is not taken into account. In this study, Equation (4) is introduced with the intention of overcoming these restrictions. Therefore, the efficiency of each material was defined in terms of tar conversion (X_{tar}) calculated as grams of EB removed per gram of material excluding thermal cracking according to the following equation:

$$X_{tar} = \int_{t_0}^{t} \frac{C_0 - C_t - C^*}{m_{material}} Q_{gas} \quad (4)$$

where C_0 is the inlet ethylbenzene concentration (g/Nm^3), C_t is outlet ethylbenzene concentration at time t (g/Nm^3), C^* is ethylbenzene thermally cracked at time t (g/Nm^3), Q_{gas} is the inlet total gas flow (Nm^3/min) and $m_{material}$ is the initial mass of material (g). The figure 2 gives a graphical explanation of the above equation: the curve in red represents the thermal cracking and the blue breakthrough curve is relative to a material. The area between these 2 curves is proportional to the material efficiency.

3. Results and discussion

3.1. Characterization of materials

3.1.1. Chemical composition

The chemical characterization of the biomass and the chars is presented in Table 4. It can be noted that the pyrolysis at 500 °C increases significantly the C fraction in the char from 47.5 to 78.4 % while decreasing H (5.8 to 3.1 %), N (2.3 to 1.3 %) and O (44.1 to 15.5 %) contents. This result is due to the release of these elements within the form of gases and tars during the pyrolysis [32]. This also explains the increase of fixed carbon (60.2 %) and ash (5.7 %). Similarly, the HHV increases from 18.3 to 28.1 MJ/kg due to higher C fraction. Traces of K, Ca and P are found in the biomass and represent between 0.4 and 2.4 % in the char. It can be noticed that Mg is detected in BH-Char but not in the biomass since this element is more concentrated after pyrolysis and it is difficult to detect by X-ray fluorescence analysis [33].

Significant differences between BH-CO_2 and BH-H_2O are found as a result of the activation method as well as in their by-products (gas and condensable). The physical activation with CO_2 changes the char composition by boosting the percentage of C (83.3 %) while the activation with steam results in a lower C content (72.3 %). The activation with steam results also in higher O (11.8 % vs 8.4 %) and ash (11.2 % vs 7.9 %) contents in BH-H_2O compared to BH-CO_2. This results are in accordance with the reactions R 4 - R 6 [34], which show that the activation process releases H_2, CO_2 and CO. The high H_2 content (52 %) in the steam activation is justified by the partial gasification of BH with H_2O involving reactions R 4- R 47. On the other hand, the CO_2 activation produces mainly CO (20 %) according to reaction R 6. The methane production is observed during pyrolysis in both activations while the high content of CO_2 (75 %) is mostly due to the excess of injected CO_2 as oxidizing agent (70 %) in CO_2 activation.

H_2O Activation $\quad C + H_2O \rightarrow CO + H_2$ **R 4**

$\quad CO + H_2O \leftrightarrow H_2 + CO_2$ **R 47**

CO_2 Activation $\quad C + CO_2 \rightarrow 2CO$ **R 6**

The mineral compounds are mainly constituted of the potassium, calcium and magnesium which represent respectively 3.1, 2.4 and 1.4 % in BH-CO_2 and 3.9, 3.4 and 2.6 % in BH-H_2O. The K is the main mineral constituent in BH-CO_2 and BH-H_2O. Concerning the calcium, its lower content in BH-CO_2 compared to BH-H_2O seems indicated that under CO_2 atmosphere more Ca is released from the solid phase. In gasification processes conducted between 800 and 900 °C, the behavior of Ca and K has been already studied by many authors since these both elements can improve the production of gas, and its quality by increasing the H_2 concentration and reducing the formation of tars [35–38].

Bai et al. [38], demonstrated that K content in the coal char was not influenced by the gasification agent (steam or CO_2) at 800 °C. In the same way, they concluded that the calcium release depends on the oxidizing agent and is more volatilized during the CO_2 gasification. The activation under CO_2 is carried out with a partial pressure P_{CO2} close to 0.70 atm. During the steam activation some CO_2 is produced by the water gas shift reaction thus P_{CO2} is 0.08 atm and P_{H2O} is 0.12 atm at 850 °C as explained in Figure 6-3 (adapted from [37]). Therefore, the calcium in BH-CO_2 should be present within the $CaCO_3$ and CaO forms corresponding to the equilibrium curve and within the calcium oxide CaO in BH-H_2O. Knowing the melting point of this element which are at 825°C and 2613 °C for $CaCO_3$ and CaO respectively, we can explained the partial realeased of Ca during the CO_2 activation. Moreover the Ca compounds can agglomerate and sinter resulting in clusters whereas it presents an homogeneous surface distribution under steam gasification [38,39]. Another research team has stated that the active form which could destabilize the tars and lead to the fragmentation of the aromatic rings during the gasification

could be the calcium oxide CaO [37]. In the same way, it seems that more Mg is released in CO_2 activation which is in agreement with the work of Guizani *et al.*, [40].
According to Table 4, the activation process also influences the surface pH of BH-Char. The activation with CO_2 and steam lead to a basic character of BH-CO_2 and BH-H_2O (11.9 and 11.7 respectively) which is well known for physical activation [41]. These results can be explained by the release of acidic functional groups (carboxylic type, anhydride, etc) composed of O and H during pyrolysis at temperatures from 380 – 720 °C [42,43] and also by the presence of the alkaline oxides. And finally, the HHV of BH-CO_2 and BH-H_2O are not impacted by the activation mode with respective values of 29.2 and 27.7 MJ/kg.

3.1.2. Textural properties

The activation method induces great differences in the textural properties of activated chars as depicted in Table 6. The nitrogen gas adsorption isotherm analysis shows that the activation with steam creates a higher porosity than the activation with CO_2. The BET surface area and total pore volume of BH-H_2O reaches respectively 997 m^2/g and 0.681cm^3/g which are significantly higher compared to BH-CO_2 (578 m^2/g and 0.291 cm^3/g). Another difference consists in the balance of pores. The CO_2 activation develops 96 % of micropores (0.261 cm^3/g) while the steam activation creates higher porosity distributed in 71 % of micropores (0.419 cm^3/g) and 29 % of mesopores (0.175 cm^3/g). In agreement with the mercury porosimetry, BH-H_2O presents the highest porosity according to the total pore volume (0.938 cm^3/g) and the distribution is oriented to 25 % of mesopores and 75 % of macropores. This results must be seen as regard that mercury porosimetry allows only measuring a partial mesopore volume since this method this method measures the mesopores contained between 8 and 50 nm (according IUPAC $2 < V_{meso} < 50$ nm). The mesoporous volumes measured by the mercury porosimetry are ranged in the standard deviation of the volumes measured by the nitrogen gas adsorption isotherm analysis which confirms the well balance porosity of this sample. In the case of BH-CO_2, the total pore volume is much lower (0.555 cm^3/g) compared to BH-H_2O. The mesopore volume is again poor and is overestimated in comparison with the N_2 adsorption. These 2 techniques are based on different assumptions with different molecules (N_2 and Hg) that can create some disparities especially with low ranges. Another interest of this technique is to evaluate the porosity of pyrolysis chars reputed difficult by N_2 adsorption because of the lack of micropores and/or mesopores. The V_{Total} of BH-Char is quite high with 0.540 cm^3/g and leading to 80 % of macropores. This confirms that chars are known to be mainly macroporous [44] and allow to estimate a partly of the mesoporosity (0.111 cm^3/g) those contained between 8 and 50 nm. This latter is interesting since the N_2 adsorption/desorption isotherms are often incomplete because the hysteresis loop determining the mesoporosity is rarely close. The last parameter determined by the mercury porosimetry is the real density. BH-char has lower density (0.19 g/cm^3) than activated carbons (0.25 and 0.22 g/cm^3) due to the lower ash content of the first.

The higher surface area resulting from steam activation is in agreement with the work of other authors. Yang *et al.*, [45] reported that the activation of walnut shells with H_2O or CO_2 under the same conditions led to activated carbons with higher surface area (771 m^2/g) and pore volume (V_{total} = 0.499 cm^3/g) with steam activation than CO_2 activation (552 m^2/g and 0.293 cm^3/g respectively). The same trend was reported by Guizani *et al.*, [40] in the gasification of chars under steam or CO_2. They demonstrated that for the same char conversion degree (i.e. 50 %), H_2O-chars presented higher surface area (1225 m^2/g) and pore volume than CO_2-chars (842 m^2/g). Some authors have also shown that the CO_2 activation creates mainly microporosity while the steam activation results in a higher degree of mesoporosity [46] with a better balance between micro- and meso-pores since in this case the mechanism of porosity development consists in increasing the pore depth and the pore diameter [47].

3.2. Mass and energy balances of pyrolysis and activation processes

The mass and energy balances of pyrolysis and activations are calculated to evaluate the process efficiency in terms of energy recovery (Table 7). The mass balances of the pyrolysis and the H_2O activation are ranged between 79 and 85 %. The mass loss is mainly due to incomplete bio-oil recovery, notably light tars and steam in the cold trap and consequently not taken into account in the calculation. In the literature, it is specified that the mass loss is contained between 7 and 20 wt% [48]. The mass balance of the CO_2 activation is complete which means that all the byproducts are considered. The NER of the pyrolysis conducted at 500 °C is close to 1.5. The energy held by the char, the oily liquid phase and the gas is consequently higher than the electrical energy required for the heating. Gaunt and Lehmann, [49] have reported higher NER from 2 to 7 dedicated to slow pyrolysis but in that case, the latent heat of the gas was recovered in order to decrease the electrical consumption. In this study, the gas phase has a low LHV (6 MJ/kg) due to its high content in CO_2 (58 % of the produced gas) but it represents close to 25 % of the byproducts. Moreover the degradation of lignin accounting for 27 % in BH (Table 4), is high energy demanding since this molecule starts decomposing at 400 - 550 °C [26]. Nevertheless, the pyrolysis char that represents 38 % of the byproducts, still contents most of the energy coming from the biomass with a LHV of 27.5 MJ/kg. Even if the materials produced from both activations exhibit high added values as activated carbons, the NER of these processes conducted at 850 °C are very low (0.29 and 0.13). This can be explained by the energy demand for the heating which is very high and close to 30 MJ for 1 kg of biomass and since no energy recovery is made at the laboratory scale with the latent heat of the gas phase. Regarding the CO_2 activation, it can be noted that the CO_2 is in large excess leading to 75 % of the produced gas (Table 66) which totally collapses the LHV of the gas phase. As far as the H_2O activation is concerned, the steam excess is found in the liquid phase with a poor LHV of 5.7 MJ/kg. However the composition of the gas phase has a H_2/CO ratio close to 2 and is quite interesting to serve as precursor for Fischer Tropsch process [50].

3.3. Catalytic cracking experiments

The breakthrough curves of ethylbenzene (EB) through a fixed bed of BH-Char, BH-CO_2 or BH-H_2O are presented in Figure 6-4. They have been obtained with an initial concentration of 40 g/Nm^3 in EB at 650 °C. In order to evaluate the participation of the thermal cracking in the catalytic cracking process, the experiment is carried out with an empty column (black curve in Figure 6-4). The EB concentration in the outlet gas starts rising at t = 2 min and is stabilized after 160 min at C_t = 0.6 C_0 which means that 40 % of ethylbenzene is thermally cracked in these conditions. The breakthrough curve obtained with the pyrolysis char shows that BH-Char loses its reactivity after 13 min when the concentration of EB starts to increase (Figure 6-4). This curve is then close to the thermal cracking which implies that this sample does not present any performance to improve the degradation of EB. This observation is confirmed by the calculation of EB conversion at 60, 100 and 180 min (Figure 6-5): X_{EB} is negative with respective values of -0.024, -0.036, -0.062 g_{EB}/g_{char} which means that the EB removal is lower or equal than the thermal cracking considering the deviation of the last one. This may be due to the char porosity restricted to macropores which are too width to adsorb a molecule as EB with a critical diameter close to 0.663 nm [51]. According to the literature, the pore diameters close to the molecular diameter of the adsorbate are more reactive due to the beneficial intermolecular attraction forces [30]. Other similar results have been reported for the cracking of naphthalene [30] and benzene [29] where the pyrolysis chars demonstrated a lower tar conversion than the thermal cracking. All these investigations seem denote that raw pyrolysis chars are not suitable for tar catalytic cracking.

As far as activated carbons are concerned, Figure 6-4 shows that the breakthrough is delayed to 18 min with BH-CO_2 and 22 min with BH-H_2O and that BH-H_2O develops a clearly higher performance of EB cracking. The tar conversion is confirmed by where it reaches 0.951 $g_{EB}/g_{BH\text{-}H2O}$ and 0.502 $g_{EB}/g_{BH\text{-}CO2}$ at t = 180 min. It can be noted that the experiment has been stopped at 180 min in order to compare the different materials. The breakthrough curve of BH-CO_2 meets

the plateau of the thermal cracking around 140 min which is not the case of BH-H_2O. This means that the performance of BH-H_2O is clearly higher if the experiment lasts longer than 180 min. The superiority of BH-H_2O can be due to many factors. On one hand, this activated carbon presents the highest microporous volume which serves as active sites for the EB removal. Secondly BH-H_2O also possesses some mesoporosity which is known to favor the mass transfer to the microporosity. This trend is observed by Hosokai et al., [52] during the benzene and naphthalene conversion over charcoal. It is also probable that the mesopores do not contribute directly to the tar conversion, but they are responsible for the long-time stability of the char. And BH-CO_2 would be then lacking of micropores to be likewise attractive. On the other hand, the superiority of BH-H_2O can also be explained by its mineral composition. It has been shown that the main mineral constituent is the calcium (5.8 %, Table 4) and that the likely active form is CaO which is known to destabilize the tars [31]. In BH-CO_2, the calcium content is lesser (1.9 %) and the forms would be CaO (50 %) and $CaCO_3$ (50 %). Activated carbons developing micro and mesopores and provided with calcium, in particular within the form of CaO, appear to be attractive materials for the catalytic cracking of tars.

3.4. Catalyst deactivation

The heterogeneous conversion of tar molecules over chars leads to release of H_2 and to a deposition of coke on the surface of samples [30,31]. This carbon deposit has been related to the loss of reactivity and reduces the porous volume of materials. This deactivation has been verified on the BH-Char: it has lost 30 % of its weight during the experiment (Table 69) and this can be attributed to a partial gasification. This assumption has been verified by an experiment (data not shown) carried out with the column filled with BH-Char at 650 °C under syngas atmosphere (N_2, CO) without ethylbenzene. The porosity has also decreased: -26 % and -36 % on the macroporous and mesoporous volumes respectively. These changes are also noticeable with BH-CO_2 and BH-H_2O. BH-Char and BH-CO_2 have similar decrease of porous volume while BH-H_2O presents the lowest decrease, the highest weight gain (+16 %) and highest efficiency of BH-H_2O which is 1.9 times compared to BH-CO_2 at 180 min. In addition, it could be noted that the LHV of used activated carbons remains unchanged. Consequently, it seems that BH-H_2O is more resistant to the deactivation and exhibits a longer lifetime.

4. Conclusions and outlook

This paper investigated the catalytic activity of pyrolysis chars produced from BH in the cracking of ethylbenzene as a model of the light aromatic compounds, and highlighted the impact of the oxidizing agent used to activate the char (steam or carbon dioxide). The physical activation of pyrolyisis chars modifies their chemical and textural characteristics. The CO_2 activation provides activated carbons with more carbon and less ash content compared to steam activation. Indeed, the activation agent influences the volatilization of mineral elements from the solid phase: with CO_2, more Ca and Mg are released and the calcium compounds remaining in the solid phase are found like CaO and $CaCO_3$ forms. CO_2 activation results also in a higher relative microporosity (89 %) than activation with steam (61 %) whereas the steam activation allows reaching the higher surface area. In terms of energy efficiency, the slow pyrolysis presents a higher NER compared to the activations in the case of our study.

The pyrolysis char has not demonstrated any interest in the EB catalytic cracking whereas the activated carbons have highlighted higher performances. This is due to their porosity which is more developed and their higher ash content. The porosity seems to be an important parameter in the tar cracking since BH-H_2O, which presents the higher porosity, has developed a better catalytic effect and was more resistant to the deactivation. Indeed, the EB catalytic conversion reaches 0.951 $g_{EB}/g_{BH\text{-}H2O}$ after 180 min of treatment. BH-H_2O would be a promising activated carbon for the catalytic cracking of tars if the energy efficiency of its production is optimized. In

a biorefinery frame, it can be taken advantage of the gas phase composition in Fischer Tropsch synthesis or recover the latent heat of this gas phase to meet the energy demand or recover the energy hold in used activated carbon.
ACs are amorphous carbonaceous materials (80-95 % of carbon) characterized by high surface area (500 to 2000 m^2/g), microporous structure, and high degree of surface reactivity [53]. Thus, on the basis of their characteristics, BH-H_2O and BH-CO_2 have all the qualities to be considered as activated carbons. During ACs production, raw materials undergo a first carbonization process (or pyrolysis), then a physical activation is conducted. The physical activation can be seen as a partial gasification; thus the chars of pyrogasification can be considered as activated carbons. Regarding the results of this study and considering that the pyrogasification is similar to a pyrolysis follows by a physical activation; it seems more interesting to use the chars from pyro-gasification than pyrolysis to crack the tars in syngas.

5. Acknowledgements

The authors would like to thank L'Agence de l'Environnement et de la Maîtrise de l'Energie (ADEME) and Region Pays de la Loire for their financial support which allowed the development of this study.

6. References

[1] V. Benedetti, F. Patuzzi, M. Baratieri, Gasification Char as a Potential Substitute of Activated Carbon in Adsorption Applications, Energy Procedia. 105 (2017) 712–717. doi:https://doi.org/10.1016/j.egypro.2017.03.380.

[2] V. Benedetti, F. Patuzzi, M. Baratieri, Characterization of char from biomass gasification and its similarities with activated carbon in adsorption applications, Appl. Energy. 227 (2018) 92–99. doi:https://doi.org/10.1016/j.apenergy.2017.08.076.

[3] T.A. Milne, R.J. Evans, Biomass Gasifier " Tars ": Their Nature , Formation , and Conversion Biomass Gasifier " Tars ": Their Nature , Formation , and Conversion, (1998).

[4] A. Villot, Y. Gonthier, E. Gonze, A. Bernis, S. Ravel, M. Grateau, J. Guillaudeau, Separation of particles from syngas at high-temperatures with an electrostatic precipitator, Sep. Purif. Technol. 92 (2012) 181–190. doi:https://doi.org/10.1016/j.seppur.2011.04.028.

[5] N. Abdoulmoumine, S. Adhikari, A. Kulkarni, S. Chattanathan, A review on biomass gasification syngas cleanup, Appl. Energy. 155 (2015) 294–307. doi:10.1016/j.apenergy.2015.05.095.

[6] R. Coll, J. Salvadó, X. Farriol, D. Montané, Steam reforming model compounds of biomass gasification tars: conversion at different operating conditions and tendency towards coke formation, Fuel Process. Technol. 74 (2001) 19–31. doi:10.1016/S0378-3820(01)00214-4.

[7] P.J. Woolcock, R.C. Brown, A review of cleaning technologies for biomass-derived syngas, Biomass and Bioenergy. 52 (2013) 54–84. doi:10.1016/j.biombioe.2013.02.036.

[8] S.A. Nair, A.J.M. Pemen, K. Yan, F.M. van Gompel, H.E.M. van Leuken, E.J.M. van Heesch, K.J. Ptasinski, A.A.H. Drinkenburg, Tar removal from biomass-derived fuel gas by pulsed corona discharges, Fuel Process. Technol. 84 (2003) 161–173. doi:https://doi.org/10.1016/S0378-3820(03)00053-5.

[9] S. Mani, J.R. Kastner, A. Juneja, Catalytic decomposition of toluene using a biomass derived catalyst, Fuel Process. Technol. 114 (2013) 118–125. doi:10.1016/j.fuproc.2013.03.015.

[10] Z. Abu El-Rub, E.A. Bramer, G. Brem, Experimental comparison of biomass chars with other catalysts for tar reduction, Fuel. 87 (2008) 2243–2252. doi:10.1016/j.fuel.2008.01.004.

[11] Y. Shen, P. Zhao, Q. Shao, D. Ma, F. Takahashi, K. Yoshikawa, In-situ catalytic conversion of tar using rice husk char-supported nickel-iron catalysts for biomass pyrolysis/gasification, Appl. Catal. B Environ. 152–153 (2014) 140–151. doi:10.1016/j.apcatb.2014.01.032.

[12] Y. Zhang, S. Kajitani, M. Ashizawa, Y. Oki, Tar destruction and coke formation during rapid pyrolysis and gasification of biomass in a drop-tube furnace, Fuel. 89 (2010) 302–309. doi:https://doi.org/10.1016/j.fuel.2009.08.045.

[13] M. Bläsing, M. Müller, Investigations on the influence of steam on the release of sodium, potassium, chlorine, and sulphur species during high temperature gasification of coal, Fuel. (2011).

[14] M. Hervy, S. Berhanu, E. Weiss-Hortala, A. Chesnaud, C. Gérente, A. Villot, D. Pham Minh, A. Thorel, L. Le Coq, A. Nzihou, Multi-scale characterisation of chars mineral species for tar cracking, Fuel. 189 (2017) 88–97. doi:10.1016/j.fuel.2016.10.089.

[15] A.N. M. Hervy, C. Gerente, A. Villot, L. Le-Coq, E. Weiss-Hortala, D. Pham Minh, Recycling of pyrolysis chars from food waste, wastewater treatment sludge and wood for the syngas purification, in: R.D.T. and A.S. J.W.C. Wong, M. Nelles (Ed.), Int. Conf. Solid Waste – Knowl. Transf. Sustain. Resour. Manag., 2015.

[16] M. Hervy, A. Villot, C. Gérente, D. Pham Minh, E. Weiss-Hortala, A. Nzihou, L. Le Coq, Catalytic cracking of ethylbenzene as tar surrogate using pyrolysis chars from wastes, Biomass and Bioenergy. 117 (2018) 86–95. doi:https://doi.org/10.1016/j.biombioe.2018.07.020.

[17] K. Lazdovica, V. Kampars, L. Liepina, M. Vilka, Comparative study on thermal pyrolysis of buckwheat and wheat straws by using TGA-FTIR and Py-GC/MS methods, J. Anal. Appl. Pyrolysis. (2017) 1–15. doi:10.1016/j.jaap.2017.03.010.

[18] E. Mura, O. Debono, A. Villot, F. Paviet, Pyrolysis of biomass in a semi-industrial scale reactor: Study of the fuel-nitrogen oxidation during combustion of volatiles, Biomass and Bioenergy. (2013). doi:10.1016/j.biombioe.2013.09.001.

[19] J. Torres-Pérez, C. Gérente, Y. Andrès, Sustainable Activated Carbons from Agricultural Residues Dedicated to Antibiotic Removal by Adsorption, Chinese J. Chem. Eng. 20 (2012) 524–529. http://www.sciencedirect.com/science/article/pii/S1004954111602140.

[20] J. Torres-Perez, C. Gerente, Y. Andres, Conversion of agricultural residues into activated carbons for water purification: Application to arsenate removal, J. Environ. Sci. Heal. - Part A Toxic/Hazardous Subst. Environ. Eng. 47 (2012) 1173–1185. doi:10.1080/10934529.2012.668390.

[21] P. Lodeiro, S.M. Kwan, J.T. Perez, L.F. González, C. Gérente, Y. Andrès, G. McKay, Novel Fe loaded activated carbons with tailored properties for As(V) removal: Adsorption study correlated with carbon surface chemistry, Chem. Eng. J. 215–216 (2013) 105–112. doi:10.1016/j.cej.2012.11.052.

[22] M.M. Diémé, M. Hervy, S.N. Diop, C. Gérente, A. Villot, Y. Andres, C.K. Diawara, Sustainable Conversion of Agriculture and Food Waste into Activated Carbons Devoted to Fluoride Removal from Drinking Water in Senegal, Int. J. Chem. 8 (2015) 8. doi:10.5539/ijc.v8n1p8.

[23] M.M. Dieme, A. Villot, C. Gerente, Y. Andres, S.N. Diop, C.K. Diawara, Sustainable conversion of agriculture wastes into activated carbons: energy balance and arsenic

removal from water, Environ. Technol. 3330 (2016) 1–8. doi:10.1080/09593330.2016.1193225.

[24] I. Galan, F.P. Glasser, C. Andrade, Calcium carbonate decomposition, J. Therm. Anal. Calorim. 111 (2013) 1197–1202. doi:10.1007/s10973-012-2290-x.

[25] P.G. González, T. Hernández, L. García, The use of experimental design and response surface methodologies for the synthesis of chemically activated carbons produced from bamboo, Fuel Process. Technol. 127 (2014) 133–139. doi:10.1016/j.fuproc.2014.05.035.

[26] J.F. Saldarriaga, R. Aguado, A. Pablos, M. Amutio, M. Olazar, J. Bilbao, Fast characterization of biomass fuels by thermogravimetric analysis (TGA), Fuel. 140 (2015) 744–751. doi:10.1016/j.fuel.2014.10.024.

[27] J.A. Conesa, A. Domene, Biomasses pyrolysis and combustion kinetics through n-th order parallel reactions, Thermochim. Acta. 523 (2011) 176–181. doi:10.1016/j.tca.2011.05.021.

[28] M. Shahbaz, S. yusup, A. Inayat, D.O. Patrick, M. Ammar, The influence of catalysts in biomass steam gasification and catalytic potential of coal bottom ash in biomass steam gasification: A review, Renew. Sustain. Energy Rev. 73 (2017) 468–476. doi:10.1016/j.rser.2017.01.153.

[29] L. Burhenne, T. Aicher, Benzene removal over a fixed bed of wood char: The effect of pyrolysis temperature and activation with CO2 on the char reactivity, Fuel Process. Technol. 127 (2014) 140–148. doi:10.1016/j.fuproc.2014.05.034.

[30] F. Nestler, L. Burhenne, M.J. Amtenbrink, T. Aicher, Catalytic decomposition of biomass tars: The impact of wood char surface characteristics on the catalytic performance for naphthalene removal, Fuel Process. Technol. 145 (2016) 31–41. doi:10.1016/j.fuproc.2016.01.020.

[31] Y. Zhang, W. Wu, S. Zhao, Y. Long, Y. Luo, Experimental study on pyrolysis tar removal over rice straw char and inner pore structure evolution of char, Fuel Process. Technol. 134 (2015) 333–344. doi:10.1016/j.fuproc.2015.01.047.

[32] M.A. Yahya, Z. Al-Qodah, C.W.Z. Ngah, Agricultural bio-waste materials as potential sustainable precursors used for activated carbon production: A review, Renew. Sustain. Energy Rev. 46 (2015) 218–235. doi:10.1016/j.rser.2015.02.051.

[33] K.E. Young, C.A. Evans, K. V. Hodges, J.E. Bleacher, T.G. Graff, A review of the handheld X-ray fluorescence spectrometer as a tool for field geologic investigations on Earth and in planetary surface exploration, Appl. Geochemistry. 72 (2016) 77–87. doi:10.1016/j.apgeochem.2016.07.003.

[34] P. Mondal, G.S. Dang, M.O. Garg, Syngas production through gasification and cleanup for downstream applications - Recent developments, Fuel Process. Technol. 92 (2011) 1395–1410. doi:10.1016/j.fuproc.2011.03.021.

[35] Y. Huang, X. Yin, C. Wu, C. Wang, J. Xie, Z. Zhou, L. Ma, H. Li, Effects of metal catalysts on CO2gasification reactivity of biomass char, Biotechnol. Adv. 27 (2009) 568–572. doi:10.1016/j.biotechadv.2009.04.013.

[36] C. Dupont, S. Jacob, K.O. Marrakchy, C. Hognon, M. Grateau, F. Labalette, D. Da Silva Perez, How inorganic elements of biomass influence char steam gasification kinetics, Energy. 109 (2016) 430–435. doi:10.1016/j.energy.2016.04.094.

[37] C. Shuai, S. Hu, L. He, J. Xiang, L. Sun, S. Su, L. Jiang, Q. Chen, C. Xu, The synergistic effect of Ca(OH)2 on the process of lignite steam gasification to produce hydrogen-rich gas, Int. J. Hydrogen Energy. 39 (2014) 15506–15516. doi:10.1016/j.ijhydene.2014.07.111.

[38] Y. Bai, S. Zhu, K. Luo, M. Gao, L. Yan, F. Li, Coal char gasification in H2O/CO2 : Release of

alkali and alkaline earth metallic species and their effects on reactivity, Appl. Therm. Eng. 112 (2017) 156–163. doi:10.1016/j.applthermaleng.2016.10.044.

[39] M. Gao, Z. Yang, Y. Wang, Y. Bai, F. Li, K. Xie, Impact of calcium on the synergistic effect for the reactivity of coal char gasification in H2O/CO2 mixtures, Fuel. 189 (2017) 312–321. doi:10.1016/j.fuel.2016.10.100.

[40] C. Guizani, M. Jeguirim, R. Gadiou, F.J. Escudero Sanz, S. Salvador, Biomass char gasification by H2O, CO2and their mixture: Evolution of chemical, textural and structural properties of the chars, Energy. 112 (2016) 133–145. doi:10.1016/j.energy.2016.06.065.

[41] P. Nowicki, J. Kazmierczak, R. Pietrzak, Comparison of physicochemical and sorption properties of activated carbons prepared by physical and chemical activation of cherry stones, Powder Technol. 269 (2015) 312–319. doi:10.1016/j.powtec.2014.09.023.

[42] M. Ducousso, E. Weiss-Hortala, A. Nzihou, M.J. Castaldi, Reactivity enhancement of gasification biochars for catalytic applications, Fuel. 159 (2015) 491–499. doi:10.1016/j.fuel.2015.06.100.

[43] N.B. Klinghoffer, M.J. Castaldi, A. Nzihou, Influence of char composition and inorganics on catalytic activity of char from biomass gasification, Fuel. 157 (2015) 37–47. doi:10.1016/j.fuel.2015.04.036.

[44] C.E. Brewer, V.J. Chuang, C.A. Masiello, H. Gonnermann, X. Gao, B. Dugan, L.E. Driver, P. Panzacchi, K. Zygourakis, C.A. Davies, New approaches to measuring biochar density and porosity, Biomass and Bioenergy. 66 (2014) 176–185. doi:10.1016/j.biombioe.2014.03.059.

[45] L. Yang, T. Huang, X. Jiang, W. Jiang, Effect of steam and CO2 activation on characteristics and desulfurization performance of pyrolusite modified activated carbon, Adsorption. 22 (2016) 1099–1107. doi:10.1007/s10450-016-9832-7.

[46] T. Yang, A.C. Lua, Characteristics of activated carbons prepared from pistachio-nut shells by potassium hydroxide activation, Microporous Mesoporous Mater. 63 (2003) 113–124. doi:10.1016/S1387-1811(03)00456-6.

[47] M. Ruiz-Fernández, M. Alexandre-Franco, C. Fernández-González, V. Gómez-Serrano, Development of activated carbon from vine shoots by physical and chemical activation methods. Some insight into activation mechanisms, Adsorption. 17 (2011) 621–629. doi:10.1007/s10450-011-9347-1.

[48] J. Park, Y. Lee, C. Ryu, Y.-K. Park, Slow pyrolysis of rice straw: Analysis of products properties, carbon and energy yields, Bioresour. Technol. 155 (2014) 63–70. doi:10.1016/j.biortech.2013.12.084.

[49] J.L. Gaunt, J. Lehmann, Energy balance and emissions associated with biochar sequestration and pyrolysis bioenergy production, Environ. Sci. Technol. 42 (2008) 4152–4158. doi:10.1021/es071361i.

[50] M.I. Jahirul, M.G. Rasul, A.A. Chowdhury, N. Ashwath, Biofuels production through biomass pyrolysis- A technological review, Energies. 5 (2012) 4952–5001. doi:10.3390/en5124952.

[51] M.M. Hossain, L. Atanda, N. Al-Yassir, S. Al-Khattaf, Kinetics modeling of ethylbenzene dehydrogenation to styrene over a mesoporous alumina supported iron catalyst, Chem. Eng. J. 207–208 (2012) 308–321. doi:10.1016/j.cej.2012.06.108.

[52] S. Hosokai, K. Kumabe, M. Ohshita, K. Norinaga, C.Z. Li, J. ichiro Hayashi, Mechanism of decomposition of aromatics over charcoal and necessary condition for maintaining its activity, Fuel. 87 (2008) 2914–2922. doi:10.1016/j.fuel.2008.04.019.

[53] H. Marsh, F. Rodríguez-Reinoso, CHAPTER 4 - Characterization of Activated Carbon, in: H.

Marsh, F.B.T.-A.C. Rodríguez-Reinoso (Eds.), Elsevier Science Ltd, Oxford, 2006: pp. 143–242. doi:https://doi.org/10.1016/B978-008044463-5/50018-2.

Table 4. Chemical characterization of materials.

Analysis	Composition	BH	BH-Char	BH-CO_2	BH-H_2O
Ultimate analysis (wt.%)	C	47.5 ± 0.6	78.4 ± 1.0	83.3 ± 0.3	72.3 ± 1.9
	H	5.8 ± 0.3	3.1 ± 0.1	1.1 ± 0.1	0.9 ± 0.2
	N	2.3 ± 0.8	1.3 ± 0.2	1.5 ± 0.1	1.7 ± 0.2
	S	n.d	n.d	n.d	n.d
	O	44.1 ± 1.1	15.5 ± 0.8	8.4 ± 0.5	11.8 ± 0.6
Thermogravimetric analysis (wt.%)	Cellulose	20,4	*	*	*
	Hemicellulose	18,5	*	*	*
	Lignin	27	*	*	*
Proximate analysis (wt.%)	Moisture	12.5 ± 0.1	5.4 ± 0.1	0.9 ± 0.0	6.3 ± 0.5
	Volatile matter	66.9 ± 0.6	28.7 ± 0.6	29.1 ± 0.2	52.1 ± 0.8
	Fixed carbon	18.1 ± 0.7	60.2 ± 0.6	62.2 ± 0.3	30.3 ± 1.1
	Ash	2.6 ± 0.1	5.7 ± 0.1	7.9 ± 0.1	11.2 ± 0.2
Main mineral composition (wt.%)	K	Trace	2.4 ± 0.1	3.1 ± 0.1	3.9 ± 0.2
	Ca	Trace	1.5 ± 0.1	2.4 ± 0.1	3.4 ± 0.1
	P	Trace	0.4 ± 0.1	0.8 ± 0.1	0.8 ± 0.1
	Mg	n.d	0.8 ± 0.1	1.4 ± 0.1	2.6 ± 0.1
High heating values (MJ/kg)	HHV	18.3 ± 0.2	28.1 ± 0.6	29.2 ± 0.2	27.7 ± 0.9
pH_{pzc}		*	5,7	11,9	11,7

*n.d: non-detectable. *Not valid for this material*

Table 66. Composition of produced gas in pyrolysis and activation processes.

Process	H_2 (mol.%)	CH_4 (mol.%)	CO (mol.%)	CO_2 (mol.%)	C_xH_y (mol.%)
Pyrolysis (500 °C)	2	11	25	58	5
CO_2 Activation (850 °C)	3	1	20	75*	0
H_2O Activation (850 °C)	52	4	25	19	0.4

**The high content of CO_2 is due to the injected CO_2 as oxidizing agent (70 %) in CO_2 activation*

Table 6. Textural properties of fresh materials.

Analysis	Parameter	BH-Char	BH-CO_2	BH-H_2O
N_2 Adsorption /Desorption	V_{Total} (cm^3/g)	*	0.291 ± 0.011	0.681 ± 0.136
	V_{Micro} (cm^3/g)	*	0.261 ± 0.004	0.419 ± 0.010
	V_{Meso} (cm^3/g)	*	0.012 ± 0.010	0.175 ± 0.083
	BET Surface (m^2/g)	*	578 ± 4	997 ± 81
Mercury porosimetry	V_{Total} (cm^3/g)	0.540 ± 0.084	0.555 ± 0.092	0.938 ± 0.069
	V_{Meso} (cm^3/g)	0.111 ± 0.012	0.070 ± 0.004	0.226 ± 0.006
	V_{macro} (cm^3/g)	0.421 ± 0.072	0.480 ± 0.088	0.688 ± 0.084
	ρ_{real} (g/cm^3)	0.191 ± 0.018	0.247 ± 0.013	0.216 ± 0.005

*Micro: D_p< 2 nm; Meso: 2 < D_p < 50 nm; Macro: D_p > 50 nm.*Not valid for this material. The V_{meso} giving by the mercury porosimetry is incomplete since the measure is conducted between 8 and 50 nm.*

Table 7. Mass and energy balances of pyrolysis and activation processes.

		BH-CO_2 (2-step)			BH-CO_2 (1-step)			MH-CO_2 (2-step)			MH-CO_2 (1-step)		
		Mass fraction (wt.%)	**LHV (MJ/Kg)**	**Energy ($MJ/Kg_{Biomass}$)**	**Mass fraction (wt.%)**	**LHV (MJ/Kg)**	**Energy ($MJ/Kg_{Biomass}$)**	**Mass fraction (wt.%)**	**LHV (MJ/Kg)**	**Energy ($MJ/Kg_{Biomass}$)**	**Mass fraction (wt.%)**	**LHV (MJ/Kg)**	**Energy ($MJ/Kg_{Biomass}$)**
Inlet	Biomass	100	16.8 ± 0.2		100	16.8 ± 0.2		100	17.1 ± 0.8		100	17.1 ± 0.8	
	Electrical consumption		-	38	-	-	30.2			37.9	-	-	29.7
Outlet	AC	5.0± 0.4	28.3 ± 0.2	1.4 ± 0.1	5.7 ± 0.1	29.2 ± 0.6	1.7 ± 0.1	5.8 ± 0.4	18.7 ± 0.5	1.1 ± 0.1	7.0 ± 0.3	17.7 ± 0.1	1.23 ± 0.05
	Aqueous phase	3.3	0	0	1.9	0	0	3.7	0	0.0	1.7	0	0
	Oily phase	0.4	23.06 ± 0.25	0.2	0.8	20.76 ± 0.12	0.2	1.4	10.02	0.1	0.7	24.00	0.2
	Gas	67.8 ± 0.6	2.9 ± 0.3	2.0 ± 0.2	91.6 ± 1.8	2.2 ± 0.1	2.0 ± 0.1	56.8 ± 5.3	2.6 ± 0.6	1.5 ± 0.2	78.2 ± 1.2	1.82 ± 0.03	1.42 ± 0.01
Performance indicators:	**Target products:**	**Oil and gas**	**AC, oil and gas**		**Oil and gas**	**AC, oil and gas**		**Oil and gas**	**All**		**Oil and gas**	**AC, oil and gas**	
	AEE*	**12.4 ± 0.6 %**	**20.8 ± 0.8 %**		**13.1 ± 0.2 %**	**23.0 ± 0.2 %**		**9.3 ± 1.0 %**	**15.7 ± 1.2 %**		**9.35 ± 0.01 %**	**16.5 ± 0.3 %**	
	AEE elec**	**3.8 ± 0.3 %**	**6.4 ± 0.4 %**		**4.7 ± 0.1 %**	**8.2 ± 0.2 %**		**2.9 ± 0.5 %**	**4.9 ± 0.6 %**		**3.42 ± 0.02 %**	**5.3 ± 0.1 %**	
	NER***		**0.092 ± 0.013**		**-**	**0.128 ± 0.001**			**0.071 ± 0.009**		**-**	**0.095 ± 0.002**	

**Energy in MJ calculated for 1 kg of biomass*

Table 69. Change of porous volume and weight of samples after EB conversion at 650 °C and EB = 40 g/Nm^3.

Analysis	**Parameter**	**BH-Char**	**BH-CO_2**	**BH-H_2O**
Mercury porosimetry	ΔV_{Total} (%)	-28	-31	-12
	ΔV_{Meso} (%)	-36	-12	-22
	ΔV_{macro} (%)	-26	-34	-7
Weight variation	Δm (wt.%)	-30	+4	+16

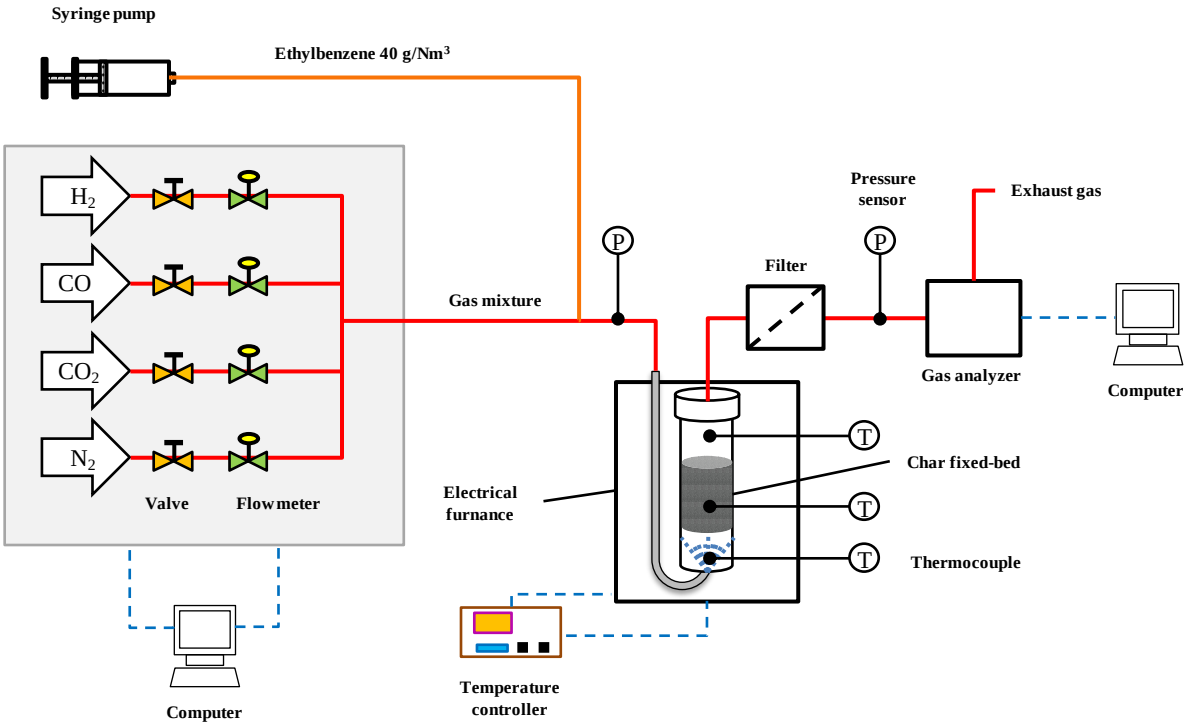

Figure 6-1. Experimental configuration of syngas treatment pilot.

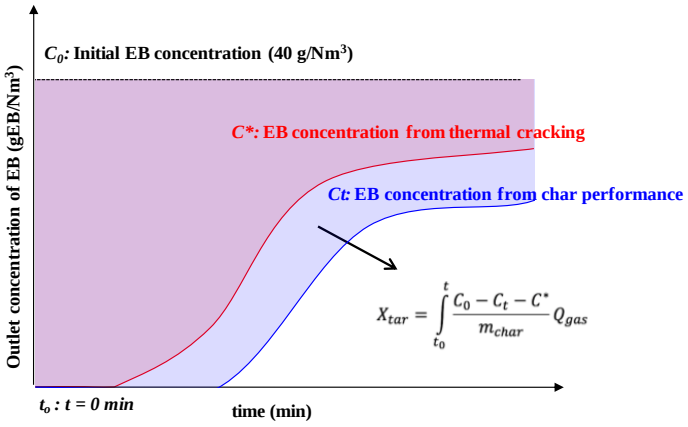

Figure 6-2. Calculation method of performance defined as tar conversion due to presence of chars.

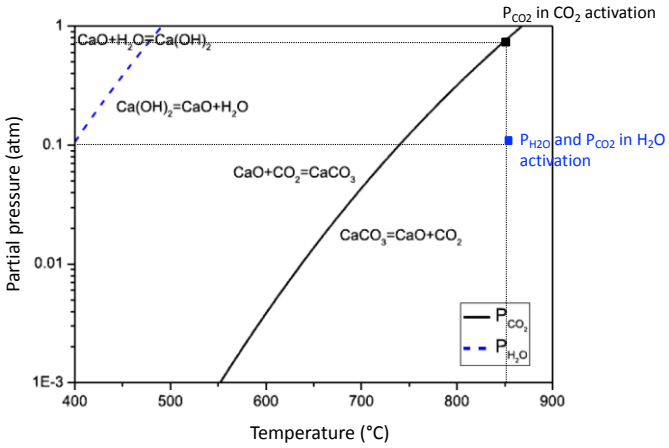

Figure 6-3. Reactions of $Ca(OH)_2$ and $CaCO_3$ in function of partial pressure of H_2O and CO_2 taken from [37]. In our work: in CO_2 activation P_{CO2} = 0.70 atm; Steam activation P_{CO2} = 0.085 atm and P_{H2O} = 0.12 atm at 850 °C.

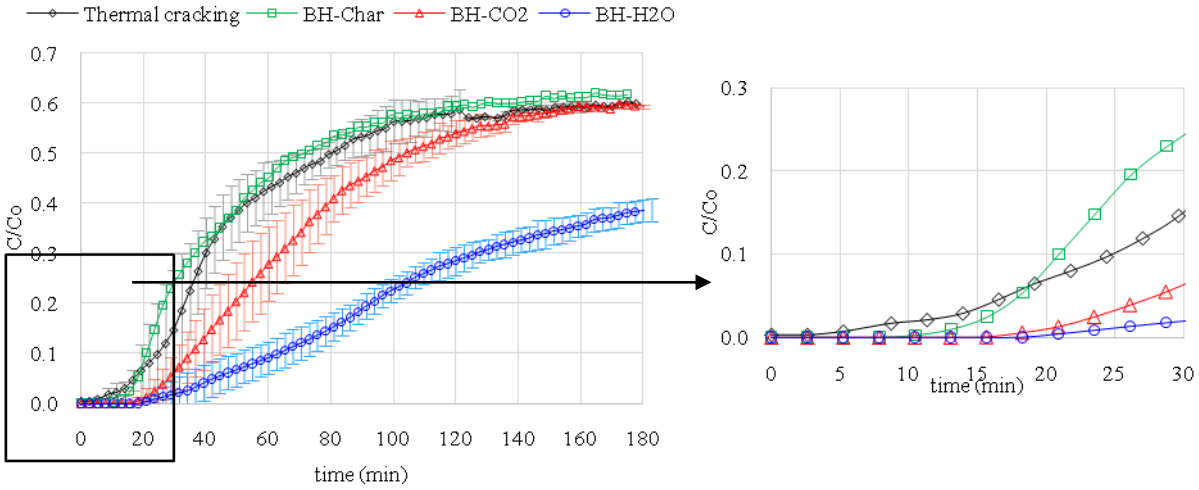

Figure 6-4. Removal of ethylbenzene due to thermal cracking and materials over time at 650 °C, EB = 40 g/Nm³.

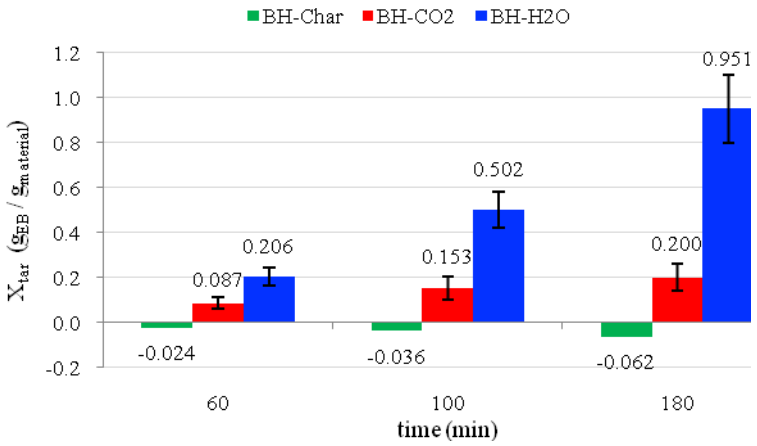

Figure 6-5. Performance of materials to crack ethylbenzene apart from thermal cracking at 650 °C, EB = 40 g/Nm³.

UNIVERSITE BRETAGNE SCIENCES LOIRE POUR L'INGENIEUR

IMT Atlantique
Bretagne-Pays de la Loire
École Mines-Télécom

Titre : Valorisation énergétique et matière de chars issus de biomasses résiduelles

Mots clés : activation, bilan énergétique, biomasse, chars, économie circulaire, épuration de gaz, pyrolyse.

Résumé : L'objectif de la thèse est d'étudier la valorisation des chars de biomasse. Dans ce contexte de transition énergétique, les biomasses sélectionnées sont les écales de sarrasin et de millet, assez peu étudiées jusqu'à maintenant, produites localement pour contribuer au développement de l'économie circulaire et qui ne compromettent pas une filière de valorisation connue. Dans ce travail, la valorisation matière est abordée à travers la réutilisation de ces résidus dans des procédés d'épuration catalytique de syngaz ou d'épuration de biogaz pour lesquels les polluants sont respectivement les goudrons et le sulfure d'hydrogène. Des bilans énergétiques relatifs à la production de ces chars ont été établis et des indicateurs d'efficacité énergétiques ont été calculés. Pour ce faire, les chars ont été produits à 500 °C puis caractérisés par des analyses chimiques et physiques. Afin de leur conférer de meilleures propriétés poreuses nécessaires pour les applications d'épuration de gaz en lit fixe, des activations ont été réalisées à 850 °C avec du CO_2 ou de la vapeur d'eau. Les écales de sarrasin se révèlent être une biomasse assez classique et la particularité des écales de millet est de présenter des taux élevés en silicium. Si les chars de pyrolyse ont montré une efficacité faible dans l'épuration des gaz, l'activation leur ouvre de nouvelles potentialités, notamment pour les écales de sarrasin qui s'apparentent alors à des charbons actifs. Les chars des écales de sarrasin démontrent leur intérêt lorsqu'ils sont activés à la vapeur d'eau pour la purification du syngaz et ils conservent leur pouvoir calorifique (PCI) que permet d'envisager une valorisation énergétique par gazéification. Ces résultats montrent également qu'en fonction de la nature de la biomasse et du type d'activation, les objectifs de valorisation matière et énergie sont parfois incompatibles.

Title : Study of chars prepared from biomass wastes: material and energy recovery

Keywords: activation, energy balance, biomass, chars, circular economy, gas purification, pyrolysis.

Abstract : The aim of the thesis is to study the valorization of chars prepared from biomass wastes. In this context of energy transition, the selected biomasses are the buckwheat and millet husks since they are barely studied until now. In addition these wastes are produced locally, contribute to the development of the circular economy and do not compromise a known value chain. In this work, material recovery is approached through the reuse of these residues in syngas and biogas cleaning processes in order to remove key pollutants such as tars and hydrogen sulfide, respectively. Energy balances from the production of these chars have been established and energy efficiency indicators have been calculated. The chars were produced at 500 °C and then characterized by chemical and physical analysis. In order to provide them porous properties necessary for fixed-bed gas cleaning applications, activations were carried out at 850°C with CO_2 or steam. Buckwheat husks turn out to be a fairly conventional biomass and the particularity of millet husks is to have high levels of silicon. If pyrolysis chars have shown a low efficiency in the purification of gases, activation opens up new potential for them, especially for materials from buckwheat husks, which are similar to activated carbons. When activated with steam these chars show interesting efficiency for the purification of syngas and they conserve their calorific value (LHV) which makes it possible to consider an energy recovery through gasification. Results from this study also show that depending on the nature of biomass and type of activation, the material valorization and energy recovery are sometimes incompatible.